

Intraarticular pharmacokinetics of biologics and drug-delivery strategies to extend transsynovial permeation

Dissertation
zur
Erlangung des Doktorgrades (Dr. rer. nat.)
der
Mathematisch-Naturwissenschaftlichen Fakultät
der
Rheinischen Friedrich-Wilhelms-Universität Bonn

Vorgelegt von
Tobias Siefen

Aus
Düsseldorf

Bonn, 2022

Angefertigt mit Genehmigung der Mathematisch-Naturwissenschaftlichen Fakultät
der Rheinischen Friedrich-Wilhelms-Universität Bonn

1. Gutachter: Prof. Dr. Alf Lamprecht
2. Gutachter: Prof. Dr. Karl Wagner
Tag der Promotion: 26.01.2023
Erscheinungsjahr 2023

Table of content

Acknowledgements	
Summary	
1. Introduction	1
1.1 References	3
2. Assessment of joint pharmacokinetics and consequences for the intraarticular delivery of biologics	5
2.1 Graphical Abstract	6
2.2 Abstract	6
2.3 Keywords	6
2.4 Introduction	7
2.5 The synovial joint	8
2.5.1 The synovial membrane	9
2.5.2 Articular cartilage	10
2.6 Osteoarthritis pathology	11
2.6.1 Cartilage degeneration	12
2.6.2 Synovitis	12
2.6.3 Alterations in synovial fluid	13
2.7 Kinetics of IA applied molecules	13
2.7.1 Elimination of injected drugs from the joint	13
2.7.2 Impact of the synovial fluid on drug kinetics	14
2.7.3 Drug distribution into cartilage	14
2.8 Biorelevant models for articular kinetics	16
2.8.1 <i>In-vitro</i> versus <i>in-vivo</i> testing of drug formulations	16
2.8.2 Assessment of joint residence time	17
2.8.3 Assessment of cartilage penetration	18
2.9 Potential biologics for the treatment of OA	18
2.10 Intraarticular formulation principles for biologics	20
2.10.1 Viscosity increase	22
2.10.2 Immobilizing hydrogel systems	23
2.10.3 Encapsulation in multiparticulate systems	24
2.10.4 Bioadhesive strategies	27
2.10.5 Drug targeting	29
2.11 General discussion	31
2.11.1 Models	31
2.11.2 Drug delivery strategies	32
2.12 Conclusion	34
2.13 Author contributions	35

2.14	References	36
3.	Aims and scope	58
4.	An ex-vivo model for transsynovial drug permeation of intraarticular injectables in naive and arthritic synovium	59
4.1	Graphical abstract.....	60
4.2	Abstract	60
4.3	Keywords	60
4.4	Introduction	61
4.5	Materials and methods	63
4.5.1	Reagents and materials	63
4.5.2	<i>Ex-vivo</i> transsynovial permeation model	64
4.5.3	Incubation of synovium with LPS and analysis of inflammatory response	66
4.5.4	<i>In-vivo-in-vitro</i> -correlation (IVIVC).....	67
4.5.5	Statistical analysis	67
4.6	Results.....	68
4.6.1	Characterization of the transsynovial permeation model	68
4.6.2	Characterization of the transsynovial permeation of the <i>ex-vivo</i> synovitis model.....	71
4.6.3	Transsynovial permeability from synovitis model.....	72
4.7	Discussion	78
4.8	Conclusion.....	83
4.9	Acknowledgements.....	84
4.10	Author contributions.....	84
4.11	Supplementary Data.....	85
4.12	References	86
5.	Co-formulations of adalimumab with hyaluronic acid / polyvinylpyrrolidone to combine intraarticular drug delivery and viscosupplementation.....	92
5.1	Graphical abstract.....	93
5.2	Abstract	93
5.3	Keywords	93
5.4	Introduction	94
5.5	Materials and methods	96
5.5.1	Reagents and Materials.....	96
5.5.2	Design of experiments (DOE).....	96
5.5.3	Preparation of the ADA loaded HA/PVP formulations.....	97
5.5.4	Rheology	97
5.5.5	Conjugation of fluorophores.....	98

5.5.6	<i>Ex-vivo</i> transsynovial permeability	98
5.5.7	Isothermal titration calorimetry	99
5.5.8	Activity of ADA in presence of HA and PVP	100
5.5.9	Statistical analysis	100
5.6	Results	101
5.6.1	Rheology of HA/PVP mixtures	101
5.6.2	FITC-HA <i>ex-vivo</i> transsynovial permeability	106
5.6.3	FITC- ADA and FITC 150 kDa <i>ex-vivo</i> transsynovial permeability	106
5.6.4	Isothermal titration calorimetry	110
5.6.5	ADA activity in presence of polymers	111
5.7	Discussion	112
5.7.1	Rheology	112
5.7.2	Transsynovial permeability	114
5.8	Conclusion	116
5.9	Acknowledgements	117
5.10	Author contributions	117
5.11	Supplementary data	118
5.12	References	121
6.	Polyelectrolyte nanocomplexes to increase intraarticular residence of adalimumab injections	127
6.1	Graphical abstract	128
6.2	Abstract	128
6.3	Keywords	128
6.4	Introduction	129
6.5	Methods	131
6.5.1	Reagents and materials	131
6.5.2	Potentiometric titration	131
6.5.3	Biotinylation and conjugation of fluorophores	132
6.5.4	Preparation and characterization of ADA-nanocomplexes	133
6.5.5	Permeation studies	135
6.5.6	Tissue viability	137
6.5.7	TNF- α FLISA	137
6.5.8	Statistical analysis	138
6.6	Results	138
6.6.1	ADA-Nanocomplex formation and analysis	138
6.6.2	Synovial permeation	139
6.6.3	ADA-nanocomplex antigen recognition	144
6.6.4	Synovial cell viability in presence of nanocomplexes	145
6.7	Discussion	146
6.8	Conclusion	149

6.9	Acknowledgements.....	150
6.10	Author contributions.....	150
6.11	Supplementary data.....	151
6.12	References	155
7.	Summary and outlook.....	160
7.1	References	165
8.	Appendix.....	168
8.1	List of abbreviations.....	168
8.2	List of publications	170

Acknowledgements

First of all, I would like to thank my supervisor, Prof. Dr. Alf Lamprecht, for giving me the opportunity to research in his working group on this interesting topic. The many academic discussions and constructive talks have supported me enormously in the development of my thesis and also in my personal development. Thank you for your ideas, for your drive, for your criticism and above all for your openness. At the same time, these conversations were both entertaining and cheerful, so that the work was also connected with a lot of enjoyment. Thank you very much for the very pleasant cooperation and the trust!

I would like to sincerely thank Prof. Dr. Karl Wagner for providing the second examination report and for the numerous good discussions in the professional and private context.

I would like to thank Prof. Dr. Günther Weindl and Prof. Dr. Andreas Schieber for their willingness to participate in the examination committee.

Many thanks to Ferring Pharmaceuticals and my supervisors at the company, Crilles Casper Larsen, Alfred Liang, John Lokhnauth, Simon Bjerregaard, Daniel Plaksin and Camilla Borglin, who placed their confidence in me and whose support and advice I could always count on. The meetings were always enjoyable and productive gatherings.

A special thanks to my colleagues in pharmaceutical technology. You have made the institute a place I have gladly come to, even in stressful times. Besides the scientific discourses on technological issues of all kinds, there was always a lot of joking, laughing, and making true friends. Many thanks to my office, to Rafael, Ozan, Marius, and Christian for the wonderful time together and for making the institute feel like a second home for a few years. Thank you for your support, advice, and encouragement over the years. In particular, I would like to mention Thilo and Tim, with whom I was fortunate to share hobbies, holidays, and many wonderful experiences beyond university.

To my friends Julian, Marci, Luke, Flo, Charly, Aron, Fabi, Franzi, Gina, Basti, Jojo and Luki, I would like to thank you for your constant support and the backing you gave me in every phase of my PhD and my life. You are the best!

Many thanks to my parents and my brother. I wouldn't have been able to do any of this without your help and I am infinitely grateful for your endless support throughout all aspects of my life, for your patience, your love, and your advice, even in difficult times.

And last but not least special thanks to Theresa. For always believing in me and standing by me on every beautiful and every difficult day. You are truly the best person and made my time the best it could ever have been.

Summary

A local injection is often considered the only appropriate route of administration for active pharmaceutical ingredients that cannot cross biomembranes easily or that are not sufficiently stable in the gastrointestinal tract and therefore do not reach their site of action in the required quantity. Intraarticular injections provide the opportunity to deliver biologics directly to their site of action for a local and efficient treatment of osteoarthritis. However, the synovial joint is a challenging site of administration since the drug is rapidly eliminated across the synovial membrane and has limited distribution into cartilage, resulting in unsatisfactory therapeutic efficacy. In order to rationally develop appropriate drug delivery systems, it is essential to thoroughly understand the unique biopharmaceutical environments and kinetics in the joint to adequately simulate them in relevant experimental models. In this context, the estimation of joint residence time of a drug is one of the key requirements for rational development of intraarticular therapeutics. There is a great need for a predictive model to reduce the high number of animal experiments in early-stage development. In this work, a Franz-cell based porcine *ex-vivo* permeation model is proposed, and transsynovial permeation of fluorescently labeled model substances in the range of potential drug candidates have been determined. In addition, an inflammatory model was assessed for its effect on permeation of solutes. Size-dependent permeability in varying degrees of synovitis-like inflammation was observed for the analytes, whereby synovial inflammation led to a reduced size selectivity of the synovial membrane. Besides offering biorelevant insights into articular pharmacokinetics this work aims to reveal how this knowledge can be transferred into designing rationally derived formulation strategies to affect the joint residence time using the anti-inflammatory biologic adalimumab as an example. Polymer-based formulations present an attractive strategy for the intraarticular drug-delivery to refrain biologicals from early leakage from the joint. In this study, co-formulations of hyaluronic acid and polyvinylpyrrolidone were investigated for their potential as viscosupplements and their influence on the transsynovial loss of adalimumab. For this purpose, the polymer mixtures were

Summary

evaluated for their viscosity and elasticity behavior and their potential to restore the rheological properties of the synovial fluid over the range of joint motion while at the same time assessing their influence on the permeation of adalimumab across a porcine ex-vivo synovial membrane was determined. The formulations showed significant influence on transsynovial permeation kinetics of adalimumab and hyaluronic acid, which could be decelerated up to 5- and 3-fold, respectively. Besides viscosity effects, adalimumab was retained primarily by an electrostatic interaction with hyaluronic acid. Moreover, polymer-mediated stabilization of the antibody activity was detected. In a second drug-delivery approach, the biopharmaceutical environment of the joint space was exploited via positively charged nanocomplexes. The extracellular matrix of the synovium consists of a collagen network with enmeshed aggrecan galactosamine glycans, generating a high fixed negative charge density. By linking adalimumab with different molar equivalents of cationic diethylaminoethyl-dextran using avidin mediated nanocomplexes, the flux through porcine synovium was significantly decelerated whereby immobilization in superficial tissue layers was revealed by confocal laser scanning microscopy. The prepared carriers exhibited excellent intra-tissue stability, while retaining antigen recognition of adalimumab. In addition, the nanocomplexes did not show any adverse effects on synovial cells, resulting in unchanged viability compared with adalimumab alone. To conclude, an *ex-vivo* permeation model has been successfully introduced as a tool that allows for biorelevant screening of drug release as well as pharmacokinetics at an early stage of development, that might narrow the gap between dissolution and *in-vivo* testing through enhanced understanding of material-tissue interactions. The approach thus enables researchers to observe, evaluate, and adapt the design of efficient and intelligent drug carriers directly within their biopharmaceutical environment.

1. Introduction

Local injections are often the only reasonable route of administration for active pharmaceutical ingredients (API) which are unable to sufficiently overcome biomembranes or do not exhibit stability in the gastrointestinal tract and thus do not reach their dedicated sites of action in the required quantities. Depending on the site and form of administration, the injection can aim for both systemic and local effects [1]. To ensure satisfactory success of therapy and reduce frequent injections, there are a variety of pharmaceutical drug delivery systems to design parenteral depot formulations and achieve controlled release of the active ingredient from its dosage form. The dosage forms for controlled parenteral delivery systems are as diverse as the sites of their administration. Depending on the therapeutic regimen, local parenteral depots can be administered e.g., intratumorally, intraocularly, intrathecally, or intraarticularly [2]. Due to these very different sites of application, a high heterogeneity of the biopharmaceutical environments exists, which, just like the release from the drug delivery system itself, has a great influence on the pharmacokinetics and thus ultimately on the effect of the therapy. However, in early stages of development, the true impact of the injection site on the controlled parenteral delivery system is often underestimated. To test the release from these dosage forms, simple *in-vitro* test models are commonly used that measure the dissolution rate but fail to account for how the drug delivery system interplays with surrounding tissues, which can lead to misinterpretation of drug elimination and distribution kinetics [3,4]. Focusing on intraarticular injections, this work aims to raise awareness of the relevance of test methodologies that closely simulate the biopharmaceutical environment to provide profound information on release profile as well as pharmacokinetics for a more comprehensive assessment of controlled injectable drug delivery systems for biologics.

In recent years, targeted biologic therapies such as monoclonal antibodies have changed treatment paradigms and prognoses for many chronic diseases, with great resources being invested in novel therapeutic regimens and innovative drug delivery strategies [5]. Osteoarthritis (OA) represents the most frequent musculoskeletal disease diagnosed in more than 20% of US adults [6]. It leads to degeneration of cartilage and inflammation of the joint lead to pain, stiffness, and loss of mobility, which in turn dramatically impairs quality of life [7,8] and places a high burden on the individual and on the healthcare system respectively [9]. Despite the increasing incidence of OA worldwide, advanced therapeutic strategies have received little attention to date, with biologics yet to find their way into existing treatment regimens.

This is the case regardless of the fact that current research efforts have identified numerous targets and pathomechanisms, including proinflammatory cytokines and catabolic proteases that potentially allow for more causal therapeutic approaches [10,11]. With some of the investigational biologics, such as the tumor necrosis factor α (TNF- α) inhibitor adalimumab (ADA), being already well established with other indications [12], IA administered agents require drug delivery strategies yet to be adapted to the application in the joint space in order to exert their effect. ADA, even as an immediate release injectable, has been reported to have a beneficial effect on the progression and symptoms of OA in clinical trials and thus represents a promising drug candidate for more progressive drug delivery systems for OA therapy in order to unlock the full potential of the agent [13,14]. Since ADA is a monoclonal antibody (mAb), which represent the largest and most relevant category of biologics, it further qualifies as an excellent model drug with a high translational capacity to other biologics and was therefore chosen as suitable agent to develop and test novel IA formulation approaches. Thereby, it has to be considered that proteins are usually much more sensitive to chemical and physical stresses so that more precautionary approaches have to be taken to applied processes and excipients [15,16].

1.1 References

- [1] Y. Shi, L. Li, Current advances in sustained-release systems for parenteral drug delivery, *Expert Opin. Drug Deliv.* 2 (2005) 1039–1058. <https://doi.org/10.1517/17425247.2.6.1039>.
- [2] V. Imran, B. Denish, R. Saketh, R. Javia, Ankit, Parenteral Controlled and Prolonged Drug Delivery Systems: Therapeutic Needs and Formulation Strategies, in: A. Misra, A. Shahiwala (Eds.), *Nov. Drug Deliv. Technol. Innov. Strateg. Drug Re-Position.*, Springer Singapore, Singapore, 2019. https://doi.org/doi.org/10.1007/978-981-13-3642-3_7.
- [3] A. Seidlitz, W. Weitschies, In-vitro dissolution methods for controlled release parenterals and their applicability to drug-eluting stent testing, *J. Pharm. Pharmacol.* 64 (2012) 969–985. <https://doi.org/10.1111/j.2042-7158.2011.01439.x>.
- [4] C. Larsen, S.W. Larsen, H. Jensen, A. Yaghmur, J. Østergaard, Role of *in vitro* release models in formulation development and quality control of parenteral depots, *Expert Opin. Drug Deliv.* 6 (2009) 1283–1295. <https://doi.org/10.1517/17425240903307431>.
- [5] B. Coiffier, Preparing for a new generation of biologic therapies: understanding the development and potential of biosimilar cancer therapeutics, *Future Oncol.* 13 (2017) 1–3. <https://doi.org/10.2217/fon-2017-0157>.
- [6] C.G. Helmick, D.T. Felson, R.C. Lawrence, S. Gabriel, R. Hirsch, C.K. Kwoh, M.H. Liang, H.M. Kremers, M.D. Mayes, P.A. Merkel, S.R. Pillemer, J.D. Reveille, J.H. Stone, National Arthritis Data Workgroup, Estimates of the prevalence of arthritis and other rheumatic conditions in the United States: Part I, *Arthritis Rheum.* 58 (2008) 15–25. <https://doi.org/10.1002/art.23177>.
- [7] D. Pereira, E. Ramos, J. Branco, Osteoarthritis, *Acta Médica Port.* 28 (2014) 99–106.
- [8] M.B. Goldring, S.R. Goldring, Osteoarthritis, *J. Cell. Physiol.* 213 (2007) 626–634. <https://doi.org/10.1002/jcp.21258>.
- [9] P.A. Laires, H. Canhão, A.M. Rodrigues, M. Eusébio, M. Gouveia, J.C. Branco, The impact of osteoarthritis on early exit from work: results from a population-based study, *BMC Public Health.* 18 (2018) 472. <https://doi.org/10.1186/s12889-018-5381-1>.
- [10] M.B. Goldring, Anticytokine therapy for osteoarthritis, *Expert Opin Biol Ther.* (2001) 13.

- [11] A.E. Weber, I.K. Bolia, N.A. Trasolini, Biological strategies for osteoarthritis: from early diagnosis to treatment, *Int. Orthop.* 45 (2021) 335–344. <https://doi.org/10.1007/s00264-020-04838-w>.
- [12] Abbvie. Humira (adalimumab) [package insert], US Food Drug Administration Website. (n.d.). https://www.accessdata.fda.gov/drugsatfda_docs/label/2015/125057s394lbl.pdf (accessed January 27, 2022).
- [13] W.P. Maksymowych, A.S. Russell, P. Chiu, A. Yan, N. Jones, T. Clare, R.G. Lambert, Targeting tumour necrosis factor alleviates signs and symptoms of inflammatory osteoarthritis of the knee, *Arthritis Res. Ther.* 14 (2012) R206. <https://doi.org/10.1186/ar4044>.
- [14] J. Wang, Efficacy and safety of adalimumab by intra-articular injection for moderate to severe knee osteoarthritis: An open-label randomized controlled trial, *J. Int. Med. Res.* 46 (2018) 326–334. <https://doi.org/10.1177/0300060517723182>.
- [15] R. Vaishya, V. Khurana, S. Patel, A.K. Mitra, Long-term delivery of protein therapeutics, *Expert Opin. Drug Deliv.* 12 (2015) 415–440. <https://doi.org/10.1517/17425247.2015.961420>.
- [16] W. Jiskoot, T.W. Randolph, D.B. Volkin, C. Russell Middaugh, C. Schöneich, G. Winter, W. Friess, D.J.A. Crommelin, J.F. Carpenter, Protein Instability and Immunogenicity: Roadblocks to Clinical Application of Injectable Protein Delivery Systems for Sustained Release, *J. Pharm. Sci.* 101 (2012) 946–954. <https://doi.org/10.1002/jps.23018>.

2. Assessment of joint pharmacokinetics and consequences for the intraarticular delivery of biologics

Tobias Siefen¹, Simon Bjerregaard², Camilla Borglin², Alf Lamprecht^{1,3}

¹Department of Pharmaceutics, Institute of Pharmacy, University of Bonn, Bonn, Germany.

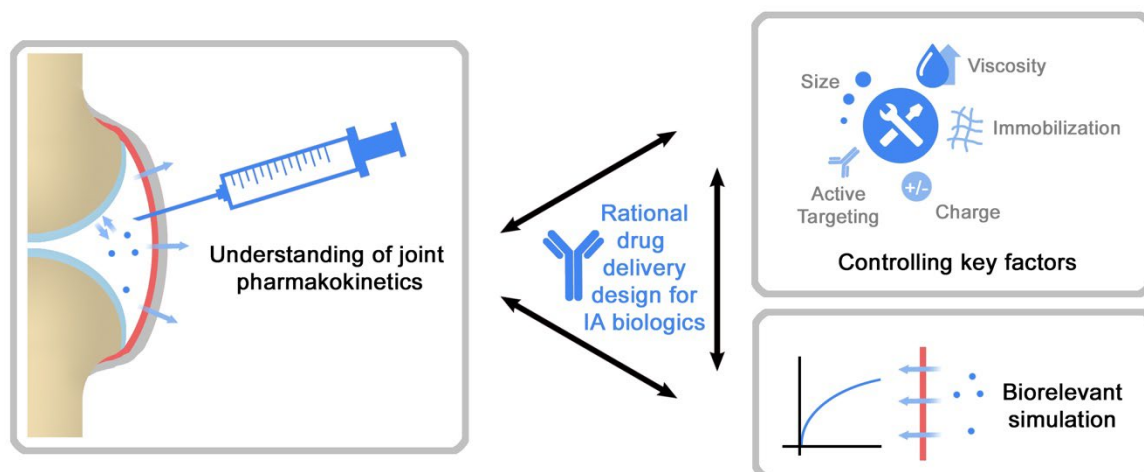
²Ferring Pharmaceuticals A/S, Copenhagen, Denmark

³PEPITE (EA4267), University of Burgundy/Franche-Comté, Besançon, France.

This work is published as

Siefen T, Bjerregaard S, Borglin C, Lamprecht A. Assessment of joint pharmacokinetics and consequences for the intraarticular delivery of biologics. *J Control Release*. 2022 Jun 14:S0168-3659(22)00343-1. doi: 10.1016/j.jconrel.2022.06.015.

2.1 Graphical Abstract



2.2 Abstract

Intraarticular (IA) injections provide the opportunity to deliver biologics directly to their site of action for a local and efficient treatment of osteoarthritis. However, the synovial joint is a challenging site of administration since the drug is rapidly eliminated across the synovial membrane and has limited distribution into cartilage, resulting in unsatisfactory therapeutic efficacy. In order to rationally develop appropriate drug delivery systems, it is essential to thoroughly understand the unique biopharmaceutical environments and kinetics in the joint to adequately simulate them in relevant experimental models. This review presents a detailed view on articular kinetics and drug-tissue interplay of IA administered drugs and summarizes how these can be translated into reasonable formulation strategies by identification of key factors through which the joint residence time can be prolonged and specific structures can be targeted. In this way, pros and cons of the delivery approaches for biologics will be evaluated and the extent to which biorelevant models are applicable to gain mechanistic insights and ameliorate formulation design is discussed.

2.3 Keywords

intraarticular injection, articular pharmacokinetics, joint residence time, cartilage diffusion

2.4 Introduction

The synovial joint represents a unique site for drug application that involves complex pharmacokinetics, such that intraarticular (IA) administered therapeutic agents may fail to exert their potential effects and remain inadequate. Upon injection, the agents are subject to rapid elimination across the synovial tissue into surrounding vessels, resulting in a therapeutically deficient residence time in the joint or failure to reach their site of action due to insufficient distribution into the avascular articular cartilage [1]. In the early stages of formulation development, it is therefore important to accurately mimic the joint environment and its specific biopharmaceutical characteristics through appropriate test models so that drug-tissue interplay in the joint can be thoroughly analyzed and comprehensive drug delivery systems can be designed on a rational basis. Indeed, provided these pharmacokinetic challenges were controlled, IA injections appear to be the ideal therapeutic approach for joint diseases such as osteoarthritis (OA), where typically only individual joints are involved and no extraarticular manifestations are entailed [2]. Locally administered drugs generally offer the advantages of high efficiency while reducing the amount of active ingredient and thus the costs and systemic exposure of the therapy and enable the administration of progressive therapeutics, such as macromolecular agents, autologous blood products and gene or cell-based treatments, which would be unavailable or insufficiently effective via the oral or systemic route [3]. However, to date, current treatment options remain limited, and no targeted treatments have been approved [4]. Consequently, only pain-reducing or mobility-improving agents are being injected into the joint space at present. Whereas these can temporarily reduce the burden of disease and provide symptomatic benefit, neither cure nor sustained improvement of the clinical progression of the disease can be achieved [5]. Thereby, among the IA injectables, hyaluronic acid (HA) and corticosteroids present by far the most frequently applied agents [6], with analgesics, such as NSAIDs or local anesthetics being less commonly applied [7,8]. However, at present there is only one approved drug (Zilretta® - Triamcinolone acetonide PLGA microspheres) with a sustained release formulation [9]. Over the past years, a lot of research has been conducted to gain deeper knowledge on the etiology and pathogenesis of OA and a number of potential targets for a directed therapeutic approach have been identified [10–12]. These findings could lead to a more causal and profound modulation of OA in future treatment regimens via target-specific biologics, as has already successfully been introduced for other chronic diseases. However, achieving these aims will require the development of dedicated drug delivery systems that overcome biopharmaceutical articular challenges while ensuring the stability and bioactivity of non-cellular biologics. This first

requires a profound knowledge of the distribution and elimination processes of the drug and its delivery system in the different compartments of the synovial joint in the healthy as well as in the arthritic state, and models to adequately mimic these processes in the laboratory.

2.5 The synovial joint

Synovial joints are complex structures whose principal function is to provide stability and mobility through flexible junction of adjacent bones. Essentially, within the joint, there are two relevant target tissues regarding the potential deployment of therapeutics in OA: the synovial membrane enclosing the joint cavity and the bone-covering articular cartilage (**Fig. 2-1**). In addition, the SF, which fills the synovial cavity, has a vital role for the interaction of different cells and tissues within the joint and interferes with injected dosage forms, thereby affecting their distribution and properties.

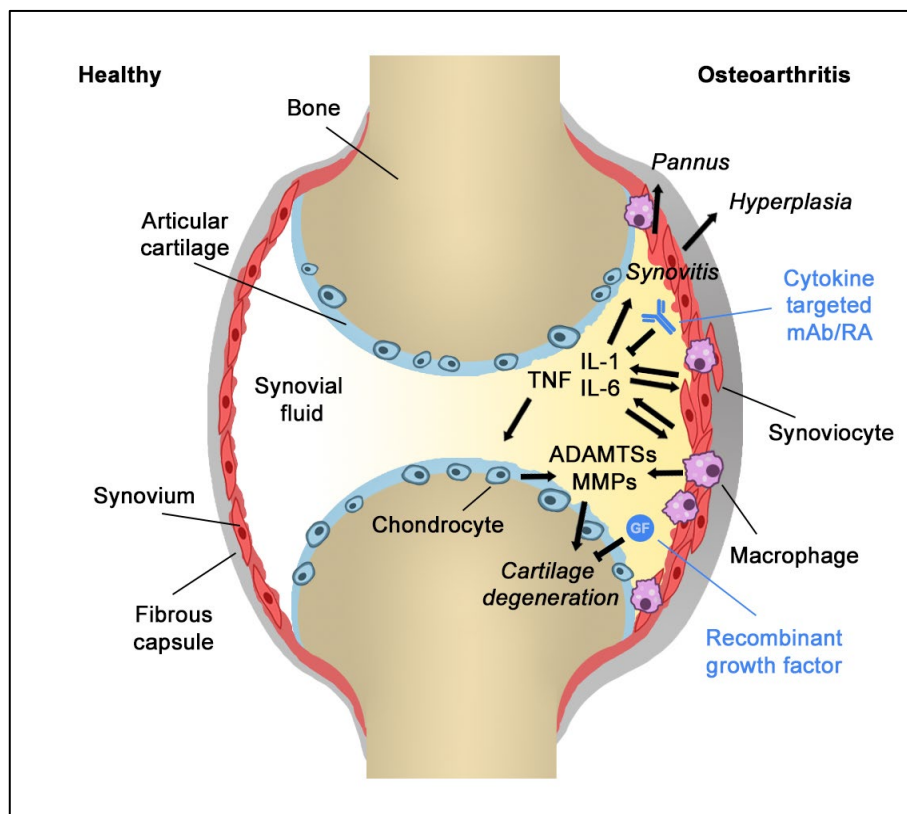


Fig. 2-1: Schematic illustration of the structure of a synovial joint in its healthy and arthritic state. Thereby, the key pathophysiological processes are depicted, which can be pharmacologically intervened by biologics.

2.5.1 The synovial membrane

The synovial membrane represents the innermost layer of the synovial joint capsule and consists of two layers: A connective tissue called subsynovium, which can be of fibrous, adipose or areolar structure and a more cellular intimal lining, which is mainly composed of 1-4 layers of fibroblast-like synoviocytes and macrophage-like synoviocytes [13]. The intima forms a compact yet discontinuous interface without any intercellular junctions or presence of a basement membrane [14] and thus, despite its apparent resemblance to other body surface or cavity lining epithelia, it is an entirely unique structure in the human body (**Fig. 2-2A**) [15]. The principal functions of the synovial membrane are to maintain homeostasis by controlling fluid and nutrient exchange within the joint compartments as well as to secrete HA into the plasma ultrafiltrate and thus regulate SF properties. Due to the microporous structure of the intima, diffusion is predominantly controlled by the subsynovial tissue, which is composed of collagen bundles (**Fig. 2-2B**), fibronectin and enmeshed proteoglycans and covered by a polarization layer of secreted hyaluronic acid [16,17].

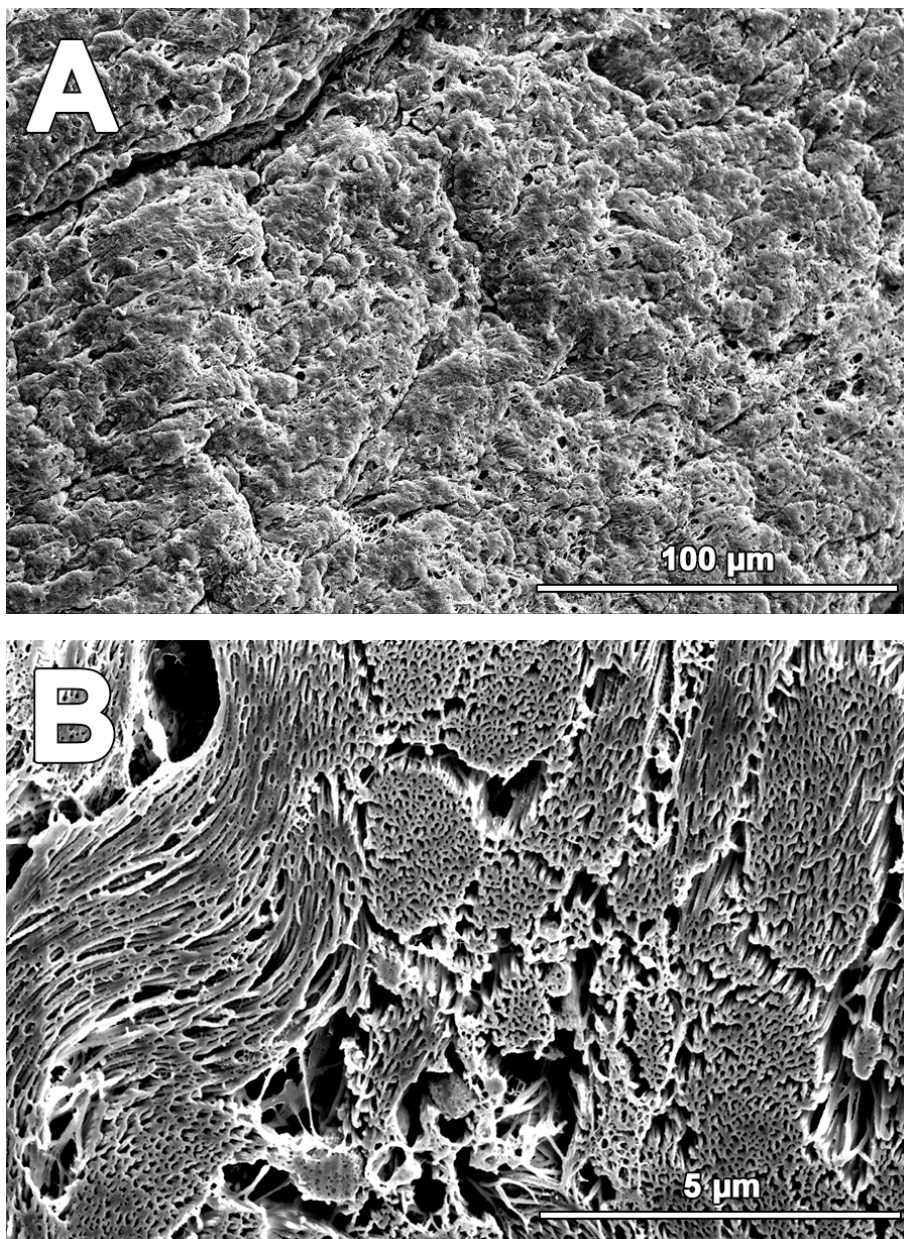


Fig. 2-2: Electron microscopic image (unpublished data) of the synovial membrane surface (**A**). In this overview image, the intimal layer consisting of synoviocytes with intracellular gaps can be seen. The intima represents a densely populated cellular region that is one to three cells thick. It is covered with the synovial fluid of the polarization layer, which has been freeze-dried in the fixation process, giving it a uniform surface. The cross-section (**B**) shows a closer look at the extracellular network of the subintima, which is built up from a loosely packed fibrillar ultrastructure consisting of collagens III, IV, V and VI with a small amount of type I collagen.

2.5.2 Articular cartilage

Articular cartilage covers the interfacing bones of the joint with a uniform and smooth surface and, together with the SF, assures for almost frictionless movement. The cartilage presents an entirely avascular and alymphatic tissue and is thus reliant on diffusion from the SF for its supply of nutrients [18]. Cartilage constitutes predominantly

of water (70%) and a high negatively charged and dense network of collagen and interwoven aggrecan proteoglycans, wherein chondrocytes are embedded [19]. The chondrocytes function as metabolically active cells that maintain the composition of the cartilage by regulating anabolic and catabolic processes of this unique complex structure [20].

2.6 Osteoarthritis pathology

OA is a chronic degenerative disorder that affects only one or a few synovial joints, and causes pain, stiffness, and loss of mobility [2]. Although OA is often described as a pathological destruction of the cartilage, it is in fact a disease of the whole joint associated with changes in articular cartilage, synovial membrane, bone, and SF. Focal lesions in cartilage caused by adverse effects of trauma, abnormal load on healthy cartilage or normal load on abnormal cartilage are assumed to initiate OA [10]. It should however be noted that the exact etiology is still not fully understood and both systemic and local biomechanical factors are thought to contribute to the development of the disease [21]. OA conditions lead to a stimulation of the chondrocytes in the cartilage which react with an upregulation of cytokines and proteases such as metalloproteases (MMPs) and aggrecanases of the ADAMTS (a disintegrin and metalloproteinase with thrombospondin motifs) family. These proteases cause degeneration of the cartilage extracellular matrix (ECM), whose fragments in turn trigger the release of inflammatory mediators such as tumor necrosis factor- α (TNF- α) and interleukin 1 β (IL-1 β) by chondrocytes and synoviocytes [22], which promote inflammatory processes throughout the joint and drive the progression of the disease. This positive feedback loop leads to proceeding degeneration of the cartilage matrix and inflammation of the synovial membrane, which leads to hyperplasia of the synovial intima, cellular infiltration of immune cells, and pannus formation of the fibrous capsule, causing pain and loss of mobility (**Fig. 2-1**). The activated macrophages within the synovial membrane play another key role in OA pathology by further fueling the disease particularly through the production of MMPs [23,24]. The resulting mechanical stress resulting from a decrease of the lubricating properties of the SF and the breakdown of the protective cartilage layer causes remodeling and sclerosis of the underlying bones as well as formation of osteophytes within the joint [25]. While the processes involved in osteoarthritis can generally serve as an efficient compensating system for existing fissures, that result in a structurally altered but symptom-free joint, overwhelming deterioration or impaired repair mechanisms may fail to provide

adequate recovery from trauma and can lead to progressive tissue damage and malalignment of associated symptoms as described above.

2.6.1 Cartilage degeneration

Cartilage has a very limited capacity for self-healing, so that its degradation is widely considered to be the most critical pathophysiologic issue in OA. In the course of OA, there is a disturbance of the chondrocyte function resulting in a deterioration of the structural properties of the cartilage. This dysregulation is particularly mediated by catabolic cytokines, with both autocrine and paracrine mechanisms described [26]. In addition, chemokines and proteases such as MMPs and ADAMTs, that originate from the inflamed synovium, can provoke or intensify ECM degeneration [27]. To inhibit cartilage degradation, both the blockade of catabolic proinflammatory cytokines and the supplement of anabolic growth factors offer possible therapeutic approaches. In addition, the suppression of MMP activity and the associated prevention of cartilage breakdown presents a potential therapeutic aim [28]. However, while it is sufficient to prolong the residence time in the joint for drugs whose site of action is the synovium or SF, it is mandatory for drugs aiming for cartilage protection to penetrate deep tissue layers and reach the chondrocytes of the avascular cartilage, which requires appropriate drug delivery strategies.

2.6.2 Synovitis

Since the synovial membrane functions as the principal immunoreactive system of the joint, it plays a pivotal role in the development and progression of OA. Synovitis, the inflammation of the synovial membrane, is present in the majority of OA patients [29]. While OA is not classically considered an inflammatory disease as it is for example the case for rheumatoid arthritis, current research increasingly recognizes the role of synovitis to be an important determinant for clinical symptoms that reflects of the structural progression of the disease. The synoviocytes release an array of proinflammatory mediators, including the major cytokines IL-1 β and TNF- α among others, whose inhibition may provide opportunities for therapy with monoclonal antibodies (mAb) or other targeted agents [30]. In turn, the mediators TNF- α and IL-1 β released by the macrophages induce the formation of interleukin 6 (IL-6), nerve growth factor (NGF) and other chemokines, as well as catabolic MMPs and ADAMTs, which further amplify inflammation and promote breakdown of the articular cartilage [31,32].

2.6.3 Alterations in synovial fluid

The SF that fills the joint cavity is a plasma ultrafiltrate that is enriched with HA secreted by the synoviocytes and serves as a lubricant and nutrient supplier for the avascular cartilage [33]. Pathophysiological changes associated with OA may cause a decrease in SF viscosity due to increased activity of galactosamine glycan (GAG) degrading hyaluronidases [34,35]. The resulting breakdown of hyaluronic acid chains into smaller fragments, leads to a loss of lubricating properties of SF and elevated mechanical stress on articular cartilage [36], whereby HA fragments may even further stimulate the inflammatory process [37].

2.7 Kinetics of IA applied molecules

2.7.1 Elimination of injected drugs from the joint

Small molecules have a half-life of usually less than 2 h (0.1-6 h) in the joint cavity [38]. While these primarily exit the joint via blood vessels, macromolecular agents are largely eliminated from the joint cavity via the lymphatic vasculature of the synovial tissue. Although bulk flow of proteins into lymphatics has at many times been assumed [39], it appears more likely that there is a certain size-dependency in the IA clearance of macromolecules (see **Fig. 2-1**) [40–43], whereby it should be mentioned that molecular size has far a greater impact on the ingress of molecules from systemic circulation into the joint, than on the elimination from it [44]. Therein, the discriminating influencing variable appears to be the effective pore size of approximately 33-59 nm as predetermined by the dense structure of the synovial ECM [45], rather than the micrometer wide gaps of the intimal layer. In addition, IA outflow of molecules is restricted by a concentration polarization layer on the surface of the intima, which is formed through accumulation of secreted hyaluronic acid on the tissue surface [46]. Nevertheless, fluid exchange in the joint represents a yet relatively unconstrained system and rapid elimination of IA drugs from the joint space occurs, which leads to insufficient therapeutic success. In OA, both pannus development and alteration in the distribution of joint lymphatics lead to a change in the diffusion path of IA injected agents through the synovial tissue, which is accompanied by catabolic enzyme activity and further inflammatory processes that result in tissue remodeling and alteration of permeability. Hence elimination kinetics of macromolecules of the synovial tissue are significantly different in the inflamed state. However, the true impact of OA on clearance remains unclarified. While some studies have identified an accelerated elimination which has been attributed to an increase in the number of lymphatic vessels

and enhanced tissue permeability [47–49], other publications describe a reduction in the elimination rate of macromolecules [50,51]. These differences could be due to the state of disease or accordingly to the experimental model used. In mild OA, for example, the number of capillary lymphatic vessels is increased, but in severe disease the number of mature lymphatics is decreased [52,53]. In addition, *ex-vivo* permeation studies have shown that enzymatic activity leads to depletion of the enmeshed proteoglycans and thereby to a reduction in the size selectivity of the membrane under inflammation [40]. Similar implications for the mechanism behind inflamed state permeability were derived based on *in-vivo* injection of enzymes or enzyme inhibitors [54,55], so that, taken together, evidence exists that the exact inflammatory state of the joint must be considered for an accurate assessment of kinetics.

2.7.2 Impact of the synovial fluid on drug kinetics

SF can have considerable influence on the pharmacokinetics of drug delivery systems in the joint space. Since it is highly viscous, its hyaluronan gel network sterically impedes the passive diffusion of macromolecules in a size-dependent manner [56]. Electrostatic interaction of the anionic HA with drugs or their carriers can increase the hydrodynamic diameter by formation of self-assembling nano- or microparticulate systems, thereby reducing diffusion into the dense ECM of the synovial membrane or cartilage [57]. In addition, charge-induced interactions with the ECM of cartilage or synovial membrane are diminished by a reduced zeta potential of drug-HA complexes [58]. Depending on the defined therapeutic goal of the injected drug, the interactions with SF can be both considered advantageous or considered as a challenge, as they may prolong the retention time in the joint but as at the same time the penetration into the cartilage is hindered. However, it is advisable to integrate the effect of SF on the drug delivery system in the development of the formulation strategy, as it may exhibit significant influence.

2.7.3 Drug distribution into cartilage

Generally, the cartilage causes a substantial hindrance for the drug to reach the chondrocytes and thereby its effective site of action due to the dense hydrophilic matrix composition creating a fine porous network with an effective pore size of approximately 6 nm [59]. Furthermore, the high negative-fixed charge resulting from the high content of GAGs and proteoglycans in the tissue represents an additional barrier that impedes the deep penetration of drugs into the tissue [60]. In general, there is a partition equilibrium between the SF and the cartilage, which shifts as the molecular size of the

drug increases (see **Fig. 2-3**). Steric hindrance to the diffusion of macromolecules occurs due to the tight and anisotropic ECM. However, even large molecules, up to an approximately 16 nm radius, diffuse through the entire cartilage matrix, albeit a decrease in the partition coefficient with increasing size appears evident [61,62]. Thereby, linear molecules permeate through the tissue more easily than spherical molecule such as mAbs [63] and an increase in hydrophilicity leads to an increased permeability across the articular cartilage [64]. In addition, molecular charge has a significant influence on the permeability of cartilage. The distribution equilibrium of charged solutes is subject to the Donnan effect, which is due to the difference in electrical potential between the joint cavity and the high negative fixed charge of the cartilage [65]. Small cationic solutes accordingly have a higher partition coefficient, penetrate deeper into the tissue and are longer retained in the cartilage [41], whereby the opposite applies to anionic solutes [66]. This influence of charge can already be observed in differences in the pI value of proteins. An antibody with a pI of 5.9 for example shows a 20 % higher local diffusivity compared to an antibody with a pI value of 4.7 [61]. However, if the total positive net charge is increased above a certain threshold, immobilization on the surface of the cartilage occurs due to strong electrostatic interactions and deep zones of the cartilage remain unreached [67]. In this way, the total residence time in the joint can be influenced as well as the chondrocytes can be reached. The local composition of the cartilage undergoes structural breakdown of the ECM during the course of OA, resulting in a change in the diffusivity of drugs in the tissue [68]. As previously described, it is most notably GAGs that control cartilage permeability. Degradation of their structural integrity by MMPs and other catabolic enzymes causes enhanced diffusivity of cartilage as the effective pore size enlarges [69,70]. Accordingly, in analogy to the synovial membrane, permeation rates, but not distribution coefficients, of large macromolecules such as proteins are affected more strongly than those of small molecules [71]. In this way, an increased uptake into the cartilage after mechanical injury could be shown for Fab fragments, that could be further amplified by TNF- α , which acts as an inflammatory mediator [72]. Beyond that, the altered ECM leads to a change in convection, which additionally enhances drug penetration due to increased fluid flow. This likewise causes a more pronounced enhancement of the penetration of macromolecules compared to small molecules [73]. Hence, the pathological state could indeed facilitate the reachability of chondrocytes by the drug, although a pathologically accelerated clearance from the joint *in-vivo* might offset the herein described effects.

2 Assessment of joint pharmacokinetics and consequences for the intraarticular delivery of biologics

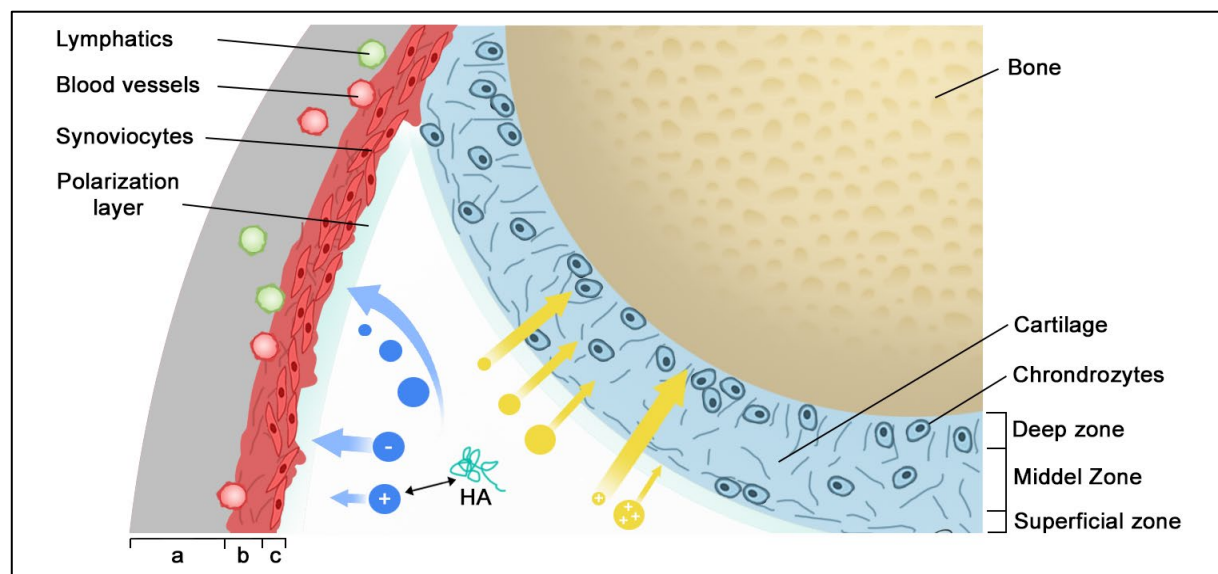


Fig. 2-3: Schematic illustration of the pharmacokinetics of IA injected molecules. The agents leave the joint space into surrounding lymphatic or blood vessels in a size-dependent manner (blue), which is determined by the ECM of the subsynovium. Thereby charge, partly due to interaction with endogenous HA, has a hindering influence on permeation. Penetration of cartilage (yellow) is limited by the hydrodynamic radius, so that molecules above a certain size do not or not sufficiently reach the deep zones of the cartilage. Positive charged molecules penetrate faster and deeper into the cartilage due to the Donnan effect. However, above a certain net charge or size, superficial immobilization of the molecule occurs. a: fibrous capsule; b: subsynovium; c: intimal layer.

2.8 Biorelevant models for articular kinetics

2.8.1 *In-vitro* versus *in-vivo* testing of drug formulations

A wide variety of *in-vitro*, *ex-vivo*, and *in-vivo* models have been used in research to develop new OA drugs to assess the pharmacokinetics of the applied drug and to evaluate the impact of pathological processes on their elimination and distribution. Animal models are frequently used, as they allow investigation of physiological and metabolic factors as well as long-term changes in tissue structure and joint organization [74]. While animal models provide valuable information, they are very complex in their interpretation, entail ethical considerations and are demanding as well as costly in their execution. Reducing this complexity by means of suitable *ex-vitro* or *in-vitro* models to individual joint compartments or processes can provide more specific information about isolated events or mechanisms in the joint, since the number of variables and influences is reduced, and causal relationships can be identified more readily. Animal models for OA have been described in detail elsewhere [75–78], but this paper will provide an overview of current *in-vitro*, and *ex-vivo* models for articular pharmacokinetics in the healthy and OA joints to evaluate how these processes can

be simulated in the laboratory in a biorelevant approach to provide a platform for the rational design of formulations in the early stages of development.

2.8.2 Assessment of joint residence time

Since the joint residence time represents one of the most crucial criteria when developing IA drug formulations, its appropriate simulation is essential for a biorelevant assessment of novel drug formulations. In this context, a simple yet accurate *in-vitro* test model is required to adequately evaluate both drug release from the dosage form as well as its synovial elimination. However, there is generally no approved model to test dissolution of parenteral sustained release drugs, especially for IA injection, so that there are different approaches in research. Simple artificial membranes are most commonly used, for example in the form of rotating dialysis membranes [79,80] or assimilable membrane separated diffusion chambers [57,81]. While these allow for testing of the release kinetics from the dosage form, they fail to predict the interaction with the tissue and the effective duration of joint residence, since their structural composition and chemical properties do not reasonably mimic the physiological state [40]. A substantially higher information value is achieved from using *ex-vivo* synovium as a permeation barrier, with explants from porcine joints being used most frequently [82,83]. These are considered to have excellent transferability to human synovial tissue, making them a suitable surrogate [84]. However, beside the advantage of high biorelevance and a favorable *in-vitro-in-vivo* correlation, *ex-vivo* models entail the drawback of lower replicability across different laboratories. Tissue engineered cell culture models also provide a relevant, yet simple assessment of synovial permeation kinetics [85], but lack organically grown ECM, which however is ultimately one of the most important determinants of elimination kinetics. Since the clearance of drugs in the OA joint is altered by both changes in the SF and inflamed tissue, it's of particular interest to integrate these conditions into the test model, since IA drug formulations are usually injected into pathologically affected joints. Advanced *in-vitro* test systems mimic the arthritic environment through modification in the composition of the medium or a change of pore size of the membrane to gain more relevant insights [86,87]. Again, improved simulation can be achieved using *ex-vivo* tissue or cell-culture models, whose living cells offer the prospect to induce true inflammatory events through incubation with proinflammatory agents, such as lipopolysaccharides or interleukins and thus assessment of the impact of synovitis on the permeation of the drug formulation across the synovium [40,85].

2.8.3 Assessment of cartilage penetration

In vitro, determination of absorption kinetics into cartilage is approached almost exclusively with explanted material since, as with the synovial membrane, the unique properties of the tissue are demanding to mimic artificially. To measure diffusion of pharmaceutical dosage forms, different techniques have proven successful. One method is to place harvested cartilage in a solution of analyte and indirectly infer penetration from the decrease of drug concentration in the surrounding medium. Once saturation has been reached, it is then also possible to calculate the desorption by replacing the solution in the bath [88,89]. Another method to analyze diffusion is based on the use of a two-chamber diffusion model with an explant as a barrier between the two chambers [64,90]. Thereby, labeling by means of conjugated fluorophores or radiolabeling is common for both models. As it is not possible to gain insight into distinct diffusion through the different layers of the cartilage with these methods, examination of labeled molecules within the previously incubated tissue by means of fluorescence microscopy, CT or NMR is commonly employed to obtain diffusion gradients within the tissue [91–94]. In addition, fluorescence recovery after photobleaching (FRAP) is widely used to quantify site-specific diffusion dynamics but is restricted to small regions within the cartilage rather than providing broader information pertaining to the tissue as a whole [62,95]. For biorelevant conclusions, the use of tissue in a state resembling that of the diseased cartilage is recommended since factors such as inflammation or traumatic injuries relevantly affect the permeability of the cartilage. For this purpose, the harvested tissue may be treated *ex-vivo* with collagenases or cytokines such as TNF- α , or mechanical injury may be applied by compression to mimic the arthritic state before permeability studies are performed. [72,74,96].

2.9 Potential biologics for the treatment of OA

While small molecules, especially corticosteroids are already used for the treatment of OA, there are no approved biologic agents for IA injection yet. Nevertheless, research has revealed a number of very promising candidates [97–99], provided an appropriate delivery ensures sufficient residence time at the site of action, as well as sufficient preservation of the bioactivity of the biologic. Among a few others, mAbs, mainly targeting the inhibition of proinflammatory mediators, and growth factors for cartilage regeneration have proven to be effective (**Tab. 2-1**). In particular, the cytokines TNF- α and IL-1 β have been implicated in the development and progression of OA [100]. On this basis, the anti-TNF- α agents infliximab, etanercept, and adalimumab have been shown to significantly improve OA and to be well tolerated in clinical trials after IA

administration [101–105]. Significant improvement in clinical condition including pain relief and prevention of cartilage degradation after IA injection was also described for the IL-1 receptor antagonist (RA) anakinra and evaluated as a potential therapeutic approach [24,106,107]. In addition to receptor antagonists of the main inflammatory mediators, tanezumab, a mAb that blocks NGF, has been associated with a significant improvement in OA symptoms and has been successfully tested clinically [108,109]. The US Food and Drug Administration (FDA) has approved the NGF antibody Solensia (frunevetmab injection), the first drug to treat pain associated with osteoarthritis in cats and the first new veterinary monoclonal antibody (mAb) drug in early 2022 [110]. However, in 2021, the FDA decided against approving the NGF antibody tanezumab for use in human therapy [111]. There are no FDA-approved antibody therapies for OA in humans to date. Anabolic-acting agents are also of great relevance in research on the therapy of OA. Among them, the exogenous addition of the recombinant growth factors insulin-like growth factor 1 (IGF-1), bone morphogenetic protein 7 (BMP-7), Fibroblast Growth Factor 18 (FGF-18) and calcitonin has been particularly successful, which have been shown to induce cartilage repair and thus alleviate symptoms without causing adverse events in clinical studies [112–116]. However, none of these biologics achieves sufficient therapeutic efficacy without a residence prolonging formulation strategy.

2 Assessment of joint pharmacokinetics and consequences for the intraarticular delivery of biologics

Tab. 2-1: Potential treatment options for OA with non-cellular biologics as were tested in clinical or animal trials; *IR:* Immediate release; *SR:* sustained release; *SC:* subcutaneous; *IV:* intravenous, *TRN:* Trial registration number.

Type	Therapeutic	Release	Application	Reference
TNF- α inhibitor	Adalimumab	IR	IA/SC	Human: NCT00686439 [103] Human: No TRN [104] Human: NCT00597623 [117] Human: Case report [118] Human: NCT00296894 [119]
	Infliximab	IR	IA	Human: Case report [101] Human: No TRN [102]
	Etanercept	IR	IA	Human: No TRN [105] Human: NTR-1210 [120]
IL-1 β RA	Anakinra	IR/SR	IA	Human: No TRN [121] Mouse [106] Dog [122]
NGF inhibitor	Tanezumab	IR	IV	Human: NCT00394563 [108] Human: NCT00864097 [109]
Growth factor	IGF-1	SR	IA	Rat [123] Rabbit [124]
	BMP-7	SR	IA	Hunter: NCT00456157 [112] Mouse [125] Pig [126] Rabbit [127]
	TGF- β	SR	IA	Mouse [128] Rabbit [129]
	FGF-18	SR	IA	Human: NCT01033994 [130] Rabbit [131]
	Calcitonin	SR	IA	Rabbit [116] Mouse [132]

2.10 Intraarticular formulation principles for biologics

IA injections of biologics such as mAbs, RA or growth factors promise a wide range of novel therapeutic approaches to control OA more effectively if adequately delivered [133–135]. In comparison to small molecules [136], however, they exhibit distinctly different physicochemical and biopharmaceutical characteristics due to their complicated shape based on secondary, tertiary and (sometimes) quaternary structures [137,138]. In view of their divergent kinetics within the joint, as well as the demanding formulation requirements that apply for proteinaceous drugs, focus will be placed on IA drug-delivery strategies of non-cellular biologics. In this context, the effect on the joint residence time, the stability of the dosage form and the active ingredient and the targeting of specific structures are considered. Articular pharmacokinetics represents the logical starting point for drug delivery design, from which the formulation must be developed and examined. Based on this, three principal strategies were identified to manipulate the fate of biologics in the joint (see **Fig. 2-4**). The viscosity of a formulation can be increased by a polymer network which leads to steric obstruction of diffusion or restriction of release via protein-polymer interactions that determine the dwell time in the joint. Therein, it is important to ensure that adequate injectability is

maintained if viscosity is adjusted, which makes it is a common principle in the formulation of IA injections to create thermoresponsive or other in situ gelling systems to ensure satisfactory applicability of the dosage form even through small needles [139]. Another approach is to increase the size of the drug dosage form, through the immobilization of the drug in nano- or microspheres, liposomes, or dendrimers, so that transsynovial diffusion is restricted and in joint residence time is prolonged. These delivery systems exhibit considerable impact on biocompatibility, immune response, and the drug stability of the therapeutic *in-vivo*. Moreover, sustained release can be achieved via entrapment of the biologic in a hydrogel matrix, where the drug is physically immobilized or chemically linked to the polymer matrix and the drug is released by degradation mechanisms. Both carrier size and polymeric network systems can be combined and further optimized by bioadhesive qualities or passive and active targeting strategies to selectively reach specific cells or structures within the joint. In addition to the key requirement of extended joint residence time and enhancement of the drugs permeation properties, it is essential for drug delivery systems for biologics to provide sufficient stability of the active ingredient as well as excellent properties suitable for parenteral dosage forms [140]. Generally, IA applications must meet most of the criteria that apply to other injection formulations, including sterility and compatibility with physiological conditions at the site of application. Thereby, the manufacturing process for protein carriers must be designed to ensure that their therapeutic activity is not compromised. Unlike many small molecules, it usually requires that neither organic solvents nor elevated temperatures or high shear rates stress are involved [5]. Accordingly, more elaborate, and gentle techniques or multistep processes are to be favored and careful selection of the retarding excipients is required. A wide range of polymers have proven suitable for the formulation of drug delivery systems for biologics, including synthetic polymers, natural polymers, and their derivatives, as well as endogenous macromolecules from the ECM of joint tissues (**Tab. 2-2**) [141–144]. Thereby, an appropriate formulation should further enhance the stability of the three-dimensional protein folding and thus the preservation of its bioactivity compared to a pure protein solution due to immobilization or restriction of mobility.

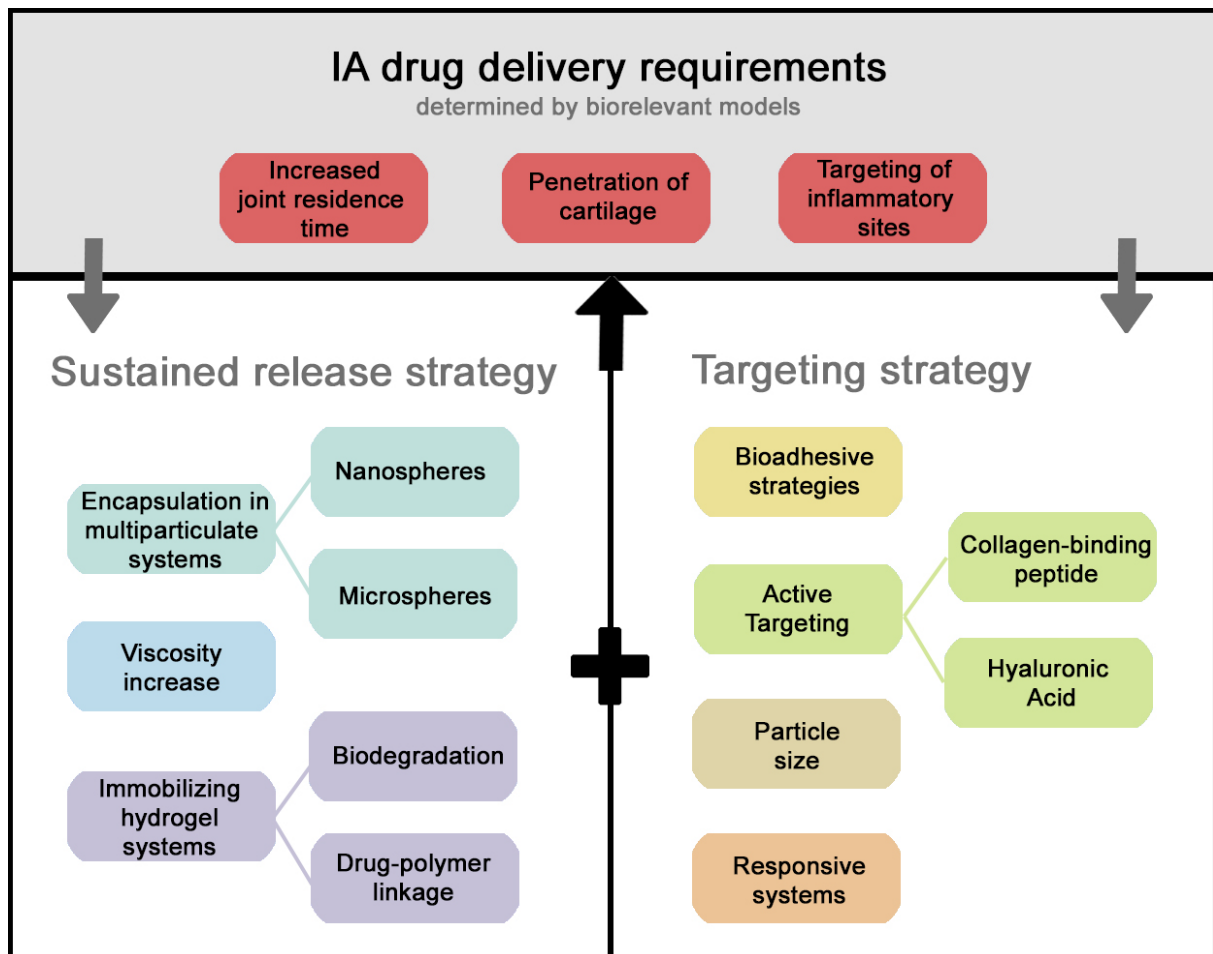


Fig. 2-4: Schematic representation the approach to rational design IA drug delivery systems in early stages of development and presentation of its formulation principles. Thereby, the three pharmacokinetic requirements: Increase of joint residence time, targeted or responsive delivery to inflammatory sites, and access to deep cartilage structures can be achieved by biopharmaceutically derived combinations of sustained release strategies and targeting strategies.

2.10.1 Viscosity increase

OA is associated with a collapse in SF viscosity. The viscosity in turn influences the fluid egress from the joint, so that a formulation with elevated viscosity can not only restore SF properties, but at the same time interfere with the diffusion and synovial outflow of macromolecules. Prolongation of the joint residence time by increasing the viscosity of the formulation, and thus steric obstruction of the free diffusion of macromolecular drugs through a fine polymer network, represents a simple yet effective approach for sustained IA drug delivery systems. This is achieved most particularly through the formation of hydrogels, which are cross-linked hydrophilic polymers that retain large amounts of water and provide a three-dimensional network structure. In general, given that the pores of the network are larger than the

hydrodynamic radius of an embedded protein, diffusion is the driving release mechanism, which is dependent on both the size of the protein and the hydrogel mesh size as well as on protein-polymer interaction [145,146]. Diffusion-driven release usually implies that the release is proportional to the square root of time, where a burst release within the first 24 hours is typically present and retention is seldom prolonged for more than 2 weeks [147,148]. In this way, a thermoresponsive hydrogel of HA and Pluronic F127 with infliximab incorporated, was shown to be an easily injectable and diffusion-controlled drug delivery system. It was seen to ameliorate clinical symptoms and decreasing cytokine levels, with approximately half of the dose released on the first day and 95% of infliximab released within the first 14 days [149]. Following the same principle, embedding IGF-1 in a viscous HA formulation showed a prolongation of the release and an improved clinical effect, in particular a decrease in the number of cartilage surface lesions and nearly normal microarchitectural properties [124], which thus proves a general validity of viscosity as a factor for the rational modulation of the joint residence time for biologics. In addition to pure viscosity, interactions between the agent and the gel scaffold can influence diffusion, so that depending on the agents' charge, tailored formulations can be designed to take advantage of these attributes [150]. Transsynovial permeation of the TNF-binding mAb adalimumab was prolonged fivefold by increasing viscosity using a co-formulation of HA and polyvinylpyrrolidone, with electrostatic protein-polymer interactions substantially controlling drug leakage [151]. Through the use of the endogenous lubricants together with a synthetic polymer, the formulation additionally offered viscosupplementative properties that could concomitantly restore the rheological properties of the synovial fluid upon injection of the formulation. Additionally, the polymer mixture did not affect the bioactivity of the mAb, but rather provides increased stability of the protein. This represents a general advantage of hydrogels. Hydrogels usually offer high biocompatibility since they exhibit a high structural similarity to the natural ECM and, since very mild conditions are used in their production, the process is well suited for the maintenance of the protein stability. In addition, the integrity of the fragile 3D structure of the protein is preserved by restriction of mobility within the network matrix of the polymer gel while a high water content still provided [145,152].

2.10.2 Immobilizing hydrogel systems

Besides diffusion-driven release from hydrogels, full immobilization of the biologic in the three-dimensional scaffold can be achieved [153]. This applies if the mesh size is below the hydrodynamic radius of the embedded cargo or if the drug is covalently linked to the polymer matrix. The active ingredient is then released either by

degradation of the polymer or cleavage of a drug-polymer linkage. One potential strategy was to attach biologics to a PEG hydrogel via degradable carbamate linkers in order to control their release [154]. This resulted in a 5-fold retardation of the release of unmodified and bioactive protein. However, it should be noted that only 60% of the initial dose was released. Incomplete release is a common challenge in immobilization strategies due to strong chemical bonds. Moreover, though long-term release of the therapeutic molecule can be achieved via chemical or physical immobilization, this method can lead to denaturalization of protein drugs, as harsh conditions are often required to achieve sufficient entrapment. [155]. Nano- or microparticulate carriers can be incorporated within hydrogels in order to increase the hydrodynamic radius of the cargo and thus immobilize the active ingredient bound therein. This is why, in the case of a HA gel loaded with PLGA nanoparticles, a significantly prolonged release of the model drug was achieved compared to the nanoparticles or hydrogel alone [81]. Bioresponsive systems represent a further development of this formulation strategy. In this way, a biologic drug may be attached to the polymer using a responsive cleavable linker or by introduction of predetermined breaking points into the hydrogel framework. These smart drug delivery systems are capable to titrate their release via an on-demand hydrogel degradation, that is depending on the inflammatory state [80]. However, responsive IA formulations are currently only described for small molecules and not for the much more sensitive protein drugs, but smart systems for the delivery of macromolecular drugs may yet present an emerging area of interest that could offer promising opportunities. In-situ-forming depots are a further development of hydrogel systems, which represent an appealing strategy since they form the hydrogel network upon injection into the joint, thus ensuring excellent injectability or extended storability of the protein. Thereby, rapid formation of the drug depot in the joint is essential to achieve the desired effects. A copolymer-based system consisting of PEG or methoxy-PEG and polylactic acid was tested to prolong the residence time of mAbs in the joint cavity [156]. The formulation resulted in an increased concentration of proteins in the synovial gap over several weeks without diminishing the activity of the mAbs. However, the formulation also induced inflammatory reactions, which was explained with the high quantity of injected foreign material. Nevertheless, if further developed in situ forming depots represent a very promising approach in the development of IA dosage forms especially as scaffolds for growth factors in the regeneration of cartilage.

2.10.3 Encapsulation in multiparticulate systems

It is of great importance to be aware of the permeation properties and the pore size of the synovial membrane in the healthy and especially in the arthritic state in order to

rationally adapt a drug delivery system to these parameters and to actively control the resulting pharmacokinetics [157]. It is therefore an effective strategy to prolong the residence time of injected therapeutic biologics by increasing the hydrodynamic radius of the delivery system and immobilize them within nanoparticulate or microparticulate drug carriers [75]. In this process, the drug is encapsulated in a polymeric matrix, whereby microparticles sustain the release of the drug from its matrix far more effectively compared to nanoparticles [158]. However, for both nanoparticles and microparticles, the effective change in the hydrodynamic radius of the drug dosage form relevantly influences the duration of the joint residence, as well as the distribution within the tissues of the different compartments of the synovial joint. Therapeutic proteins such as mAbs typically have a hydrodynamic radius of approximately 5 nm [159] and can thus permeate comparatively unimpeded across the 33-59 nm sized pores of the ECM into surrounding lymphatic vessels. Enlargement, by conjugation or encapsulation within a particulate carrier, results in sterically hindered diffusion of the particle in the SF and across the synovial membrane, so that it escapes the synovial cavity either more slowly or not at all, but only after biodegradation of the particle. For instance, for IL-1 RA self-assembled Poly(2-hydroxyethyl methacrylate)-pyridine nanoparticles, it was shown that particles with diameter of 500 nm led to a 3-fold increase in half-life in the joint compared to free RA, while particles of 900 nm size led to about 4-fold increase in half-life. However, the latter also showed an increased retention time of 14 days (30% remaining in the joint cavity), whereas free protein or 500 nm particles were eliminated from the joint cavity during this period. In the same way, it was shown for the biodistribution of polylactic acid particles that 300 nm particles slowly emerged from the joint in an *in-vivo* study in mice, while 3 or 10 μm particles of the same material were retained for several weeks [160]. However, significant differences due to the pathophysiologically altered tissue permeability in synovitis were evident and in the arthritic state, complete retention was described only for the 10 μm particles. The size of the particle has a relevant influence on the biocompatibility of the therapeutic agent, which in turn affects particle distribution and joint residence time. For example, polymeric microspheres in the size range of 35-105 μm were found biocompatible, whereas smaller microspheres (1-20 μm) were reported to elicit an inflammatory response, which was attributed to larger phagocytizable fractions [161,162], although it is also conceivable that this finding is related to the higher amount of surfactant required for precipitation. Due to antibody opsonization of smaller particles in plasma-derived fluids, phagocytosis is induced in synovial macrophages and leads to cell activation, which may cause local inflammation that might be adversarial to OA therapy [163]. In the same context, when 26 μm

microparticles and 265 nm nanoparticles of a DL-lactide/glycoside copolymer (PLGA) were compared, the microparticles were likewise found to be non-phagocytosed but to granulate on the synovial intima [164]. This suggests that larger microparticles may be appropriate for local drug delivery to the synovial surface, whereas the nanospheres were phagocytosed, and therefore represent a strategy to target macrophages and reach deeper structures of the synovial tissue. In that way, the mere change of size, especially the creation of nanoparticles, can therefore be interpreted as a form of targeting, since the release is not essentially affected, but the distribution of the drug is specifically controlled. However, contrary to the above, a study investigating on the inflammatory response to beta-tricalcium phosphate particles of different sizes in vitro, reported larger particles of 20-40 μm size to show a stronger induction of proinflammatory mediators than smaller particles [165]. This suggests that in addition to size, shape must also be considered, and rough, irregular particles appear to provoke greater inflammation with a concomitant increase in size. It must therefore be concluded that particles of any size, albeit with different mechanisms and at varying intensities, are generally capable of inducing inflammatory processes upon injection into the synovial joint [166,167]. Besides endogenous biodegradation mechanisms, particles can further be reduced by means of bioresponsive formulations in which a modified polymers react to certain stimuli in the joint and thus tailors the release of the active ingredient or affects the size of a particle. Among simple physiological or pathophysiological joint conditions such as body heat or pH-value, inflammation associated enzymes or similar are of particular importance as triggering stimuli. In this way, passive targeting of inflamed cartilage by polyethylene glycol (PEG) coated poly(N-isopropylacrylamide) nanoparticles was described that protect the drug from premature extracellular digestion, but after cellular uptake by immune cells are degraded via sensitive disulfide cross-links and subsequently release an anti-inflammatory peptide intracellularly [168]. Similar studies such as disulfide-crosslinked chitosan/HA layer-by-layer self-assembled microcapsules, that enable redox-responsive controlled intracellular release of proteins, thereby providing superior activity maintenance, confirm the feasibility of this concept [169]. The unique physiological conditions of cartilage require that prolonged drug delivery to the chondrocytes or the articular ECM can only be achieved if the drug is released from an immobilized depot, ideally from the interface between the SF and the cartilage, or if sustained release systems form a depot in the cartilage itself. To penetrate the cartilage in full depth, the size of the particles should not exceed a diameter of about 50 nm, which implies that size alone is not a suitable factor to promote accumulation, since it rather causes exclusion from the tissue. It is therefore advisable to design

targeted or bioadhesive formulations to achieve the desired penetration of the deep cartilage tissue. Following this concept, however, larger particles may be equally effective if they bind to the cartilage interface and from there, gradually release the active ingredient which then diffuses into the tissue [170]. Encapsulation or immobilization of proteins on particles can result in a significant amelioration of protein stability *in-vivo* and maintain its activity over a prolonged period of time. Microspheres of polycaprolactone and a copolymer of PEG and methoxy-PEG were shown to retain near total activity of etanercept, a TNF- α RA, in SF after 90 days [171]. In the same way, nanocomplexes composed of cationic charged proteins and HA formed by complex coadsorption have been confirmed to significantly increase bioactivity and physical stability over time as compared to pure protein and to maintain full activity of the drug for several days or even weeks. [172,173]. However, rather hydrophobic drug delivery systems such as PLGA, which is the most frequently used polymer for particle manufacturing, show inferior preservation of protein structure than more hydrophilic polymers which are for example used for hydrogel formation [174].

2.10.4 Bioadhesive strategies

Modification of the charge of a carrier or hydrogel matrix can change the articular kinetics of the drug form and passively target the agent to accumulate in specific tissues or on structures via bioadhesion [175]. It is however important to note that charge-mediated bioadhesion is a rather nonspecific way of targeting and should therefore be distinguished from other passive and active targeting strategies that are aimed towards more specifically defined target sites. The charge of the particulate carrier used can be utilized to increase the residence time in the joint through interaction with the microenvironment in the joint space. Uncharged nanoparticles, such as PEG-coated nanoparticles, are able to diffuse rapidly within the SF [176], while cationic particles can form aggregates with the anionic HA of the SF, increasing their size and thus decelerating their mobility in the synovial cavity and their diffusivity across the synovial tissue [41,177]. Chitosan, which itself already exhibits bioadhesive and anti-inflammatory activity, is a commonly used excipient for nanoparticle formation, often through electrostatic interaction together with hyaluronic acid [132,178]. Chitosan-HA microspheres showed that incorporation of an IL-1 RA, after a burst release, resulted in linear release kinetics over eight days and effectively suppressed IL-1 β -induced inflammation and apoptosis [179]. Following the same concept, self-assembled networks of intraarticular injected cationic dextran and Eudragit RL100 nanoparticles interacting with endogenous HA were found to significantly prolong the retention time in the joint, with 70% of the incorporated

fluorescently labeled protein remaining in the joint cavity after 7 days. [57]. Moreover, it has been shown for differently charged polyvinyl acetate nanoparticles that particularly cationic particles associate with macrophages and other immune cells, suggesting passive targeting of inflamed tissue by utilizing cationic polymers [180]. Liposomal preparations require the use of organic solvents, which can cause degradation of proteinaceous drugs. In addition, liposomes generally exhibit relatively rapid release and shorter joint retention with more polar drugs, such as proteins [3]. Nonetheless, it was shown that liposomal administration of lactoferrin alleviated arthritic symptoms after intraarticular injection for 2 weeks instead of 3-4 days with free protein. Here, positively charged liposomes were formulated and the increased therapeutic effect was attributed to enhanced tissue retention and selective adhesion onto dendritic cells [181]. Moreover, cargo free multilamellar vesicles were shown to exhibit biolubricant properties and have the potential to effectively reduce articular friction, which may offer multimodal therapy concepts by combining drug carrier and viscosupplementation [182]. Particulate carriers can be used to promote biologics uptake into cartilage by passive targeting or bioadhesion via nonspecific electrostatic interactions. Cationic multi-armed avidin nano constructs with a size <10 nm and a positive charge were shown to effectively penetrate cartilage [183]. The protein avidin was used to deliver drugs across the full thickness of the cartilage via conjugation using hydrolysable ester linkers. Avidin was found to have a half-life of 29 h in cartilage, which represents a significant increase over neutravidin, being the same size but uncharged, which was scarcely present in the cartilage after only 24 h [184]. In the same way, insulin-like growth factor-1 was successfully retained in cartilage for 4 weeks via formulation using cationic polyglutamic acid and polyarginine nanoplexes, whereby cartilage degradation and interleukin-1 mediated inflammation were mitigated over several weeks [185]. In addition to more conventional particulate carriers, scalable cationic dendrimers were found to be a versatile carrier for conjugation to a variety of drugs, that can control the residence time and penetration depth in cartilage. Conjugation of IGF-1 to PAMAM dendrimers showed improved pharmacokinetics and efficacy in the clinic with a more than 10 fold increased joint residence time and an 70% uptake into the targeted tissue [186]. Biocompatibility of the pharmacokinetically versatile cationic polymers must however be considered, as they may impact the homeostasis of the ECM as well as lead to destabilization of cell membranes. Furthermore, interaction may occur with the applied therapeutic biologics and negatively influence their activity as well as with serum proteins, causing toxicity especially if the agents enter the systemic circulation [187]. Taken together, cationic charge presents one of the most promising concepts for IA injections due to its

simplicity and efficiency for both its residence time increasing properties and affinity for articular cartilage.

2.10.5 Drug targeting

Directed therapy can be achieved via targeting of moieties that possess high affinity for specific molecules (receptors, structural proteins, markers, antigens, etc.) abundantly expressed in the target [188]. At its simplest, a biologic drug can be directly linked to a targeting agent. One such example is the fusion of IGF-1 with a heparin-binding domain, which was able to prolong the retention in cartilage from less than one day to 8 days, thereby providing a significant therapeutic advantage over sole IGF-1 [123]. More commonly the targeting agents are tethered on the surface of particulate systems. It was shown that PLGA nanoparticles carrying a collagen type II binding peptide and thus selectively binding to cartilage tissue resulted in increased association into the tissue compared to passive targeting via charged and uncharged nanoparticles [189]. Moreover, an enhanced binding of the collagen-binding particles in the arthritic state was shown. Based on a similar concept, a significantly increased uptake of FGF-18 nanoparticles was shown [190], where a fusion protein of FGF-18 and a peptide known to bind selectively to collagen II of the cartilage, but not of the synovium, was expressed and conjugated to poly (propylene sulfide) nanoparticles. The targeted peptide extended the injection interval from bi-weekly to bi-monthly. Besides targeting of collagen entities, it was demonstrated that targeting chondrocytes directly via the CD-44 receptor by means of HA coated nanoparticles leads to increased articular residence and chondrocytic accumulation and may represent another promising and simple delivery strategy for macromolecules [191,192]. However, despite the higher effectiveness of drug targeting strategies, it should be considered that passive targeting strategies involve less customization, which not only simplifies production and thus reduces costs but also creates more readily transferable systems.

2 Assessment of joint pharmacokinetics and consequences for the intraarticular delivery of biologics

Tab. 2-2: Overview of polymer compounds, which were used in research studies to influence the joint residence time of protein drugs after IA injection and their respective features.

Material	Biodegradable	Attributes	Potential mechanisms of leakage prolongation	Targeting features	References
Natural Polymers (and derivates)					
Hyaluronic Acid (HA) / Crosslinked HA	Yes (Hyaluronidases)	Endogenous lubricant of SF, Viscosupplementative, Rapid elimination (linear derivates) Retains bioactivity, Anti-inflammatory effect	Viscosity Increase, Encapsulation	CD-44	[81,124,149,173,191]
Chitosan	Yes (pH, enzymes)	Self-assembling, Anti-inflammatory effect	Encapsulation, Viscosity increase	Bioadhesion	[169,179]
Cationic dextran	Yes (Enzymes, hydrolysis)	Cartilage targeting, In-situ network with SF	Encapsulation	Bioadhesion, Immobilization	[57]
Synthetic Polymers					
Poly-hydroxyethylmethacrylate-pyridine	Yes (Hydrolysis)	Self-assembling, Retain bioactivity	Encapsulation	None	[193]
Poloxamer	Partially (Enzymes)	Thermoresponsive, Retain Bioactivity	Viscosity increase, Immobilization	None	[149]
Polyethylenglykol (PEG) / Methoxy-PEG	Partially (Enzymes)	Retain bioactivity, in-situ formation, potential proinflammatory	Viscosity increase, Immobilization	None	[154,156,171]
Poly lactic acid / glycolic acid (PLGA)	Yes (Hydrolysis)	Long experience, low toxicity	Encapsulation	None	[81,160,164]
Poly(N-isopropylacrylamide) (PNIPA)	Yes (pH)	Thermoresponsive Cartilage targeting, Intracellular delivery	Encapsulation	Bioadhesion	[168]
Polyvinylpyrrolidone (PVP)	Partially (Enzymes)	Viscosupplementative, FDA approved for parenteral application, Retain bioactivity, Size dependent accumulation	Viscosity increase	None	[151]
Poly(amidoamine) (PAMAM)	Yes (pH)	Scalable dendrimers, Cartilage targeting, Retain bioactivity	Encapsulation	Bioadhesion	[186]
Polyglutamine/Polyarginine	Yes (Proteases)	Cartilage targeting, Intracellular delivery, Retain bioactivity, FDA inactive excipient list	Encapsulation	Bioadhesion	[185]

2.11 General discussion

2.11.1 Models

Currently, most formulations are tested in simple dissolution apparatus and then administered directly to an animal model. However, a further intermediate step would be useful in most cases, at which the formulation can be optimized with regard to its pharmacokinetic target parameters. While current *in-vitro* methods only provide information on the release from the drug delivery system itself, animal models are often complex in their interpretation, so that individual parameters such as transsynovial permeation, cartilage penetration or tissue adhesion cannot be precisely estimated in isolation due to many influencing variables [194]. Furthermore, animal models are time and cost intensive and not well suited for screening experiments. Biorelevant *ex-vivo* models allow for this intermediate step. A major advantage of using functionally isolated tissues from the joint compartments is the retainment of the three-dimensional multi-layered assembly and the expression of transport and drug metabolism proteins. Therefore, this model allows for intercellular interplay and communication while maintaining anatomical and structural diversity of a tissue and mimics *in-vivo* conditions better than *in vitro* models. This preservation of tissue architecture enables biorelevant diffusion models, which also provides a system for studying therapeutic efficacy and cytotoxicity as well as give admissible insights into pharmacokinetic differences between healthy and OA tissue. Known advantages of this system over *in-vivo* experiments include: no influence of movement or extra-articular processes, no limitation of drug concentration administered, and full control of the physiological environment while reducing animal consumption. However, it remains a major difficulty to fully replicate the complex *in-vivo* conditions and important details, such as the presence of the injection site, are not represented. In addition, *ex-vivo* models show more difficult inter-laboratory transferability compared to less diverse *in-vitro* systems and a restricted run time of the assay due to the limited viability of the tissue. While the use of *ex-vivo* synovium or *ex-vivo* cartilage to simultaneously assess release and permeability is not yet well established, for a rational formulation development, all steps: *in vitro* release, *ex-vivo* biodistribution and *in-vivo* performance are of great relevance, and their consideration leads to a faster and deeper understanding of the developed drug delivery system, so that a wide establishment of the proposed sequence of pharmacokinetic tests should be pursued in the pharmaceutical development of IA injectables. This is because only the accurate detection of drug

delivery system-tissue interplay at in the early phases of research enables the rational design and profiling of the desired pharmacokinetics.

2.11.2 Drug delivery strategies

Numerous IA formulation systems have been tested to prolong the joint residence time of biologics, based essentially on the principles of either diffusion-controlled retardation via viscosity increase or degradation-controlled release of the drug from an enclosing polymer, wherein the latter can be in the form of a monolithic hydrogel matrix or multiparticulate systems. In detail, however, the choice of strategy and the additives used have many decisive consequences not only for the joint residence time, but also for the articular biodistribution, drug stability, applicability of the injection and the biocompatibility of the dosage form. Since there is no single best approach and the formulation strategy will always depend on the biologic used and the origin of its target structure, the drug delivery system must be developed in frequent exchange with biorelevant testing of pharmacokinetic and pharmacodynamic objectives. The work process should follow a cycle in which first the biopharmaceutical parameters of the drug alone are assessed in comparison to known model compounds, then rational intervention approaches for formulation and targeting strategies are identified, and after their deployment, the drug delivery system is reassessed by biorelevant methods. The cycle should involve multiple rounds to refine and optimize the profile of the formulation before conducting in vivo trials, thus saving time as well as resources by pursuing only proven high-potential candidates. However, a number of general assumptions can be derived from the research conducted to date, which will facilitate finding an orientation for the formulation design of biologics. First of all, it must be acknowledged that, despite some existing clinical trials with biologics as simple aqueous solutions, a prolongation of the duration of action in the joint is essential for all drugs in order to develop promising therapeutic treatment regimens. For acute therapy regimens, a duration of action of a few days to weeks may be sufficient, whereas for chronic treatment strategies, a joint residence of weeks to months should be aimed for in order to avoid frequent injections. Therefore, in order to make biological agents for IA injections actually clinically applicable in the future, it is of absolute necessity to no longer isolate the agents from their drug delivery system, but to consider them together as one therapeutic agent. Prolonged joint residence time can be achieved most reasonable with immobilized agents, either bound in hydrogel systems or encapsulated in multiparticulate systems of several micrometers in

size. On the other hand, due to the simple formulation and better translation from existing approaches as well as the generally better tolerability and protein stability, diffusion-controlled retardation is the simplest and thus most effective way for more acute indications such as inflammatory events, especially since viscosupplementative properties can be utilized simultaneously to alleviate clinical symptoms. Generally speaking, combination therapy targeting more than one site/symptom may be a more efficient IA drug delivery strategy for OA therapy. Stimuli-responsive hydrogels that respond to temperature, pH, and inflammation represent a promising option for future developments. They often consist of novel polymers or combinations of polymers. Further studies are needed in this area to develop controllable hydrogel systems by synthesis or combination that are sensitive to external biochemical, physical, and chemical stimuli without the risk of dose dumping in the event of overstimulation. Thereby, it is of utmost importance to carefully examine biocompatibility, pharmacokinetics of the polymers, and potential cytotoxicity in order to ensure a safe applicability of these novel polymers in practice. The assessments of biocompatibility should include evaluation of swelling, inflammation, and histopathological analysis in the joint. Apart from prolongation of joint residence time some therapies require targeting strategies to achieve sufficient effect. In this way, for anti-inflammatory biologics nanoencapsulation may be more suitable for delivery to inflamed synovial tissue, since nanospheres are extensively phagocytosed by macrophages existing in the epithelium synovial lining cells, so that uptake and accumulation of nanospheres at inflamed sites within these immune cells compared to other cellular or extracellular compartments occurs. The macrophages then generate through the synovial tissues and deep tissue layers may be reached. Special requirements apply to dosage forms that need to reach the chondrocytes in deep cartilage layers. Here, the hydrodynamic radius of the dosage form must not exceed the pore size of the cartilage to facilitate full permeation of the tissue. However, in most cases there is still insufficient penetration, so accumulation should be promoted by bioadhesion through cationic charge or passive targeting strategies aiming at specific collagen fragments. Thereby, bioadhesion appears to be the tool of choice for targeting chondrocytes based on current knowledge. While way to proceed before protein agents would be widely introduced. A general problem of IA formulation development is the small selection of approved excipients for parenteral use, which considerably complicates the introduction of a new drug delivery systems into actual therapy regimens, so that an expansion of the possibilities would be

desirable in the near future in order to draw from a more versatile toolbox of substances. However, the fundamental principles are available to researchers today, as outlined in this manuscript, enabling them to further explore and implement therapy relevant concepts in a simple and accessible approach. much more straightforward to execute compared to active targeting, it is nonetheless highly efficient owing to the Donnan effect. However, the cationic polymers employed for this purpose will require in-depth investigation of their toxicity and distribution, as well as elimination, in order to ensure the safety of the therapy. Generally, it can be argued that commercialization of applications based on hydrogels and multiparticulate carriers could be required for their efficient use in the clinical setting. IA injections are still in their early days in terms of formulation and in spite of some very promising research and concept studies, there is certainly still a fair.

2.12 Conclusion

Biologics bring great expectations as a therapeutic option for many chronic diseases. The fact that they have not yet found their way into the treatment of OA can be explained by the challenging biopharmaceutical conditions that limit the success of the therapy. However, these limitations can be overcome to achieve the intended treatment outcome through intelligent design of drug delivery systems, as current research is increasingly demonstrating with a variety of approaches. In this regard, it is essential to precisely understand and simulate the physiological and anatomical conditions in this route of administration and the resulting drug elimination or distribution kinetics by relevant models. Deriving from this, several factors have emerged to as effective and tunable formulation principles in the rational development of IA injections of biologics with prolonged residence time and targeting properties. In particular, the size of potential carriers, the viscosity of the formulation, the level and mechanism of immobilization, the charge and further passive or active targeting strategies can be thoroughly adjusted in order to access the full potential of the drug. Hence, future efforts should conceptualize and understand the drug delivery system not in isolation, but always in the context of the unique characteristics of its application site, which will help to achieve effective targeted biologic-based therapies with comparatively simple but well-designed strategies.

2.13 Author contributions

Conceptualization, T.S and A.L.; writing—original draft preparation, T.S.; writing—review and editing, T.S., A.L., S.B.; visualization, T.S.; supervision, A.L.; project administration A.L., S.B., C.B.

All authors have read and agreed to the published version of the manuscript.

2.14 References

- [1] S.H.R. Edwards, Intra-articular drug delivery: The challenge to extend drug residence time within the joint, *Vet. J.* 190 (2011) 15–21. <https://doi.org/10.1016/j.tvjl.2010.09.019>.
- [2] M.B. Goldring, S.R. Goldring, Osteoarthritis, *J. Cell. Physiol.* 213 (2007) 626–634. <https://doi.org/10.1002/jcp.21258>.
- [3] C.H. Evans, V.B. Kraus, L.A. Setton, Progress in intra-articular therapy, *Nat. Rev. Rheumatol.* 10 (2014) 11–22. <https://doi.org/10.1038/nrrheum.2013.159>.
- [4] W. Zhang, R.W. Moskowitz, G. Nuki, S. Abramson, R.D. Altman, N. Arden, S. Bierma-Zeinstra, K.D. Brandt, P. Croft, M. Doherty, M. Dougados, M. Hochberg, D.J. Hunter, K. Kwok, L.S. Lohmander, P. Tugwell, OARSI recommendations for the management of hip and knee osteoarthritis, Part II: OARSI evidence-based, expert consensus guidelines, *Osteoarthritis Cartilage.* 16 (2008) 137–162. <https://doi.org/10.1016/j.joca.2007.12.013>.
- [5] N. Gerwin, C. Hops, A. Lucke, Intraarticular drug delivery in osteoarthritis, *Adv. Drug Deliv. Rev.* 58 (2006) 226–242. <https://doi.org/10.1016/j.addr.2006.01.018>.
- [6] A. Dhawan, R.C. Mather, V. Karas, M.B. Ellman, B.B. Young, B.R. Bach, B.J. Cole, An Epidemiologic Analysis of Clinical Practice Guidelines for Non-Arthroplasty Treatment of Osteoarthritis of the Knee, *Arthrosc. J. Arthrosc. Relat. Surg.* 30 (2014) 65–71. <https://doi.org/10.1016/j.arthro.2013.09.002>.
- [7] J. Uson, S.C. Rodríguez-García, R. Castellanos-Moreira, T.W. O’Neill, M. Doherty, M. Boesen, H. Pandit, I. Möller Parera, V. Vardanyan, L. Terslev, W.U. Kampen, M.-A. D’Agostino, F. Berenbaum, E. Nikiphorou, I.A. Pitsillidou, J. de la Torre-Aboki, L. Carmona, E. Naredo, EULAR recommendations for intra-articular therapies, *Ann. Rheum. Dis.* 80 (2021) 1299–1305. <https://doi.org/10.1136/annrheumdis-2021-220266>.
- [8] C. Place, R. Tischler, Are intra-articular NSAID injections as effective as intra-articular corticosteroid injections for the treatment of knee osteoarthritis?, *Evid.-Based Pract.* 22 (2019) 14–15. <https://doi.org/10.1097/EBP.0000000000000296>.

- [9] J. Paik, S.T. Duggan, S.J. Keam, Triamcinolone Acetonide Extended-Release: A Review in Osteoarthritis Pain of the Knee, *Drugs*. 79 (2019) 455–462. <https://doi.org/10.1007/s40265-019-01083-3>.
- [10] M.B. Goldring, M. Otero, Inflammation in osteoarthritis, *Curr. Opin. Rheumatol.* 23 (2011) 471–478. <https://doi.org/10.1097/BOR.0b013e328349c2b1>.
- [11] B. Xia, Di Chen, J. Zhang, S. Hu, H. Jin, P. Tong, Osteoarthritis Pathogenesis: A Review of Molecular Mechanisms, *Calcif. Tissue Int.* 95 (2014) 495–505. <https://doi.org/10.1007/s00223-014-9917-9>.
- [12] R.F. Loeser, Molecular mechanisms of cartilage destruction: Mechanics, inflammatory mediators, and aging collide, *Arthritis Rheum.* 54 (2006) 1357–1360. <https://doi.org/10.1002/art.21813>.
- [13] M.D. Smith, The Normal Synovium, *Open Rheumatol. J.* 5 (2011) 100–106. <https://doi.org/10.2174/1874312901105010100>.
- [14] L.C. Dijkgraaf, L.G.M. de Boni, G. Boering, R.S.B. Liem, Structure of the normal synovial membrane of the temporomandibular joint: A review of the literature, *J. Oral Maxillofac. Surg.* 54 (1996) 332–338. [https://doi.org/10.1016/S0278-2391\(96\)90755-7](https://doi.org/10.1016/S0278-2391(96)90755-7).
- [15] T. Iwanga, M. Shikichi, H. Kitamura, H. Yanase, K. Nozawa-loue, Morphology and Functional Roles of Synoviocytes in the Joint, *Arch. Histol. Cytol.* 63 (2000) 17–31. <https://doi.org/10.1679/aohc.63.17>.
- [16] F.M. Price, J.R. Levick, R.M. Mason, Glycosaminoglycan concentration in synovium and other tissues of rabbit knee in relation to synovial hydraulic resistance., *J. Physiol.* 495 (1996) 803–820. <https://doi.org/10.1113/jphysiol.1996.sp021634>.
- [17] S. Sabaratnam, R.M. Mason, J.R. Levick, Molecular sieving of hyaluronan by synovial interstitial matrix and lymphatic capillary endothelium evaluated by lymph analysis in rabbits, *Microvasc. Res.* 66 (2003) 227–236. <https://doi.org/10.1016/j.mvr.2003.08.003>.
- [18] A.J. Fox, A. Bedi, S.A. Rodeo, The Basic Science of Articular Cartilage: Structure, Composition, and Function, *Sports Health Multidiscip. Approach.* 1 (2009) 461–468. <https://doi.org/10.1177/1941738109350438>.

- [19] A.G. Bajpayee, A.J. Grodzinsky, Cartilage-targeting drug delivery: can electrostatic interactions help?, *Nat. Rev. Rheumatol.* 13 (2017) 183–193. <https://doi.org/10.1038/nrrheum.2016.210>.
- [20] M.B. Goldring, Update on the biology of the chondrocyte and new approaches to treating cartilage diseases, *Best Pract. Res. Clin. Rheumatol.* 20 (2006) 1003–1025. <https://doi.org/10.1016/j.berh.2006.06.003>.
- [21] D.T. Felson, Osteoarthritis: New Insights. Part 1: The Disease and Its Risk Factors, *Ann. Intern. Med.* 133 (2000) 635. <https://doi.org/10.7326/0003-4819-133-8-200010170-00016>.
- [22] T. Yasuda, Cartilage destruction by matrix degradation products, *Mod. Rheumatol.* 16 (2006) 197–205. <https://doi.org/10.3109/s10165-006-0490-6>.
- [23] A.B. Blom, P.L. van Lent, S. Libregts, A.E. Holthuysen, P.M. van der Kraan, N. van Rooijen, W.B. van den Berg, Crucial role of macrophages in matrix metalloproteinase-mediated cartilage destruction during experimental osteoarthritis: Involvement of matrix metalloproteinase 3, *Arthritis Rheum.* 56 (2007) 147–157. <https://doi.org/10.1002/art.22337>.
- [24] V.B. Kraus, G. McDaniel, J.L. Huebner, T.V. Stabler, C.F. Pieper, S.W. Shipes, N.A. Petry, P.S. Low, J. Shen, T.A. McNearney, P. Mitchell, Direct in vivo evidence of activated macrophages in human osteoarthritis, *Osteoarthritis Cartilage.* 24 (2016) 1613–1621. <https://doi.org/10.1016/j.joca.2016.04.010>.
- [25] P.M. van der Kraan, W.B. van den Berg, Osteophytes: relevance and biology, *Osteoarthritis Cartilage.* 15 (2007) 237–244. <https://doi.org/10.1016/j.joca.2006.11.006>.
- [26] S.R. Goldring, M.B. Goldring, The Role of Cytokines in Cartilage Matrix Degeneration in Osteoarthritis, *Clin. Orthop.* 427 (2004) S27–S36. <https://doi.org/10.1097/01.blo.0000144854.66565.8f>.
- [27] P. Bhattaram, U. Chandrasekharan, The joint synovium: A critical determinant of articular cartilage fate in inflammatory joint diseases, *Semin. Cell Dev. Biol.* 62 (2017) 86–93. <https://doi.org/10.1016/j.semcdb.2016.05.009>.
- [28] T.A. Holland, A.G. Mikos, Advances in drug delivery for articular cartilage, *J. Controlled Release.* 86 (2003) 1–14. [https://doi.org/10.1016/S0168-3659\(02\)00373-5](https://doi.org/10.1016/S0168-3659(02)00373-5).
- [29] D. Goldenberg, M. Egan, A. Cohen, Inflammatory synovitis in degenerative joint disease, *J. Rheumatol.* 9 (1982) 204–209.

- [30] J. Sellam, F. Berenbaum, The role of synovitis in pathophysiology and clinical symptoms of osteoarthritis, *Nat. Rev. Rheumatol.* 6 (2010) 625–635. <https://doi.org/10.1038/nrrheum.2010.159>.
- [31] G.-H. Yuan, M. Tanaka, K. Masuko-Hongo, A. Shibakawa, T. Kato, K. Nishioka, H. Nakamura, Characterization of cells from pannus-like tissue over articular cartilage of advanced osteoarthritis, *Osteoarthritis Cartilage.* 12 (2004) 38–45. <https://doi.org/10.1016/j.joca.2003.08.004>.
- [32] C. Kjelgaard-Petersen, A.S. Siebuhr, T. Christiansen, C. Ladel, M. Karsdal, A.-C. Bay-Jensen, Synovitis biomarkers: *ex vivo* characterization of three biomarkers for identification of inflammatory osteoarthritis, *Biomarkers.* 20 (2015) 547–556. <https://doi.org/10.3109/1354750X.2015.1105497>.
- [33] N. Volpi, J. Schiller, R. Stern, L. Soltes, Role, Metabolism, Chemical Modifications and Applications of Hyaluronan, *Curr. Med. Chem.* 16 (2009) 1718–1745. <https://doi.org/10.2174/092986709788186138>.
- [34] W.J. McCarty, J.C. Cheng, B.C. Hansen, T. Yamaguchi, G.S. Firestein, K. Masuda, R.L. Sah, The biophysical mechanisms of altered hyaluronan concentration in synovial fluid after anterior cruciate ligament transection, *Arthritis Rheum.* 64 (2012) 3993–4003. <https://doi.org/10.1002/art.37682>.
- [35] D. Mazzucco, G. McKinley, R.D. Scott, M. Spector, Rheology of joint fluid in total knee arthroplasty patients, *J. Orthop. Res.* 20 (2002) 1157–1163. [https://doi.org/10.1016/S0736-0266\(02\)00050-5](https://doi.org/10.1016/S0736-0266(02)00050-5).
- [36] H. Fam, J.T. Bryant, M. Kontopoulou, Rheological properties of synovial fluids, *Biorheology.* 44 (2007) 59–74.
- [37] D. Jiang, J. Liang, P.W. Noble, Hyaluronan in Tissue Injury and Repair, *Annu. Rev. Cell Dev. Biol.* 23 (2007) 435–461. <https://doi.org/10.1146/annurev.cellbio.23.090506.123337>.
- [38] C. Larsen, J. Østergaard, S.W. Larsen, H. Jensen, S. Jacobsen, C. Lindegaard, P.H. Andersen, Intra-articular depot formulation principles: Role in the management of postoperative pain and arthritic disorders, *J. Pharm. Sci.* 97 (2008) 4622–4654. <https://doi.org/10.1002/jps.21346>.
- [39] P.A. Simkin, J.E. Bassett, Pathways of Microvascular Permeability in the Synovium of Normal and Diseased Human Knees, *J. Rheumatol.* 38 (2011) 2635–2642. <https://doi.org/10.3899/jrheum.110785>.

- [40] T. Siefen, J. Lokhnauth, A. Liang, C.C. Larsen, A. Lamprecht, An ex-vivo model for transsynovial drug permeation of intraarticular injectables in naive and arthritic synovium, *J. Controlled Release*. (2021). <https://doi.org/10.1016/j.jconrel.2021.03.008>.
- [41] B. Sterner, M. Harms, S. Wöll, M. Weigandt, M. Windbergs, C.M. Lehr, The effect of polymer size and charge of molecules on permeation through synovial membrane and accumulation in hyaline articular cartilage, *Eur. J. Pharm. Biopharm.* 101 (2016) 126–136. <https://doi.org/10.1016/j.ejpb.2016.02.004>.
- [42] D. Scott, P.J. Coleman, R.M. Mason, J.R. Levick, Action of polysaccharides of similar average mass but differing molecular volume and charge on fluid drainage through synovial interstitium in rabbit knees, *J. Physiol.* 528 (2000) 609–618. <https://doi.org/10.1111/j.1469-7793.2000.00609.x>.
- [43] P. Lent, L.A. Bersselaar, G. J. F. Grutters, W. Berg, Fate of antigen after intravenous and intraarticular injection into mice. Role of molecular weight and charge, *J. Rheumatol.* 16 (1989) 1295–303.
- [44] J.R. Levick, Permeability of Rheumatoid and Normal Human Synovium to Specific Plasma Proteins, *Arthritis Rheum.* 24 (1981) 1550–1560. <https://doi.org/10.1002/art.1780241215>.
- [45] S. Sabaratnam, V. Arunan, P.J. Coleman, R.M. Mason, J.R. Levick, Size selectivity of hyaluronan molecular sieving by extracellular matrix in rabbit synovial joints: Hyaluronan chain length and interstitial matrix sieving, *J. Physiol.* 567 (2005) 569–581. <https://doi.org/10.1113/jphysiol.2005.088906>.
- [46] J.R. Levick, J.N. McDonald, Fluid movement across synovium in healthy joints: role of synovial fluid macromolecules., *Ann. Rheum. Dis.* 54 (1995) 417–423. <https://doi.org/10.1136/ard.54.5.417>.
- [47] H. Xu, J. Edwards, S. Banerji, R. Prevo, D.G. Jackson, N.A. Athanasou, Distribution of lymphatic vessels in normal and arthritic human synovial tissues, *Ann. Rheum. Dis.* 62 (2003) 1227–1229. <https://doi.org/10.1136/ard.2003.005876>.
- [48] S.L. Myers, K.D. Brandt, O. Eilam, Even low-grade synovitis significantly accelerates the clearance of protein from the canine knee: implications for measurement of synovial fluid “markers” of osteoarthritis, *Arthritis Rheum.* 38 (1995) 1085–1091. <https://doi.org/10.1002/art.1780380810>.

- [49] A. Mathiessen, P.G. Conaghan, Synovitis in osteoarthritis: current understanding with therapeutic implications, *Arthritis Res. Ther.* 19 (2017) 18. <https://doi.org/10.1186/s13075-017-1229-9>.
- [50] T.K. Mwangi, I.M. Berke, E.H. Nieves, R.D. Bell, S.B. Adams, L.A. Setton, Intra-articular clearance of labeled dextrans from naive and arthritic rat knee joints, *J. Controlled Release.* 283 (2018) 76–83. <https://doi.org/10.1016/j.jconrel.2018.05.029>.
- [51] I. Reimann, D. Vittas, S.L. Nielsen, E. Svalastoga, Lymphatic transport from normal and synovitic knees in rabbits, *Acta Orthop. Scand.* 60 (1989) 185–187. <https://doi.org/10.3109/17453678909149250>.
- [52] J. Shi, Q. Liang, M. Zuscik, J. Shen, D. Chen, H. Xu, Y.-J. Wang, Y. Chen, R.W. Wood, J. Li, B.F. Boyce, L. Xing, Distribution and Alteration of Lymphatic Vessels in Knee Joints of Normal and Osteoarthritic Mice, *Arthritis Rheumatol.* 66 (2014) 657–666. <https://doi.org/10.1002/art.38278>.
- [53] F. Ikomi, Y. Kawai, T. Ohhashi, Recent Advance in Lymph Dynamic Analysis in Lymphatics and Lymph Nodes, *Ann. Vasc. Dis.* 5 (2012) 258–268. <https://doi.org/10.3400/avd.ra.12.00046>.
- [54] P.J. Coleman, D. Scott, R.M. Mason, J.R. Levick, Characterization of the effect of high molecular weight hyaluronan on trans-synovial flow in rabbit knees, *J. Physiol.* 514 (Pt 1) (1999) 265–282. <https://doi.org/10.1111/j.1469-7793.1999.265af.x>.
- [55] D. Scott, P.J. Coleman, A. Abiona, D.E. Ashhurst, R.M. Mason, J.R. Levick, Effect of depletion of glycosaminoglycans and non-collagenous proteins on interstitial hydraulic permeability in rabbit synovium, *J. Physiol.* 511 (1998) 629–643. <https://doi.org/10.1111/j.1469-7793.1998.629bh.x>.
- [56] P. Gribbon, B.C. Heng, T.E. Hardingham, The Molecular Basis of the Solution Properties of Hyaluronan Investigated by Confocal Fluorescence Recovery After Photobleaching, *Biophys. J.* 77 (1999) 2210–2216. [https://doi.org/10.1016/S0006-3495\(99\)77061-X](https://doi.org/10.1016/S0006-3495(99)77061-X).
- [57] M. Morgen, D. Tung, B. Boras, W. Miller, A.-M. Malfait, M. Tortorella, Nanoparticles for Improved Local Retention after Intra-Articular Injection into the Knee Joint, *Pharm. Res.* 30 (2013) 257–268. <https://doi.org/10.1007/s11095-012-0870-x>.

- [58] S. Brown, J. Pistiner, I.M. Adjei, B. Sharma, Nanoparticle Properties for Delivery to Cartilage: The Implications of Disease State, Synovial Fluid, and Off-Target Uptake, *Mol. Pharm.* 16 (2019) 469–479. <https://doi.org/10.1021/acs.molpharmaceut.7b00484>.
- [59] C.W. McCutchen, The frictional properties of animal joints, *Wear.* 5 (1962) 1–17. [https://doi.org/10.1016/0043-1648\(62\)90176-X](https://doi.org/10.1016/0043-1648(62)90176-X).
- [60] A. Vedadghavami, C. Zhang, A.G. Bajpayee, Overcoming negatively charged tissue barriers: Drug delivery using cationic peptides and proteins, *Nano Today.* 34 (2020) 100898. <https://doi.org/10.1016/j.nantod.2020.100898>.
- [61] C.D. DiDomenico, A. Goodearl, A. Yarilina, V. Sun, S. Mitra, A.S. Sterman, L.J. Bonassar, The Effect of Antibody Size and Mechanical Loading on Solute Diffusion Through the Articular Surface of Cartilage, *J. Biomech. Eng.* 139 (2017) 091005. <https://doi.org/10.1115/1.4037202>.
- [62] H.A. Leddy, F. Guilak, Site-Specific Molecular Diffusion in Articular Cartilage Measured using Fluorescence Recovery after Photobleaching, *Ann. Biomed. Eng.* 31 (2003) 753–760. <https://doi.org/10.1114/1.1581879>.
- [63] C.D. DiDomenico, M. Lintz, L.J. Bonassar, Molecular transport in articular cartilage — what have we learned from the past 50 years?, *Nat. Rev. Rheumatol.* 14 (2018) 393–403. <https://doi.org/10.1038/s41584-018-0033-5>.
- [64] S.X. Peng, E.C. Von Bargen, D.M. Bornes, S. Pikul, Permeability of Articular Cartilage to Matrix Metalloprotease Inhibitors, *Pharm. Res.* 15 (1998) 1414–1418. <https://doi.org/10.1023/A:1011905806123>.
- [65] F.G. Donnan, Theorie der Membrangleichgewichte und Membranpotentiale bei Vorhandensein von nicht dialysierenden Elektrolyten. Ein Beitrag zur physikalisch-chemischen Physiologie., *Z. Für Elektrochem. Angew. Phys. Chem.* 17 (1911) 572–581. <https://doi.org/10.1002/bbpc.19110171405>.
- [66] A. Maroudas, Transport of solutes through cartilage: permeability to large molecules, *J. Anat.* 122 (1976) 335–347.
- [67] A. Vedadghavami, E.K. Wagner, S. Mehta, T. He, C. Zhang, A.G. Bajpayee, Cartilage penetrating cationic peptide carriers for applications in drug delivery to avascular negatively charged tissues, *Acta Biomater.* 93 (2019) 258–269. <https://doi.org/10.1016/j.actbio.2018.12.004>.

- [68] M. Maldonado, J. Nam, The Role of Changes in Extracellular Matrix of Cartilage in the Presence of Inflammation on the Pathology of Osteoarthritis, *BioMed Res. Int.* 2013 (2013) 1–10. <https://doi.org/10.1155/2013/284873>.
- [69] L.J. Bonassar, E.H. Frank, J.C. Murray, C.G. Paguio, V.L. Moore, M.W. Lark, J.D. Sandy, J.-J. Wu, D.R. Eyre, A.J. Grodzinsky, Changes in cartilage composition and physical properties due to stromelysin degradation, *Arthritis Rheum.* 38 (1995) 173–183. <https://doi.org/10.1002/art.1780380205>.
- [70] A.R. Poole, M.E.J. Barratt, H.B. Fell, The Role of Soft Connective Tissue in the Breakdown of Pig Articular Cartilage Cultivated in the Presence of Complement-Sufficient Antiserum to Pig Erythrocytes, *Int. Arch. Allergy Immunol.* 44 (1973) 469–488. <https://doi.org/10.1159/000230952>.
- [71] P.A. Torzilli, J.M. Arduino, J.D. Gregory, M. Bansal, Effect of proteoglycan removal on solute mobility in articular cartilage, *J. Biomech.* 30 (1997) 895–902. [https://doi.org/10.1016/S0021-9290\(97\)00059-6](https://doi.org/10.1016/S0021-9290(97)00059-6).
- [72] S. Byun, Y.L. Sinskey, Y.C.S. Lu, T. Ort, K. Kavalkovich, P. Sivakumar, E.B. Hunziker, E.H. Frank, A.J. Grodzinsky, Transport of anti-IL-6 antigen binding fragments into cartilage and the effects of injury, *Arch. Biochem. Biophys.* 532 (2013) 15–22. <https://doi.org/10.1016/j.abb.2012.12.020>.
- [73] A.M. Garcia, E.H. Frank, P.E. Grimshaw, A.J. Grodzinsky, Contributions of Fluid Convection and Electrical Migration to Transport in Cartilage: Relevance to Loading, *Arch. Biochem. Biophys.* 333 (1996) 317–325. <https://doi.org/10.1006/abbi.1996.0397>.
- [74] S. Grenier, M.M. Bhargava, P.A. Torzilli, An in vitro model for the pathological degradation of articular cartilage in osteoarthritis, *J. Biomech.* 47 (2014) 645–652. <https://doi.org/10.1016/j.jbiomech.2013.11.050>.
- [75] D.T. Holyoak, Y.F. Tian, M.C. van der Meulen, A. Singh, Osteoarthritis: Pathology, mouse models, and nanoparticle injectable systems for targeted treatment, *Ann. Biomed. Eng.* 44 (2016) 2062–2075. <https://doi.org/10.1007/s10439-016-1600-z>.
- [76] M.H. Gregory, N. Capito, K. Kuroki, A.M. Stoker, J.L. Cook, S.L. Sherman, A Review of Translational Animal Models for Knee Osteoarthritis, *Arthritis.* 2012 (2012) 1–14. <https://doi.org/10.1155/2012/764621>.

- [77] W. N. D'Souza, G. Y. Ng, B. D. Youngblood, W. Tsuji, S. G. Lehto, A Review of Current Animal Models of Osteoarthritis Pain, *Curr. Pharm. Biotechnol.* 12 (2011) 1596–1612. <https://doi.org/10.2174/138920111798357320>.
- [78] C. Little, M. Smith, Animal Models of Osteoarthritis, *Curr. Rheumatol. Rev.* 4 (2008) 175–182. <https://doi.org/10.2174/157339708785133523>.
- [79] B.T. Pedersen, J. Østergaard, S.W. Larsen, C. Larsen, Characterization of the rotating dialysis cell as an in vitro model potentially useful for simulation of the pharmacokinetic fate of intra-articularly administered drugs, *Eur. J. Pharm. Sci.* 25 (2005) 73–79. <https://doi.org/10.1016/j.ejps.2005.01.019>.
- [80] N. Joshi, J. Yan, S. Levy, S. Bhagchandani, K.V. Slaughter, N.E. Sherman, J. Amirault, Y. Wang, L. Riegel, X. He, T.S. Rui, M. Valic, P.K. Vemula, O.R. Miranda, O. Levy, E.M. Gravallesse, A.O. Aliprantis, J. Ermann, J.M. Karp, Towards an arthritis flare-responsive drug delivery system, *Nat. Commun.* 9 (2018). <https://doi.org/10.1038/s41467-018-03691-1>.
- [81] T. Noda, T. Okuda, R. Mizuno, T. Ozeki, H. Okamoto, Two-Step Sustained-Release PLGA/Hyaluronic Acid Gel Formulation for Intra-articular Administration, *Biol. Pharm. Bull.* 41 (2018) 937–943. <https://doi.org/10.1248/bpb.b18-00091>.
- [82] R. Labens, B.D.X. Lascelles, A.N. Charlton, N.R. Ferrero, A.J. Van Wettere, X.-R. Xia, A.T. Blikslager, Ex vivo effect of gold nanoparticles on porcine synovial membrane, *Tissue Barriers.* 1 (2013). <https://doi.org/10.4161/tisb.24314>.
- [83] Y. Guang, T.M. McGrath, N. Klug, R. Nims, C.-C. Shih, P.O. Bayguinov, F. Guilak, C.T.N. Pham, J.A.J. Fitzpatrick, L.A. Setton, Combined Experimental Approach and Finite Element Modeling of Small Molecule Transport Through Joint Synovium to Measure Effective Diffusivity, *J. Biomech. Eng.* (2019). <https://doi.org/10.1115/1.4044892>.
- [84] Y. Guang, A.L. Davis, T.M. McGrath, C.T.N. Pham, J.A.J. Fitzpatrick, L.A. Setton, Size-Dependent Effective Diffusivity in Healthy Human and Porcine Joint Synovium, *Ann. Biomed. Eng.* (2021). <https://doi.org/10.1007/s10439-020-02717-4>.
- [85] R.M. Stefani, S.S. Halder, E.G. Estell, A.J. Lee, A.M. Silverstein, E. Sobczak, N.O. Chahine, G.A. Ateshian, R.P. Shah, C.T. Hung, A Functional Tissue-Engineered Synovium Model to Study Osteoarthritis Progression and Treatment, *Tissue Eng. Part A* (2018). <https://doi.org/10.1089/ten.tea.2018.0142>.

- [86] N. Mertz, J. Østergaard, A. Yagmur, S.W. Larsen, Transport characteristics in a novel in vitro release model for testing the performance of intra-articular injectables, *Int. J. Pharm.* 566 (2019) 445–453. <https://doi.org/10.1016/j.ijpharm.2019.04.083>.
- [87] B. Sterner, M. Harms, M. Weigandt, M. Windbergs, C.M. Lehr, Crystal suspensions of poorly soluble peptides for intra-articular application: A novel approach for biorelevant assessment of their in vitro release, *Int. J. Pharm.* 461 (2014) 46–53. <https://doi.org/10.1016/j.ijpharm.2013.11.031>.
- [88] A. Maroudas, Distribution and Diffusion of Solutes in Articular Cartilage, *Biophys. J.* 10 (1970) 365–379. [https://doi.org/10.1016/S0006-3495\(70\)86307-X](https://doi.org/10.1016/S0006-3495(70)86307-X).
- [89] Y. Shafieyan, N. Khosravi, M. Moeini, T.M. Quinn, Diffusion of MRI and CT Contrast Agents in Articular Cartilage under Static Compression, *Biophys. J.* 107 (2014) 485–492. <https://doi.org/10.1016/j.bpj.2014.04.041>.
- [90] A.M. Garcia, N. Szasz, S.B. Trippel, T.I. Morales, A.J. Grodzinsky, E.H. Frank, Transport and binding of insulin-like growth factor I through articular cartilage, *Arch. Biochem. Biophys.* 415 (2003) 69–79. [https://doi.org/10.1016/S0003-9861\(03\)00215-7](https://doi.org/10.1016/S0003-9861(03)00215-7).
- [91] C.D. DiDomenico, Z. Xiang Wang, L.J. Bonassar, Cyclic Mechanical Loading Enhances Transport of Antibodies Into Articular Cartilage, *J. Biomech. Eng.* 139 (2017) 011012. <https://doi.org/10.1115/1.4035265>.
- [92] A.G. Bajpayee, C.R. Wong, M.G. Bawendi, E.H. Frank, A.J. Grodzinsky, Avidin as a model for charge driven transport into cartilage and drug delivery for treating early stage post-traumatic osteoarthritis, *Biomaterials.* 35 (2014) 538–549. <https://doi.org/10.1016/j.biomaterials.2013.09.091>.
- [93] B.D. Foy, J. Blake, Diffusion of Paramagnetically Labeled Proteins in Cartilage: Enhancement of the 1-D NMR Imaging Technique, *J. Magn. Reson.* 148 (2001) 126–134. <https://doi.org/10.1006/jmre.2000.2216>.
- [94] J.T.J. Honkanen, M.J. Turunen, J.D. Freedman, S. Saarakkala, M.W. Grinstaff, J.H. Ylärinne, J.S. Jurvelin, J. Töyräs, Cationic Contrast Agent Diffusion Differs Between Cartilage and Meniscus, *Ann. Biomed. Eng.* 44 (2016) 2913–2921. <https://doi.org/10.1007/s10439-016-1629-z>.

- [95] F. Travascio, F. Devaux, M. Volz, A.R. Jackson, Molecular and macromolecular diffusion in human meniscus: relationships with tissue structure and composition, *Osteoarthritis Cartilage*. 28 (2020) 375–382. <https://doi.org/10.1016/j.joca.2019.12.006>.
- [96] H.C. Chin, M. Moeini, T.M. Quinn, Solute transport across the articular surface of injured cartilage, *Arch. Biochem. Biophys.* 535 (2013) 241–247. <https://doi.org/10.1016/j.abb.2013.04.011>.
- [97] A.E. Weber, I.K. Bolia, N.A. Trasolini, Biological strategies for osteoarthritis: from early diagnosis to treatment, *Int. Orthop.* 45 (2021) 335–344. <https://doi.org/10.1007/s00264-020-04838-w>.
- [98] I.A. Jones, R. Togashi, M.L. Wilson, N. Heckmann, C.T. Vangsness, Intra-articular treatment options for knee osteoarthritis, *Nat. Rev. Rheumatol.* 15 (2019) 77–90. <https://doi.org/10.1038/s41584-018-0123-4>.
- [99] Y. Wu, E.L. Goh, D. Wang, S. Ma, Novel treatments for osteoarthritis: a recent update, *Open Access Rheumatol. Res. Rev.* (2018). <https://doi.org/10.2147/OARRR.S176666>.
- [100] X. Chevalier, F. Eymard, P. Richette, Biologic agents in osteoarthritis: hopes and disappointments, *Nat. Rev. Rheumatol.* 9 (2013) 400–410. <https://doi.org/10.1038/nrrheum.2013.44>.
- [101] G.T. Sakellariou, G. Kakavouli, I. Chatzigiannis, Intraarticular injection of infliximab., *J. Rheumatol.* 33 (2006) 1912–1913.
- [102] A. Fioravanti, M. Fabbroni, A. Cerase, M. Galeazzi, Treatment of erosive osteoarthritis of the hands by intra-articular infliximab injections: a pilot study, *Rheumatol. Int.* 29 (2009) 961–965. <https://doi.org/10.1007/s00296-009-0872-0>.
- [103] W.P. Maksymowych, A.S. Russell, P. Chiu, A. Yan, N. Jones, T. Clare, R.G. Lambert, Targeting tumour necrosis factor alleviates signs and symptoms of inflammatory osteoarthritis of the knee, *Arthritis Res. Ther.* 14 (2012) R206. <https://doi.org/10.1186/ar4044>.
- [104] J. Wang, Efficacy and safety of adalimumab by intra-articular injection for moderate to severe knee osteoarthritis: An open-label randomized controlled trial, *J. Int. Med. Res.* 46 (2018) 326–334. <https://doi.org/10.1177/0300060517723182>.

[105] S. Ohtori, S. Orita, K. Yamauchi, Y. Eguchi, N. Ochiai, S. Kishida, K. Kuniyoshi, Y. Aoki, J. Nakamura, T. Ishikawa, M. Miyagi, H. Kamoda, M. Suzuki, G. Kubota, Y. Sakuma, Y. Oikawa, K. Inage, T. Sainoh, J. Sato, Y. Shiga, K. Abe, K. Fujimoto, H. Kanamoto, T. Toyone, G. Inoue, K. Takahashi, Efficacy of Direct Injection of Etanercept into Knee Joints for Pain in Moderate and Severe Knee Osteoarthritis, *Yonsei Med. J.* 56 (2015) 1379–1383. <https://doi.org/10.3349/ymj.2015.56.5.1379>.

[106] K. Kimmerling, B. Furman, D. Mangiapani, M. Moverman, S. Sinclair, J. Huebner, A. Chilkoti, V. Kraus, L. Setton, F. Guilak, S. Olson, Sustained intra-articular delivery of IL-1Ra from a thermally-responsive elastin-like polypeptide as a therapy for post-traumatic arthritis, *Eur. Cell. Mater.* 29 (2015) 124–140. <https://doi.org/10.22203/eCM.v029a10>.

[107] X. Chevalier, B. Giraudeau, T. Conrozier, J. Marliere, P. Kiefer, P. Goupille, Safety study of intraarticular injection of interleukin 1 receptor antagonist in patients with painful knee osteoarthritis: a multicenter study., *J. Rheumatol.* 32 (2005) 1317–1323.

[108] N.E. Lane, T.J. Schnitzer, C.A. Birbara, M. Mokhtarani, D.L. Shelton, M.D. Smith, M.T. Brown, Tanezumab for the Treatment of Pain from Osteoarthritis of the Knee, *N. Engl. J. Med.* 363 (2010) 1521–1531. <https://doi.org/10.1056/NEJMoa0901510>.

[109] A.R. Balanescu, E. Feist, G. Wolfram, I. Davignon, M.D. Smith, M.T. Brown, C.R. West, Efficacy and safety of tanezumab added on to diclofenac sustained release in patients with knee or hip osteoarthritis: a double-blind, placebo-controlled, parallel-group, multicentre phase III randomised clinical trial, *Ann. Rheum. Dis.* 73 (2014) 1665–1672. <https://doi.org/10.1136/annrheumdis-2012-203164>.

[110] FDA, FDA Approves Novel Treatment to Control Pain in Cats with Osteoarthritis, First Monoclonal Antibody Drug for Use in Any Animal Species, 2022. <https://animaldrugsatfda.fda.gov/adafda/app/search/public/document/download/Foi/11817>.

[111] FDA, Joint Meeting of Arthritis Advisory Committee and Drug Safety and Risk Management Advisory Committee, 2021. <https://www.fda.gov/media/146867/download>.

- [112] D.J. Hunter, M.C. Pike, B.L. Jonas, E. Kissin, J. Krop, T. McAlindon, Phase 1 safety and tolerability study of BMP-7 in symptomatic knee osteoarthritis, *BMC Musculoskelet. Disord.* 11 (2010) 232. <https://doi.org/10.1186/1471-2474-11-232>.
- [113] K. Stewart, M. Pabbruwe, S. Dickinson, T. Sims, A.P. Hollander, J.B. Chaudhuri, The Effect of Growth Factor Treatment on Meniscal Chondrocyte Proliferation and Differentiation on Polyglycolic Acid Scaffolds, *Tissue Eng.* 13 (2007) 271–280. <https://doi.org/10.1089/ten.2006.0242>.
- [114] E.E. Moore, A.M. Bendele, D.L. Thompson, A. Littau, K.S. Waggle, B. Reardon, J.L. Ellsworth, Fibroblast growth factor-18 stimulates chondrogenesis and cartilage repair in a rat model of injury-induced osteoarthritis, *Osteoarthritis Cartilage.* 13 (2005) 623–631. <https://doi.org/10.1016/j.joca.2005.03.003>.
- [115] C. Wen, L. Xu, X. Xu, D. Wang, Y. Liang, L. Duan, Insulin-like growth factor-1 in articular cartilage repair for osteoarthritis treatment, *Arthritis Res. Ther.* 23 (2021) 277. <https://doi.org/10.1186/s13075-021-02662-0>.
- [116] A. Mero, M. Campisi, M. Favero, C. Barbera, C. Secchieri, J.M. Dayer, M.B. Goldring, S.R. Goldring, G. Pasut, A hyaluronic acid–salmon calcitonin conjugate for the local treatment of osteoarthritis: Chondro-protective effect in a rabbit model of early OA, *J. Controlled Release.* 187 (2014) 30–38. <https://doi.org/10.1016/j.jconrel.2014.05.008>.
- [117] X. Chevalier, P. Ravaut, E. Maheu, G. Baron, A. Rialland, P. Vergnaud, C. Roux, Y. Maugars, D. Mulleman, C. Lukas, D. Wendling, P. Lafforgue, D. Loeuille, V. Foltz, P. Richette, Adalimumab in patients with hand osteoarthritis refractory to analgesics and NSAIDs: a randomised, multicentre, double-blind, placebo-controlled trial, *Ann. Rheum. Dis.* 74 (2015) 1697–1705. <https://doi.org/10.1136/annrheumdis-2014-205348>.
- [118] A. Vasudeva, S.L. Yadav, S. Nanda, S. Sahu, Assessment of pain and structure after an intra-articular injection of adalimumab in osteoarthritis of the knee: A case report, *Medicine (Baltimore).* 99 (2020) e21131. <https://doi.org/10.1097/MD.00000000000021131>.
- [119] G. Verbruggen, R. Wittoek, B.V. Cruyssen, D. Elewaut, Tumour necrosis factor blockade for the treatment of erosive osteoarthritis of the interphalangeal finger joints: a double blind, randomised trial on structure modification, *Ann. Rheum. Dis.* 71 (2012) 891. <https://doi.org/10.1136/ard.2011.149849>.

- [120] C. Aalbers, D. Gerlag, K. Vos, M. Vervoordeldonk, R. Landewé, P.P. Tak, Intra-articular etanercept treatment in inflammatory arthritis: A randomized double-blind placebo-controlled proof of mechanism clinical trial validating TNF as a potential therapeutic target for local treatment, *Joint Bone Spine*. 82 (2015) 338–344. <https://doi.org/10.1016/j.jbspin.2015.03.002>.
- [121] X. Chevalier, P. Goupille, A.D. Beaulieu, F.X. Burch, W.G. Bensen, T. Conrozier, D. Loeuille, A.J. Kivitz, D. Silver, B.E. Appleton, Intraarticular injection of anakinra in osteoarthritis of the knee: A multicenter, randomized, double-blind, placebo-controlled study, *Arthritis Care Res.* 61 (2009) 344–352. <https://doi.org/10.1002/art.24096>.
- [122] J.P. Caron, J.C. Fernandes, J. Martel-Pelletier, G. Tardif, F. Mineau, C. Geng, J.-P. Pelletier, Chondroprotective effect of intraarticular injections of interleukin-1 receptor antagonist in experimental osteoarthritis. Suppression of collagenase-1 expression, *Arthritis Rheum.* 39 (1996) 1535–1544. <https://doi.org/10.1002/art.1780390914>.
- [123] F.S. Loffredo, J.R. Pancoast, L. Cai, T. Vannelli, J.Z. Dong, R.T. Lee, P. Patwari, Targeted Delivery to Cartilage Is Critical for In Vivo Efficacy of Insulin-like Growth Factor 1 in a Rat Model of Osteoarthritis: Efficacy of Cartilage-Targeted Delivery, *Arthritis Rheumatol.* 66 (2014) 1247–1255. <https://doi.org/10.1002/art.38357>.
- [124] X.-W. Liu, J. Hu, C. Man, B. Zhang, Y.-Q. Ma, S.-S. Zhu, Insulin-like growth factor-1 suspended in hyaluronan improves cartilage and subchondral cancellous bone repair in osteoarthritis of temporomandibular joint, *Int. J. Oral Maxillofac. Surg.* 40 (2011) 184–190. <https://doi.org/10.1016/j.ijom.2010.10.003>.
- [125] P.P. Srinivasan, S.Y. McCoy, A.K. Jha, W. Yang, X. Jia, M.C. Farach-Carson, C.B. Kirn-Safran, Injectable Perlecan Domain 1-Hyaluronan Microgels Potentiate the Cartilage Repair Effect of BMP2 in a Murine Model of Early Osteoarthritis, *Biomed. Mater. Bristol Engl.* 7 (2012) 024109. <https://doi.org/10.1088/1748-6041/7/2/024109>.
- [126] K. Gavenis, N. Heussen, M. Hofman, S. Andereya, U. Schneider, B. Schmidt-Rohlfing, Cell-free repair of small cartilage defects in the Goettinger minipig: The effects of BMP-7 continuously released by poly(lactic-co-glycolid acid) microspheres, *J. Biomater. Appl.* 28 (2014) 1008–1015. <https://doi.org/10.1177/0885328213491440>.

- [127] J. Shi, X. Zhang, J. Zhu, Y. Pi, X. Hu, C. Zhou, Y. Ao, Nanoparticle Delivery of the Bone Morphogenetic Protein 4 Gene to Adipose-Derived Stem Cells Promotes Articular Cartilage Repair In Vitro and In Vivo, *Arthrosc. J. Arthrosc. Relat. Surg.* 29 (2013) 2001-2011.e2. <https://doi.org/10.1016/j.arthro.2013.09.076>.
- [128] L. Bian, D.Y. Zhai, E. Tous, R. Rai, R.L. Mauck, J.A. Burdick, Enhanced MSC chondrogenesis following delivery of TGF- β 3 from alginate microspheres within hyaluronic acid hydrogels in vitro and in vivo, *Biomaterials.* 32 (2011) 6425–6434. <https://doi.org/10.1016/j.biomaterials.2011.05.033>.
- [129] H. Diao, J. Wang, C. Shen, S. Xia, T. Guo, L. Dong, C. Zhang, J. Chen, J. Zhao, J. Zhang, Improved Cartilage Regeneration Utilizing Mesenchymal Stem Cells in TGF- β 1 Gene-Activated Scaffolds, *Tissue Eng. Part A.* 15 (2009) 2687–2698. <https://doi.org/10.1089/ten.tea.2008.0621>.
- [130] L.S. Lohmander, S. Hellot, D. Dreher, E.F.W. Krantz, D.S. Kruger, A. Guermazi, F. Eckstein, Intraarticular Sprifermin (Recombinant Human Fibroblast Growth Factor 18) in Knee Osteoarthritis: A Randomized, Double-Blind, Placebo-Controlled Trial: Sprifermin Effects in Knee Osteoarthritis, *Arthritis Rheumatol.* 66 (2014) 1820–1831. <https://doi.org/10.1002/art.38614>.
- [131] P. Cuevas, J. Burgos, A. Baird, Basic fibroblast growth factor (FGF) promotes cartilage repair in vivo, *Biochem. Biophys. Res. Commun.* 156 (1988) 611–618. [https://doi.org/10.1016/S0006-291X\(88\)80887-8](https://doi.org/10.1016/S0006-291X(88)80887-8).
- [132] S.M. Ryan, J. McMorro, A. Umerska, H.B. Patel, K.N. Kornerup, L. Tajber, E.P. Murphy, M. Perretti, O.I. Corrigan, D.J. Brayden, An intra-articular salmon calcitonin-based nanocomplex reduces experimental inflammatory arthritis, *J. Controlled Release.* 167 (2013) 120–129. <https://doi.org/10.1016/j.jconrel.2013.01.027>.
- [133] X. Chevalier, F. Kempta-Lepka, Are biologics a treatment option in osteoarthritis?, *Therapy.* 7 (2010) 675–683. <https://doi.org/10.2217/thy.10.66>.
- [134] C. Wenham, M. McDermott, P. Conaghan, Biological Therapies in Osteoarthritis, *Curr. Pharm. Des.* 21 (2015) 2206–2215. <https://doi.org/10.2174/1381612821666150310144940>.
- [135] M.B. Goldring, Anticytokine therapy for osteoarthritis, *Expert Opin Biol Ther.* (2001) 13.

- [136] P. Maudens, O. Jordan, E. Allémann, Recent advances in intra-articular drug delivery systems for osteoarthritis therapy, *Drug Discov. Today*. 23 (2018) 1761–1775. <https://doi.org/10.1016/j.drudis.2018.05.023>.
- [137] A.L. Daugherty, R.J. Msrny, Formulation and delivery issues for monoclonal antibody therapeutics, *Adv. Drug Deliv. Rev.* 58 (2006) 686–706. <https://doi.org/10.1016/j.addr.2006.03.011>.
- [138] D.J.A. Crommelin, R.D. Sindelar, B. Meibohm, eds., *Pharmaceutical Biotechnology: Fundamentals and Applications*, Springer International Publishing, Cham, 2019. <https://doi.org/10.1007/978-3-030-00710-2>.
- [139] W. Rungseewijitprapa, R. Bodmeier, Injectability of biodegradable in situ forming microparticle systems (ISM), *Eur. J. Pharm. Sci.* 36 (2009) 524–531. <https://doi.org/10.1016/j.ejps.2008.12.003>.
- [140] W. Jiskoot, T.W. Randolph, D.B. Volkin, C. Russell Middaugh, C. Schöneich, G. Winter, W. Friess, D.J.A. Crommelin, J.F. Carpenter, Protein Instability and Immunogenicity: Roadblocks to Clinical Application of Injectable Protein Delivery Systems for Sustained Release, *J. Pharm. Sci.* 101 (2012) 946–954. <https://doi.org/10.1002/jps.23018>.
- [141] L. Kou, S. Xiao, R. Sun, S. Bao, Q. Yao, R. Chen, Biomaterial-engineered intra-articular drug delivery systems for osteoarthritis therapy, *Drug Deliv.* 26 (2019) 870–885. <https://doi.org/10.1080/10717544.2019.1660434>.
- [142] R. Vaishya, V. Khurana, S. Patel, A.K. Mitra, Long-term delivery of protein therapeutics, *Expert Opin. Drug Deliv.* 12 (2015) 415–440. <https://doi.org/10.1517/17425247.2015.961420>.
- [143] F. Wu, T. Jin, Polymer-Based Sustained-Release Dosage Forms for Protein Drugs, Challenges, and Recent Advances, *AAPS PharmSciTech.* 9 (2008) 1218–1229. <https://doi.org/10.1208/s12249-008-9148-3>.
- [144] F. Raza, H. Zafar, Y. Zhu, Y. Ren, A. -Ullah, A. Khan, X. He, H. Han, M. Aquib, K. Boakye-Yiadom, L. Ge, A Review on Recent Advances in Stabilizing Peptides/Proteins upon Fabrication in Hydrogels from Biodegradable Polymers, *Pharmaceutics.* 10 (2018) 16. <https://doi.org/10.3390/pharmaceutics10010016>.
- [145] T. Vermonden, R. Censi, W.E. Hennink, Hydrogels for Protein Delivery, *Chem. Rev.* 112 (2012) 2853–2888. <https://doi.org/10.1021/cr200157d>.

- [146] R. Censi, T. Vermonden, M.J. van Steenberg, H. Deschout, K. Braeckmans, S.C. De Smedt, C.F. van Nostrum, P. di Martino, W.E. Hennink, Photopolymerized thermosensitive hydrogels for tailorable diffusion-controlled protein delivery, *J. Controlled Release*. 140 (2009) 230–236. <https://doi.org/10.1016/j.jconrel.2009.06.003>.
- [147] K.L. Spiller, G. Vunjak-Novakovic, Clinical translation of controlled protein delivery systems for tissue engineering, *Drug Deliv. Transl. Res.* 5 (2015) 101–115. <https://doi.org/10.1007/s13346-013-0135-1>.
- [148] R. Censi, P. Di Martino, T. Vermonden, W.E. Hennink, Hydrogels for protein delivery in tissue engineering, *J. Controlled Release*. 161 (2012) 680–692. <https://doi.org/10.1016/j.jconrel.2012.03.002>.
- [149] W. Chen, Z. Li, Z. Wang, H. Gao, J. Ding, Z. He, Intraarticular Injection of Infliximab-Loaded Thermosensitive Hydrogel Alleviates Pain and Protects Cartilage in Rheumatoid Arthritis, *J. Pain Res.* Volume 13 (2020) 3315–3329. <https://doi.org/10.2147/JPR.S283518>.
- [150] J.P. Schillemans, E. Verheyen, A. Barendregt, W.E. Hennink, C.F. Van Nostrum, Anionic and cationic dextran hydrogels for post-loading and release of proteins, *J. Controlled Release*. 150 (2011) 266–271. <https://doi.org/10.1016/j.jconrel.2010.11.027>.
- [151] T. Siefen, J. Lokhnauth, A. Liang, C.C. Larsen, S. Bjerregaard, A. Lamprecht, Co-formulations of adalimumab with hyaluronic acid / polyvinylpyrrolidone to combine intraarticular drug delivery and viscosupplementation, *Eur. J. Pharm. Biopharm.* in Press (2022).
- [152] S. Mantha, S. Pillai, P. Khayambashi, A. Upadhyay, Y. Zhang, O. Tao, H.M. Pham, S.D. Tran, Smart Hydrogels in Tissue Engineering and Regenerative Medicine, *Materials*. 12 (2019) 3323. <https://doi.org/10.3390/ma12203323>.
- [153] Z. He, B. Wang, C. Hu, J. Zhao, An overview of hydrogel-based intra-articular drug delivery for the treatment of osteoarthritis, *Colloids Surf. Biointerfaces*. 154 (2017) 33–39. <https://doi.org/10.1016/j.colsurfb.2017.03.003>.
- [154] N. Hammer, F.P. Brandl, S. Kirchhof, A.M. Goepferich, Cleavable carbamate linkers for controlled protein delivery from hydrogels, *J. Controlled Release*. 183 (2014) 67–76. <https://doi.org/10.1016/j.jconrel.2014.03.031>.

- [155] A. Rey-Rico, H. Madry, M. Cucchiarini, Hydrogel-Based Controlled Delivery Systems for Articular Cartilage Repair, *BioMed Res. Int.* 2016 (2016) 1–12. <https://doi.org/10.1155/2016/1215263>.
- [156] A. Fayd'herbe De Maudave, W. Leconet, K. Toupet, M. Constantinides, G. Bossis, M. de Toledo, J. Vialaret, C. Hirtz, A. Lopez-Noriega, C. Jorgensen, D. Noël, P. Louis-Plence, S. Grizot, M. Villalba, Intra-articular delivery of full-length antibodies through the use of an in situ forming depot, *J. Controlled Release.* 341 (2022) 578–590. <https://doi.org/10.1016/j.jconrel.2021.12.010>.
- [157] Y. Cao, Y. Ma, Y. Tao, W. Lin, P. Wang, Intra-Articular Drug Delivery for Osteoarthritis Treatment, *Pharmaceutics.* 13 (2021) 2166. <https://doi.org/10.3390/pharmaceutics13122166>.
- [158] W. Chen, A. Palazzo, W.E. Hennink, R.J. Kok, Effect of Particle Size on Drug Loading and Release Kinetics of Gefitinib-Loaded PLGA Microspheres, *Mol. Pharm.* 14 (2017) 459–467. <https://doi.org/10.1021/acs.molpharmaceut.6b00896>.
- [159] C.E. Espinosa-de la Garza, M.P. Miranda-Hernández, L. Acosta-Flores, N.O. Pérez, L.F. Flores-Ortiz, E. Medina-Rivero, Analysis of therapeutic proteins and peptides using multiangle light scattering coupled to ultra high performance liquid chromatography: Liquid Chromatography, *J. Sep. Sci.* 38 (2015) 1537–1543. <https://doi.org/10.1002/jssc.201400863>.
- [160] J. Pradal, P. Maudens, C. Gabay, C.A. Seemayer, O. Jordan, E. Allémann, Effect of particle size on the biodistribution of nano- and microparticles following intra-articular injection in mice, *Int. J. Pharm.* 498 (2016) 119–129. <https://doi.org/10.1016/j.ijpharm.2015.12.015>.
- [161] R.T. Liggins, T. Cruz, W. Min, L. Liang, W.L. Hunter, H.M. Burt, Intra-articular treatment of arthritis with microsphere formulations of paclitaxel: biocompatibility and efficacy determinations in rabbits, *Inflamm. Res.* 53 (2004). <https://doi.org/10.1007/s00011-004-1273-1>.
- [162] H. Chikaura, Y. Nakashima, Y. Fujiwara, Y. Komohara, M. Takeya, Y. Nakanishi, Effect of particle size on biological response by human monocyte-derived macrophages, *Biosurface Biotribology.* 2 (2016) 18–25. <https://doi.org/10.1016/j.bsbt.2016.02.003>.

- [163] J.K. Jackson, C.M.K. Springate, W.L. Hunter, H.M. Burt, Neutrophil activation by plasma opsonized polymeric microspheres: inhibitory effect of Pluronic F127, *Biomaterials*. 21 (2000) 1483–1491. [https://doi.org/10.1016/S0142-9612\(00\)00034-X](https://doi.org/10.1016/S0142-9612(00)00034-X).
- [164] E. Horisawa, K. Kubota, I. Tuboi, K. Sato, H. Yamamoto, H. Takeuchi, Y. Kawashima, Size-Dependency of DL-Lactide/Glycolide Copolymer Particulates for Intra-Articular Delivery System on Phagocytosis in Rat Synovium, *Pharm. Res.* 19 (2002) 132–139. <https://doi.org/10.1023/A:1014260513728>.
- [165] T. Lange, A.F. Schilling, F. Peters, J. Mujas, D. Wicklein, M. Amling, Size dependent induction of proinflammatory cytokines and cytotoxicity of particulate beta-tricalciumphosphate in vitro, *Biomaterials*. 32 (2011) 4067–4075. <https://doi.org/10.1016/j.biomaterials.2011.02.039>.
- [166] S.P. Zysk, H.H. Gebhard, T. Kalteis, M. Schmitt-Sody, V. Jansson, K. Messmer, A. Veihelmann, Particles of All Sizes Provoke Inflammatory Responses In Vivo, *Clin. Orthop. Relat. Res.* 433 (2005). <https://doi.org/doi:10.1097/01.blo.0000150311.33227.b1>.
- [167] P.A. Dieppe, M. Doherty, The Role of Particles in the Pathogenesis of Joint Disease, in: C.L. Berry (Ed.), *Bone Jt. Dis.*, Springer Berlin Heidelberg, Berlin, Heidelberg, 1982: pp. 199–233.
- [168] J.B. Lin, S. Poh, A. Panitch, Controlled release of anti-inflammatory peptides from reducible thermosensitive nanoparticles suppresses cartilage inflammation, *Nanomedicine Nanotechnol. Biol. Med.* 12 (2016) 2095–2100. <https://doi.org/10.1016/j.nano.2016.05.010>.
- [169] Y. Yang, H. Zhu, J. Wang, Q. Fang, Z. Peng, Enzymatically Disulfide-Crosslinked Chitosan/Hyaluronic Acid Layer-by-Layer Self-Assembled Microcapsules for Redox-Responsive Controlled Release of Protein, *ACS Appl. Mater. Interfaces*. 10 (2018) 33493–33506. <https://doi.org/10.1021/acsami.8b07120>.
- [170] X. Li, B. Dai, J. Guo, L. Zheng, Q. Guo, J. Peng, J. Xu, L. Qin, Nanoparticle–Cartilage Interaction: Pathology-Based Intra-articular Drug Delivery for Osteoarthritis Therapy, *Nano-Micro Lett.* 13 (2021) 149. <https://doi.org/10.1007/s40820-021-00670-y>.

- [171] Ö. Erdemli, S. Özen, D. Keskin, A. Usanmaz, E.D. Batu, B. Atilla, A. Tezcaner, In vitro evaluation of effects of sustained anti-TNF release from MPEG-PCL-MPEG and PCL microspheres on human rheumatoid arthritis synoviocytes, *J. Biomater. Appl.* 29 (2014) 524–542. <https://doi.org/10.1177/0885328214535958>.
- [172] S.J. Na, S.Y. Chae, S. Lee, K. Park, K. Kim, J.H. Park, I.C. Kwon, S.Y. Jeong, K.C. Lee, Stability and bioactivity of nanocomplex of TNF-related apoptosis-inducing ligand, *Int. J. Pharm.* 363 (2008) 149–154. <https://doi.org/10.1016/j.ijpharm.2008.07.013>.
- [173] J.J. Water, M.M. Schack, A. Velazquez-Campoy, M.J. Maltesen, M. van de Weert, L. Jorgensen, Complex coacervates of hyaluronic acid and lysozyme: Effect on protein structure and physical stability, *Eur. J. Pharm. Biopharm.* 88 (2014) 325–331. <https://doi.org/10.1016/j.ejpb.2014.09.001>.
- [174] M. van de Weert, W.E. Hennink, W. Jiskoot, Protein Instability in Poly(Lactic-co-Glycolic Acid) Microparticles, *Pharm. Res.* 17 (2000) 1159–1167. <https://doi.org/10.1023/A:1026498209874>.
- [175] S. Mehta, T. He, A.G. Bajpayee, Recent advances in targeted drug delivery for treatment of osteoarthritis, *Curr. Opin. Rheumatol.* 33 (2021) 94–109. <https://doi.org/10.1097/BOR.0000000000000761>.
- [176] M. Unni, S. Savliwala, B.D. Partain, L. Maldonado-Camargo, Q. Zhang, S. Narayanan, E.M. Dufresne, J. Ilavsky, P. Grybos, A. Koziol, P. Maj, R. Szczygiel, K.D. Allen, C.M. Rinaldi-Ramos, Fast nanoparticle rotational and translational diffusion in synovial fluid and hyaluronic acid solutions, *Sci. Adv.* 7 (2021) eabf8467. <https://doi.org/10.1126/sciadv.abf8467>.
- [177] S.R. Kim, M.J. Ho, E. Lee, J.W. Lee, Y.W. Choi, M.J. Kang, Cationic PLGA/Eudragit RL nanoparticles for increasing retention time in synovial cavity after intra-articular injection in knee joint, *Int. J. Nanomedicine.* 10 (2015) 5263–5271. <https://doi.org/10.2147/IJN.S88363>.
- [178] H.D. Jhundoo, T. Siefen, A. Liang, C. Schmidt, J. Lokhnauth, A. Béduneau, Y. Pellequer, C.C. Larsen, A. Lamprecht, Anti-Inflammatory Activity of Chitosan and 5-Amino Salicylic Acid Combinations in Experimental Colitis, *Pharmaceutics.* 12 (2020) 1038. <https://doi.org/10.3390/pharmaceutics12111038>.

[179] B. Qiu, M. Gong, Q.-T. He, P.-H. Zhou, Controlled Release of Interleukin-1 Receptor Antagonist from Hyaluronic Acid-Chitosan Microspheres Attenuates Interleukin-1 β -Induced Inflammation and Apoptosis in Chondrocytes, *BioMed Res. Int.* 2016 (2016). <https://doi.org/10.1155/2016/6290957>.

[180] J. Youshia, M.E. Ali, V. Stein, A. Lamprecht, Nanoparticles' properties modify cell type-dependent distribution in immune cells, *Nanomedicine Nanotechnol. Biol. Med.* 29 (2020) 102244. <https://doi.org/10.1016/j.nano.2020.102244>.

[181] M. Trif, A. Roseanu, J.H. Brock, J.M. Brewer, Designing Lipid Nanostructures for Local Delivery of Biologically Active Macromolecules, *J. Liposome Res.* 17 (2007) 237–248. <https://doi.org/10.1080/08982100701530027>.

[182] S. Sivan, A. Schroeder, G. Verberne, Y. Merkher, D. Diminsky, A. Prieve, A. Maroudas, G. Halperin, D. Nitzan, I. Etsion, Y. Barenholz, Liposomes Act as Effective Biolubricants for Friction Reduction in Human Synovial Joints, *Langmuir.* 26 (2010) 1107–1116. <https://doi.org/10.1021/la9024712>.

[183] T. He, C. Zhang, A. Vedadghavami, S. Mehta, H.A. Clark, R.M. Porter, A.G. Bajpayee, Multi-arm Avidin nano-construct for intra-cartilage delivery of small molecule drugs, *J. Controlled Release.* 318 (2020) 109–123. <https://doi.org/10.1016/j.jconrel.2019.12.020>.

[184] A.G. Bajpayee, M. Scheu, A.J. Grodzinsky, R.M. Porter, Electrostatic interactions enable rapid penetration, enhanced uptake and retention of intra-articular injected avidin in rat knee joints: avidin for intra-articular drug delivery, *J. Orthop. Res.* 32 (2014) 1044–1051. <https://doi.org/10.1002/jor.22630>.

[185] N.J. Shah, B.C. Geiger, M.A. Quadir, N. Hyder, Y. Krishnan, A.J. Grodzinsky, P.T. Hammond, Synthetic nanoscale electrostatic particles as growth factor carriers for cartilage repair, *Bioeng. Transl. Med.* 1 (2016) 347–356. <https://doi.org/10.1002/btm2.10043>.

[186] B.C. Geiger, S. Wang, R.F. Padera, A.J. Grodzinsky, P.T. Hammond, Cartilage-penetrating nanocarriers improve delivery and efficacy of growth factor treatment of osteoarthritis, *Sci. Transl. Med.* 10 (2018) eaat8800. <https://doi.org/10.1126/scitranslmed.aat8800>.

[187] H. Lv, S. Zhang, B. Wang, S. Cui, J. Yan, Toxicity of cationic lipids and cationic polymers in gene delivery, *J. Controlled Release.* 114 (2006) 100–109. <https://doi.org/10.1016/j.jconrel.2006.04.014>.

- [188] M. Shetab Boushehri, D. Dietrich, A. Lamprecht, Nanotechnology as a Platform for the Development of Injectable Parenteral Formulations: A Comprehensive Review of the Know-Hows and State of the Art, *Pharmaceutics*. 12 (2020) 510. <https://doi.org/10.3390/pharmaceutics12060510>.
- [189] S. Brown, S. Kumar, B. Sharma, Intra-articular targeting of nanomaterials for the treatment of osteoarthritis, *Acta Biomater.* 93 (2019) 239–257. <https://doi.org/10.1016/j.actbio.2019.03.010>.
- [190] D.A. Rothenfluh, H. Bermudez, C.P. O’Neil, J.A. Hubbell, Biofunctional polymer nanoparticles for intra-articular targeting and retention in cartilage, *Nat. Mater.* 7 (2008) 248–254. <https://doi.org/10.1038/nmat2116>.
- [191] Z. Chen, J. Chen, L. Wu, W. Li, Chen J., H. Cheng, J. Pan, B. Cai, Hyaluronic acid-coated bovine serum albumin nanoparticles loaded with brucine as selective nanovectors for intra-articular injection, *Int. J. Nanomedicine*. (2013) 3843. <https://doi.org/10.2147/IJN.S50721>.
- [192] H. Laroui, L. Grossin, M. Léonard, J.-F. Stoltz, P. Gillet, P. Netter, E. Dellacherie, Hyaluronate-Covered Nanoparticles for the Therapeutic Targeting of Cartilage, *Biomacromolecules*. 8 (2007) 3879–3885. <https://doi.org/10.1021/bm700836y>.
- [193] A. Singh, R. Agarwal, C.A. Diaz-Ruiz, N.J. Willett, P. Wang, L.A. Lee, Q. Wang, R.E. Guldberg, A.J. García, Nanoengineered Particles for Enhanced Intra-Articular Retention and Delivery of Proteins, *Adv. Healthc. Mater.* 3 (2014) 1562–1567. <https://doi.org/10.1002/adhm.201400051>.
- [194] M.A. Tryfonidou, G. de Vries, W.E. Hennink, L.B. Creemers, “Old Drugs, New Tricks” – Local controlled drug release systems for treatment of degenerative joint disease, *Adv. Drug Deliv. Rev.* 160 (2020) 170–185. <https://doi.org/10.1016/j.addr.2020.10.012>.

3. Aims and scope

The aim of this work is to reveal both how an *ex-vivo* test model for permeation across the synovial membrane offers biorelevant insights into articular pharmacokinetics and how this knowledge can be used to design rationally derived formulation strategies to affect the joint residence time of the active ingredient ADA. The first drug delivery approach presents the joint leakage prolonging effect mediated by augmented viscosity and polymer-drug interaction. In this context, the hyaluronic acid (HA) – polyvinylpyrrolidone (PVP) co-formulated hydrogel network simultaneously provided a viscosupplementing system to restore the lubricating capacity of the joint. The second delivery approach presented takes advantage of the endogenous bioelectricity in the joint so that the drug is superficially immobilized in the synovium via avidin-biotin intermediated nanocomplexes of ADA with cationic diethylaminoethyl-dextran. These two very different designed approaches were assessed for their *ex-vivo* synovial permeability as an indicator of joint retention, with ancillary assessments of conservation of antigen recognition of ADA, as well as tracking biocompatibility and intra-tissue stability of the formulation. Thus, from rather conventional to pioneering, IA drug delivery strategies will be investigated and evaluated using advanced early development testing strategies that allow biorelevant estimation of pharmacokinetics in the joint.

4 An ex-vivo model for transsynovial drug permeation of intraarticular injectables in naive and arthritic synovium

4. An ex-vivo model for transsynovial drug permeation of intraarticular injectables in naive and arthritic synovium

Tobias Siefen¹, John Lokhnauth², Alfred Liang³, Crilles Casper Larsen⁴, Alf Lamprecht^{1,5}

¹Department of Pharmaceutics, Institute of Pharmacy, University of Bonn, Bonn, Germany

²Tris Pharma, Monmouth Junction, NJ 08852, USA

³Vytaderm, Fair Lawn, NJ 07410, USA

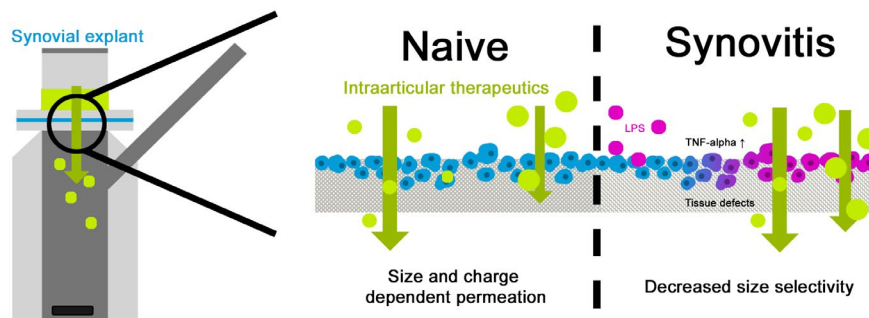
⁴Ferring Pharmaceuticals Inc, Parsippany, New Jersey, USA

⁵PEPITE (EA4267), University of Burgundy/Franche-Comté, Besançon, France

This work is published as

T. Siefen, J. Lokhnauth, A. Liang, C. C. Larsen, and A. Lamprecht, "An ex-vivo model for transsynovial drug permeation of intraarticular injectables in naive and arthritic synovium," *Journal of Controlled Release*, Mar. 2021, doi: 10.1016/j.jconrel.2021.03.008.

4.1 Graphical abstract



4.2 Abstract

Estimation of joint residence time of a drug is a key requirement for rational development of intraarticular therapeutics. There is a great need for a predictive model to reduce the high number of animal experiments in early-stage development. Here, a Franz-cell based porcine *ex-vivo* permeation model is proposed, and transsynovial permeation of fluorescently labeled dextrans in the range of potential drug candidates (10-150 kDa), as well as a small molecule (fluorescein sodium) and charged dextran derivatives, have been determined. In addition, a lipopolysaccharide (LPS) -induced synovitis model was assessed for inflammatory biomarker levels and its effect on permeation of the solutes. Size-dependent permeability was observed for the analytes, which distinctly differed from findings with an artificial polycarbonate membrane, which is a widely used model. LPS was found to successfully stimulate an inflammatory response and led to a reduced size selectivity of the synovial membrane. 150 kDa dextran flux was accelerated approximately 2.5-fold in the inflamed state, whereas the permeation of smaller molecules was little affected. Moreover, by varying the LPS concentrations, the *ex-vivo* model was shown to produce varying degrees of synovitis-like inflammation. A simple and highly relevant *ex-vivo* tool for investigation of transsynovial permeation was developed, offering the further advantage of mimicking synovitis-induced permeability changes. Thus, this model provides a promising method for formulation screening, while reducing the need for animal experiments.

4.3 Keywords

formulation development, permeability, synovitis, joint residence time, Franz-cell

4.4 Introduction

Intraarticular (IA) injections offer several advantages for treatment of arthritic joints. High local drug concentrations while maintaining small total drug load may increase efficacy and decrease cost of therapy. However, after IA injection the drug appears to be rapidly cleared through the synovial membrane into surrounding blood capillaries or lymphatic vessels [1]. The potential benefits of prolonged retention time of the drug do not only arise from the effective duration of action within the joint, but also from the enhancement of patient compliance and the reduced risk of infection due to high injection frequency [2]. Despite an increasing number of therapeutic approaches in IA treatment, including nanoparticles, liposomes, and hydrogel formulations in research [3,4], a suitable test system to examine drug retention and escape from the joint is lacking. Animal experiments to examine transsynovial transport are commonly used to provide relevant clearance data but entail ethical issues as well as imprecise sampling methods and high cost, making them unsuitable for screening purposes and early-stage development. However, with no regulatory approved, *in-vitro* model for sustained parenteral drug delivery, various test systems have been used in recent years. Application of USP (United States Pharmacopeia) apparatus III (reciprocal cylinder) and IV (flow through cell) have been investigated for their general adaptability for sustained parenteral drug testing [5]. IA injectables were most commonly assayed using the rotating dialysis cell model [6,7] or assimilable membrane separated diffusion chambers such as the Ussing chamber or vertical permeation cells [8,9]. These models typically use an artificial membrane and can supplement routine parenteral delivery tests and quality control. However, they are expected to be applicable primarily for simple drug formulations [10] and do not necessarily reflect physiological environment. As an artificial membrane does not adequately mirror the synovium's specific structure and properties, its usage may result in inaccurate measurement of the effective drug clearance from the joint, where transport is controlled by multiple mechanisms. Due to the physiological complexity of the joint, drug elimination is typically studied using a high number of animal experiments. To efficiently reduce animal studies an *ex-vivo* model that more closely represents physiological synovial permeability is required. This is especially true since the synovium features a unique two-layered architecture. It consists of a 1-4 cells thick discontinuous intimal layer, which is composed of fibroblast-like B cells and macrophage-like A cells, and the subsynovium, comprised of loose connective tissue and fat cells [11,12]. The combination of intercellular gaps, dense extracellular network and enmeshed

4 An ex-vivo model for transsynovial drug permeation of intraarticular injectables in naive and arthritic synovium

proteoglycans determine an effective pore size of approximately 50-100 nm to create a pathway for fluid drainage [11,13]. However, true morphology of pores is believed to be far more complex than that of a cylindrical pore [14]. Moreover, extracellular matrix is highly anionic [15] and cell-secreted hyaluronan forms a charged polarization layer [16] which can affect trans-synovial permeation. Thus, close resemblance to physiological morphology is crucial to precisely discriminate between specific drugs or complex formulations and display a biorelevant permeation profile. As IA injections are ordinarily applied to arthritic joints, it is of additional importance to evaluate the impact of pathologic changes due to synovitis on the permeation of the drug. Animal studies may offer insight into arthritic permeability, but involve chronic pain, loss of mobility and surgery of the animals. Besides ethical issues, these animal models make it challenging to gain insight on individual factors such as synovial permeability, as *in-vivo* data result from a multitude of influencing variables. *In-vitro* tests to mimic arthritic synovial permeability have been developed [17,18] but are currently based on artificial membranes and mimic the arthritic joint by diversification of media compounds or membrane pore size. *Ex-vivo* tissue testing provides a method to evaluate physiological permeation characteristics of therapeutic molecules and was first introduced to investigate the permeation of gold nanoparticles [19]. More recently, synovial explants were used for evaluation of size-selective diffusion of polyethylene glycol polymers [20], and a multiphasic computational model of a small molecule was established with the help of *ex-vivo* data to estimate the influence of intimal layer and matrix diffusivity [21]. To expand the understanding of *ex-vivo* drug permeation through the synovial membrane, we introduce and characterize a Franz-cell-based, vertical diffusion model to link synovial permeability to the influence of molecular size and viability of the explant. As porcine anatomy and physiology are generally believed to exhibit high similarities to human [22], use of a standardized porcine *ex vivo* model for IA permeability provides a new surrogate for transsynovial elimination. Biochemical modification can be made to the test model to gain additional insight into transport mechanisms, offering another major advantage of the *ex-vivo* model and providing decisive benefits for specific experimental objectives, such as pathologic state investigations [23]. Clearance from the arthritic joint differs from the naive joint, due to numerous morphological and biochemical alterations associated with synovitis, as the course of disease progresses [24,25]. As IA injections are ordinarily administered to pathologic joints, a permeation model that is capable of simulating synovitis as seen in arthritic diseases would be of

great value. In the present work, the development of a transsynovial permeation model for determination of drug diffusion profiles and pathologic model adjustment is pursued. To identify its characteristics, we focus on the suitability of distinctive permeation between specific macromolecules with different physicochemical properties and link them to the underlying mechanisms for naive and arthritic joints as stated in literature. Fluorescently-labeled dextrans of different molecular sizes served as adaptable and easily traceable standard markers for macromolecular substances were chosen for investigation of synovial permeability. Sizes were chosen to match those of possible drug candidates for IA injection (10-150 kDa).

4.5 Materials and methods

4.5.1 Reagents and materials

Fluorescein-isothiocyanate-dextrans (FITC-dextrans) sized 10, 40, 70, 150 and 500 kDa fluorescein-isothiocyanate–diethylaminoethyl–dextran (FITC-DEAE-dextran) and fluorescein-isothiocyanate–carboxymethyl–dextran (FITC-CM-dextran) with MW 150 kDa were all purchased from Sigma-Aldrich (St. Louis, USA). Methylthiazolyldiphenyl-tetrazolium bromide (MTT reagent) was supplied by Sigma-Aldrich (St. Louis, USA). Lipopolysaccharides (LPS) from *Salmonella enterica* serotype Minnesota were purchased from Sigma-Aldrich (St. Louis, USA). Protease inhibitor cocktail containing 4-(2-aminoethyl)benzenesulfonyl fluoride hydrochloride (AEBSF) at 2 mM, Aprotinin at 0.3 μ M, Bestatin at 116 μ M, trans-Epoxy succinyl-L-leucylamido(4-guanidino)butane (E-64) at 14 μ M, Leupeptin at 1 μ M and Ethylenediaminetetraacetic acid (EDTA) at 1 mM was purchased from Sigma-Aldrich (St. Louis, USA) Porcine tumor necrosis factor alpha ELISA kit was received from Sigma-Aldrich (St. Louis, USA). Hematoxylin-eosin (H&E) fast staining kits were purchased from Carl Roth (Karlsruhe, Germany). Dulbecco minimum essential media (DMEM), fetal bovine serum (FBS) and penicillin plus streptomycin were obtained from Biochrom (Berlin, Germany). Chemicals for preparation of buffers were of analytical grade. Deionized water was used throughout the experiments. Pig feet of Class E pigs (Regulation EU No 1308/2013), 5-7 months old, following the routine slaughtering procedure, were obtained from a local commercial slaughterhouse.

4.5.2 Ex-vivo transsynovial permeation model

4.5.2.1 Synovium explant harvest

On the day of slaughter for human consumption, lower limbs from domestic pigs were received prior to each experiment and synovial tissue was contiguously dissected from the articulation metacarpophalangeus. To do so a dorsal incision was made approximately 1 cm proximal to the metacarpal heads. Skin and subcutaneous fat layers were elevated, and extensor tendons and ligaments were transected. Following careful removal of loose areolar tissue, exposed synovial membrane separated by a sagittal ridge, was dissected undermining the synovium in that area. The tissue was attached to a thin ring to avoid movement during the permeation test and thickness was measured using a Mitutoyo Absolute indicator (Mitutoyo, Neuss, Germany). The tissue was stored in phosphate-buffered saline (PBS) at 4 °C until the start of experiment (< 30 min).

4.5.2.2 Franz-cell experiments

The permeation experiments were performed on custom-made Franz cells with an orifice diameter of 1.0 cm, resulting in a total diffusional area of 0.785 cm². Basolateral- and luminal-representing chambers were divided by the harvested porcine synovium and two thin foamed Teflon seals. The Franz cells were adjusted to 37 ± 0.5 °C and PBS buffer (pH 7.4) was used as acceptor fluid unless otherwise stated. The basolateral side consists of 5.0 ml acceptor fluid stirred at 150 rpm. To prevent bacterial growth during the experiment, 0.05% sodium azide was added to the buffer. Sample solutions, each containing differently sized or charged FITC-dextrans (FITC-dextran 10, 40, 70, 150 kDa, negatively charged FITC-CM-dextran 150 kDa and positively charged FITC-DEAE-dextran 150 kDa) or fluorescein sodium (SM) were prepared at a concentration of 2.5 mg/ml in PBS buffer. 0.2 ml of fluorescently labeled analyte was added to the luminal side of the membrane to start the permeation test. Sink conditions were maintained as the dextran concentration in the basolateral chamber did not exceed 10% of its saturation solubility. For comparison, all dextrans, as well as fluorescein sodium, were additionally tested using an artificial Whatman® polycarbonate filter membrane by Sigma-Aldrich (St. Louis, USA) with a pore size of 50 nm under the same conditions. To identify the influence of the explant cell viability on the transsynovial permeability, permeation profiles of differently treated synovium explants were compared. Non-viable tissue was obtained by devitalization with 10% sodium azide [26]. Full viability, as preliminarily identified (see below), was

4 An ex-vivo model for transsynovial drug permeation of intraarticular injectables in naive and arthritic synovium

reached by replacing the fluid in the acceptor chamber by DMEM. 10 kDa and 150 kDa FITC-dextran, representing the smallest and largest macromolecules tested, were analyzed, and compared to the results of untreated synovium in previous experiments. The luminal compartment was sealed by parafilm to minimize evaporation effects. 0.5 ml samples were withdrawn from the basolateral chamber by a 1.0 ml syringe at predetermined intervals and replaced with acceptor fluid. Fluorescence quantification was performed utilizing a plate reader (PerkinElmer Victor Multilabel reader) at an excitation of 485 nm and an emission of 535 nm for fluorescein labeled molecules. Since analyte is removed from the acceptor chamber with each sample draw, the cumulative amount permeated is calculated from

$$M_i = V_s \sum_{i=0}^{t-1} C_{i-1} + V_A C_t$$

where, V_A is the total volume of the acceptor chamber, C_t is the concentration at each sampling time, V_s is the volume of the withdrawn sample and C_i represents the concentration of analyte at time i . The cumulative mass was then divided by the total diffusional area (0.785 cm^2) for normalization. Plots of cumulative amount permeated per area against time were derived and the percentage permeation amount of the applied dose was calculated. The fluxes were from the slope calculated by linear regression interpolation of the experimental data at steady state, hence describing the mass per time and area diffused across the membrane in $\mu\text{g}/(\text{cm}^2 \cdot \text{h})$. The flux is considered as a surrogate parameter for the permeability of the synovial membrane to a specific substance.

4.5.2.3 Viability test

Synovial membrane was assayed for viability by measuring tetrazolium reductase activity, which reflects the number of viable cells present. Harvested tissue sized approximately 1 cm in diameter was weighed and placed into a vessel containing either PBS buffer or DMEM, 10% FBS, penicillin and streptomycin. Analogous to the total time of permeation experiments, incubation time was set 0 h, 24 h or 48 h at $37 \pm 0.5 \text{ }^\circ\text{C}$. Media was subsequently replaced by 1 mg/ml MTT reagent and samples were incubated for 2 h at $37 \pm 0.5 \text{ }^\circ\text{C}$. The explant was placed into 3 ml dimethyl sulfoxide (DMSO) and disintegrated with the IKA Ultra Turrax (Staufen, Germany). Following centrifugation, the supernatant absorption was detected at 540 nm. For positive control, viability was determined immediately after dissection without further treatment steps. As a negative control, tissue discs were

4 An ex-vivo model for transsynovial drug permeation of intraarticular injectables in naive and arthritic synovium

devitalized by 10% sodium azide and subsequently treated in the exact same manner. Sodium azide is an inhibitor of the mitochondrial respiratory chain and induces apoptosis at the given concentration [26]. Results were normalized by tissue weight. Mean viability was calculated from 5 samples for each treatment. Results were expressed as the percentage of positive control after subtraction of the negative control, which was considered 100%, as no absolute viability of cells can be estimated in tissue samples via MTT assay.

4.5.3 Incubation of synovium with LPS and analysis of inflammatory response

Harvested synovial tissue explants were weighed and incubated with either 1 µg/ml, 5 µg/ml, 10 µg/ml or 20 µg/ml LPS for 24 h at 37 ± 0.5 °C. For viability testing explants were incubated in PBS for 24 h or 48 h at 37 ± 0.5 °C after LPS incubation. Subsequently an MTT assay was performed analogous to naive tissue viability test. Sampling intervals were after 0 h, 24 h in LPS, and after 24 h (48 h total) and 48 h (72 h total) in PBS. Additionally, naive synovial membrane was compared to LPS inflamed tissue by histological image analysis. The tissue was fixed in 4% phosphate-buffered formaldehyde solution for 24 h. After dehydration in increasing ethanol concentrations, xylol and paraffin, the sample was embedded into a paraffin block. Thin cross sections (4 µm thickness) were cut with a Leica RM 2155 (Wetzlar, Germany) microtome and stained subsequently to hydration with hematoxylin and eosin according to the manufacturer recommendations. Microscopic examination was performed with a Leica DM 2700 M (Wetzlar, Germany) microscope. TNF-alpha was quantified following incubation with 0, 1, 5, 10 and 20 µg/ml LPS for 24 h at 37 °C in DMEM+FBS. Sampling intervals were equal to those of the viability test. TNF-alpha was consecutively quantified using a porcine tumor necrosis factor alpha ELISA Kit. The assay was performed according to the manufacturer's instructions and results were normalized by explant's weight (concentration per gram explant) and cell viability (%). Mean TNF-alpha concentration was calculated from four samples for each treatment. For assessment of the transepithelial electrical resistance (TEER) synovial explant (n=6) was attached to a Corning Costar Transwell 6.5 mm insert. For incubation 0.6 ml of DMEM+FBS as a control, LPS 10 µg/ml or 20 µg/ml in DMEM was added per well and 0.1 ml of the respective media was added into the insert. Incubation was performed analogous to the permeation test for 24 h at 37 ± 0.5 °C. After equilibration electrical resistance was measured using a Millicell-ERS2 (Merck, Germany) at predetermined

4 An ex-vivo model for transsynovial drug permeation of intraarticular injectables in naive and arthritic synovium

intervals. TEER values for each group were averaged and data was expressed in Ω/cm^2 and normalized by the baseline resistance values.

4.5.3.1 Dependency of transsynovial permeation on inflammation of explant

After incubation with 10 $\mu\text{g}/\text{ml}$ LPS for 24 h, which preliminarily indicated favorable inflammatory response (see below), synovial permeability was tested using inflamed tissue. All FITC-dextrans and derivatives tested above, as well as fluorescein sodium, were analyzed and compared to the results obtained using naive explant. 150 kDa FITC dextran was additionally tested using synovium incubated by either 1 $\mu\text{g}/\text{ml}$, 5 $\mu\text{g}/\text{ml}$ or 20 $\mu\text{g}/\text{ml}$ for 24 h to mimic different degrees of inflammation and its effect on transsynovial permeation. To evaluate the hypothesis of ECM depletion by catabolic enzymes as the main cause for altered permeation in the synovitis model, protease inhibitors at the given concentration were added to the incubation media containing 10 $\mu\text{g}/\text{ml}$ or 20 $\mu\text{g}/\text{ml}$ LPS and permeability was tested subsequently using 150 kDa FITC-dextran. The resulting permeation profile was compared to naive synovium and inflamed tissue, respectively.

4.5.4 *In-vivo-in-vitro*-correlation (IVIVC)

To establish a level A correlation, IVIVC literature data of intraarticular injected FITC-dextrans (10 kDa and 500 kDa) into healthy rats [27] was used and correlated with corresponding data from the same molecules in our *ex-vivo* or *in-vitro* artificial membrane model. For the *in-vivo* data, *in-vivo* elimination in percent was obtained by calculating the reciprocal value of the normalized fluorescence intensity in the joint gap as measured by *in-vivo* imaging. *In-vivo* elimination in percent was drawn against cumulated amount permeated *ex-vivo* in a Levy-Plot was fitted to correlate the corresponding times [28]. The Levy-plot generate a time scaling factor for the *ex-vivo* permeation data. Time scaled values were interpolated using a four-parameter logistic regression to calculate interrelated time scaled *ex-vivo* values. These were plotted against *in-vivo* elimination to obtain a Level A IVIVC, which was analyzed by linear regression. All calculations were performed using GraphPad Prism 8.

4.5.5 Statistical analysis

Data was presented as mean \pm standard deviation. Comparison of permeation profiles was assessed using their flux within the linear region as calculated from linear regression. Statistical significance was determined by one-way analysis of

variance test (one-way ANOVA) followed by either Dunnett's or Tukey-Kramer multiple comparison test. Differences were considered significant at $p < 0.05$. Statistical analysis was performed using GraphPad Prism 8 software.

4.6 Results

4.6.1 Characterization of the transsynovial permeation model

Average harvested porcine synovial tissue thickness was measured $272 \pm 85 \mu\text{m}$. The explant was assayed for cell metabolic activity by measuring enzymatic reduction of tetrazolium dye MTT, which reflects the number of viable cells present. The untreated synovial tissue measured immediately after dissection, which served as a positive control, showed an UV-absorption of 0.381 ± 0.071 in the colorimetric assay after normalization by tissue weight and was set as 100% viability after subtraction of the negative control which measured approximately 0.053 ± 0.007 . Following incubation in PBS-buffer, viability dropped significantly within 24 h ($p < 0.05$) to about 50% (**Fig. 4-1**), compared to positive control. No further significant decline was observed after 48 h, but viability stayed at a proportionate level. In contrast, no significant change ($p > 0.05$) was found throughout the whole experiment when the explant was incubated in DMEM + 10 % FBS.

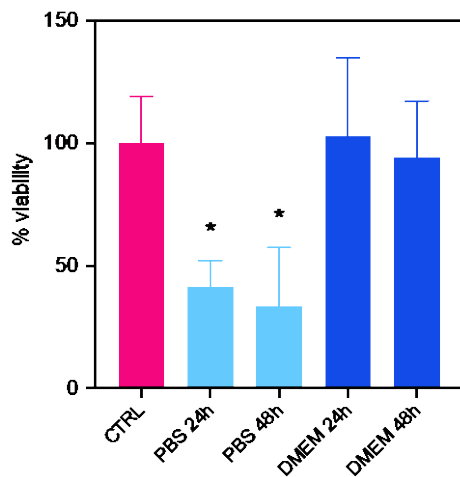


Fig. 4-1: Viability changes of synovium samples in percent of positive control at 37 °C in different media after 24 h and 48 h. * $p < 0.05$ vs CTRL.

As depicted in **Fig. 4-2**, cumulative amount permeated from luminal to basolateral chamber of the test system was found to depend on the molecular weight of the analyte. Fluorescein sodium, as a model substance for small molecules, was the

4 An ex-vivo model for transsynovial drug permeation of intraarticular injectables in naive and arthritic synovium

only sample to completely permeate the tissue within 48 h of measuring. The fluorescein sodium flux was significantly different from tested dextrans ($p < 0.05$). Overall, flux for all FITC-dextrans sequentially decreased with increasing molecular weight. Permeation of 500 kDa FITC-dextran was measured for correlation with *in-vivo* elimination data and was found to permeate slightly slower than the 150 kDa FITC-dextran (**Sup. Fig. 4-1**). Permeation of charged dextran derivatives is depicted in **Fig. 4-3**. Diffusion of anionic FITC-CM-dextran was faster compared to unmodified FITC-dextran, but the difference was not significant. FITC-DEAE-dextran was observed to diffuse through the synovial membrane at not more than 5 % within 48 h, resulting in a considerably slower permeation, when compared to the other derivatives ($p < 0.05$). No significant difference ($p > 0.05$) could be found, when comparing the permeability using DMEM as acceptor fluid or devitalized tissue, to data generated using PBS as acceptor phase (**Fig. 4-4**). Neither 10 kDa FITC-dextran nor 150 kDa, representing the smallest and largest macromolecule tested, showed any impact of cell viability on diffusion respectively. To evaluate the differences of the *ex-vivo* model compared to frequently used artificial membranes, the measured fluxes were normalized and plotted against the normalized fluxes obtained from the artificial 50 nm polycarbonate membrane. As **Fig. 4-5** shows, the use of an artificial membrane can over-estimate effective drug clearance from the joint concerning their relative quantities. The scatter plot indicates a poor correlation of fluxes, reflected by the goodness of fit for the linear regression ($R^2 = 0.7502$).

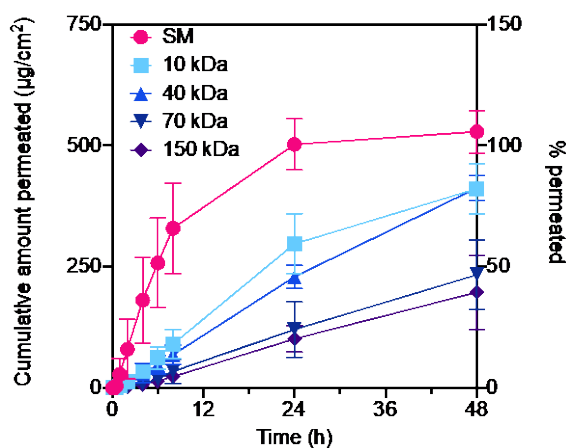


Fig. 4-2: Cumulative amount permeated of differently sized dextrans (10 kDa, 40 kDa, 70 kDa and 150 kDa FITC-dextran) and fluorescein sodium (SM).

4 An ex-vivo model for transsynovial drug permeation of intraarticular injectables in naive and arthritic synovium

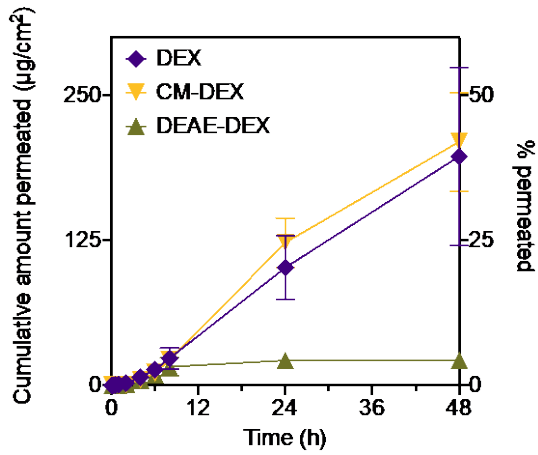


Fig. 4-3: Cumulative amount permeated of negatively charged 150 kDa FITC-CM-dextran and positively charged 150 kDa FITC-DEAE-dextran as compared to uncharged 150 kDa FITC-dextran.

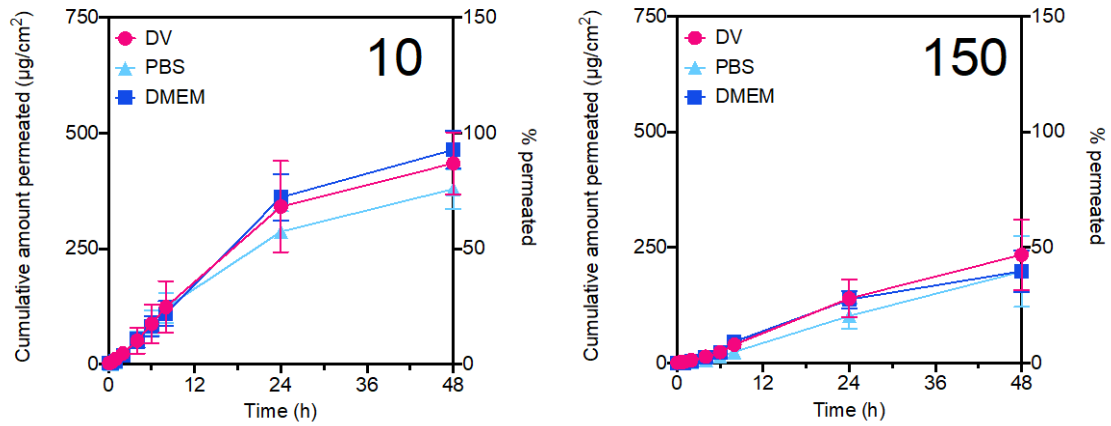


Fig. 4-4: Permeation data comparing devitalized tissue (DV) and experiments using either DMEM (fully viable over 48 h) or PBS (partly viable over 48 h) as acceptor fluid. No significant differences could be seen ($p < 0.05$) for 10 kDa FITC-dextran (**10**) and 150 kDa FITC-dextran (**150**).

4 An ex-vivo model for transsynovial drug permeation of intraarticular injectables in naive and arthritic synovium

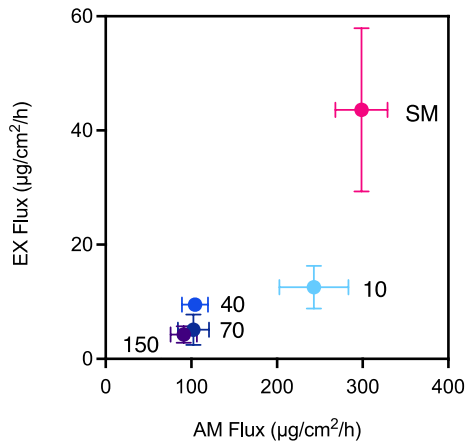


Fig. 4-5: Scatter plot of flux in synovial explant (EX) and corresponding data with an artificial polycarbonate membrane (50 nm) (AM). FITC dextrans ranging from 10 – 150 kDa as well as fluorescein sodium (SM) were evaluated. Linear regression ($R^2 = 0.7502$) reflects poor correlation of size discrimination.

4.6.2 Characterization of the transsynovial permeation of the ex-vivo synovitis model

The metabolic activity of the cells was measured using the MTT assay as a surrogate for viability after LPS treatment. The positive control corresponding to freshly dissected synovial tissue showed an absorption of 0.429 ± 0.078 , which was normalized as 100% viability after subtraction of the negative control which measured 0.052 ± 0.006 . No significant reduction of cell survival was observed when incubated in DMEM+FBS, showing an average viability close to 100 % after 24 h ($p > 0.05$). LPS incubation for 24 h led to concentration dependent decline in viability, being significant for concentrations larger than 5 µg/ml ($p < 0.05$). Values were found ranging from 90% viability (1 µg/ml) to approx. 60% viability for 20 µg/ml (**Fig. 4-6**). After a media change and another 24 h of incubation in PBS, viability of all samples including control dropped significantly to approximately 50%, to 35% viability ($p < 0.05$). Yet, except for 10 µg/ml LPS, no significant difference ($p > 0.05$) was observed compared to 0 µg/ml LPS at the same time, though the average values tended to decrease with increasing LPS concentration. Another decrease of viability was assessed after 48 h in PBS, where control was measured to be 45% viable at the end of the test and all LPS concentrations showed comparable viabilities around 30% to 25%, again being significantly lower than positive control ($p < 0.05$). **Fig. 4-7** shows concentration in ng/ml of TNF-alpha normalized by weight of synovial explant (concentration per gram of explant) and viable cells (%). TNF-alpha was shown to be significantly increased for all concentrations of LPS after 24 h of incubation ($p < 0.05$). During the subsequent permeation test, incubation time is prolonged

for another 48 h, which culminates in a further rise of TNF-alpha level for 10 and 20 µg/ml LPS at the measured timepoints. Overall, an increasingly LPS-dependent segmentation of TNF-alpha concentrations can be observed over the course of the permeation test. As shown in **Fig. 4-8** TEER of naive synovium remained constant over a period of 24 h in DMEM, whereas LPS treated tissue electrical resistance decreased with increasing amount of LPS. Though a general trend could be observed, only the 24 h value of the 20 µg/ml LPS sample was significantly different to the control ($p < 0.05$) due to high variability of the measured data. As seen in **Fig. 4-9A** the H&E-stained naive synovial tissue slice exhibits the characteristic intimal cell layer of 1-4 cells covering a dense extracellular matrix of collagenous network. Few cells and occasional blood vessels are visible within the subintimal matrix. The *ex-vivo* synovitis (10 µg/ml LPS for 24 h) slice (**Fig. 4-9B**) shows no signs of hyperplasia of the intimal layer. Clustering and infiltration of cells into the ECM as well as tissue defects were observed in some samples. However, due to high interindividual variability within all samples, a valid assessment of the *ex-vivo* inflammatory state of the tissue by image analysis remains difficult.

4.6.3 Transsynovial permeability from synovitis model

Following incubation with 10 µg/ml LPS for 24h, FITC-dextran, derivatives and fluorescein sodium were tested to elucidate the impact of inflammation on the permeation profile (**Fig. 4-10**). No significant change was detected for the smaller sized molecules, although a small acceleration was observed ($p > 0.05$). The molecular radius is the most relevant factor that defines passive diffusion through the joint. Increasing molecular radii led to an asymptotic decrease in flux in both naive and synovitic synovium. However, large macromolecules, especially 150 kDa FITC-dextran but also 70 kDa FITC-dextran and 40 kDa FITC-dextran, diffused through the inflamed synovium significantly faster when compared to naive tissue ($p < 0.05$) (**Fig. 4-11A**). In conclusion, a sequential size-discriminate effect was observed within the range of tested molecules. These findings become more apparent when comparing the respective flux ratios, indicating an up to approximately 2.5-fold acceleration of permeation in inflamed tissue (**Fig. 4-11B**). No differences were observed for the positively charged DEAE-FITC-dextran, whereas the negatively charged CM-FITC-dextran was affected similarly as the uncharged FITC-dextran (**Fig. 4-10**). Since large molecules depict most considerable differences in permeation with 10 µg/ml, 150 kDa FITC-dextran was chosen for additional investigation of different synovitis degrees induced by

4 An ex-vivo model for transsynovial drug permeation of intraarticular injectables in naive and arthritic synovium

increasing LPS concentrations (**Fig. 4-12A**). LPS concentrations of 5 $\mu\text{g/ml}$ or greater entail a significant rise in flux ($p < 0.05$) as compared to the naive control, and an overall trend of concentration-dependent sequential arrangement was observed, although not all concentrations were significantly different from each other ($p > 0.05$). Low-grade inflammation already leads to a significant rise in flux, depicted by the respective flux ratio (**Fig. 4-12B**). Acceleration culminates in a 3.7-fold flux rise after incubation with 20 $\mu\text{g/ml}$ LPS. As shown in (**Fig. 4-12C+D**) the addition of protease inhibitors to the 10 and 20 $\mu\text{g/ml}$ LPS incubation media was able to prevent acceleration of the 150 kDa FITC-dextran permeation and resulted in fluxes not significantly different to the naive synovium flux ($p < 0.05$). Though both concentrations showed the same trend, differences in flux between LPS incubation with and without protease inhibitor were only significant for the 20 $\mu\text{g/ml}$ LPS concentration ($p < 0.05$).

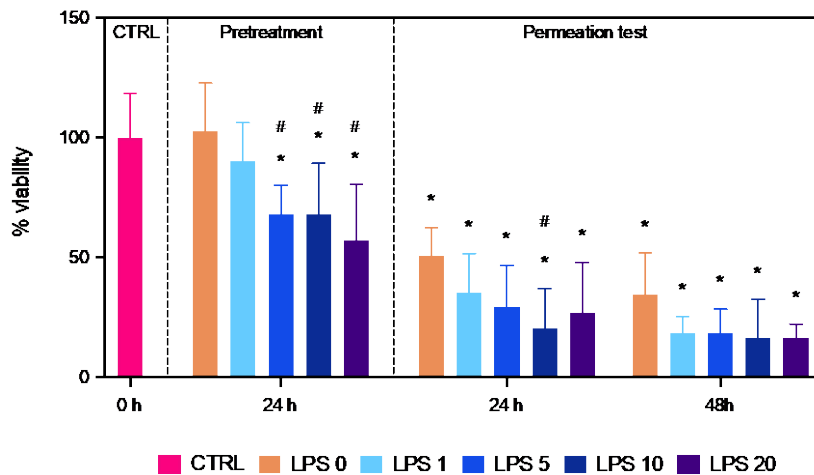


Fig. 4-6: Viability changes of explant after incubation with 1 $\mu\text{g/ml}$, 5 $\mu\text{g/ml}$, 10 $\mu\text{g/ml}$ and 20 $\mu\text{g/ml}$ LPS for 24 h and during subsequent permeation test, where PBS presents surrounding media at the timepoints 24 h (48 h total) and 48 h (72 h) in percent of positive control. * $p < 0.05$ vs CTRL; # $p < 0.05$ vs. LPS 0 incubated for the same time.

4 An ex-vivo model for transsynovial drug permeation of intraarticular injectables in naive and arthritic synovium

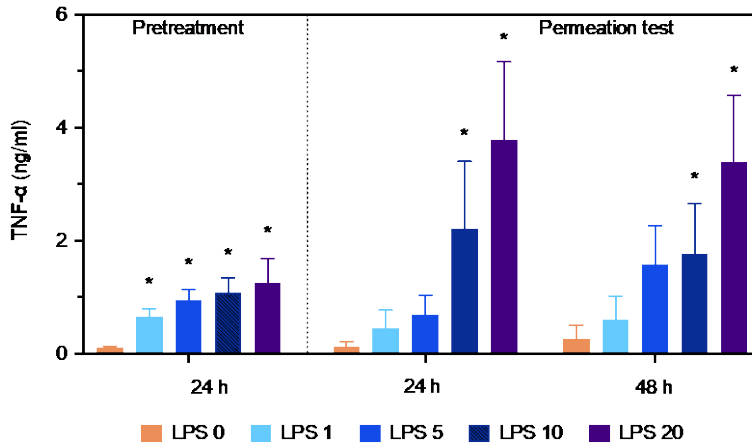


Fig. 4-7: Concentration of TNF-alpha normalized by weight of tissue (concentration/gram explant) and viable cells (%) as observed in negative control (LPS0) and after LPS incubation with 1 $\mu\text{g/ml}$, 5 $\mu\text{g/ml}$, 10 $\mu\text{g/ml}$ and 20 $\mu\text{g/ml}$ for 24 h in DMEM and during subsequent permeation test, where PBS presents the surrounding media after 24 h (48 h total) and 48 (72 h); * $p < 0.05$ vs. LPS 0 incubated for the same time.

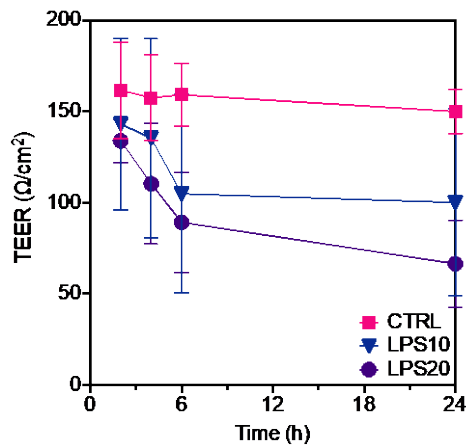


Fig. 4-8: TEER measurement of naive tissue and LPS 10 $\mu\text{g/ml}$ and 20 $\mu\text{g/ml}$ treated synovium over 24 h.

4 An ex-vivo model for transsynovial drug permeation of intraarticular injectables in naive and arthritic synovium

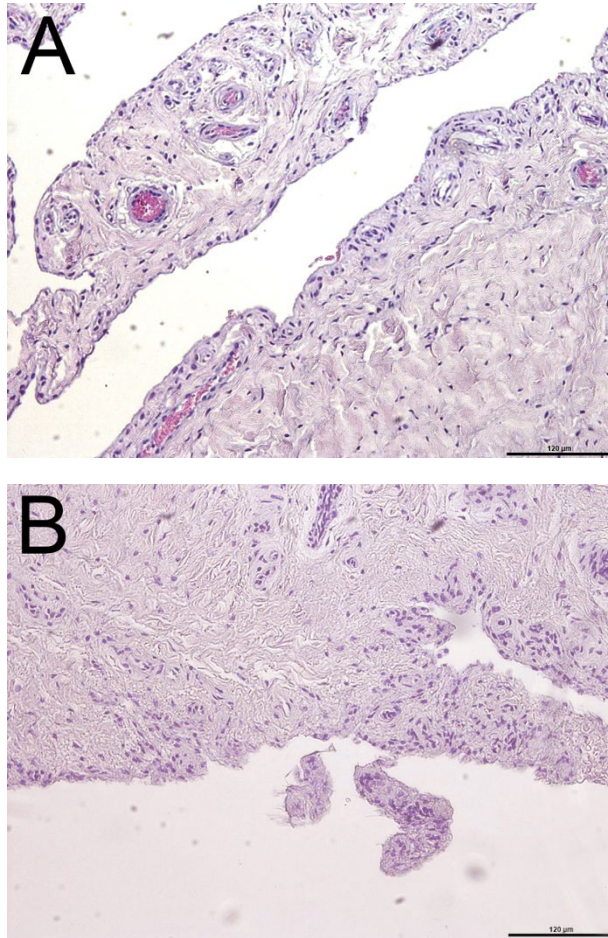


Fig. 4-9: H&E-stained synovial tissue. Histological appearance of naive explant (**A**) and 10 µg/ml LPS incubated (24 h) synovium (**B**). Scale bars are 120 µm.

4 An ex-vivo model for transsynovial drug permeation of intraarticular injectables in naive and arthritic synovium

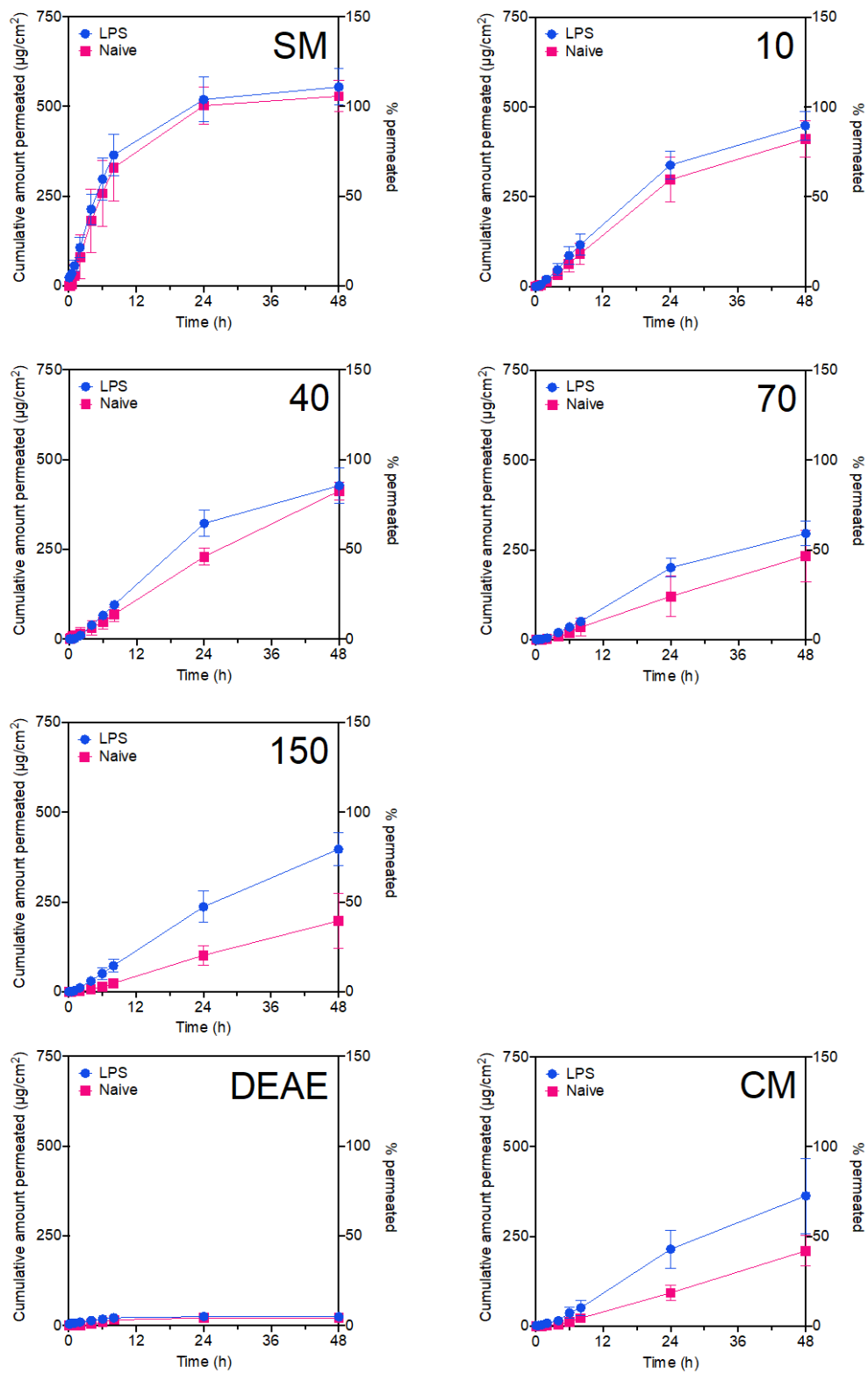


Fig. 4-10: Comparison of dextran permeation in naive tissue and 10 µg/ml LPS ex vivo inflamed (24 h) explant for fluorescein sodium (**SM**), 10 kDa (**10**), 40 kDa (**40**), 70 kDa (**70**), 150 kDa FITC-dextran (**150**), 150 kDa FITC-DEAE-dextran (**DEAE**) and 150 kDa FITC-CM-dextran (**CM**).

4 An ex-vivo model for transsynovial drug permeation of intraarticular injectables in naive and arthritic synovium

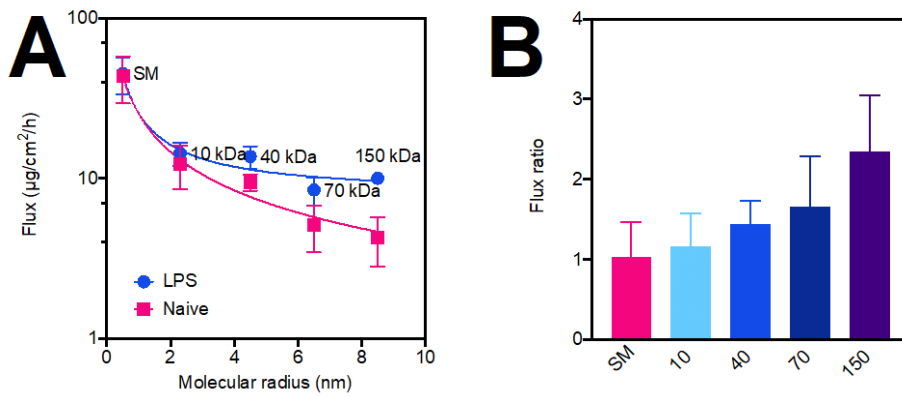


Fig. 4-11: (A) Rise in divergence from pathologic to naive flux with increasing molecular size becomes perceptible when molecular radius is plotted against flux for arthritic and naive synovium. **(B)** Flux ratio, describing the relative acceleration of permeability for differently sized dextrans (SM=fluorescein sodium; 10-150 kDa FITC-dextrans).

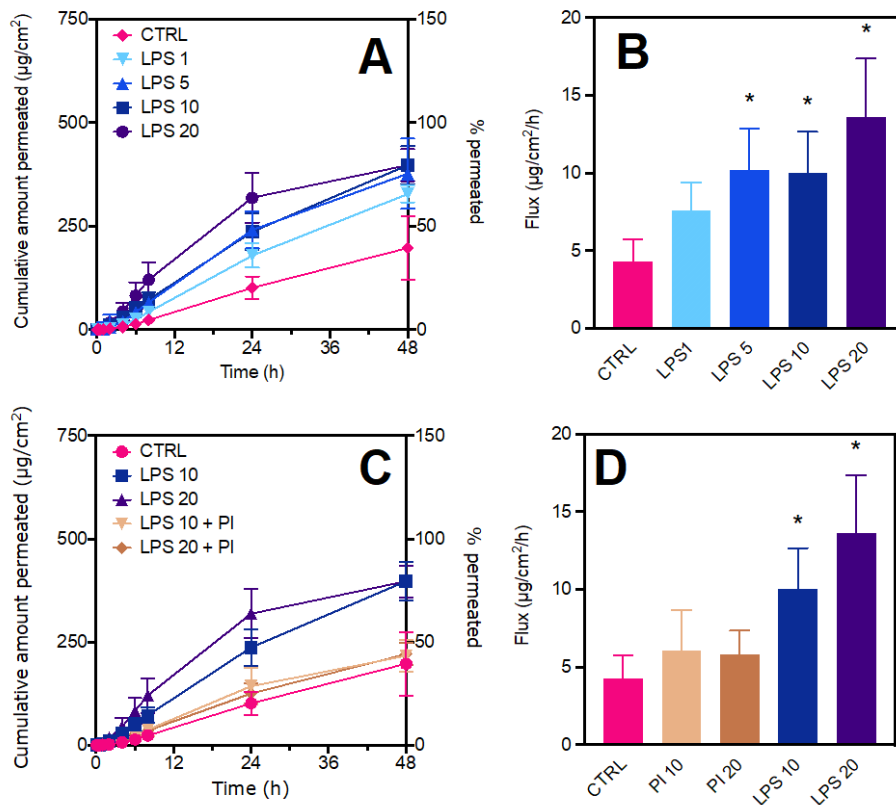


Fig. 4-12: (A) Cumulative amount permeated of 150 kDa dextran in naive tissue and in different stages of arthritic synovium as induced by increasing concentrations of LPS (µg/ml) *ex-vivo*. **(B)** Flux for 150 kDa FITC-dextran, describing the acceleration of permeation for different concentrations of LPS (µg/ml) to mimic increasing grades of synovitis in comparison to naive explant flux. * $p < 0.05$ vs CTRL **(C)** Cumulative amount permeated of 150 kDa dextran in naive tissue and in arthritic synovium as induced by LPS (10 and 20 µg/ml) *ex-vivo* with and without addition of a protease inhibitors (PI). **(D)** Flux of 150 kDa FITC-dextran, describing the acceleration of permeation after LPS (µg/ml) incubation with and without addition of a protease inhibitors in comparison to naive explant flux. * $p < 0.05$ vs CTRL.

4.7 Discussion

Viability of the synovial explant was assessed in this *ex-vivo* model using a metabolic activity assay. While no reduction of viability was observed using DMEM + FBS, viability dropped significantly when PBS was used as the fluid. Similar results were observed in previous studies showing more than 80-90% of equine synovium to be viable after several days of culturing in DMEM [29,30]. However, in consecutive tests, permeability of differently sized dextrans (10 kDa and 150 kDa) appeared to be independent from the state of synovial viability, confirming PBS as a suitable acceptor receptor fluid for non-metabolic preparations according to the OECD guidelines [31]. These findings are in line with the theory of molecular sieving by the porous synovial extracellular network rather than cellular processes or intercellular junctions [32]. Yet, viable synovial cells offer the prospect of biochemical intervention prior to or during the permeation testing to modify the permeation model according to the experimental objective. Elimination of macromolecules from the joint gap was often described as a non-selective bulk flow into lymphatics [33]. However, more recent studies investigating the *in-vivo* clearance of differently sized macromolecules [34,35] report size discriminative transport profiles. Differences in clearance of macromolecules may have been underestimated due to complex measurability and distinction of *in-vivo* joint-elimination. *Ex-vivo* experiments allow a reduction of interference factors and a simplification of experimental setup and analytics, that allow a more isolated observation of synovial permeability. Dextrans are strongly hydrophilic molecules, and their permeation profile is mainly driven by passive diffusion and convection. Linear kinetics were found for all tested substances until approaching the end of luminal drug depot. Given that transsynovial permeability for uncharged molecules relies on steric exclusion defined by the dense extracellular matrix, differentiation by molecular size of the analyte could be expected. To assess if the *ex-vivo* model is biorelevant, the results of the size-dependent permeation (10 kDa and 500 kDa) *ex-vivo* were correlated to intraarticular elimination of dextrans of the same size after injection into naive rat joints as reported by Mwangi et al. [27]. A good correlation ($R^2 = 0.9551$) was received from the establishment of a linear level A *in-vitro-in-vivo*-correlation (IVIVC) (**Fig. 4-13A**). The IVIVC supports similar relative permeation or elimination rates in both systems and therefore the transferability of the results. However, *in-vivo* clearance appears to be considerably faster than the measured *ex-vivo* permeability, necessitating the application of a Levy-plot and consequential time scaling for predictive assessments. Differences to diffusion

times *in-vivo* are believed to derive from varying interspecies concentration-to-surface ratios and diverging thickness of tissue as well as the lack of intraarticular pressure and joint movement. Comparably good correlation could not be achieved using the artificial membrane ($R^2 = 0.9066$), which thus appears to have a lower relevance of the results for *in-vivo* prediction of the joint residence time (**Fig. 4-13B**). The dextrans tested represent the size range of potential drugs for OA treatment and suggest high molecular weight macromolecules as promising candidates for prolonged joint residence, as these exhibit fluxes more than 10-times slower than small molecules. The estimated clearance of differently sized proteins *in-vivo* confirms the determined results and consequently the *ex-vivo* model applicability for permeation testing [35]. The measured *ex-vivo* permeation was compared with an artificial membrane of 50 nm pore size, which was assessed by a previous study to most appropriately mimic synovial retention of macromolecules [36]. Despite these findings, the poor goodness of fit of the linear regression in the respective scatter plot reflects the inaccuracy of measuring joint residence time of differently sized molecules using an artificial membrane. This is especially true for the 10 kDa-sized macromolecules, indicating a divergence in molecular cutoff of the different membranes. The observed discrepancies are probably due to the inability of the artificial membrane to represent the *in-vivo* complexity of nanosized biostructures, multi-layer architecture and physiological properties, making it a less appropriate research tool for clearance screening of differently sized analytes. However, it should be noted that diverging thickness of the synovium as a result of the operating procedure leads to longer permeation times and herein higher apparent residence times. High molecular weight molecules will be more affected than low molecular weight molecules, which makes it challenging to translate results across laboratories or species. This challenge is seen as a disadvantage to commercially available artificial membranes, which tend to generate more reproducible results. To overcome this issue, normalization through standard molecules and standardized techniques as performed in this work may be applied. Chemical modified derivatives of 150 kDa dextran, that contain negatively (FITC-CM-dextran) or positively (FITC-DEAE-dextran) charged functional groups were used to investigate the influence of analyte charge on the transsynovial permeation. For the polyanionic CM-Dextran no difference could be observed compared to uncharged dextran. Though the FITC molecule itself is negatively charged already, a further increase of the negative net charge by introduction of the carboxymethyl-group does not appear to significantly influence the permeability. In contrast, cationic FITC-DEAE-

4 An ex-vivo model for transsynovial drug permeation of intraarticular injectables in naive and arthritic synovium

Dextran exhibited considerable reduction in permeability. The anionic extracellular matrix of the synovium, as well as the polarization layer formed by secreted glycosaminoglycans, creates a high negative fixed charge density barrier. As a result, strong association due to electrostatic interaction hinders the permeation of the molecule through the synovium. This effect has previously been described for the penetration into articular cartilage, where molecules appear to either penetrate facile with low cationic net charge or being trapped in superficial zones with a high molecular net charge [37]. These findings appear to be true for the synovial membrane, likewise, as was shown in the permeation experiments and confocal laser scanning microscopy (Data not shown). Both cationic and anionic charge exhibited comparable effects on the diffusion of 150 kDa dextrans in vitreous humor [38], indicating the presence of glycosaminoglycans as the main influence of the electro-diffusive permeation. Since viable cells provide the potential application of biochemical alteration, a pathologic synovitis model to mimic the permeability of an arthritic joint was developed by inflammation of the explant and subsequent permeation testing. The synovial explant was inflamed using LPS, which has previously been shown to increase cytokines in *ex-vivo* synovium [39]. TNF-alpha was chosen as marker cytokine to indicate the degree of inflammation, as it is known to play a key role in the pathology of arthritis [40]. TNF-alpha increased in a concentration-dependent manner, proving the presence of a strong inflammatory response. The increase was especially distinct for 10 µg/ml LPS and 20 µg/ml LPS. Corresponding TNF-alpha ranges were witnessed by *Lu et al.*, who further tested additional inflammatory markers to verify the LPS effect on the synovial explant [41]. As expected, no hyperplasia of the intimal layer was detectable by image analysis, as no cells can migrate into the tissue *ex-vivo*, and incubation time is insufficient for noticeable mitosis activity, which might be considered as a disadvantage of this model. However, as diffusion is believed to be determined by passive diffusion through the extracellular matrix, a change of the intimal layer thickness is believed to be a less relevant factor for drug permeation studies [21]. *In-vivo*, transsynovial influx from the blood capillaries into the synovial gap showed reduced selectivity of the membrane in arthritic state. Permeability to large molecules is increased, whereas smaller molecules are little affected [42]. Likewise, discrimination of macromolecular permeation was observed in the *ex-vivo* model. Despite differences not being as substantial as for the influx, synovitis may significantly affect the residence time of a locally injected therapeutic. Whereas smaller FITC-dextrans as well as fluorescein sodium were little affected

4 An ex-vivo model for transsynovial drug permeation of intraarticular injectables in naive and arthritic synovium

by the inflammatory state of synovium, increasing size of FITC-dextran corresponds with significantly increasing transsynovial permeation. These findings become more perceptible by calculating the flux ratio, which describes the relative acceleration of transsynovial flux from naive to inflamed state. Whereas small molecules result in a flux ratio of approx. 1.0, implying no flux increase due to immunogenic effects, 150 kDa dextran undergoes an approximately 2.5-fold acceleration when compared to naive synovium. In accordance, acceleration of clearance from synovitis was likewise proven by *in-vivo* studies for different proteins, being most significant for large molecular radii [24,35]. Depending on the state of disease and intraindividual manifestations, synovitis may arise from low-grade to highly inflamed states in arthritis. LPS has been shown to cause a defective barrier, which results in a concentration-dependent increase in transsynovial permeability. Even low-grade inflammations already showed a decisive acceleration with a 1.7-fold flux increase for 1 µg/ml LPS. Maximum increase was observed after incubation with 20 µg/ml with a 3.2-fold flux. These findings are in agreement with a study of protein clearance in canine joint synovitis [24], which describes a 2-3-fold increase in clearance for low-grade synovitis as found in arthritis. An increase of inflammatory permeability of cartilage was explained by a sharp rise of catabolic enzymes and glycosaminoglycan/collagen turnover in LPS treated cartilage within 24 h [43,44] leading to massive cartilage matrix break down through NF-κB and PI-3K pathways [45]. This hypothesis was tested for transferability to *ex-vivo* synovium by addition of a protease inhibitors to the LPS incubation media. Protease inhibitors were able to maintain a flux close to that of naive synovium, suggesting that the LPS treatment-induced permeability changes in our synovitis model may have their cause in the degradation of the extracellular matrix protein network by catabolic enzymes, which, along with glycosaminoglycans, are considered the main contributor to synovial hydraulic resistance [46]. Conversely, it was also reported that synovial enzymatic depletion of proteoglycans and glycoproteins leads to high rates of fluid and macromolecule loss in living joints [32]. Further effects such as LPS induced hyperpermeability of the fibroblast-like-synoviocytes [47] may play a contributory role. These effects were affirmed by the TEER measurements that likewise indicate an altered barrier function of the synovial membrane after exposure to LPS. However, it should be noted that the *ex-vivo* synovitis model cannot directly be translated to synovial clearance *in-vivo*, as not all pathologic changes that arise within the joint are covered. The observed impact of increased permeability of the synovial extracellular matrix as a diffusion

4 An ex-vivo model for transsynovial drug permeation of intraarticular injectables in naive and arthritic synovium

barrier is opposed by an impaired lymphatic drainage due to reorganization of lymphatic vessels [48] and hypertrophy, both of which extend the pathlength of diffusion (**Fig. 4-14**). With some studies conversely indicating a prolongation rather than acceleration [27], effective clearance may vary from the results presented herein, depending on specific state of disease, or applied pathologic model, as IA clearance increases at the onset of synovitis and then declines as inflammation progresses to a more chronic phase [49]. Nevertheless, the simulation of the pathologic synovial permeability allows potential benefits for formulation testing and rational development of new intraarticular therapeutics, by providing a more relevant model for the determination of drug elimination and assessment of retentive strategies, thereby reducing the need for animal experiments.

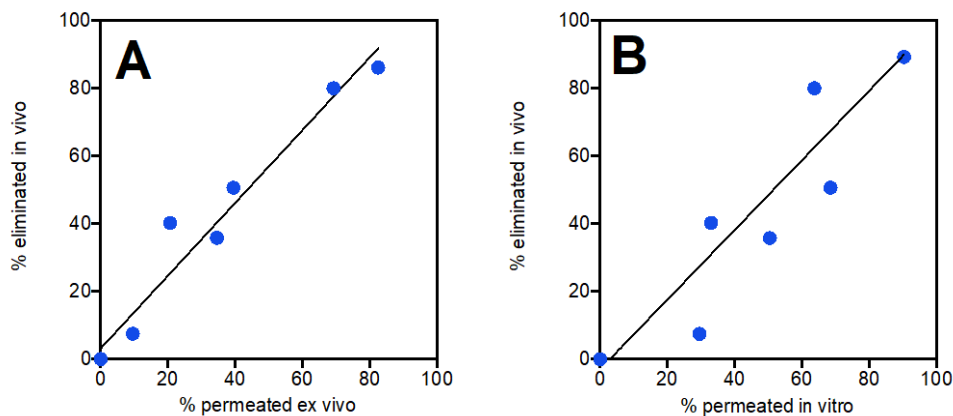


Fig. 4-13: IVIVC of 10 kDa and 500 kDa FITC dextran in the *ex-vivo* model (**A**) or the *in vitro* (artificial membrane) model (**B**) and as quantified via *in-vivo* imaging after injection into rat joints [27]. Time-scaling was performed using a Levy-plot (**Sup. Fig. 4-2**). *Ex-vivo*: $R^2=0.9551$, intercept=3.175, slope=1.076. *In-vitro*: $R^2=0.9066$, intercept=-2.991, slope=1.030

4 An ex-vivo model for transsynovial drug permeation of intraarticular injectables in naive and arthritic synovium

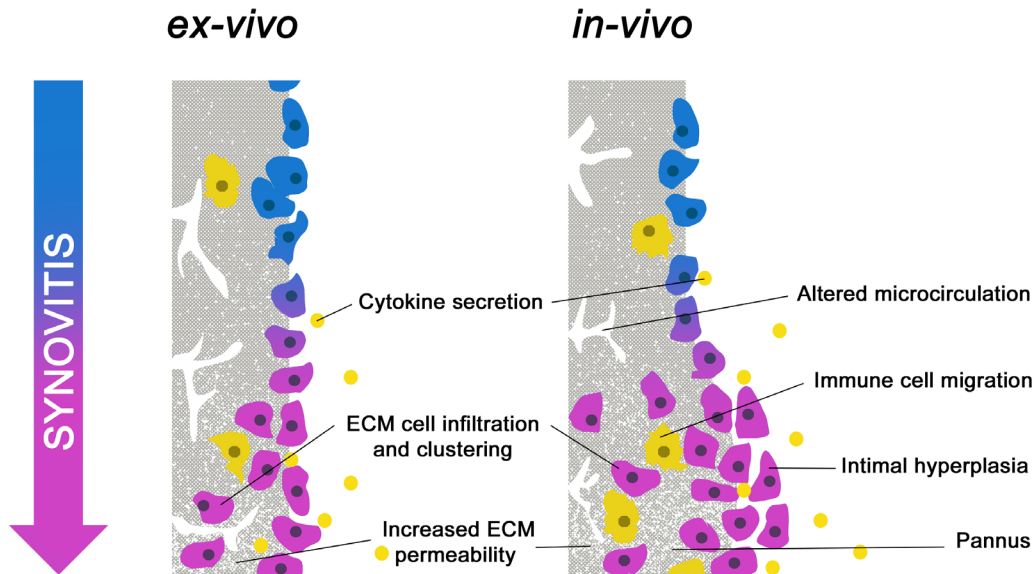


Fig. 4-14: Capabilities and limitations of the *ex-vivo* synovitis model derive from its resemblance of the pathologic processes observed *in-vivo*, as not all mechanisms may be mimicked within the model.

4.8 Conclusion

In this work, an *ex-vivo* synovial permeation model was employed as a promising tool for relevant assessment of the synovial permeability to macromolecules for early-stage development of IA injectables. With a level A IVIVC we were able to confirm that the *ex-vivo* model is able to partially simulate the *in-vivo* permeation and supports its biorelevance. Meanwhile, comparable results could not be provided by the artificial membranes, that lack the unique two-layered synovial architecture and the morphology of the extracellular matrix as diffusion barrier. Thus, an improved *ex-vivo* assessment and screening of promising drug candidates or formulations for IA injections is possible without the need for animal studies. The proposed model offers the ability to relevantly distinguish multiple physicochemical drug parameters and give a valuable insight into the transport mechanisms and clearance characteristics of tested IA injectables. Further, the use of viable synovial explants offers the prospect of a synovitis model for advanced permeability simulations, which cannot be done using artificial membranes. LPS has been shown to increase permeability, whereby this effect could be antagonized by protease inhibitors, suggesting that inflammation-related enzymatic catabolism may play a role in this process. Imitation of the pathological state within the proposed *ex-vivo* model therefore allows elucidation of

4 An ex-vivo model for transsynovial drug permeation of intraarticular injectables in naive and arthritic synovium

fundamental permeation kinetics and provides a more relevant insight into synovial permeability, as injections are ordinarily applied to pathologic joints.

4.9 Acknowledgements

Ferring Pharmaceuticals Inc. sponsored the research that is the subject of the manuscript. Employees of the sponsor were involved in the conceptualization and design of the study.

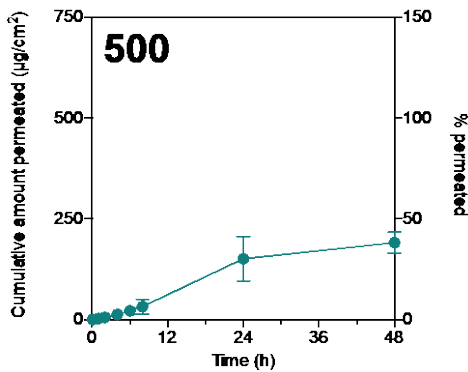
4.10 Author contributions

Conceptualization, T.S., A.La.; methodology, T.S.; software, T.S.; validation, T.S.; formal analysis, T.S.; investigation, T.S.; resources, A.La., J.L., A.Li., C.C.L.; data curation, T.S.; writing-original draft preparation, T.S.; writing-review and editing, T.S., A.La.; visualization, T.S.; supervision, A.La.; project administration A.La., J.L., A.Li., C.C.L.; funding acquisition, A.La., J.L., A.Li., C.C.L.

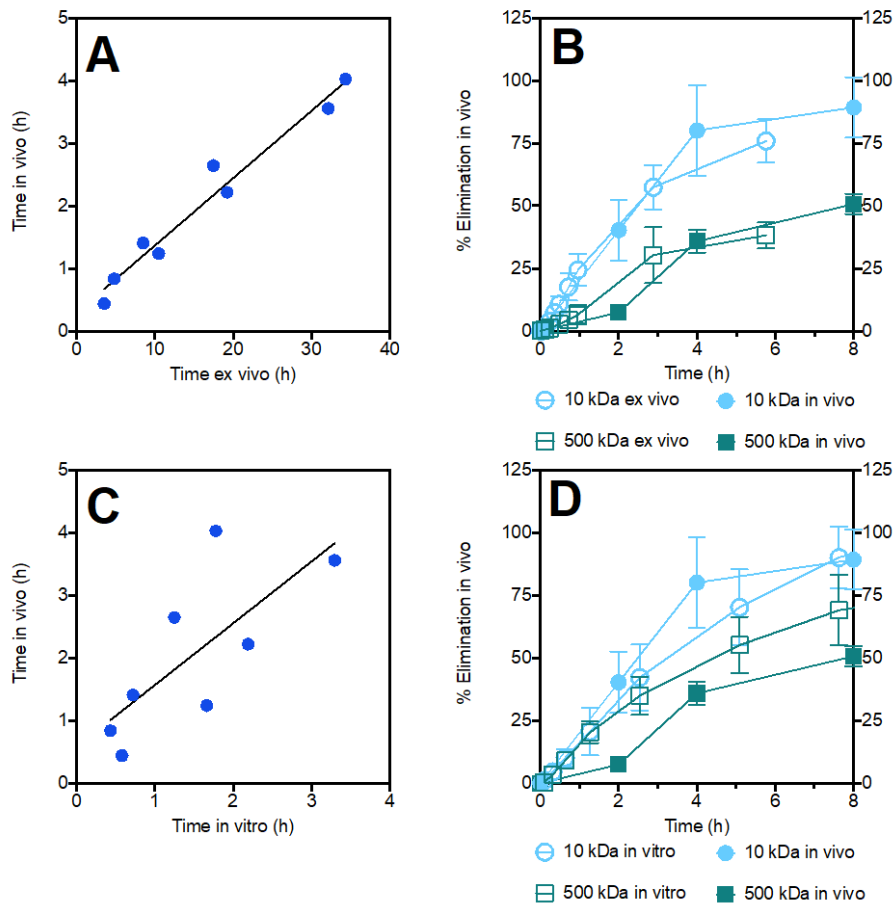
All authors have read and agreed to the published version of the manuscript.

4 An ex-vivo model for transsynovial drug permeation of intraarticular injectables in naive and arthritic synovium

4.11 Supplementary Data



Sup. Fig. 4-1 Cumulative amount permeated of 500 kDa FITC-dextran for IVIVC.



Sup. Fig. 4-2 (A) Levy Plot for *in-vivo* vs. *ex-vivo* for a given fraction eliminated or permeated from 10 kDa FITC-dextran and 500 kDa FITC-dextran. $R^2=0.9686$, intercept=0.2935, slope=0.1076 (B) Elimination and permeation profiles of 10 kDa FITC-dextran and 500 kDa FITC-dextran after time scaling. The panel is limited to time equal to 8 h to facilitate viewing the overlapping of the processes [27]. (C) Levy Plot for *in vivo* vs. *in vitro* (artificial membrane) for a given fraction eliminated or permeated from 10 kDa FITC-dextran and 500 kDa FITC-dextran. $R^2=0.5363$, intercept=0.5809, slope=0.9862. (D) Elimination and permeation profiles of 10 kDa FITC-dextran and 500 kDa FITC-dextran after time scaling for the artificial membrane.

4.12 References

- [1] S.H.R. Edwards, Intra-articular drug delivery: The challenge to extend drug residence time within the joint, *Vet. J.* 190 (2011) 15–21. <https://doi.org/10.1016/j.tvjl.2010.09.019>.
- [2] K.M. Ross, J.S. Mehr, B.L. Carothers, R.D. Greeley, I. Benowitz, D. Henry, L.A. McHugh, L. DiFedele, E. Adler, S. Naqvi, L. Taylor, E. Lifshitz, C. Tan, B.E. Montana, Bacterial septic arthritis infections associated with intra-articular injection practices for osteoarthritis knee pain—New Jersey, 2017, *Infect. Control Hosp. Epidemiol.* 40 (2019) 1013–1018. <https://doi.org/10.1017/ice.2019.168>.
- [3] M.F. Rai, C.T. Pham, Intra-articular drug delivery systems for joint diseases, *Curr. Opin. Pharmacol.* 40 (2018) 67–73. <https://doi.org/10.1016/j.coph.2018.03.013>.
- [4] M.L. Kang, G.-I. Im, Drug delivery systems for intra-articular treatment of osteoarthritis, *Expert Opin. Drug Deliv.* 11 (2014) 269–282. <https://doi.org/10.1517/17425247.2014.867325>.
- [5] D.J. Burgess, D.J.A. Crommelin, A.S. Hussain, M.-L. Chen, Assuring quality and performance of sustained and controlled release parenterals: EUFEPS workshop report, *AAPS PharmSci.* 6 (2004) 100–111. <https://doi.org/10.1208/ps060111>.
- [6] B.T. Pedersen, J. Østergaard, S.W. Larsen, C. Larsen, Characterization of the rotating dialysis cell as an in vitro model potentially useful for simulation of the pharmacokinetic fate of intra-articularly administered drugs, *Eur. J. Pharm. Sci.* 25 (2005) 73–79. <https://doi.org/10.1016/j.ejps.2005.01.019>.
- [7] N. Joshi, J. Yan, S. Levy, S. Bhagchandani, K.V. Slaughter, N.E. Sherman, J. Amirault, Y. Wang, L. Riegel, X. He, T.S. Rui, M. Valic, P.K. Vemula, O.R. Miranda, O. Levy, E.M. Gravallesse, A.O. Aliprantis, J. Ermann, J.M. Karp, Towards an arthritis flare-responsive drug delivery system, *Nat. Commun.* 9 (2018). <https://doi.org/10.1038/s41467-018-03691-1>.
- [8] T. Noda, T. Okuda, R. Mizuno, T. Ozeki, H. Okamoto, Two-Step Sustained-Release PLGA/Hyaluronic Acid Gel Formulation for Intra-articular Administration, *Biol. Pharm. Bull.* 41 (2018) 937–943. <https://doi.org/10.1248/bpb.b18-00091>.

- [9] M. Morgen, D. Tung, B. Boras, W. Miller, A.-M. Malfait, M. Tortorella, Nanoparticles for Improved Local Retention after Intra-Articular Injection into the Knee Joint, *Pharm. Res.* 30 (2013) 257–268. <https://doi.org/10.1007/s11095-012-0870-x>.
- [10] C. Larsen, J. Østergaard, S.W. Larsen, H. Jensen, S. Jacobsen, C. Lindegaard, P.H. Andersen, Intra-articular depot formulation principles: Role in the management of postoperative pain and arthritic disorders, *J. Pharm. Sci.* 97 (2008) 4622–4654. <https://doi.org/10.1002/jps.21346>.
- [11] S. Sabaratnam, V. Arunan, P.J. Coleman, R.M. Mason, J.R. Levick, Size selectivity of hyaluronan molecular sieving by extracellular matrix in rabbit synovial joints: Hyaluronan chain length and interstitial matrix sieving, *J. Physiol.* 567 (2005) 569–581. <https://doi.org/10.1113/jphysiol.2005.088906>.
- [12] J.R. Levick, Microvascular Architecture and Exchange in Synovial Joints, *Microcirculation.* 2 (1995) 217–233. <https://doi.org/10.3109/10739689509146768>.
- [13] T. Iwanga, M. Shikichi, H. Kitamura, H. Yanase, K. Nozawa-loue, Morphology and Functional Roles of Synoviocytes in the Joint, *Arch. Histol. Cytol.* 63 (2000) 17–31. <https://doi.org/10.1679/aohc.63.17>.
- [14] D. Scott, P.J. Coleman, R.M. Mason, J.R. Levick, Action of polysaccharides of similar average mass but differing molecular volume and charge on fluid drainage through synovial interstitium in rabbit knees, *J. Physiol.* 528 (2000) 609–618. <https://doi.org/10.1111/j.1469-7793.2000.00609.x>.
- [15] C.H. Evans, V.B. Kraus, L.A. Setton, Progress in intra-articular therapy, *Nat. Rev. Rheumatol.* 10 (2014) 11–22. <https://doi.org/10.1038/nrrheum.2013.159>.
- [16] V.C. Hascall, K.E. Kuettner, The Many Faces of Osteoarthritis, (2002). <http://dx.doi.org/10.1007/978-3-0348-8133-3>.
- [17] N. Mertz, J. Østergaard, A. Yaghmur, S.W. Larsen, Transport characteristics in a novel in vitro release model for testing the performance of intra-articular injectables, *Int. J. Pharm.* 566 (2019) 445–453. <https://doi.org/10.1016/j.ijpharm.2019.04.083>.

- [18] B. Sterner, M. Harms, M. Weigandt, M. Windbergs, C.M. Lehr, Crystal suspensions of poorly soluble peptides for intra-articular application: A novel approach for biorelevant assessment of their in vitro release, *Int. J. Pharm.* 461 (2014) 46–53. <https://doi.org/10.1016/j.ijpharm.2013.11.031>.
- [19] R. Labens, B.D.X. Lascelles, A.N. Charlton, N.R. Ferrero, A.J. Van Wettere, X.-R. Xia, A.T. Blikslager, Ex vivo effect of gold nanoparticles on porcine synovial membrane, *Tissue Barriers*. 1 (2013). <https://doi.org/10.4161/tisb.24314>.
- [20] B. Sterner, M. Harms, S. Wöll, M. Weigandt, M. Windbergs, C.M. Lehr, The effect of polymer size and charge of molecules on permeation through synovial membrane and accumulation in hyaline articular cartilage, *Eur. J. Pharm. Biopharm.* 101 (2016) 126–136. <https://doi.org/10.1016/j.ejpb.2016.02.004>.
- [21] Y. Guang, T.M. McGrath, N. Klug, R. Nims, C.-C. Shih, P.O. Bayguinov, F. Guilak, C.T.N. Pham, J.A.J. Fitzpatrick, L.A. Setton, Combined Experimental Approach and Finite Element Modeling of Small Molecule Transport Through Joint Synovium to Measure Effective Diffusivity, *J. Biomech. Eng.* (2019). <https://doi.org/10.1115/1.4044892>.
- [22] OECD, Joint Meeting of the Chemicals Committee and the Working Party on Chemicals, Pesticides and Biotechnology. 2004. Guidance Document for the Conduct of Skin Absorption Studies. OECD Environmental Health and Safety Publications Series on Testing and Assessment. Number 28. Environment Directorate Organisation for Economic Co-operation and Development. Paris., (2004). [http://www.oecd.org/officialdocuments/publicdisplaydocumentpdf/?cote=env/jm/mono\(2004\)2&doclanguage=en](http://www.oecd.org/officialdocuments/publicdisplaydocumentpdf/?cote=env/jm/mono(2004)2&doclanguage=en).
- [23] C.A. Squier, M.J. Mantz, P.M. Schlievert, C.C. Davis, Porcine Vagina Ex Vivo as a Model for Studying Permeability and Pathogenesis in Mucosa, *J. Pharm. Sci.* 97 (2008) 9–21. <https://doi.org/10.1002/jps.21077>.
- [24] S.L. Myers, K.D. Brandt, O. Eilam, Even low-grade synovitis significantly accelerates the clearance of protein from the canine knee: implications for measurement of synovial fluid “markers” of osteoarthritis, *Arthritis Rheum.* 38 (1995) 1085–1091. <https://doi.org/10.1002/art.1780380810>.

- [25] A. Mathiessen, P.G. Conaghan, Synovitis in osteoarthritis: current understanding with therapeutic implications, *Arthritis Res. Ther.* 19 (2017) 18. <https://doi.org/10.1186/s13075-017-1229-9>.
- [26] J. Weyermann, D. Lochmann, A. Zimmer, A practical note on the use of cytotoxicity assays, *Int. J. Pharm.* 288 (2005) 369–376. <https://doi.org/10.1016/j.ijpharm.2004.09.018>.
- [27] T.K. Mwangi, I.M. Berke, E.H. Nieves, R.D. Bell, S.B. Adams, L.A. Setton, Intra-articular clearance of labeled dextrans from naive and arthritic rat knee joints, *J. Controlled Release.* 283 (2018) 76–83. <https://doi.org/10.1016/j.jconrel.2018.05.029>.
- [28] G. Levy, L.E. Hollister, Inter- and Intrasubject Variations in Drug Absorption Kinetics, *J. Pharm. Sci.* 53 (1964) 1446–1452. <https://doi.org/10.1002/jps.2600531203>.
- [29] V.L. Cook, A.L. Bertone, J.J. Kowalski, S.P. Schwendeman, A.J. Ruggles, S.E. Weisbrode, Biodegradable Drug Delivery Systems for Gentamicin Release and Treatment of Synovial Membrane Infection, *Vet. Surg.* 28 (1999) 233–241. <https://doi.org/10.1053/jvet.1999.0233>.
- [30] V.S. Moses, J. Hardy, A.L. Bertone, S.E. Weisbrode, Effects of anti-inflammatory drugs on lipopolysaccharide-challenged and -unchallenged equine synovial explants, *Am. J. Vet. Res.* 62 (2001) 54–60. <https://doi.org/10.2460/ajvr.2001.62.54>.
- [31] OECD, Guidance Document for the Conduct of Skin Absorption Studies, OECD, 2004. <https://doi.org/10.1787/9789264078796-en>.
- [32] S. Sabaratnam, P.J. Coleman, R.M. Mason, J.R. Levick, Interstitial matrix proteins determine hyaluronan reflection and fluid retention in rabbit joints: effect of protease: Hyaluronan reflection mediated by interstitial matrix proteins, *J. Physiol.* 578 (2007) 291–299. <https://doi.org/10.1113/jphysiol.2006.119446>.
- [33] G.P. Rodnan, M.J. MacLachlan, The absorption of serum albumin and gamma globulin from the knee joint of man and rabbit, *Arthritis Rheum.* 3 (1960) 152–157. <https://doi.org/10.1002/art.1780030206>.
- [34] T.N. Doan, F.C. Bernard, J.M. McKinney, J.B. Dixon, N.J. Willett, Endothelin-1 inhibits size dependent lymphatic clearance of PEG-based conjugates after intra-articular injection into the rat knee, *Acta Biomater.* 93 (2019) 270–281. <https://doi.org/10.1016/j.actbio.2019.04.025>.

- [35] P.A. Simkin, J.E. Bassett, Pathways of Microvascular Permeability in the Synovium of Normal and Diseased Human Knees, *J. Rheumatol.* 38 (2011) 2635–2642. <https://doi.org/10.3899/jrheum.110785>.
- [36] M.E. Blewis, B.J. Lao, K.D. Jadin, W.J. McCarty, W.D. Bugbee, G.S. Firestein, R.L. Sah, Semi-Permeable Membrane Retention of Synovial Fluid Lubricants Hyaluronan and Proteoglycan 4 for a Biomimetic Bioreactor, *Biotechnol. Bioeng.* 106 (2010) 149–160. <https://doi.org/10.1002/bit.22645>.
- [37] C.C. Young, A. Vedadghavami, A.G. Bajpayee, Bioelectricity for Drug Delivery: The Promise of Cationic Therapeutics, *Bioelectricity.* (2020) bioe.2020.0012. <https://doi.org/10.1089/bioe.2020.0012>.
- [38] B.T. Käsdorf, F. Arends, O. Lieleg, Diffusion Regulation in the Vitreous Humor, *Biophys. J.* 109 (2015) 2171–2181. <https://doi.org/10.1016/j.bpj.2015.10.002>.
- [39] J. Niderla-Bielinska, Influence of LPS, TNF, TGF- β 1 and IL-4 on the expression of MMPs, TIMPs and selected cytokines in rat synovial membranes incubated in vitro, *Int. J. Mol. Med.* (2010). <https://doi.org/10.3892/ijmm.2010.550>.
- [40] M.B. Goldring, M. Otero, Inflammation in osteoarthritis, *Curr. Opin. Rheumatol.* 23 (2011) 471–478. <https://doi.org/10.1097/BOR.0b013e328349c2b1>.
- [41] K. Lu, Q. Bao, D. Wang, Y. Ning, X. Xie, M. Zhou, L. Zhou, X. Zeng, J. Shan, Y. Li, Effects of All-Trans Retinoic Acid on Lipopolysaccharide-Induced Synovial Explant, *J. Nutr. Sci. Vitaminol. (Tokyo).* 65 (2019) 8–18. <https://doi.org/10.3177/jnsv.65.8>.
- [42] P.A. Simkin, J.E. Pizzorno, Synovial permeability in rheumatoid arthritis, *Arthritis Rheum.* 22 (1979) 689–696. <https://doi.org/10.1002/art.1780220701>.
- [43] J.C. de Grauw, C.H. van de Lest, P.R. van Weeren, Inflammatory mediators and cartilage biomarkers in synovial fluid after a single inflammatory insult: a longitudinal experimental study, *Arthritis Res. Ther.* 11 (2009) R35. <https://doi.org/10.1186/ar2640>.
- [44] C. Kjelgaard-Petersen, A.S. Siebuhr, T. Christiansen, C. Ladel, M. Karsdal, A.-C. Bay-Jensen, Synovitis biomarkers: ex vivo characterization of three biomarkers for identification of inflammatory osteoarthritis, *Biomarkers.* 20 (2015) 547–556. <https://doi.org/10.3109/1354750X.2015.1105497>.

- [45] W. Lorenz, C. Buhrmann, A. Mobasheri, C. Lueders, M. Shakibaei, Bacterial lipopolysaccharides form procollagen-endotoxin complexes that trigger cartilage inflammation and degeneration: implications for the development of rheumatoid arthritis, *Arthritis Res. Ther.* 15 (2013) R111. <https://doi.org/10.1186/ar4291>.
- [46] D. Scott, P.J. Coleman, A. Abiona, D.E. Ashhurst, R.M. Mason, J.R. Levick, Effect of depletion of glycosaminoglycans and non-collagenous proteins on interstitial hydraulic permeability in rabbit synovium, *J. Physiol.* 511 (1998) 629–643. <https://doi.org/10.1111/j.1469-7793.1998.629bh.x>.
- [47] R. Deng, F. Li, H. Wu, W. Wang, L. Dai, Z. Zhang, J. Fu, Anti-inflammatory Mechanism of Geniposide: Inhibiting the Hyperpermeability of Fibroblast-Like Synoviocytes via the RhoA/p38MAPK/NF- κ B/F-Actin Signal Pathway, *Front. Pharmacol.* 9 (2018) 105. <https://doi.org/10.3389/fphar.2018.00105>.
- [48] D.A. Walsh, P. Verghese, G.J. Cook, D.F. McWilliams, P.I. Mapp, S. Ashraf, D. Wilson, Lymphatic vessels in osteoarthritic human knees, *Osteoarthritis Cartilage.* 20 (2012) 405–412. <https://doi.org/10.1016/j.joca.2012.01.012>.
- [49] E.M. Bouta, R.D. Bell, H. Rahimi, L. Xing, R.W. Wood, C.O. Bingham, C.T. Ritchlin, E.M. Schwarz, Targeting lymphatic function as a novel therapeutic intervention for rheumatoid arthritis, *Nat. Rev. Rheumatol.* 14 (2018) 94–106. <https://doi.org/10.1038/nrrheum.2017.205>.

5 Co-formulations of adalimumab with hyaluronic acid / polyvinylpyrrolidone to combine intraarticular drug delivery and viscosupplementation

5. Co-formulations of adalimumab with hyaluronic acid / polyvinylpyrrolidone to combine intraarticular drug delivery and viscosupplementation

Tobias Siefen¹, Simon Bjerregaard², Daniel Plaksin², John Lokhnauth³, Alfred Liang³, Crilles Casper Larsen³, Alf Lamprecht^{1,4}

¹Department of Pharmaceutics, Institute of Pharmacy, University of Bonn, Bonn, Germany.

²Ferring Pharmaceuticals A/S, Copenhagen, Denmark

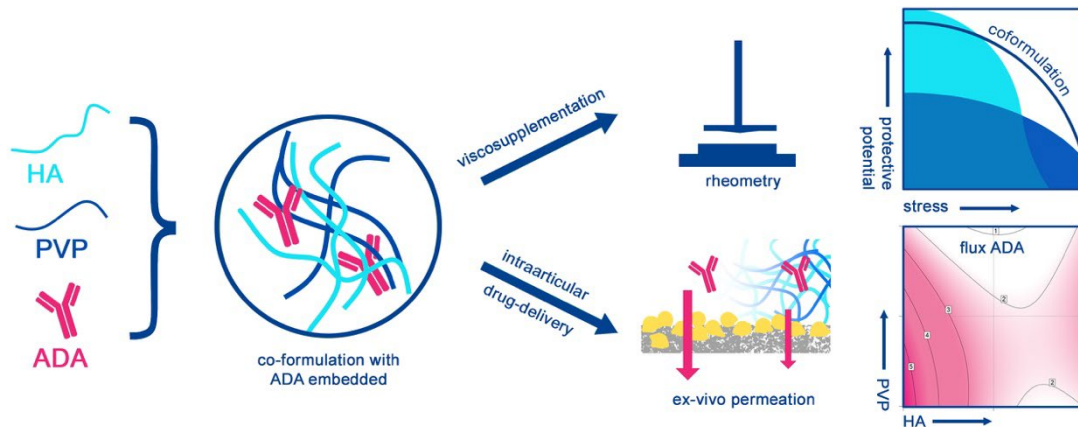
³Ferring Pharmaceuticals Inc, Parsippany, New Jersey, USA

⁴PEPITE (EA4267), University of Burgundy/Franche-Comté, Besançon, France.

This work is published as

Siefen T, Bjerregaard S, Plaksin D, Lokhnauth J, Liang A, Casper Larsen C, Lamprecht A. Co-formulations of adalimumab with hyaluronic acid / polyvinylpyrrolidone to combine intraarticular drug delivery and viscosupplementation. *Eur J Pharm Biopharm.* 2022 Jun 9:S0939-6411(22)00119-9. doi: 10.1016/j.ejpb.2022.06.002.

5.1 Graphical abstract



5.2 Abstract

Polymer-based formulations present an attractive strategy in intraarticular drug-delivery to refrain biologicals from early leakage from the joint. In this study, co-formulations of hyaluronic acid and polyvinylpyrrolidone were investigated for their potential as viscosupplements and their influence on the transsynovial loss of adalimumab. For this purpose, polymer mixtures were evaluated for their viscosity and elasticity behavior while their influence on the permeation of adalimumab across a porcine *ex-vivo* synovial membrane was determined. Hyaluronic acid showed strong shear thinning behavior and exhibited high viscosity and elasticity at low motions, while combinations with polyvinylpyrrolidone provided absorption and stiffness at high mechanical stress, so that they can potentially restore the rheological properties of the synovial fluid over the range of joint motion. In addition, the formulations showed significant influence on transsynovial permeation kinetics of adalimumab and hyaluronic acid, which could be decelerated up to 5- and 3-fold, respectively. Besides viscosity effects, adalimumab was retained primarily by an electrostatic interaction with hyaluronic acid, as detected by isothermal calibration calorimetry. Furthermore, polymer-mediated stabilization of the antibody activity was detected. In summary, hyaluronic acid - polyvinylpyrrolidone combinations can be efficiently used to prolong the residence of adalimumab in the joint cavity while simultaneously supplying viscosupplementation.

5.3 Keywords

intraarticular injection, hydrogel, *ex-vivo*, diffusion, viscosupplementation

5.4 Introduction

The synovial joint cavity is filled with synovial fluid, which in a healthy state is responsible for preventing damage and wear to the adjacent cartilage surfaces. The anionic glycosaminoglycan hyaluronic acid (HA) is the major hydrodynamic component in synovial fluid for its unique viscoelastic properties and lubricating capabilities [1]. In the course of osteoarthritis (OA), however, HA is degraded, which leads not only to a depression of viscosity and a resulting intensified mechanical stress on the chondral tissue [2], but HA fragments might even further stimulate inflammatory processes [3]. The intraarticular (IA) injection of high molecular weight HA into diseased joints has been shown to be effective in reducing pain and improving function in a broad spectrum of osteoarthritic patients [4]. The primary effect of HA is presumably mediated by increasing viscosity and restoring the natural lubrication and shock absorption of the pathologically altered synovial fluid, a therapy commonly referred to as viscosupplementation [5]. Nevertheless, further effects, such as anti-inflammatory, cytoprotective and immunoregulatory properties on disease progression must be assumed due to the limited residence time of exogenous HA and have since been confirmed in several research studies [6]. Despite the positive and well-established clinical experience with IA injections of HA, novel formulations made of chemically altered HA or artificial polymers as viscosupplements are being explored to further improve their performance for OA-therapy. Thereby, the objective is to extend the retention time of the viscosupplements, to optimize the tribological and rheological properties or to implement additional functionalities, such as a controlled drug transport [7]. However, as was concluded by a recent review on HA mediated drug delivery, there is still a need for research and development on biomaterials that can lubricate joint tissue with minimal inflammation by delivering HA in a sustained and prolonged manner [8]. Polyvinylpyrrolidone (PVP) is a biocompatible polymer with excellent solubility that has been approved by the FDA for parenteral administration (K12 PF and K19 PF) due to its low toxicity and long experience in pharmaceutical applications. [9]. Various studies have demonstrated excellent lubricating properties through formation of thin films for long-chain PVPs [10,11], so they have been successfully used in various medical applications, including the lubrication of artificial joints after total knee arthroplasty [12]. Moreover, there are early preclinical and clinical studies investigating viscosupplementation with 15% PVP solutions and observing, similar to HA, beneficial effects on the rheological properties of synovial fluid as well as on immunological processes

[13,14] and more recent studies that investigated the suitability of PVP containing hydrogel formulations for use as cartilage replacement on artificial bearing surfaces [15,16]. The blending of polymers enables the directed composition of materials that contribute different rheological properties to the polymeric solution [17]. In this study, we investigate the interplay of the two polymers HA and PVP concomitantly formulated, both of which have been shown to be appropriate candidates for IA application, in a systematic and concentration-dependent manner and evaluate their suitability as viscosupplements by means of a design of experiment (DOE). However, since viscosupplementation is considered to be only one cornerstone of a successful therapy, the aim here was to incorporate an active pharmaceutical ingredient (API) into the viscosupplement formulations that simultaneously benefits from the polymer solution viscosities of HA and PVP in view of a prolonged availability in the synovium. Since local chronic inflammation is considered one of the main causes of knee pain in OA [18], TNF- α , among IL-1, IL-6 and IL-17, is regarded as key cytokine for the onset and pathogenesis of osteoarthritis and the process of cartilage destruction [19] and can be efficiently targeted with approved antibodies, such as Adalimumab (ADA). Clinical trials and case studies reported therapeutic benefit of systemic ADA antibodies in OA, which improved patients' pain, stiffness and joint swelling [20,21]. The treatment of arthritic diseases by biologics provides a targeted and well tolerated therapy for reduction of the inflammatory processes in the joint [22]. Yet, in contrast to rheumatoid arthritis, no cytokine targeted therapy for osteoarthritis has been approved to date. As usually only few joints are affected, local injections into the joint space allow the dose to be reduced while at the same time increasing the amount of active ingredient at the actual site of action, thereby reducing systemic availability of the highly potent drug. However, rapid clearance into surrounding blood capillaries and lymphatics is the defining issue to consider when developing an intra-articular formulation [23]. The joint residence time of proteins is typically a few hours or less [24], which has been shown to be too short for an effective duration of action, necessitating frequent injections to achieve the desired therapeutic effect [25]. For this reason, in addition to the rheological investigation of the viscosupplements, this study also evaluates the formulation's potential to increase the effective residence time of the antibody ADA and HA in the joint cavity. For the evaluation of the different viscosupplement mixtures, viscosity and viscoelastic properties were measured as important flow parameters characterizing the ability to provide fluid-film lubrication in the synovial joint and

as a potentially paramount factor the retention of *ex-vivo* permeation across a porcine synovial membrane was analyzed for ADA and HA.

5.5 Materials and methods

5.5.1 Reagents and Materials

Adalimumab was obtained from the commercially available product HUMIRA® (50 mg/mL) (Abbott Laboratories). Hyaluronic Acid (HA) with an approximate MW of 2400-3600 kDa and a polydispersity index (PDI = M_w/M_n) of 1.08 was received from Ferring Pharmaceuticals (Parsippany, USA). Polyvinylpyrrolidone K90 F (PVP) with an approximate MW of 1000-1500 kDa and a PDI of 3.1 was received from BASF (Ludwigshafen, Germany). Dulbecco minimum essential media (DMEM), fetal bovine serum (FBS) and Penicillin, Streptomycin and Amphotericin B solution was purchased from Merck (Darmstadt, Germany). Fluorescein isothiocyanate 5/6 isomers were purchased from Merck (Darmstadt, Germany). 150 kDa FITC-dextran was purchased from Merck (Darmstadt, Germany). Ethylenediamine and N-ethyl-N'-(3-dimethyl-amionopropyl) carbodiimide were purchased from Merck (Darmstadt, Germany). Human TNF- α recombinant Protein was purchased from Biomol (Hamburg, Germany). All Chemicals used for preparation of buffers were of analytical grade. Deionized water was used throughout the experiments. Pig feet of Class E pigs (Regulation EU No 1308/2013), 5-7 months old, were obtained from a local commercial slaughterhouse (following routine slaughtering procedures) and were freshly used for the excision of the synovial membranes.

5.5.2 Design of experiments (DOE)

A quadratic central composite design was created in order to establish a polynomial response surface graph using Design-Expert® (Stat-Ease, USA). Numeric factors were: HA from low 0.0 mg/mL to high 20.0 mg/mL and PVP from 0.0 mg/mL to 300.0 mg/mL, which resulted in 9 different blends (HA10, HA20, PVP150, PVP300, PVP150HA10, PVP300HA10, PVP150HA20, PVP300HA20, Solution) (**Tab. 5-1**). The concentration ranges cover the spectrum in which the polymers have previously been clinically tested. Responses were: the *ex-vivo* flux of ADA, the *ex-vivo* flux of HA, ZSV, STI, G' at 2.5 Hz, $\tan\delta$ at 2.5 Hz and syringeability (23 G needle). All experiments were conducted in a randomized order and in triplicate. The collected data were modeled, and plots were

5 Co-formulations of adalimumab with hyaluronic acid / polyvinylpyrrolidone to combine intraarticular drug delivery and viscosupplementation

constructed using the same software. Correlations of the different factors and responses were calculated using Pearson multiple variables analysis.

Tab. 5-1: Composition and ratio of the investigated mixtures of HA and PVP.

Formulation	HA (mg/mL)	PVP (mg/mL)	Ratio (PVP/HA)
HA10	10	0	/
HA20	20	0	/
PVP150	0	150	/
PVP300	0	300	/
PVP150HA10	10	150	15
PVP300HA10	10	300	30
PVP150HA20	20	150	7.5
PVP300HA20	20	300	15

5.5.3 Preparation of the ADA loaded HA/PVP formulations

Based on the precedent design of experiments, 9 blends of HA and PVP with 2.5 mg/mL ADA each were prepared. The mixture stirred for 4 h using a RW 20 digital overhead stirrer at 100 rpm (IKA, Germany). After air bubbles have been removed by centrifugation, the mixture was left to swell overnight at 4 °C.

5.5.4 Rheology

To determine the formulation rheology, a HAAKE RheoStress® 1 (Haake, Karlsruhe, Germany) rheometer was used with a cone-plate geometry (25 mm diameter, 1 ° cone angle). The temperature was kept at 37 °C for all experiments. To better assess the measured values, aspirated porcine synovial fluid was also measured and compared with the polymer blends to classify their suitability for viscosupplementation. A shear rate sweep was performed at logarithmic interval from 0.01-500 s⁻¹ and subsequent reversed from the maximum shear rate to 0.01 s⁻¹. Each test was run in triplicate. The obtained viscosity data points were fitted using Carreau-Yasuda model to generate the zero-shear-viscosity (ZSV) using RheoWin® Software (Thermo Haake, Karlsruhe, Germany) software. Furthermore, a shear thinning ratio (STR= η_0/η_{300}) was calculated from the measured ZSV and the viscosity at 300 s⁻¹ to obtain an index representing the extent of shear thinning, as previously introduced for the characterization of synovial fluid samples [26,27]. All blends were measured with and without ADA, and a ZSR ratio was calculated. To evaluate whether labeling modified the rheological behavior of the HA, naive and labeled HA were additionally compared in a shear rate sweep. For assessment of the viscoelastic properties of the viscosupplements, a frequency sweep was performed at a logarithmic interval from 0.1 to 100 Hz at a low strain of 0.1 %, which was preliminarily determined to

ensure a linear shear response. For ease of comparison, the elastic moduli G' are stated for a frequency of 2.5 Hz. This corresponds approximately to the expected movement during running and has been established as a comparative parameter in previous works [28]. Additionally, the loss factor $\tan\delta$ (G''/G') is compared as a surrogate for elastic or viscous-like behavior of the viscosupplements. Syringeability was tested using a custom build extension for the Texture Analyzer TA-HDi (Stable Micro Systems, UK) equipped with a 500 N loading cell, in which a BD Luer-Lok 1 mL syringe (BD, Franklin Lakes, USA) can be attached with downward needle. The syringe was filled with the formulation and a Sterican® needle (B.Braun, Melsungen, Germany) of 23G size (0.60 x 25 mm) was screwed on the syringe tip. The measurement was performed using the compression mode at a velocity of 1 mm/s representing the manual syringe delivery to the patient [29] over a distance of 20 mm. The average maximum injection force was calculated of triplicate measurements.

5.5.5 Conjugation of fluorophores

Adalimumab was labeled with fluorescein isothiocyanate (FITC) for the *ex-vivo* permeation studies in an adapted method of the manufacturer's instructions. To remove unbound dye, the labeled antibody was purified by centrifugation using a PD Mditrap G-25 column (Merck, Darmstadt, Germany) according to the manufacturer recommendation. The molarity of the protein and degree of labeling was determined by UV-measurement with a Genesys 10S UV/VIS Spectrophotometer (Thermo-Fisher, Waltham, USA). FITC-labelled HA without significant change in molecular weight was prepared by introduction of ethylenediamine by carbodiimide reaction and subsequent FITC coupling as was previously reported [30]. After reaction with ethylenediamine and N-ethyl-N'-(3-dimethyl-amionopropyl) carbodiimide the mixture was dialyzed against distilled water. The HA derivative was then labeled using the same protocol as ADA and dialyzed again. Finally, the FITC-HA solution was freeze-dried and following reconstitution the labeling degree photometrically was determined and viscosity was measured as explained below.

5.5.6 Ex-vivo transsynovial permeability

The permeability through a porcine *ex-vivo* synovial membrane was measured in a Franz-Cell model as previously described [31] with an orifice diameter of 1.0 cm, resulting in a total diffusional area of 0.785 cm². Before each experiment, the lower limbs of domestic pigs were obtained on the day of slaughter and the

synovial tissue from the articulation metacarpophalangeus was dissected contiguously. The membrane was attached to a thin ring to avoid any movements during the permeation test. Basolateral-representing chamber, containing DMEM with 5% FBS, 1% antibiotics and antimycotics as acceptor media, and luminal-representing chamber were separated by the harvested porcine synovium. 0.2 mL of each formulation containing either FITC-labelled ADA or HA was applied on the donor cell and samples were drawn over 48 h at predetermined intervals. Sink conditions were maintained as the analyte concentration in the basolateral chamber did not exceed 10% of its saturation solubility. To evaluate the effects of ADA and HA interaction on the permeation, a 150 kDa-sized FITC-dextran was additionally tested with all formulations. Quantification of the analytes was performed utilizing a plate reader (PerkinElmer EnSpire®) at an excitation of 490 nm and an emission of 525 nm for FITC-labeled molecules. All permeability experiments were performed with n=6. The cumulative amount permeated is calculated according to the equation

$$M_i = V_s \sum_{i=0}^{t-1} C_{i-1} + V_A C_t$$

where V_A is the total volume of the acceptor chamber, C_i is the concentration at each sampling time, V_s is the volume of the withdrawn sample and C_i represents the concentration of analyte at time i . The so calculated mass was subsequently divided by the diffusional area. Plots of cumulative permeation amount per area against time were derived, and the percent permeation amount of the applied dose was calculated. Fluxes were determined from the slope at steady state computed by linear regression and thus describe the mass diffused through the membrane per time and area in $\mu\text{g}/(\text{cm}^2 \cdot \text{h})$. The flux is considered as a surrogate parameter for the permeability of the synovial membrane for ADA and HA, respectively.

5.5.7 Isothermal titration calorimetry

An interaction of the ADA or dextran with HA was evaluated by measuring binding associated thermal changes by isothermal titration calorimetry (ITC) of each molecule using a high-sensitivity Microcal isothermal titration calorimeter (VP-ITC, Northampton, MA). For this purpose, all solutions were degassed under vacuum prior to measurement to remove any gas bubbles that might be present using the Themovac-2 sample degasser and thermostat. The cell was filled with 1.43 mL of ADA solution at a concentration of 50 μM in 0.1x PBS buffer. The

syringe was loaded with 25 μ M HA (150 kDa sized to allow the measurement at reasonable viscosities) solution in the same buffer. Titration was performed at 298.15 K by making 30 injections of 10 μ l every 180 s at a rate of 30 μ l/min while the sample was stirred in the measurement well at 310 rpm. Data was analyzed using Origin® Microcal 5.0. ITC raw data were integrated, and the binding isotherm was plotted from the computed values. A curve was fitted using the 'two sets of sites' binding model and the respective parameters were calculated, since both binding of the protein to the polymer and dissociation lead to heat changes. All measurements were corrected by subtraction of heat of dilution, which was determined by titrating HA into buffer.

5.5.8 Activity of ADA in presence of HA and PVP

To assess the binding activity of the ADA to TNF- α in the presence of the polymers, a direct fluorophore-linked immunosorbent assay (FLISA) was performed, which was adapted from a previously developed ELISA for the detection of ADA [32]. For this purpose, 25 μ g/mL FITC-ADA was mixed with 0.2 mg/mL HA, 3 mg/mL PVP or 0.2 μ g/mL HA and 3 mg/mL PVP, which corresponds to the same ratio of protein to polymer as in the higher concentration formulations. All samples were prepared with n=9 and incubated at 37° C for 48 h. A 96 high protein binding well plate (NUNC Maxisorp™, Thermo-Fisher, Waltham, USA) was incubated overnight with 1 μ g/mL TNF- α at 4 °C. After blocking the remaining protein binding sites with BSA for 2 h at RT. Following three-times-washing with PBS containing 0.05 % Tween 20, 1:100 diluted standards and samples were pipetted into the wells in duplicates. Samples were allowed to incubate for 1.5 h at RT in an orbital shaker, after which the plate was washed again as previously described. Subsequently, 100 μ L of PBS was added to the wells and the fluorescence of the bound ADA was measured using a plate reader (PerkinElmer EnSpire®) at 490 nm / 525 nm.

5.5.9 Statistical analysis

Data was presented as mean \pm standard deviation. Permeation of the analytes was assessed using their flux as calculated from linear regression. Normality was analyzed by Box-Cox plot and transformation of data was applied for statistical tests according to the calculated λ -value. Statistical significance was determined by one-way analysis of variance test (one-way ANOVA) followed by Dunnett's multiple comparison test. Differences were considered significant at $p < 0.05$. Statistical analysis was performed using GraphPad Prism® 8 software. Analysis

of the DOE and establishment of response surface graphs was performed in DesignExpert®12.

5.6 Results

5.6.1 Rheology of HA/PVP mixtures

Strong non-Newtonian behavior was observed for synovial fluid and all viscosupplement samples, except for the preparations containing only PVP, which showed nearly constant viscosity over the range of measured shear rates (**Sup. Fig. 5-1**). From the profiles of the different formulations, it can be seen that HA, in particular, increases the viscosity at low shear rates, while the addition of PVP rather impacts the viscosity at high shear rates. Porcine synovial fluid exhibited a ZSV of 33 ± 9 Pas and non-significantly different ZSVs were obtained for HA10 and PVP30 (**Fig. 5-1A**), while significantly larger ZSVs were in particular measured for all formulations with HA20 ($p < 0.0001$). A Pearson correlation (**Fig. 5-2**) of the ZSV with the concentrations of HA and PVP shows a better correlation to the amount of HA ($r=0.83$) than to the one of PVP ($r=0.25$). ZSV was found to significantly decrease for HA containing formulations after addition of ADA (**Fig. 5-3A**) where HA10 is affected the most and decreased by a factor of approximately 4. Non-Newtonian shear thinning behavior was observed in the synovial fluid sample described by a large shear-thinning-index ($STI = \eta_0 / \eta_{300}$) of 214 ± 40 (**Fig. 5-1B**). Whereas PVP samples decreased the index ($r=-0.43$), as its viscosity decreases only marginally with increasing shear, HA showed a large positive correlation to the STI ($r=0.80$). All tested formulations were significantly different from the synovial fluid STI ($p < 0.05$) with HA10, PVP150HA20, and PVP300HA20 still being relatively close to the value for synovial fluid. The viscoelastic properties of the viscosupplements were evaluated on the basis of parameters relevant to the joint. At a frequency of 2.5 Hz, which approximately corresponds to motion of running, the elastic moduli G' of HA10, PVP150, PVP300 and PVP150HA10 were insignificantly different from synovial fluid ($p < 0.05$) (**Fig. 5-3B**). The loss factor $\tan\delta$ of HA20 at a frequency of 2.5 Hz (**Fig. 5-3C**) was the only one that showed no significant difference to the porcine synovial fluid ($p > 0.05$). However, with the exception of the pure PVP viscosupplements, all other formulations, especially HA10 and PVP150HA20, were in the same range with values $\tan\delta < 1$, showing predominantly elastic behavior. PVP150 behaved more like a viscous fluid, since $G' < G''$ ($\tan\delta > 1$) is

5 Co-formulations of adalimumab with hyaluronic acid / polyvinylpyrrolidone to combine intraarticular drug delivery and viscosupplementation

present. With increasing PVP concentration, the elastic character of the viscosupplements increases, with $\tan\delta > 1$ still remaining. For most of the viscosupplements, the elastic behavior increases with increasing frequency, so conversely a crossover ($\tan\delta=1$) can be observed at low frequencies, or a trend of the dynamic moduli indicated the existence of a crossover point at frequencies below 0.1 Hz (**Sup. Fig. 5-2**). For all HA-containing formulations, this crossover point was found below a frequency of 0.5 Hz and moreover HA does not significantly increase the syringeability compared to water ($p > 0.05$) at both concentrations, though a trend may be observed with increased polymer concentration (**Sup. Fig. 5-4**). PVP150 and PVP300 were found significantly harder to inject leading to injection forces in the range of 25 N. Similarly, HA10 formulations showed over additive and significantly increased syringeability for PVP150HA10 and again for PVP300HA10 compared to HA10 alone and likewise, HA20 syringeability is significantly increased by the addition of PVP150I and PVP300.

5 Co-formulations of adalimumab with hyaluronic acid / polyvinylpyrrolidone to combine intraarticular drug delivery and viscosupplementation

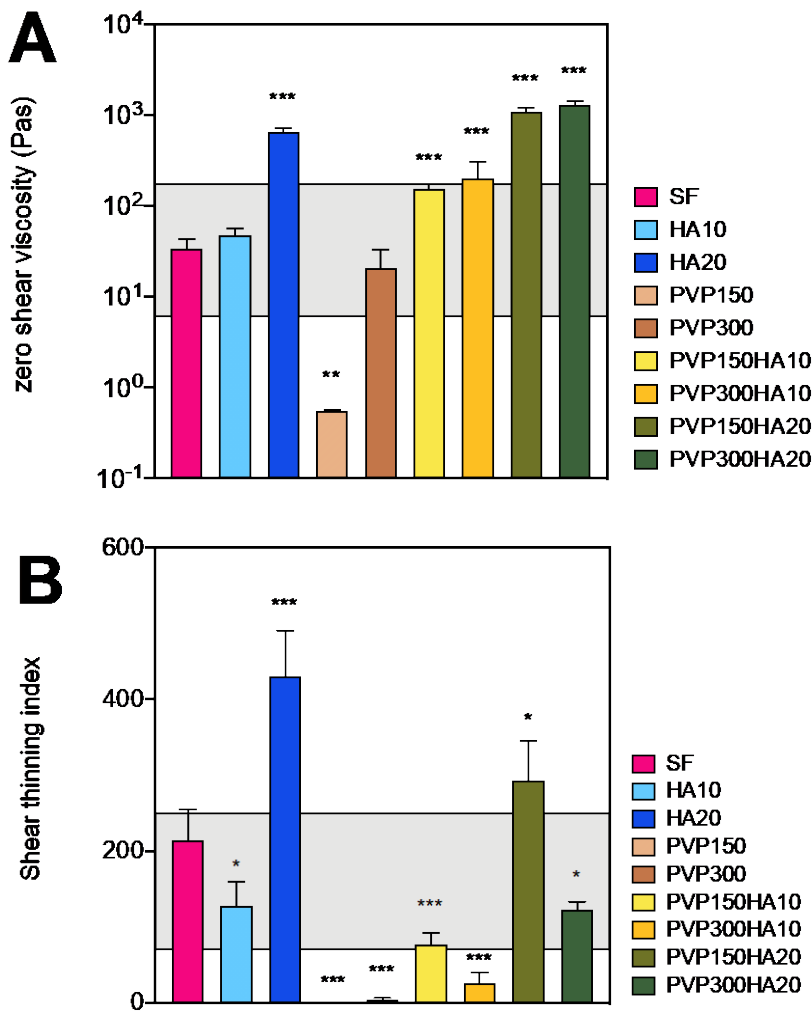


Fig. 5-1 (A) Zero shear viscosity (ZSV) in Pas of the polymeric blends as calculated using Carreau-Yasuda regression. **(B)** Shear thinning index (η_0/η_{300}). Grey area shows range of measured ZSV for human healthy synovial fluid [2]. Mean \pm SD; n=3; ANOVA + Dunnett's multiple comparison test; significant differences: '*' ($p < 0.05$), '**' ($p < 0.01$), '***' ($p < 0.001$) compared to synovial fluid.

5 Co-formulations of adalimumab with hyaluronic acid / polyvinylpyrrolidone to combine intraarticular drug delivery and viscosupplementation

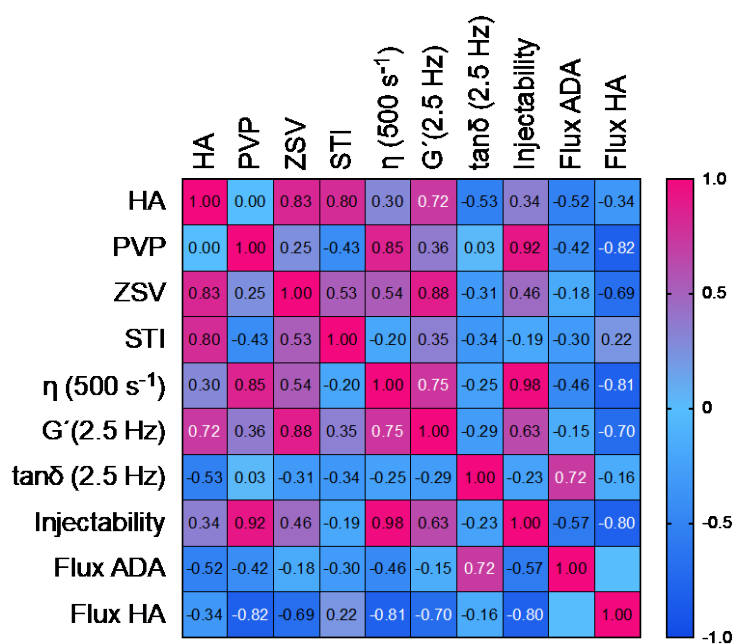


Fig. 5-2 Pearson r multiple variables correlation of the different factors and responses analyzed.

5 Co-formulations of adalimumab with hyaluronic acid / polyvinylpyrrolidone to combine intraarticular drug delivery and viscosupplementation

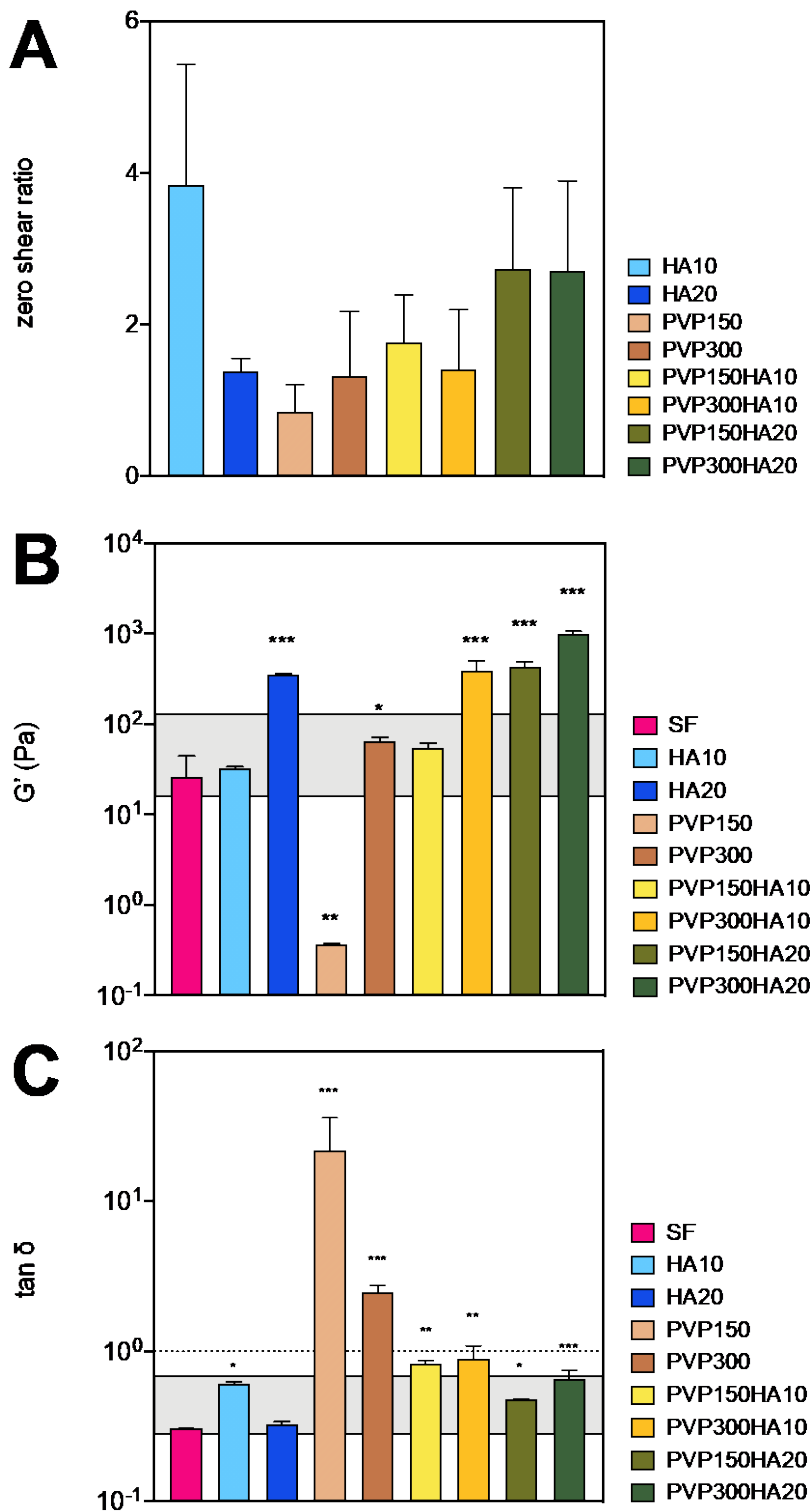


Fig. 5-3 (A) Ratio of zero shear viscosity (ZSV) describing the relative decrease of ZSV caused of addition of ADA to the sample. Mean \pm SD; n = 3. **(B)** Elastic modulus (G') and **(C)** loss factor $\tan \delta$ (G''/G') at 2.5 Hz ('Run') as measured by oscillatory rheometry. Grey area shows the range of measured values for human healthy synovial fluid [56]. The dotted line equals 1, which is the value that divides mostly elastic samples and mostly viscous samples. Mean \pm SD; n=3; ANOVA + Dunnett's multiple comparison test; significant differences: '*' ($p < 0.05$), '**' ($p < 0.01$), '***' ($p < 0.001$) compared to synovial fluid.

5.6.2 FITC-HA *ex-vivo* transsynovial permeability

HA was labeled with a degree of labeling of approximately 0.0096 molecules dye per monomer and FITC-HA (10 mg/mL) was found to exhibit the same rheological properties as the unmodified HA (data not shown). As to be seen in **Fig. 5-5A** addition of PVP150 to HA10 showed no significant decrease in flux, whereas a further increase of PVP concentration to 300 mg/mL decreased the flux significantly ($p < 0.05$). HA20 flux was significantly decreased by both PVP concentrations (**Fig. 5-5B**). However, in between PVP150HA20 and PVP300HA20 no significant difference was found ($p > 0.05$) though a trend with increasing concentration of PVP may be observed (**Fig. 5-5C**). The response surface graph (**Fig. 5-6C**) shows that a minimum HA flux was achieved by combining high HA and PVP concentrations. No significant interaction was found, which would influence the permeation of HA ($p > 0.05$).

5.6.3 FITC- ADA and FITC 150 kDa *ex-vivo* transsynovial permeability

When ADA was labeled with FITC the degree of labeling was of 7.81 molecules dye per protein. No significant difference was observed for ADA alone on transsynovial permeation whether synovial fluid or buffers were in the donor chamber (**Sup. Fig. 5-3**). The fluorescence labeled biological ADA was generally found to permeate through the porcine *ex-vivo* synovium with linear kinetics and its flux could be slowed down by adding either PVP or HA or both polymers. PVP150 did not significantly affect the ADA flux, where with PVP300 less than half of the cumulated mass was recovered from the acceptor compartment (**Fig. 5-4A**). The flux of the 300 mg/mL formulation was significantly lower than both ADA solution and 150 mg/mL formulation ($p < 0.05$). The presence of HA10 did significantly decelerate the permeation of ADA compared to its solution and this effect was stepwise further enhanced with increasing PVP concentrations (**Fig. 5-4B**). HA20 further decreased the permeation of ADA significantly as compared to H10 however, other than for HA10 addition of PVP led to a significantly higher flux of ADA, though PVP150HA20 flux was yet higher than PVP300HA20 ($p < 0.05$) (**Fig. 5-4C**). The calculated fluxes (**Fig. 5-4D**) reveal that, except for PVP150, all formulations were able to significantly slow down the permeation of ADA. The highest overall retention was achieved with the formulations HA20 and PVP300HA10, which were able to decelerate the permeation by a factor of approximately 5. In the response surface plot ADA flux minima were calculated for the region of HA 10.28 mg/mL and PVP 300 mg/mL (flux = 0.816 $\mu\text{g}/\text{cm}^2/\text{h}$) and for the region of HA 16.06 mg/mL and PVP

5 Co-formulations of adalimumab with hyaluronic acid / polyvinylpyrrolidone to combine intraarticular drug delivery and viscosupplementation

3.73 mg/mL (flux = 0.803 $\mu\text{g}/\text{cm}^2/\text{h}$) (**Fig. 5-6B**). Both factors as well as their interaction were proven to be significant with regard to their influence on the ADA flux in the quadratic model ($p < 0.05$). In contrast, the 3D-surface plot of 150 kDa dextran showed a different shape and a noticeably lower influence of HA on the flux of dextran compared to ADA (**Fig. 5-6A**). This is also shown by the finding that only the normalized dextran flux values for the HA10 and HA20 formulations differ significantly from the normalized fluxes of ADA (**Fig. 5-7**).

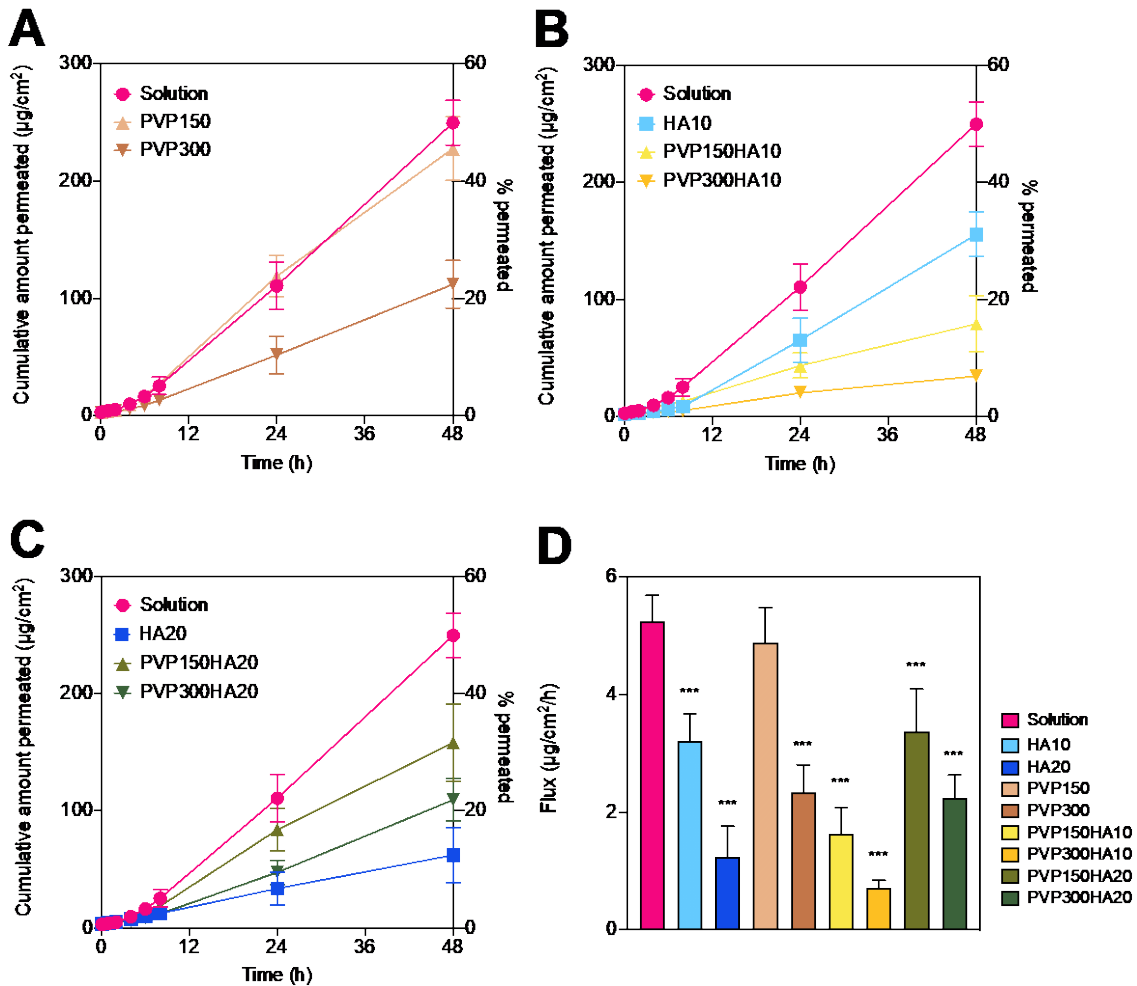


Fig. 5-4: Cumulative amount permeated of ADA through *ex-vivo* synovium as solution and with addition of viscosity modifying additives. **(A)** Comparison of ADA permeation alone and with different concentrations of PVP **(B)** Comparison of ADA permeation alone and with 10 mg/mL HA and different concentrations of PVP **(C)** Comparison of ADA permeation alone and with 20 mg/mL HA and different concentrations of PVP **(D)** Flux of ADA describing the deceleration caused by the polymer mixture. Mean \pm SD; n=6; ANOVA+ Dunnett's multiple comparison test; significant differences: '****' ($p < 0.001$) compared to Solution.

5 Co-formulations of adalimumab with hyaluronic acid / polyvinylpyrrolidone to combine intraarticular drug delivery and viscosupplementation

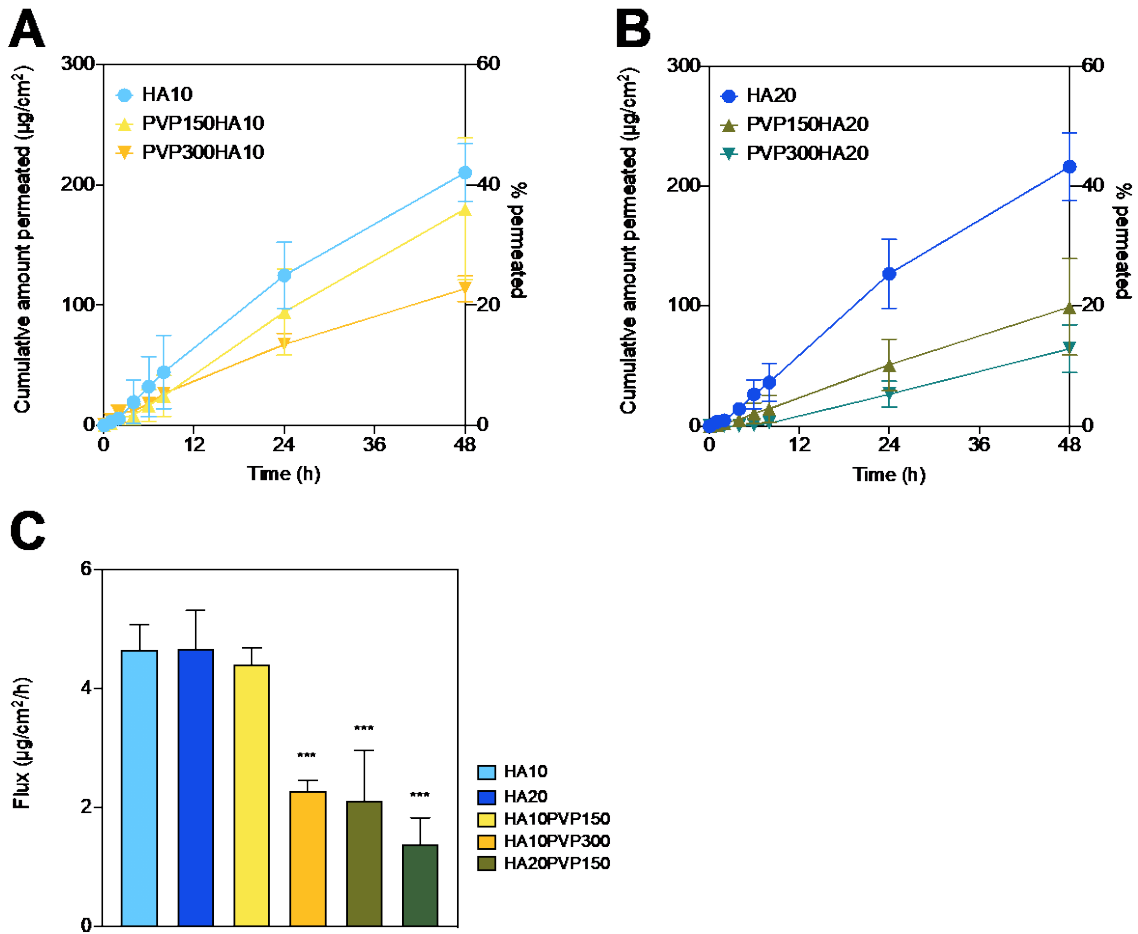


Fig. 5-5 Cumulative amount permeated of HA through ex-vivo synovium alone and with addition PVP 90. **(A)** Comparison of HA 10 mg/mL permeation alone and with different concentrations of PVP **(B)** Comparison of HA 20 mg/mL permeation alone and with different concentrations of PVP **(C)** Flux of HA describing the deceleration caused by the PVP mixture. Mean \pm SD; n=6; ANOVA+ Dunnett's multiple comparison test; significant differences: **** (p < 0.001) compared to HA10.

5 Co-formulations of adalimumab with hyaluronic acid / polyvinylpyrrolidone to combine intraarticular drug delivery and viscosupplementation

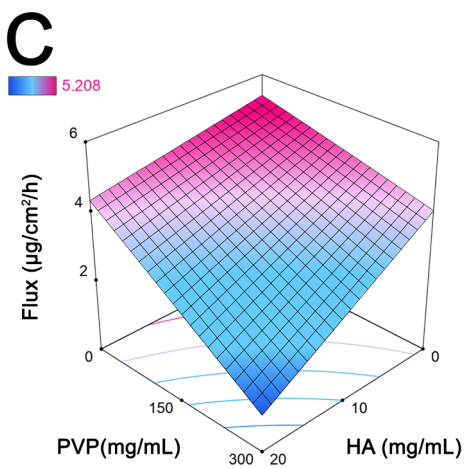
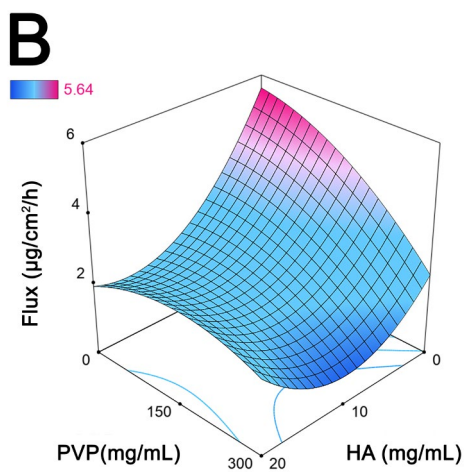
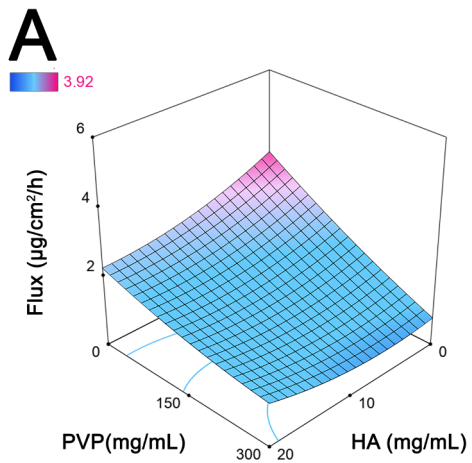


Fig. 5-6 3D Surface response plot showing the effect of HA (X1) and PVP (X2) on *ex-vivo* flux of dextran 150 kDa (Y1) (A), ADA (B) or HA (C) respectively.

5 Co-formulations of adalimumab with hyaluronic acid / polyvinylpyrrolidone to combine intraarticular drug delivery and viscosupplementation

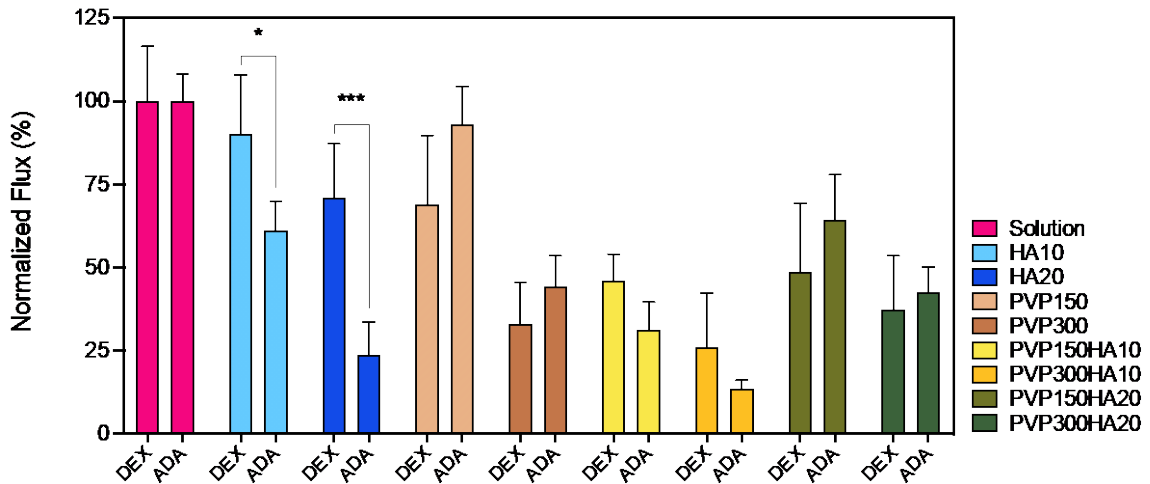


Fig. 5-7 Normalized flux of ADA through the ex-vivo synovium compared with the normalized flux of dextran 150 kDa. Mean \pm SD; n=6, Multiple t-test; significant differences: '*' ($p < 0.05$), '***' ($p < 0.001$), DEX vs. ADA.

5.6.4 Isothermal titration calorimetry

Binding isotherms of HA and ADA was found biphasic (**Fig. 5-8A**). After the resulting heat first slowly declined, it reached a minimum from which it increased sigmoidally and approaches zero. The evolved parameters resulted in a negative value of enthalpy (ΔH) for both binding sites (**Sup. Tab. 1**). In contrary, binding isotherms with dextran and HA showed values close to zero which suggested that no or very little binding occurs between the molecules at the relevant mixing ratios (**Fig. 5-8B**). As a consequence, no model could be fitted, and no binding parameters could be developed for dextran.

5 Co-formulations of adalimumab with hyaluronic acid / polyvinylpyrrolidone to combine intraarticular drug delivery and viscosupplementation

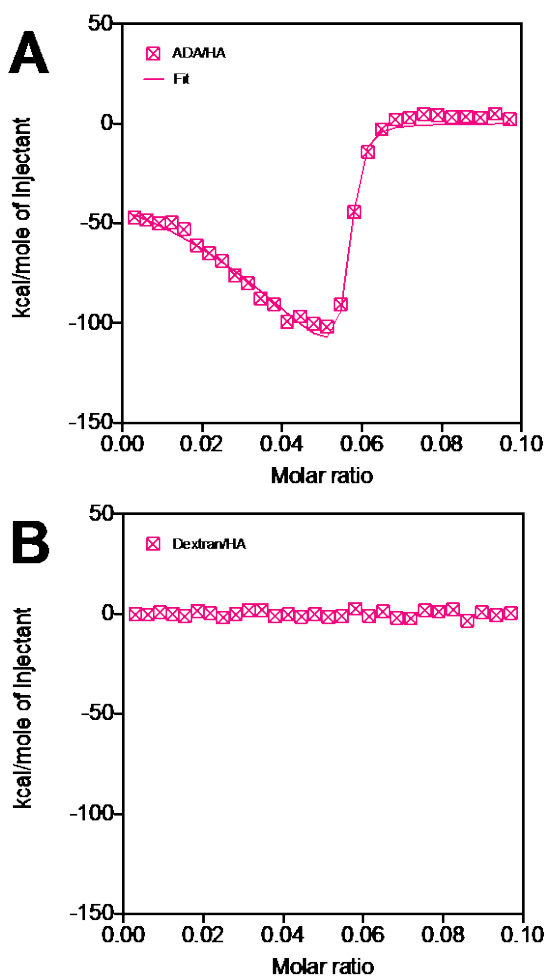


Fig. 5-8 ITC results showing the binding isotherm of HA with ADA (**A**) after subtraction of the heat of dilution and of HA with dextran 150 kDa (**B**) after subtraction of the heat of dilution. Binding isotherm obtained by integration of the raw ITC data (**Sup. Fig. 5-5**). The solid line represents the best-fit curve generated from a 'two set of sites' binding model.

5.6.5 ADA activity in presence of polymers

The measured concentration of TNF- α bound ADA after incubation for 48 h at 37° C was 17.3 ± 1.6 $\mu\text{g/mL}$ for the solution which corresponds to approximately 70% activity (**Fig. 5-9**). No significant difference was observed by addition of HA alone ($p > 0.05$), though the activity of the polymer solution was measured higher than that of the control solution. In contrast, the addition of PVP resulted in a significantly higher activity of ADA ($p < 0.05$).

5 Co-formulations of adalimumab with hyaluronic acid / polyvinylpyrrolidone to combine intraarticular drug delivery and viscosupplementation

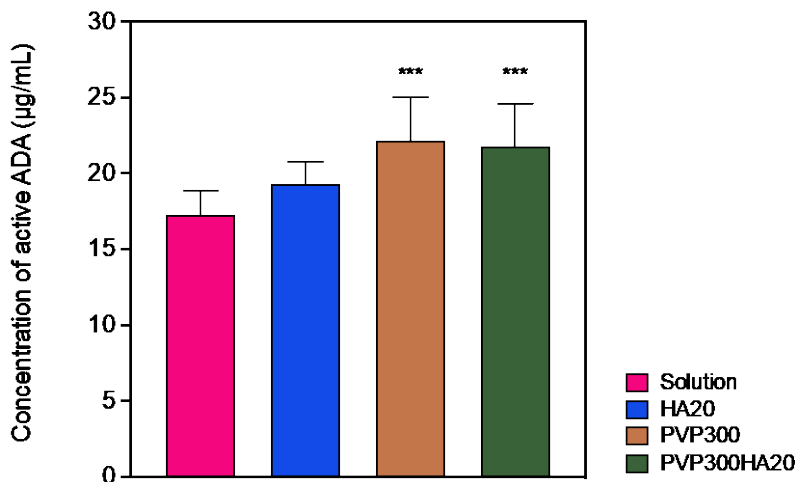


Fig. 5-9 Activity of active ADA to bind TNF- α in presence of polymers after 48 h of incubation at 37° C. 25 μ g/ml equals 100% activity compared to directly measured ADA solution. Mean \pm SD; n=9; ANOVA+ Dunnett's multiple comparison test; significant differences: '***' (p < 0.001) compared to solution.

5.7 Discussion

5.7.1 Rheology

The ZSV of healthy human synovial fluid was reported in the area of 6-175 Pas with a STI (η_0/η_{300}) of 70-250, whereas arthritic synovial fluid shows ZSVs from 0.1-1 Pas and a STI of 5-40 [2]. From these digits it becomes clear that the aim of viscosupplementation is to restore or augment the rheological properties of healthy synovial fluid. Most tested viscosupplements were insignificantly different as compared from the measured porcine synovial fluid and fell into the region described for human synovial fluid. Exceptions were the formulations with HA20, which due to the formation of a dense network, led to a sharp increase in ZSV that could be further increased by the addition of PVP. HA's intermolecular interactions via hydrogen bonds increase with its concentration or its longer polymer chains leading to more entanglements, so that higher concentrations as well as higher molecular weights cause an increase in ZSV [33]. For evaluation, it should be considered that, besides restoration of healthy synovial fluid rheological properties, there are no generally accepted rheological target values for the development of viscosupplements. Hence, higher viscosities than synovial fluid, which can for instance be achieved by cross-linking HA [34], likewise provided beneficial therapeutic effects in clinical trials. Shear thinning behavior was in the range of healthy human synovial fluid for HA10, PVP150HA10 and PVP300HA20. PVP alone exhibited an almost Newtonian behavior over the

measured shear rate range with an STI close to 1, which indicates that no network is formed by interaction of the polymer chains. While this property seems undesirable at first, PVP was yet evaluated favorable in the therapy of OA in clinical studies [13], possibly due to the excellent tribological and film building characteristics of the polymer solution [12,35], which likely enhances the physiological superficial layer covering the articular surface [4]. Since optimal articular lubrication is expected to be mediated by the synergistic action of fluid film lubrication and boundary lubrication [36,37], combination of the lubricants HA and PVP may provide these exact characteristics due to their different tribological properties. In addition, a higher viscosity at high shear rates can be advantageous from the perspective of cartilage protection under high load, where the surfaces remain more effectively preserved during stronger movements and further articular destruction may be prevented, which is also the rationale for the use of PVP in arthroplasty [16]. A low STI may further have an influence on the release of API from the viscosupplements under load and thus retain the depot effect of the viscosupplement formulation. These qualities are contrasted with the syringeability of the formulation, which, however, was measured to be adequate (26-50 N), for the viscosupplements containing PVP300 or even easy to very easy (<25 N) for all other viscosupplements [38]. During walking, running or jumping, a fast frequency and therefore mechanical stress is applied to the articular surfaces, which could be simulated by oscillatory measurements. The objective of the synovial fluid or viscosupplement is to absorb this mechanical stress through its rigidity and elasticity. Generally, a fluid with a $\tan\delta < 1$ behaves like an elastic body, that absorbs the mechanical energy and thus protects the cartilage tissue from possible mechanical damage. In addition, it has been discovered that elastic behavior led to a pain relief through desensitization of the mechanosensitive apparatus of nociceptors in the synovial tissue [39]. All viscosupplements showed at least equivalent rigidity to the synovial fluid, as can be taken from the elastic modulus values at 2.5 Hz, with only PVP150 being an exception. The formulations containing only PVP also show a $\tan\delta > 1$, which, as described above, is also not considered ideal for the shock absorption of the joint. Thus, from a rheological perspective, PVP alone is not an optimal VS. However, as a blend with HA, it is able to increase its stiffness and viscosity under load, thus enabling a rational design of the VS by synergistic rheological combination. This is especially true since for all HA-containing formulations the crossover point was found to be below a frequency of 0.5 Hz, which is generally considered to be the transfer of energy as experienced to cartilage surfaces during walking, which

implies that elastic behavior was predominant over the relevant range of joint motion.

5.7.2 Transsynovial permeability

The potential of VSs to sensitively control drug diffusion of macromolecular APIs such as ADA and thus their residence time in the joint space is also important to consider. ADA solutions permeate the synovial membrane with linear kinetics, which leads to the assumption of passive diffusion as the major path of ADA joint elimination, with no or little cellular processes contributing. As synovial permeability is dependent on the size of the molecule [40,41], ADA permeates slightly faster across the *ex-vivo* membrane than the 150 kDa dextran since, despite a comparable MW, it has a reported smaller hydrodynamic radius than the polysaccharide due to its secondary folding [42]. Although in our experiment no difference was found between SF and buffer on the permeation of ADA alone, the complex composition of the antibody *in vivo* could still be influenced by the properties of the SF, especially since their effect in combination with the different formulations was not evaluated separately. Addition of PVP leads to a concentration dependent deceleration of both ADA and dextran diffusion to similar extents. The restriction in mobility of the different macromolecules in the PVP formulations can be directly correlated to the increased ZSV as described in the Stokes-Einstein equation, with polymeric chains acting as obstacles and that alter the motion of the molecule [43]. In contrast, the pure HA hydrogel shows significant differences in the influence of the dextran and ADA. While the permeation of dextran is only marginally affected, a decrease in the transsynovial flux of ADA can be observed even with smaller amounts of HA. Since ADA has an isoelectric point of approximately 8.9 it bears a positive charge at physiological pH. What is more, the presence of basic patches in its structure result in an enhanced electrostatic interaction potential of the protein as compared to other monoclonal antibodies [42], which may further delay its diffusion in the polyelectrolyte matrix. The ITC measurements confirm this electrostatic interaction between HA and ADA for both binding sites, as a negative value of enthalpy (ΔH) is considered indicative for electrostatic and hydrogen-bonding contributions [44]. Thereby, the first binding site presumably reflects multiple binding sites of the same type of ADA to HA, whereas the second binding site might indicate size or charge restricted saturation of HA with ADA. The observed binding reaction between ADA and the negatively charged HA by ITC, whereas dextran showed no apparent interaction with the polysaccharide, suggested that

this interference, in addition to viscosity-mediated effects, was responsible for the prolongation of residence of ADA. This finding is in agreement with a significant decrease of ZSV after addition of ADA, caused by intermolecular interactions. While HA is normally present in a rod-like structure, it has been shown that the binding of cationic patches of a protein with the carbonyl groups of HA leads to an entanglement of the molecule, which induces a decrease in viscosity [45,46] but yet restricts permeation over the synovial membrane as revealed in our work. Despite the observed interaction of ADA with HA, no negative effect on ADA activity was detected. On the contrary, both polymers showed a trend towards slightly higher binding activity of ADA to TNF- α compared to the control solution, with PVP containing formulations being significantly higher. They therefore appear to have a stabilizing effect on the antibody and ameliorate the loss of activity that monoclonal antibodies generally experience due to dilution PBS [47]. This observation is consistent with previous studies of hyaluronic acid coacervates with cationic proteins, which likewise resulted in a significant improvement in stability [48] and protein stabilization through PVP by volume exclusion and soft interactions [49]. As both, ADA and HA, have a positive impact on the development of osteoarthritis and their combination additionally increases the ADA joint residence time, a dual strategy of a drug-delivering viscosupplements represents to be reasonable therapeutic approach. PVP and HA in combination can further reduce the flux by combining both diffusion-limiting mechanisms. In research, HA blends are already of importance for controlled release of antibiotics and antiseptics, for example in the field of wound healing. Among others, HA/PVP mixtures have shown a sustained release of the active ingredient because of interaction between the polymers [8]. Given the pivotal role of HA in the joint, it is reasonable to transfer these conclusions to their potential in prolonging the residence time of protein drugs in the joint space by means of formulations that are adapted to this biopharmaceutical environment. The observed synergism can be tuned to reach an optimum in ADA residence time since above a threshold ratio, flux increases again with further increase of PVP content, which is likely attributed to disruptions of the HA network by separation of interpenetrating PVP polymer chains. Taken together, it should be considered that PVP, in addition to its diffusion-restricting effect on ADA, also prolongs HA retention in the joint cavity. This reduction in HA flux can be explained, similarly to dextran, by an increase in viscosity and an associated restriction in the diffusion of the biomacromolecule, which is also reflected in good correlations of the flux with the viscosity responses. HA is particularly strongly retained because

it has a considerable hydrodynamic radius of approximately 400 nm [33]. Since from the therapeutic perspective it is desirable to maintain both HA and ADA in the joint cavity for a prolonged period of time, or in view of the drug delivery strategy alone, PVP could hence represent a beneficial excipient for IA injections, whereby desirable lubricating properties are additionally introduced into the formulation. Despite the promising properties of the PVP/HA combinations, the use of higher molecular weight PVPs may be constrained by the restricted PVP elimination *in-vivo*. Unlike short-chain PVPs, these are only renally eliminated to a very limited extent, so that due to the low biodegradability, their fate remains unclear, and storage may occur [50,51]. Although studies indicate that cumulative doses up to at least 200 g do not lead to any accumulation in tissue, a more detailed investigation of PVP elimination or accumulation after injection into the joint space would be necessary to justify an *in-vivo* application. When compared to alternate delivery approaches for monoclonal antibodies [52–54], the presented polymer mixtures exhibit multiple advantages in terms of bioactivity preservation and facile, yet efficient, prolongation of the combined residence time. They require neither organic solvents nor elevated temperatures, sonication, or exposure to high shear, all of which are widely regarded critical for preserving a protein drug's full activity, as is the case with conventional methods for the formation of particulate carriers [55]. However, the presented viscous polymer formulations are not able to extend the residence time to the same extent as microparticulate dosage forms. Yet, they provide an additional multimodal therapeutic approach and relief OA symptoms due to their viscosupplementative nature instead of potentially causing irritation due to mechanical friction. In this way, this study demonstrates general principles of rationally combining different types of polymers for intra-articular injections to achieve simultaneous multiple therapeutic goals, such as lubrication and drug release, and shows good transferability to other systems through an adoptable and rational formulation strategy.

5.8 Conclusion

The biocompatible, parenterally administrable polymers HA and PVP have different rheological properties, both of which have been shown to be beneficial in clinical trials for the treatment of OA and which can be combined to provide a sensitively adjustable formulation for viscosupplementation. Since PVP is subject to low biodegradability and has the ability to slow the clearance of HA, it may

enhance and prolong the effectiveness of IA treatment when combined with HA. Furthermore, the incorporation of ADA into the IA injection represents a promising dual therapeutic strategy, whereby the hydrogel matrix not only prolongs the joint residence time of the anti-inflammatory antibody but is itself biomechanically active. The retardation of diffusion of ADA from the hydrogel matrix is thereby achieved not only by viscosity-related properties of the polymer blend, but in particular by electrostatic interaction between ADA and HA, with the polymer combination further promoting stabilization of the antibody activity.

5.9 Acknowledgements

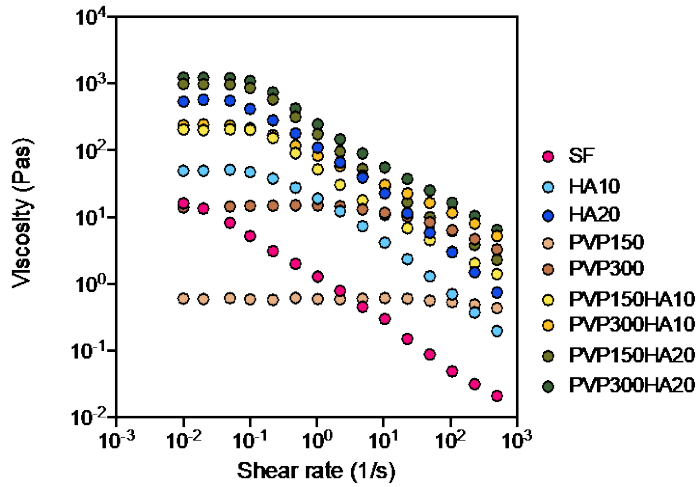
Ferring Pharmaceuticals Inc. sponsored the research that is the subject of the manuscript. Employees of the sponsor were involved in the conceptualization and design of the study.

5.10 Author contributions

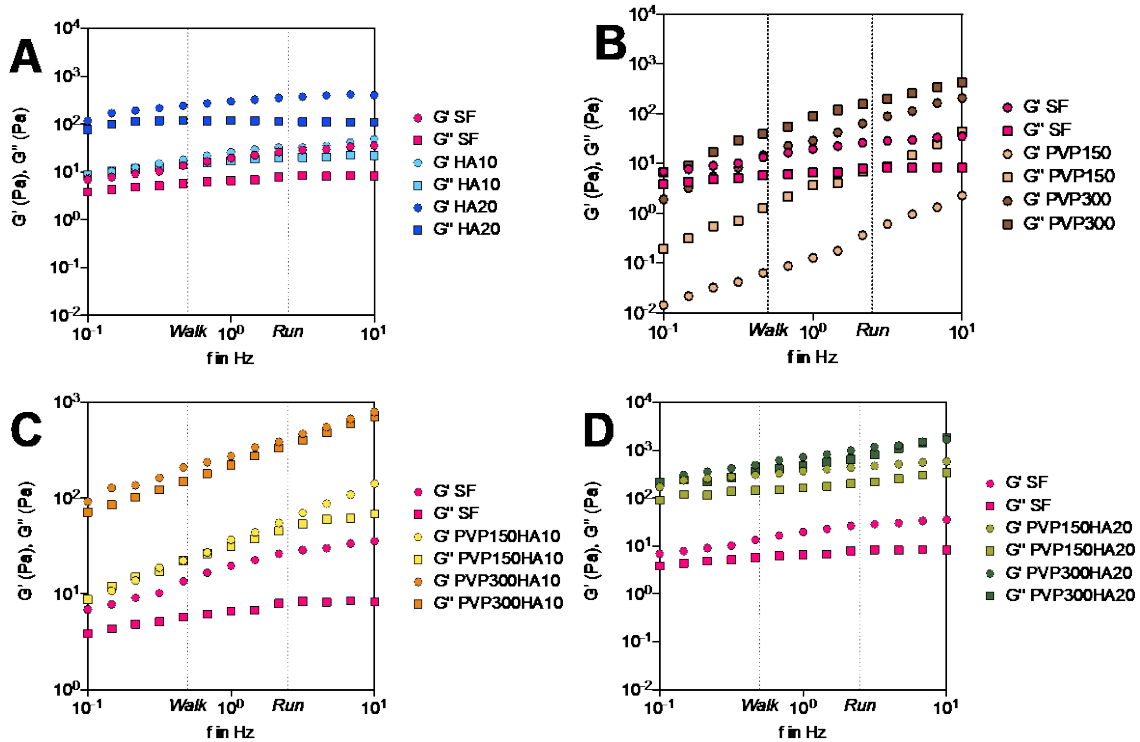
Conceptualization, T.S., A.La.; methodology, T.S.; software, T.S.; validation, T.S.; formal analysis, T.S.; investigation, T.S.; resources, A.La., S.B., D.P., J.L., A.Li., C.C.L.; data curation, T.S.; writing-original draft preparation, T.S.; writing-review and editing, T.S., A.La., S.B.; visualization, T.S.; supervision, A.La.; project administration A.La., S.B., D.P., J.L., A.Li., C.C.L.; funding acquisition, A.La., S.B., D.P., J.L., A.Li., C.C.L.

All authors have read and agreed to the published version of the manuscript.

5.11 Supplementary data

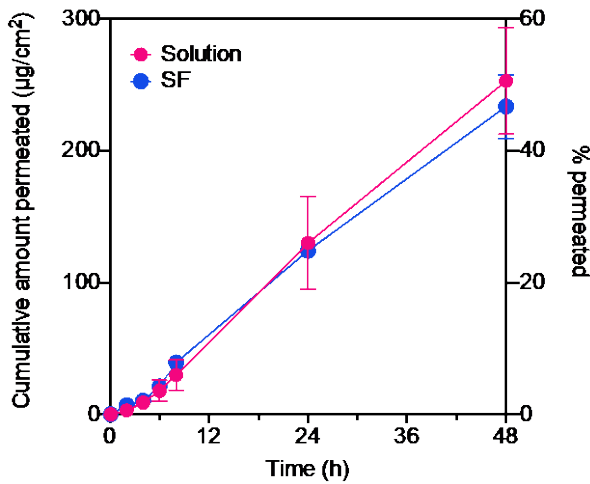


Sup. Fig. 5-1: Viscosity as a function of shear rate of synovial fluid and the different HA + PVP viscosupplements. SD was omitted for clarity reasons; n = 3.

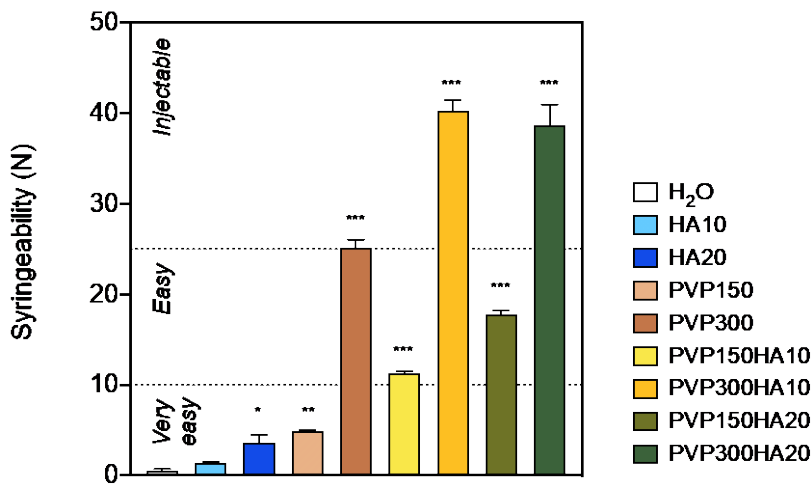


Sup. Fig. 5-2: Elastic and viscous modulus as measured by oscillatory rheometry with 0.1% stress for synovial fluid in comparison HA 10 and 20 mg/mL (A), PVP 150 mg/mL and 300 mg/mL (B), HA 10 mg/mL + PVP150 mg/mL or 300 mg/mL formulations (C) and HA 20 mg/mL + PVP150 mg/mL or 300 mg/mL (D). SD was omitted for clarity reasons; n = 3.

5 Co-formulations of adalimumab with hyaluronic acid / polyvinylpyrrolidone to combine intraarticular drug delivery and viscosupplementation

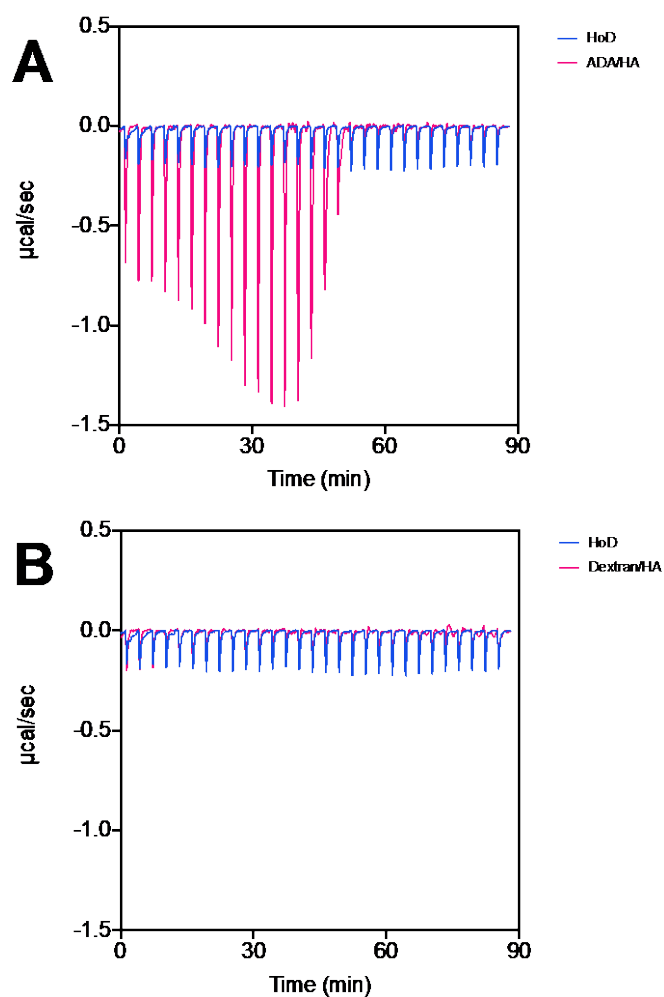


Sup. Fig. 5-3: Cumulative amount permeated of ADA through *ex-vivo* synovium as solution and with addition of synovial fluid (SF).



Sup. Fig. 5-4: Maximum injectability of intraarticular formulations in Newton (N) as measured for a syringe equipped with a 23 G needle. Dotted lines correspond to classification into <10 N "Very easy to inject", 11-25 N "Easy to inject", 26-50 N "Injectable" according to Rungseevijitprapaa and Bodmeier [38]. Mean \pm SD; n = 3; '*' ($p < 0.05$), '***' ($p < 0.01$) compared to H₂O.

5 Co-formulations of adalimumab with hyaluronic acid / polyvinylpyrrolidone to combine intraarticular drug delivery and viscosupplementation



Sup. Fig. 5-5: Raw data from titration of consecutive 10- μL injections of HA into either ADA (**A**) or dextran (**B**), represented as the heat change ($\mu\text{cal}/\text{s}$) upon injection over time.

Sup. Tab. 1: Thermodynamic properties of ADA binding to HA after subtraction of the dilution heat as derived from 'two sets of binding sites' fitting.

N_1	K_1	ΔH_1	$T\Delta S_1$	ΔG_1
0,0372	7,12E+08	-1,03E+04	1,73E+03	-1,21E+04
N_2	K_2	ΔH_2	$T\Delta S_2$	ΔG_2
0,018	2,83E+08	-2,21E+05	-2,10E+05	-1,15E+04

5.12 References

- [1] N. Volpi, J. Schiller, R. Stern, L. Soltes, Role, Metabolism, Chemical Modifications and Applications of Hyaluronan, *Curr. Med. Chem.* 16 (2009) 1718–1745. <https://doi.org/10.2174/092986709788186138>.
- [2] H. Fam, J.T. Bryant, M. Kontopoulou, Rheological properties of synovial fluids, *Biorheology.* 44 (2007) 59–74.
- [3] D. Jiang, J. Liang, P.W. Noble, Hyaluronan in Tissue Injury and Repair, *Annu. Rev. Cell Dev. Biol.* 23 (2007) 435–461. <https://doi.org/10.1146/annurev.cellbio.23.090506.123337>.
- [4] V.C. Hascall, K.E. Kuettner, The Many Faces of Osteoarthritis, (2002). <http://dx.doi.org/10.1007/978-3-0348-8133-3>.
- [5] E. Balazs, J. Denlinger, Viscosupplementation: a new concept in the treatment of osteoarthritis, *J. Rheumatol. Suppl.* 39 (1993) 3–9.
- [6] P. Ghosh, D. Guidolin, Potential mechanism of action of intra-articular hyaluronan therapy in osteoarthritis: Are the effects molecular weight dependent?, *Semin. Arthritis Rheum.* 32 (2002) 10–37. <https://doi.org/10.1053/sarh.2002.33720>.
- [7] Z. He, B. Wang, C. Hu, J. Zhao, An overview of hydrogel-based intra-articular drug delivery for the treatment of osteoarthritis, *Colloids Surf. B Biointerfaces.* 154 (2017) 33–39. <https://doi.org/10.1016/j.colsurfb.2017.03.003>.
- [8] I.S. Bayer, Hyaluronic Acid and Controlled Release: A Review, *Molecules.* 25 (2020) 2649. <https://doi.org/10.3390/molecules25112649>.
- [9] P. Franco, I. De Marco, The Use of Poly(N-vinyl pyrrolidone) in the Delivery of Drugs: A Review, *Polymers.* 12 (2020) 1114. <https://doi.org/10.3390/polym12051114>.
- [10] T. Kato, N. Kozaki, A. Takahashi, Lubrication by Thin Liquid Films of Aqueous Polymer Solutions, *Polym. J.* 18 (1986) 111–116. <https://doi.org/10.1295/polymj.18.111>.
- [11] M.W. Sulek, W. Sas, T. Wasilewski, A. Bak-Sowinska, U. Piotrowska, Polymers (Polyvinylpyrrolidones) As Active Additives Modifying the Lubricating Properties of Water, *Ind. Eng. Chem. Res.* 51 (2012) 14700–14707. <https://doi.org/10.1021/ie301431v>.

- [12] Y. Guo, Z. Hao, C. Wan, Tribological characteristics of polyvinylpyrrolidone (PVP) as a lubrication additive for artificial knee joint, *Tribol. Int.* 93 (2016) 214–219. <https://doi.org/10.1016/j.triboint.2015.08.043>.
- [13] A.A. Matulis, I.G. Dadonene, Z.K. Matskevichius, [Efficacy of polyvinylpyrrolidone solutions of various concentrations in patients with rheumatic diseases of the joints]., *Ter. Arkh.* 61 (1989) 108–112.
- [14] V.V. Vasilenkaïtis, [Artificial synovial fluid for the joints]., *Ortop. Travmatol. Protez.* (1989) 11–15.
- [15] J.K. Katta, M. Marcolongo, A. Lowman, K.A. Mansmann, Friction and wear behavior of poly(vinyl alcohol)/poly(vinyl pyrrolidone) hydrogels for articular cartilage replacement, *J. Biomed. Mater. Res. A.* 83A (2007) 471–479. <https://doi.org/10.1002/jbm.a.31238>.
- [16] Y. Kanca, P. Milner, D. Dini, A.A. Amis, Tribological properties of PVA/PVP blend hydrogels against articular cartilage, *J. Mech. Behav. Biomed. Mater.* 78 (2018) 36–45. <https://doi.org/10.1016/j.jmbbm.2017.10.027>.
- [17] T. Hoare, D. Zurakowski, R. Langer, D.S. Kohane, Rheological blends for drug delivery. I. Characterization *in vitro*, *J. Biomed. Mater. Res. A.* 9999A (2009) NA-NA. <https://doi.org/10.1002/jbm.a.32392>.
- [18] S. Orita, T. Koshi, T. Mitsuka, M. Miyagi, G. Inoue, G. Arai, T. Ishikawa, E. Hanaoka, K. Yamashita, M. Yamashita, Y. Eguchi, T. Toyone, K. Takahashi, S. Ohtori, Associations between proinflammatory cytokines in the synovial fluid and radiographic grading and pain-related scores in 47 consecutive patients with osteoarthritis of the knee, *BMC Musculoskelet. Disord.* 12 (2011) 144. <https://doi.org/10.1186/1471-2474-12-144>.
- [19] M.B. Goldring, M. Otero, Inflammation in osteoarthritis, *Curr. Opin. Rheumatol.* 23 (2011) 471–478. <https://doi.org/10.1097/BOR.0b013e328349c2b1>.
- [20] W.P. Maksymowych, A.S. Russell, P. Chiu, A. Yan, N. Jones, T. Clare, R.G. Lambert, Targeting tumour necrosis factor alleviates signs and symptoms of inflammatory osteoarthritis of the knee, *Arthritis Res. Ther.* 14 (2012) R206. <https://doi.org/10.1186/ar4044>.

- [21] G. Verbruggen, R. Wittoek, B.V. Cruyssen, D. Elewaut, Tumour necrosis factor blockade for the treatment of erosive osteoarthritis of the interphalangeal finger joints: a double blind, randomised trial on structure modification, *Ann. Rheum. Dis.* 71 (2012) 891. <https://doi.org/10.1136/ard.2011.149849>.
- [22] X. Chevalier, B. Giraudeau, T. Conrozier, J. Marliere, P. Kiefer, P. Goupille, Safety study of intraarticular injection of interleukin 1 receptor antagonist in patients with painful knee osteoarthritis: a multicenter study., *J. Rheumatol.* 32 (2005) 1317–1323.
- [23] S.H.R. Edwards, Intra-articular drug delivery: The challenge to extend drug residence time within the joint, *Vet. J.* 190 (2011) 15–21. <https://doi.org/10.1016/j.tvjl.2010.09.019>.
- [24] C.H. Evans, V.B. Kraus, L.A. Setton, Progress in intra-articular therapy, *Nat. Rev. Rheumatol.* 10 (2014) 11–22. <https://doi.org/10.1038/nrrheum.2013.159>.
- [25] X. Chevalier, P. Goupille, A.D. Beaulieu, F.X. Burch, W.G. Bensen, T. Conrozier, D. Loeuille, A.J. Kivitz, D. Silver, B.E. Appleton, Intraarticular injection of anakinra in osteoarthritis of the knee: A multicenter, randomized, double-blind, placebo-controlled study, *Arthritis Care Res.* 61 (2009) 344–352. <https://doi.org/10.1002/art.24096>.
- [26] J. Schurz, V. Ribitsch, Rheology of synovial fluid¹, *Biorheology.* 24 (1987) 385–399. <https://doi.org/10.3233/BIR-1987-24404>.
- [27] P. Bhuanantanondh, D. Grecov, E. Kwok, P. Guy, Rheology of osteoarthritic synovial fluid mixed with viscosupplements: A pilot study, *Biomed. Eng. Lett.* 1 (2011) 213–219. <https://doi.org/10.1007/s13534-011-0034-7>.
- [28] M. Chernos, D. Grecov, E. Kwok, S. Bebe, O. Babsola, T. Anastassiades, Rheological study of hyaluronic acid derivatives, *Biomed. Eng. Lett.* 7 (2017) 17–24. <https://doi.org/10.1007/s13534-017-0010-y>.
- [29] F. Cilurzo, F. Selmin, P. Minghetti, M. Adami, E. Bertoni, S. Lauria, L. Montanari, Injectability evaluation: an open issue., *AAPS PharmSciTech.* 12 (2011) 604–609. <https://doi.org/10.1208/s12249-011-9625-y>.
- [30] J. Liberda, M. Ticha, V. Jonakova Preparation of fluorescein-labelled and biotinylated derivatives of polysaccharides for lectin-saccharide binding studies, *Biotechnol. Tech.* 11 (1997) 265–268. <https://doi.org/10.1023/A:1018446723616>.

- [31] T. Siefen, J. Lokhnauth, A. Liang, C.C. Larsen, A. Lamprecht, An ex-vivo model for transsynovial drug permeation of intraarticular injectables in naive and arthritic synovium, *J. Controlled Release.* (2021). <https://doi.org/10.1016/j.jconrel.2021.03.008>.
- [32] C. Desvignes, S.R. Edupuganti, F. Darrouzain, A.-C. Dubeau, A. Loercher, G. Paintaud, D. Mulleman, Development and validation of an enzyme-linked immunosorbent assay to measure adalimumab concentration, *Bioanalysis.* 7 (2015) 1253–1260. <https://doi.org/10.4155/bio.15.30>.
- [33] M.K. Cowman, T.A. Schmidt, P. Raghavan, A. Stecco, Viscoelastic Properties of Hyaluronan in Physiological Conditions, *F1000Research.* 4 (2015) 622. <https://doi.org/10.12688/f1000research.6885.1>.
- [34] M. Nicholls, A. Manjoo, P. Shaw, F. Niazi, J. Rosen, A Comparison Between Rheological Properties of Intra-articular Hyaluronic Acid Preparations and Reported Human Synovial Fluid, *Adv. Ther.* 35 (2018) 523–530. <https://doi.org/10.1007/s12325-018-0688-y>.
- [35] E.L. Radin, I.L. Paul, P.A. Weisser, Joint Lubrication with Artificial Lubricants, *Arthritis Rheum.* 14 (1971) 126–129. <https://doi.org/10.1002/art.1780140116>.
- [36] G. Morgese, E.M. Benetti, M. Zenobi-Wong, Molecularly Engineered Biolubricants for Articular Cartilage, *Adv. Healthc. Mater.* 7 (2018) 1701463. <https://doi.org/10.1002/adhm.201701463>.
- [37] W. Lin, J. Klein, Recent Progress in Cartilage Lubrication, *Adv. Mater.* 33 (2021) 2005513. <https://doi.org/10.1002/adma.202005513>.
- [38] W. Rungseewijitprapa, R. Bodmeier, Injectability of biodegradable in situ forming microparticle systems (ISM), *Eur. J. Pharm. Sci.* 36 (2009) 524–531. <https://doi.org/10.1016/j.ejps.2008.12.003>.
- [39] E.A. Balazs, Chapter 20 - Viscoelastic Properties of Hyaluronan and Its Therapeutic Use. From Ref. 189., in: H.G. Garg, C.A. Hales (Eds.), *Chem. Biol. Hyaluronan*, Elsevier Science Ltd, Oxford, 2004: pp. 415–455. <https://doi.org/10.1016/B978-008044382-9/50051-0>.

- [40] B. Sterner, M. Harms, S. Wöll, M. Weigandt, M. Windbergs, C.M. Lehr, The effect of polymer size and charge of molecules on permeation through synovial membrane and accumulation in hyaline articular cartilage, *Eur. J. Pharm. Biopharm.* 101 (2016) 126–136. <https://doi.org/10.1016/j.ejpb.2016.02.004>.
- [41] Y. Guang, A.L. Davis, T.M. McGrath, C.T.N. Pham, J.A.J. Fitzpatrick, L.A. Setton, Size-Dependent Effective Diffusivity in Healthy Human and Porcine Joint Synovium, *Ann. Biomed. Eng.* (2021). <https://doi.org/10.1007/s10439-020-02717-4>.
- [42] A. Goyon, M. Excoffier, M.-C. Janin-Bussat, B. Bobaly, S. Fekete, D. Guillaume, A. Beck, Determination of isoelectric points and relative charge variants of 23 therapeutic monoclonal antibodies, *J. Chromatogr. B.* 1065–1066 (2017) 119–128. <https://doi.org/10.1016/j.jchromb.2017.09.033>.
- [43] E.A. Mun, C. Hannell, S.E. Rogers, P. Hole, A.C. Williams, V.V. Khutoryanskiy, On the Role of Specific Interactions in the Diffusion of Nanoparticles in Aqueous Polymer Solutions, *Langmuir.* 30 (2014) 308–317. <https://doi.org/10.1021/la4029035>.
- [44] F. Zsila, T. Juhász, G. Kohut, T. Beke-Somfai, Heparin and Heparan Sulfate Binding of the Antiparasitic Drug Imidocarb: Circular Dichroism Spectroscopy, Isothermal Titration Calorimetry, and Computational Studies, *J. Phys. Chem. B.* 122 (2018) 1781–1791. <https://doi.org/10.1021/acs.jpcc.7b08876>.
- [45] S. Xu, J. Yamanaka, S. Sato, I. Miyama, M. Yonese, Characteristics of Complexes Composed of Sodium Hyaluronate and Bovine Serum Albumin., *Chem. Pharm. Bull. (Tokyo).* 48 (2000) 779–783. <https://doi.org/10.1248/cpb.48.779>.
- [46] I. Morfin, E. Buhler, F. Cousin, I. Grillo, F. Boué, Rodlike Complexes of a Polyelectrolyte (Hyaluronan) and a Protein (Lysozyme) Observed by SANS, *Biomacromolecules.* 12 (2011) 859–870. <https://doi.org/10.1021/bm100861g>.
- [47] S.A. Giannos, E.R. Kraft, Z.-Y. Zhao, K.H. Merkle, J. Cai, Formulation Stabilization and Disaggregation of Bevacizumab, Ranibizumab and Aflibercept in Dilute Solutions, *Pharm. Res.* 35 (2018) 78. <https://doi.org/10.1007/s11095-018-2368-7>.

- [48] J.J. Water, M.M. Schack, A. Velazquez-Campoy, M.J. Maltesen, M. van de Weert, L. Jorgensen, Complex coacervates of hyaluronic acid and lysozyme: Effect on protein structure and physical stability, *Eur. J. Pharm. Biopharm.* 88 (2014) 325–331. <https://doi.org/10.1016/j.ejpb.2014.09.001>.
- [49] A.C. Miklos, C. Li, N.G. Sharaf, G.J. Pielak, Volume Exclusion and Soft Interaction Effects on Protein Stability under Crowded Conditions, *Biochemistry.* 49 (2010) 6984–6991. <https://doi.org/10.1021/bi100727y>.
- [50] Robinson, B.V, Sullivan, F.M., Borzelleca, J.F., Schwartz, S.L., PVP: A Critical Review of the Kinetics and Toxicology of Polyvinylpyrrolidone (Povidone) (1st ed.), CRC Press. (1990). <https://doi.org/10.1201/9780203741672>.
- [51] L. Vanharova, M. Julinova, R. Slavik, PVP Based Materials: Biodegradation in Different Environments, *Ecol. Chem. Eng. S.* 24 (2017) 299–309. <https://doi.org/10.1515/eces-2017-0021>.
- [52] M. Ries, B. Moulari, M.A. Shetab Boushehri, M.E. Ali, D. Molnar, A. Béduneau, Y. Pellequer, A. Lamprecht, Adalimumab Decorated Nanoparticles Enhance Antibody Stability and Therapeutic Outcome in Epithelial Colitis Targeting, *Pharmaceutics.* 14 (2022) 352. <https://doi.org/10.3390/pharmaceutics14020352>.
- [53] J. Pradal, P. Maudens, C. Gabay, C.A. Seemayer, O. Jordan, E. Allémann, Effect of particle size on the biodistribution of nano- and microparticles following intra-articular injection in mice, *Int. J. Pharm.* 498 (2016) 119–129. <https://doi.org/10.1016/j.ijpharm.2015.12.015>.
- [54] R.T. Liggins, T. Cruz, W. Min, L. Liang, W.L. Hunter, H.M. Burt, Intra-articular treatment of arthritis with microsphere formulations of paclitaxel: biocompatibility and efficacy determinations in rabbits, *Inflamm. Res.* 53 (2004). <https://doi.org/10.1007/s00011-004-1273-1>.
- [55] D.J.A. Crommelin, R.D. Sindelar, B. Meibohm, eds., *Pharmaceutical Biotechnology: Fundamentals and Applications*, Springer International Publishing, Cham, 2019. <https://doi.org/10.1007/978-3-030-00710-2>.
- [56] E.A. Balazs, The physical properties of synovial fluid and the special role of hyaluronic acid, *Disord. Knee.* (1982) 61–74.

6. Polyelectrolyte nanocomplexes to increase intraarticular residence of adalimumab injections

Tobias Siefen¹, Simon Bjerregaard², Daniel Plaksin², Camilla Borglin², Crilles Casper Larsen³, Alf Lamprecht^{1,4}

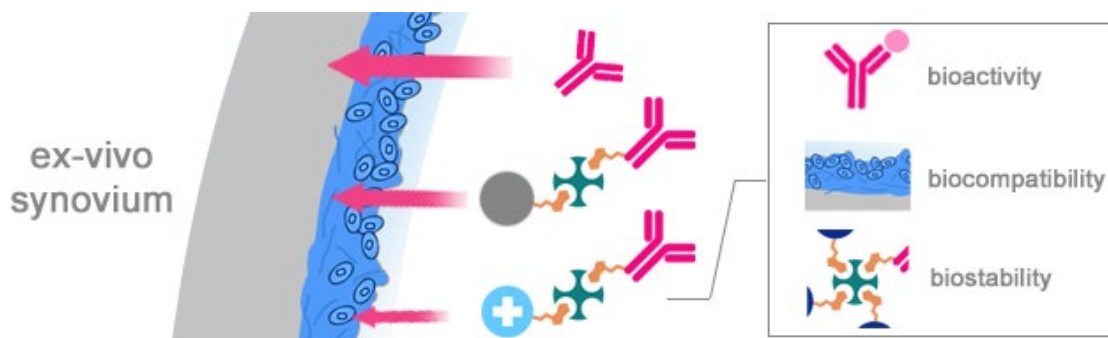
¹Department of Pharmaceutics, Institute of Pharmacy, University of Bonn, Bonn, Germany.

²Ferring Pharmaceuticals A/S, Copenhagen, Denmark

³Ferring Pharmaceuticals Inc, Parsippany, New Jersey, USA

⁴PEPITE (EA4267), University of Burgundy/Franche-Comté, Besançon, France.

6.1 Graphical abstract



6.2 Abstract

Local intraarticular injections of biologics such as the TNF- α antibody adalimumab could provide more efficient therapy for osteoarthritis but suffer from an insufficient residence time in the joint cavity due to rapid elimination across the synovial membrane. The extracellular matrix of the synovium consists of a collagen network with enmeshed aggrecan galactosamine glycans, generating a high fixed negative charge density. This biopharmaceutical environment can be taken advantage of through rationally derived drug delivery strategies that extend the duration of action in the joint. By linking adalimumab with different molar equivalents of cationic diethylaminoethyl-dextran using avidin mediated nanocomplexes, the flux through porcine synovium was decelerated from 53.3 ± 15.4 to 14.3 ± 7.2 pmol/cm²/h whereby immobilization in superficial tissue layers was revealed by confocal laser scanning microscopy. The prepared carriers exhibited excellent intra-tissue stability, while retaining up to $84.4 \pm 3.6\%$ antigen recognition of adalimumab compared to pure mAb. In addition, the nanocomplexes showed no adverse effects on synovial cells exhibiting a viability of $86.7 \pm 10.4\%$ compared to adalimumab alone. This work highlights how bioelectric-driven material-tissue interactions can be employed by avidin-biotin-linked cationic nanocomplexes to slow ex vivo permeation across the synovial membrane without limiting antibody functionality.

6.3 Keywords

Bioelectricity, ex-vivo synovium, DEAE-dextran, joint residence time

6.4 Introduction

Osteoarthritis (OA) is an irreversible joint degeneration that most frequently affects the hands, knees, hips, and spine and leads to pain, stiffness, and loss of mobility [1]. Although OA is the most common musculoskeletal disorder worldwide and the disease causes a severe reduction in the quality of life [2], until today only very limited therapeutic options are available. Since usually individual joints are affected, local therapy by means of intraarticular injections (IA) would present a logical treatment approach. In addition, local therapies generally enable the application of macromolecular agents such as therapeutic antibodies and allow delivery of the drug directly to the site of action, providing increased bioavailability while minimizing systemic side effects. Local chronic inflammation of the synovium is assumed a major source of knee pain associated with OA [3] and displays a leading contributor in the onset of the disease, as well as the process of cartilage destruction [4]. Thereby, TNF- α is considered one of the key cytokines in the pathogenesis of OA [5] and can be targeted by approved antibodies such as adalimumab (ADA). Yet, despite reports of the therapeutic effect of ADA in the management of OA [6,7], and the general potential of biologics as a highly specific and well-tolerated therapy to relieve joint inflammation, there is no approved cytokine-targeted local therapy available to date. This is primarily due to the fact that the promises of IA injections are offset by the challenge of rapid elimination from the joint cavity, which results in drug residence times of typically a few hours or less and lead to an insufficient efficacy of the therapy [8]. The synovial membrane plays a key regulatory role in defining fluid exchange in and out of the joint and its properties essentially control the elimination of macromolecular substances into surrounding blood vessels or lymphatics [9]. It is a soft tissue consisting of an intimal discontinuous cellular intimal layer and the relatively acellular subsynovium that surrounds the joint cavity [10]. Thereby, it is assumed that synovial ultrafiltration is not achieved by the intimal layer with its wide intercellular gaps, but rather by the underlying extracellular tissue, which is composed of collagen fibrils and enmeshed glycosaminoglycans, proteoglycans, and glycoproteins, thus forming a microporous network with a high negative fixed charge density [11]. As described for other negatively charged barriers in the human body, electrostatic interactions with cationic modified dosage forms can be used to enhance their transport, uptake and storage or improve their retention [12]. In this way, it was shown, that the penetration of peptides into articular cartilage can be controlled by to either deep penetration or complete immobilization at the intimal tissue surface by

increasing their cationic net charge [13]. Following the same principle, 150 kDa sized diethylaminoethyl-dextran (DEAE-dextran), a polysaccharide with a high net cationic charge that exhibits biodegradability and biocompatibility [14], was found to permeate the synovial membrane significantly slower than neutrally charged or negatively charged dextrans of the same molecular size, indicating an increased residence time of the substance in the joint cavity and within superficial layers of the tissue [15]. Therefore, to overcome the issue of rapid synovial drug elimination, the formation of multidomain nano constructs consisting of a therapeutic antibody with cationic polyelectrolytes may represent a progressive drug delivery approach for the treatment OA, aiming for improved residence time of the active substance in the synovial cavity and thus a prolonged duration of action of the drug while preserving antigen recognition. In the formation of biohybrids, among a number of other tools, the avidin-biotin interaction has gained special interest due to its enormously high, non-covalent binding strength, which makes it a convenient conjugation technique for a variety of macromolecules and a suitable drug carrier due to its low immunogenicity [16]. Avidin nanocomplexes are being explored in many medical applications and provide an adaptable system that allows facile fusion of an antibody with miscellaneous molecules of additional functionalities to improve pharmacokinetics, drug stability, or to enable combination with other synergistically acting drugs [17]. In this work, biohybrid conjugates of ADA and cationic DEAE-dextran, which are based on the principle of well characterized avidin-biotin nanocomplexes, were investigated. For this purpose, ADA-complexes were formed and characterized with different equivalents of DEAE-dextrans and analyzed with respect to their permeation across a porcine *ex-vivo* synovial membrane model and their biocompatibility and maintenance of drug bioactivity. Since not only charge by electrical interaction but also increasing size of the molecule by steric hindrance has an influence on the elimination of the applied drug carrier [18,19], synergistic combination of two mechanisms that aim for an extended joint residence time is intended via the formation of cationic nanocomplexes and a novel but yet facile and adaptable formulation strategy for IA delivery of biologics is presented.

6.5 Methods

6.5.1 Reagents and materials

Adalimumab (ADA) was obtained from the commercially available product HUMIRA® (50 mg/ml) (Abbott Laboratories, Chicago, USA). Sodium metaperiodate and EZ-link hydrazide-LC-Biotin were purchased from ThermoFisher (Waltham, USA). 2-(4'-hydroxyazobenzene)-benzoic acid (HABA) was purchased from ThermoFisher (Waltham, USA). Avidin, egg white was purchased from ThermoFisher (Waltham, USA). Rhodamine-B isothiocyanate was purchased from Merck (Darmstadt, Germany). Diethylaminoethyl-dextran (DEAE-dextran) and fluorescein labeled diethylaminoethyl-dextran (FITC-DEAE-dextran) was purchased from Merck (Darmstadt, Germany). Dulbecco minimum essential media (DMEM), fetal bovine serum (FBS) and Penicillin, Streptomycin and Amphotericin B solution was purchased from Merck (Darmstadt, Germany). Methylthiazolyldiphenyl-tetrazolium bromide (MTT reagent) was purchased from Merck (Darmstadt, Germany). Human TNF- α recombinant Protein was purchased from Biomol (Hamburg, Germany). All Chemicals used for preparation of buffers were of analytical grade. Deionized water was used throughout the experiments. Pig feet of Class E pigs (Regulation EU No 1308/2013), 5-7 months old, were received from a local commercial abattoir and were freshly used for the excision of the synovial membranes.

6.5.2 Potentiometric titration

To characterize the DEAE-dextran, its proportional composition of the monomers, its relative nitrogen content, and its effective net charge at different pH values were determined by potentiometric titration. 1000 mg of DEAE-dextran was first dissolved and, after titration with 0.1 N HCl until complete protonation of the amine groups, back-titrated with 0.1 N NaOH as was previously described [20]. The titration was performed as triplicates and the change in pH was measured using a potentiometer. To determine the proportion of the three different monomers, $\Delta\text{pH}/\Delta V$ was calculated and plotted against the molar equivalent of NaOH required to completely deionize the respective amine group. The total amount of nitrogen was calculated as follows

$$C_N[\%] = \sum_{i=1}^{N_3} \frac{n_{i(\text{NaOH})} * M_N}{Mr_{\text{DEAE}}}$$

where C_N is the total nitrogen content, n_i is the molar equivalent of NaOH to completely deionize the respective tertiary amine N_1 and N_2 (**Sup. Fig. 6-1A**). The amount of quaternary amine N_3 equals the amount of tertiary amine N_1 . M_N is the molecular mass of nitrogen and M_{rDEAE} is the relative molecular mass of DEAE-dextran. The ionized fraction for each pH value determined was calculated as follows

$$Net\ charge = A_{N_3} + \sum_{i=1}^{N_2} \frac{A_{N_i}}{10^{pH-pK_{s_i}}}$$

where A_{N_i} is the amount of amine N_1 , N_2 or N_3 per molecule of DEAE-dextran. The percent ionization was determined by dividing the calculated charge by the maximum net charge upon protonation of all amines and plotted against the pH value. Complete protonation of the DEAE-dextran was achieved by titration with 0.1 HCl. The excess acid was titrated back, where, as shown in **Sup. Fig. 6-1B**, the first maximum of $\Delta pH/\Delta V$ represents 100% ionization of the amines and was defined to be equal to 0 molar equivalents of NaOH. The following two maxima of $\Delta pH/\Delta V$ correspond to the respective complete ionization of the tertiary amines and thus serve to quantify the different monomers per dextran molecule. The dextran used was determined to contain 142.5 (15.1%) monomers c with the more basic tertiary amine 1 and 42.25 (4.95%) monomers b with the weaker tertiary amine 2, as well as 649.58 (77.95%) uncharged monomers a (**Sup. Fig. 6-1A**). The quaternary amine 3 carries a positive charge at all pH values and is not detected by the titration but equals to amine 1 in its absolute number. This composition of the DEAE-dextrans thus results in a total nitrogen content of 3.05%. As shown in **Sup. Fig. 6-1C**, the molecular charge is pH-dependent, whereby the first pka value (c) was determined to be 5.9 and the second pka value measured 9.5 (b). Together the effective total net charge was estimated +188 at physiological conditions (pH=7.4), which corresponds to an ionized fraction of 58% of the amines. A decreased pH value, such as in an inflammatory event, would accordingly result in a further increased net charge of the molecule.

6.5.3 Biotinylation and conjugation of fluorophores

For site-specific biotinylation of ADA at the glycosylation sites, the respective polysaccharides of the antibody were first oxidized using 20 mM sodium periodate in acetate buffer (pH 5.5) for 30 min at 4 °C. Excess sodium meta-periodate was subsequently separated using a PD Miditrap G-25 spin column (Merck, Darmstadt, Germany) according to the supplier's instructions with the

buffer exchanged to PBS. Hereafter, hydrazide-biotin solution in DMSO and ADA was incubated for 2 h at RT, and the unbound biotin was then removed by centrifugation. DEAE-dextran was labeled accordingly. The yield of DEAE-dextran after the labeling steps was analyzed by a phenol-sulfuric assay in a 96-well plate [21]. For this purpose, 50 μL of diluted DEAE-dextran solution mixed with 150 μL of concentrated sulfuric acid and 30 μL of phenol and heated for 5 min at 90 $^{\circ}\text{C}$ in a water bath, and subsequently measured in a plate reader at 490 nm (PerkinElmer EnSpire®). The yield of ADA was determined by UV/Vis measurement at 280 nm using a Genesys 10S UV/Vis spectrophotometer (Thermo-Fisher, Waltham, USA). The biotinylation degree was assessed using a HABA assay according to the manufacturer's instructions. For this purpose, 0.5 mg/mL avidin was added to a 72.6 $\mu\text{g}/\text{mL}$ HABA solution in PBS and 180 μL of the resulting color complex was measured in the plate reader at 500 nm. 20 μL of the diluted biotinylated sample was added and the absorbance was measured. The degree of biotinylation was calculated by the equation

$$\text{Degree of Biotinylation} = ((A_{(H/A)} - A_{(H/A/B)}) / (34,000 \text{ M}^{-1}\text{cm}^{-1} \times 0.5 \text{ cm})) / c$$

where $A_{(H/A)}$ is the absorption of the HABA/Avidin complex, $A_{(H/A/B)}$ is the absorption after addition of the sample. $34,000 \text{ M}^{-1}\text{cm}^{-1}$ equals extinction coefficient for HABA/avidin samples at 500 nm, pH 7.0, 0.5 cm is the pathlength at the given volumes and c equals the concentration of ADA or DEAE-dextran in mol/L as determined previously. ADA was labeled with rhodamine-B isothiocyanate in an adapted method from the manufacturer's protocol. To remove any unbound dye, the antibody was purified by size-exclusive centrifugation using a PD Mditrap G-25 column (Merck, Darmstadt, Germany) according to the supplier's instructions. The protein yield and the degree of labeling were determined by UV/Vis measurement at 280 nm / 555 nm using a Genesys 10S UV/VIS spectrophotometer (Thermo-Fisher, Waltham, USA).

6.5.4 Preparation and characterization of ADA-nanocomplexes

To assemble the nanocomplexes, 2.5 mg/ml of biotinylated ADA was initially combined with an equimolar amount of PBS-diluted avidin and thoroughly mixed. The preparation was then mixed with previously biotinylated 150 kDa DEAE-dextran (D) in the ratios 1:1 (ADA-D1), 1:2 (ADA-D2) and 1:3 (ADA-D3) (**Fig. 6-1**). For characterization of the complex stoichiometry, preparations were also made in ratios of 1:4 (ADA-D4) and 1:5 (ADA-D5). To investigate nanocomplexes with uncharged dextran, biotinylated 150 kDa dextran (DEX) was added to the ADA-

6 Polyelectrolyte nanocomplexes to increase intraarticular residence of adalimumab injections

avidin preparation in the same proportions. An HABA assay was performed to assess the number of biotin-occupied binding sites of avidin and thus the generated stoichiometry of the nanocomplexes [22]. Having a lower affinity to avidin than biotin, HABA gives a characteristic absorbance at 500 nm when in its complexed form with Avidin [23]. Accordingly, stoichiometry of the complexes was characterized by displacement of HABA by biotinylated DEAE-dextran from the three-remaining biotin-binding sites of ADA-Avidin. For optimization of the stoichiometry of the ADA-DEAE-dextran complexes, 1 equivalent of biotinylated ADA was added to the HABA solution alone and together with 1-5 more equivalents of biotinylated DEAE-dextran to examine the stepwise decrease in absorbance. For this purpose, the difference in absorbance at 500 nm was measured and the values obtained were normalized to the pure HABA solution as the maximum value and the ADA-D5 formulation as the minimum value. Dynamic light scattering (DLS) was used to determine the hydrodynamic radius of ADA, Biotin-conjugated ADA, DEAE-dextran, and the prepared polyelectrolyte complexes. DLS was performed using a Horiba Nano Particle Analyzer SZ-100 (Horiba, Kyoto, Japan). 200 μ L of each sample at a concentration of 10 mg/mL were analyzed in quartz micro cuvettes at a fixed angle of 173° at 25 °C (n=5). Z-average particle size and polydispersity index (PDI) were calculated using the SZ-100 internal software (Horiba, Kyoto, Japan).

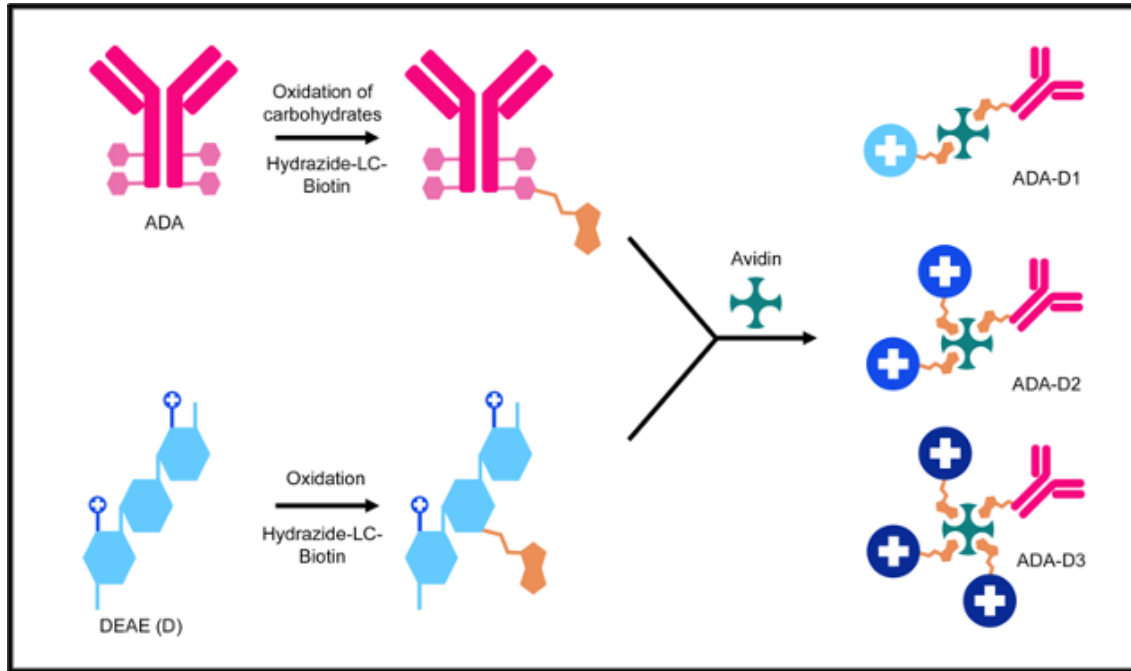


Fig. 6-1: Site-selective biotinylation of ADA after oxidation of the bound sugars by hydrazide-LC-biotin, and biotinylation of cationic DEAE-dextran by hydrazide-LC-biotin. Preparation of ADA-D(N)-nanocomplexes from the reaction of biotinylated ADA and avidin in PBS, pH 7 and subsequent addition of 1-3 molar equivalents of biotinylated DEAE-dextran to the reaction mixture to obtain ADA-D1, ADA-D2 and ADA-D3 complexes.

6.5.5 Permeation studies

Synovial explants were harvested from the lower limbs of domestic pigs obtained from a local abattoir as previously described [15]. The *ex-vivo* permeation studies were performed using a Franz cell model with diffusion area of 0.785 cm². The 5 ml acceptor chamber was filled with DMEM containing 5% FBS and 1% antibiotics and antimycotics as acceptor medium and adjusted to a temperature 37 ± 0.5 °C, stirred at 150 rpm. The prepared tissues were mounted as a diffusion barrier between the two chambers. 0.2 ml of sample with a concentration of 2.5 mg/ml rhodamine-B-labeled ADA and the respective amount of fluorescein-labeled DEAE-dextran was applied to the luminal side of the synovial membrane at t=0. All experiments were performed with a sample size of n=10. Sink conditions were present throughout the experiment as protein concentration did not exceed 10% of saturation concentration. The luminal side was sealed with Parafilm to minimize evaporation effects. At the specified time points, 0.5 ml samples were taken with a syringe and replaced with fresh media. The fluorescence signal was measured using a plate reader (PerkinElmer EnSpire®) at an excitation of 555 nm and emission of 580 nm for rhodamine-B-labeled ADA and an excitation of 490 nm and an emission of 520 nm for the fluorescein-labeled

6 Polyelectrolyte nanocomplexes to increase intraarticular residence of adalimumab injections

DEAE-dextran. Since analyte was removed with each sample draw, the cumulative permeated amount of ADA was calculated as follows.

$$M_i = V_s \sum_{i=0}^{t-1} C_{i-1} + V_A C_t$$

Where V_A is the total volume of the acceptor chamber, C_t is the concentration at each sampling time, V_s is the volume of the withdrawn sample and C_i represents the concentration of analyte at time i . The resulting mass was then divided by the diffusion area. Fluxes were determined from the steady-state slope obtained by linear regression and thus describe the mass permeated per time and area in $\mu\text{g}/(\text{cm}^2 \cdot \text{h})$. The flux is considered as a surrogate for the permeability of the synovial membrane for ADA and DEAE-dextran. The flux of DEAE-dextran in nanocomplexes of different stoichiometry was corrected to equimolar amounts to allow better comparability. To differentiate the respective influence by size or cationic charge of the complex, the experiment was also performed with nanocomplexes consisting of uncharged dextran of the same molecular mass and the determined flux was compared with the charged counterparts. To further investigate the influence of the cationic charge and its interaction with the tissue, the synovium was initially incubated with 15 mg/ml unlabeled DEAE-dextran for 4 h to block ionic interactions of the subsequently applied fluorescein-labeled sample with the membrane. In order to observe how the *in vivo* insertion of the cannula could cause a possible leakage of the active substance, the membrane was punctured with a 26G cannula in an additional experiment and the resulting permeation course of ADA and ADA-D3 was compared with the non-punctured membranes. To determine the distribution of the fluorescence-marked nanocomplexes within the synovial membrane, three additional tissue samples each were taken from the diffusion cells after 4 h and 48 h and were snap frozen. Subsequently, 50 μm thick cross-sections of the frozen synovium were made with a cryomicrotome (Slee, Mainz, Germany) and mounted on a microscope slide. The samples were visualized using a Confocal Laser Scanning Microscopy (CLSM) (Nikon Instruments Europe B.V., Amsterdam, Netherlands), whereby the diffusion of rhodamine-labeled ADA and FITC-labeled DEAE-dextran was simultaneously assessed. Pictures were taken using the same settings and the pixel density. To evaluate the acquired fluorescence signals, 50 μm Z-stacks were captured and the individual layers were summed using FIJI to achieve a normalization of the signal within the cut cross sections. Using the FIJI plot profile function, the fluorescence intensity (FI) over distance the stacks was quantified,

whereby three plot profiles were generated along a linear path in the direction of diffusion for each section. The so obtained averaged plot profiles of the three different tissue samples were then again averaged.

6.5.6 Tissue viability

The viability of the synovial tissue in the presence of the nanocomplexes was determined by measuring the tetrazolium reductase activity, which allows inference on the metabolic activity of the cells and thus indirectly on the number of viable cells present. The retrieved tissue samples were weighed and then incubated with the nanocomplex formulations in the different stoichiometric compositions (ADA-D1-3). Matching the total time of the permeation experiments, the incubation time was set to 48 h at 37 ± 0.5 °C. Subsequently, the medium was substituted by 1 mg/ml MTT reagent, and incubated for 2 h at 37 ± 0.5 °C. Then, the so-treated explant was placed into 3 ml of dimethyl sulfoxide (DMSO) and homogenized using an IKA Ultra Turrax (Staufen, Germany). After centrifugation, the absorbance of the supernatant was measured at 540 nm. For positive control, viability was determined immediately after harvest without any further treatment steps. For negative control, tissue samples were devitalized with 10% sodium azide and then treated by the same exact procedure. Sodium azide acts as an inhibitor of the mitochondrial respiratory chain and causes apoptosis at the indicated concentration [24]. Data was normalized by tissue weight. Average viability was derived from 5 samples for each treatment.

6.5.7 TNF- α FLISA

To evaluate the binding activity of fluorescently-labeled ADA to TNF- α after biotinylation, as well as after binding to avidin and after formation of the ADA-D1, ADA-D2 and ADA-D3 nanocomplexes, a direct fluorophore-linked immunosorbent assay (FLISA) was established, which was adapted to a previously developed ELISA for the detection of ADA [25]. In addition, the bioactivity of ADA and the complexes post permeation across the synovial tissue was determined by sampling from the acceptor chamber of the diffusion cells in order to evaluate the influences of the tissue on antigen recognition. Results were expressed as the active fraction of the previously measured concentrations obtained. All samples were prepared with n=3. A 96-well plate (NUNC Maxisorp™, Thermo-Fisher, Waltham, USA) was allowed to incubate overnight with 1 μ g/ml TNF- α at 4 °C. The remaining protein binding sites were blocked with BSA for 2 hours at RT, and 1:100 diluted standards and samples were

pipetted into the wells in duplicate following three times washing with PBS containing 0.05% Tween 20. The samples were then incubated at RT in an orbital shaker for 1.5 h, and then the plate was again washed as described previously. Finally, 100 μ L of PBS was added into the wells and the fluorescence of the bound ADA was measured using a plate reader (PerkinElmer EnSpire®).

6.5.8 Statistical analysis

Data was presented as mean \pm standard deviation. The permeation of the samples was evaluated by their flux calculated by linear regression. Statistical significance was assessed by one-way analysis of variance (one-way ANOVA) followed by Dunnett or Tukey multiple comparison tests. Differences were considered significant at $p < 0.05$. All statistical analysis was performed using GraphPad Prism® 8 software.

6.6 Results

6.6.1 ADA-Nanocomplex formation and analysis

Biotinylation of ADA was achieved with a yield of approx. 97% with an average binding of 1.07 molecules of biotin per protein as shown by the HABA Assay. Biotinylated DEAE-dextran was obtained with an average 1.15 molecules per polymer at a yield of approx. 93% as estimated by phenol-sulfuric carbohydrate assay. The HABA assay (**Fig. 6-2**) showed a reduction in normalized absorbance at 500 nm of about 25% with the addition of one equivalent of biotinylated ADA ($75.3 \pm 0.1\%$). Subsequent addition of 1-5 equivalents of biotinylated DEAE-dextran resulted in a further gradual decrease in absorbance of about 25% each time, leading to a value close to zero for ADA-D3 ($4.6 \pm 3.0\%$). Addition of more than 3 equivalents of DEAE-dextran did not lead to any further significant decrease in absorbance. Comparable hydrodynamic radii were observed for ADA, ADA-Biotin-conjugates, and DEAE-dextran (**Tab. 6-1**) with a non-significant increase of 4 nm after conjugation of biotin. Formation of the nanocomplexes resulted in a significant increase in size of approximately 7-9 nm per equivalent of DEAE-dextran added. On the basis of the PDI, ADA exhibited a lower polydispersity than the dextran. Compared to the monomers the PDI increased upon formation of the nanocomplexes to a magnitude of ca 0.4-0.5, with a non-significant trend of decreasing PDI with increasing DEAE-dextran equivalents.

6 Polyelectrolyte nanocomplexes to increase intraarticular residence of adalimumab injections

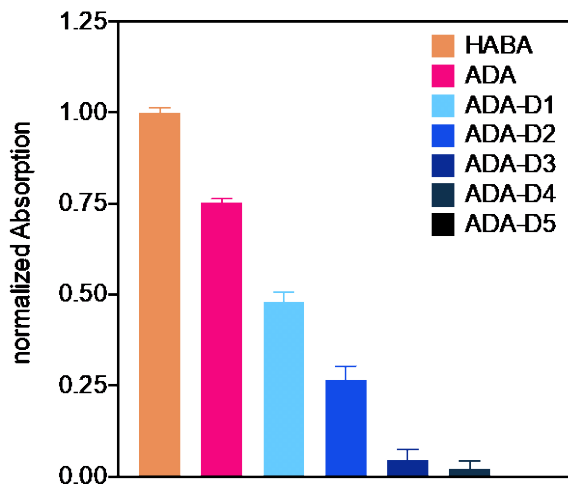


Fig. 6-2: HABA assay to determine the stoichiometry of the formed ADA-D complexes in the molar ratio 1:1-5. The measured absorbance option at 500 nm was normalized to the pure HABA-avidin complex as the maximum value, and the ADA-D5 complex as the minimum value (n=3).

Tab. 6-1 DLS results indicated as Z-average and PDI of ADA, ADA after biotinylation (ADA-Conj.), DEAE-dextran (DEAE), and ADA as nanocomplexes with DEAE-dextran in different molar ratios (ADA-D1-3). Mean \pm SD; n=5.

	ADA	ADA-Conj.	DEAE	ADA-D1	ADA-D2	ADA-D3
Z-Average (nm)	12.1	16.2	14.4	19.3	25.3	34.5
	± 1.6	± 0.8	± 1.3	± 2.6	± 2.4	± 1.3
PDI	0.24	0.23	0.29	0.47	0.40	0.39
	± 0.07	± 0.08	± 0.12	± 0.14	± 0.13	± 0.06

6.6.2 Synovial permeation

As shown in **Fig. 6-3A**, the cumulative amount of rhodamine-labeled ADA permeating from the luminal to the basolateral chamber of the test system increased linearly over time after a short initial lag time, suggesting passive diffusion across the synovial tissue. The calculated permeate fluxes are presented in **Fig. 6-3B**. A flux of 53.2 ± 15.4 pmol/cm²/h was obtained for ADA as a solution, whereas a significantly lower flux of about 15 pmol/cm²/h was obtained for the all ADA-nanocomplexes ($p < 0.001$), showing no significant difference between the different stoichiometries. Thereby ADA-D1 flux was measured 14.7 ± 9.5 pmol/cm²/h, ADA-D2 was 14.7 ± 8.7 pmol/cm²/h, and ADA-D3 showed a flux of 14.3 ± 7.2 pmol/cm²/h ($p > 0.05$). In addition to the rhodamine-labeled ADA in the respective nanocomplexes, comparable, significantly non-different flux values were obtained for the FITC-labeled DEAE-dextran in the

complexes, measuring 21.7 ± 6.9 pmol/cm²/h (ADA-D1), 18.3 ± 10.4 pmol/cm²/h (ADA-D2) and 16.7 ± 4.1 pmol/cm²/h (ADA-D3) ($p > 0.05$) (**Fig. 6-3B**). FITC-DEAE-dextran alone was found to permeated at likewise low flux across the tissue. As shown in **Fig. 6-4** nanocomplexes of the same stoichiometries were formed with uncharged dextran of the same size and compared with the cationic DEAE-dextran complexes for better evaluation and differentiation of the respective influence of size and charge. Unlike the ADA-DEAE-dextran nanocomplexes whose flux is reduced to approximately one third upon conjugation of one equivalent of DEAE-dextran and for which there were no additional significant effects from using multiple equivalents of DEAE-dextran, the use of uncharged dextran showed a size-dependent decrease of permeation across synovial tissue. While the flux of neutrally charged ADA-D1 (40.4 ± 10.0 pmol/cm²/h) is not significantly different from ADA alone (53.2 ± 15.4 pmol/cm²/h) ($p > 0.05$), the flux value of ADA-D2, which was determined 32.3 ± 10.7 pmol/cm²/h ($p < 0.05$) and of ADA-D3 that was 26.4 ± 8.9 pmol/cm²/h ($p < 0.01$) each permeated significantly slower through the tissue but could not achieve the same retention as obtained through usage of the cationic dextran in any stoichiometry, which ranged in the region of 15 pmol/cm²/h. To further investigate the effect of charge, the synovial tissue was initially incubated with a high dose of unlabeled DEAE-dextran to suppress ionic interactions of the subsequently applied sample with the membrane (**Fig. 6-5**). The previously described differences between charged and uncharged complexes were found to be no longer to be present after pretreatment of the tissue. Thereby, the charged ADA-D1 complex permeated with the approximate same flux as the uncharged complex ($p > 0.05$) which further illustrates the influence of the charge on the tissue diffusivity. Puncturing the synovial membrane with a cannula, as is the case with an *in-vivo* IA injection, led to an increase in the flux of ADA over the first 6 h, before the flux returned to the level of the impermeable membrane. For the ADA-D3 complex, no difference in flux was observed at any time point (**Sup. Fig. 6-2**). The CLSM images show the distribution of rhodamine-labeled ADA (**Fig. 6-6**) and FITC-labeled DEAE-dextran (**Sup. Fig. 6-3**), both at 4 h and 48 h after application of the respective formulations. Visually, no significant differences can be seen after 4h and ADA resides primarily in the superficial layers of the tissue. After 48 hours, however, ADA solution is distributed throughout the entire tissue, while the complexed ADA continues to adhere to the intimal layers. As the number of stoichiometrically conjugated DEAE-dextran per ADA molecule increases, the effect becomes more pronounced and the sharpness of the fluorescence gradient across the synovium

increases. For the fluorescein labeled dextran, the image is visually almost identical, though no fluorescence is observed for ADA alone. As expected, the fluorescence intensity (FI) increases with the amount of dextran, as more fluorophores are present in the sample. Plotting the fluorescence intensity against the distance in the direction diffusion proves that ADA alone penetrated the tissue significantly deeper than the nanocomplexes. Although initial differences in the plot profile were already apparent after 4 h through this processing (**Fig. 6-7A**), they became more pronounced after 48 h (**Fig. 6-7B**). Especially in deeper tissue layers, the FI level for free ADA was already observed to be higher after 4 h compared to the complexes, which showed an FI close to zero beyond a depth of more than 100 μm . Whereas the FI of ADA after 48 h showed generally a high level that declined almost linearly over the tissue depth, the nanocomplexes were entrapped in the uppermost layers of the synovial membrane, resulting in a rapid FI decrease after the first 50-100 nm. The nanocomplexes exhibit closely similar profiles, although it appears that the ADA-D1 FI decreased less rapidly when compared to ADA-D2 and ADA-D3. The plot profiles were normalized to the maximum FI, which is necessary due to the different intensity and different quantity of fluorophores. Subsequently, the distribution of FI of rhodamine-ADA and FITC-DEAE-dextran in the nanocomplexes was compared for each complex respectively, whereby it could be shown, that the distribution across the synovial membrane was close identical for the different macromolecules of the complexes for ADA-D1, ADA-D2 and ADA-D3 (**Sup. Fig. 6-4**).

6 Polyelectrolyte nanocomplexes to increase intraarticular residence of adalimumab injections

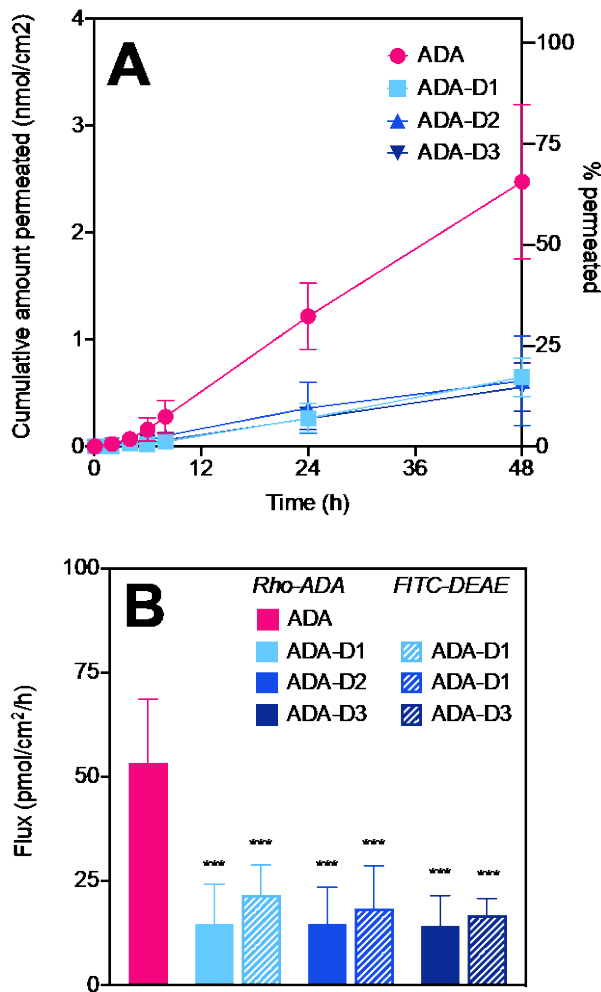


Fig. 6-3: (A) Cumulative permeation amount of rhodamine-labeled ADA solution and cationic ADA-D1, ADA-D2, and ADA-D3 nanocomplexes as measured *ex-vivo* across a porcine synovial membrane in a vertical diffusion cell. (B) Corresponding calculated flux in ng/cm²/h, which reveals the deceleration of permeation due to the formation of cationic nanocomplexes and proves the simultaneous diffusion and thus stability of the complexes in the tissue due to the non-significantly different flux rates of rhodamine-labeled ADA (*Rho-ADA*) and FITC-DEAE-dextran (*FITC-DEAE*). Mean \pm SD; n=6; ANOVA + Dunnett's multiple comparison test; significant differences: '****' (p < 0.001) compared to ADA solution.

6 Polyelectrolyte nanocomplexes to increase intraarticular residence of adalimumab injections

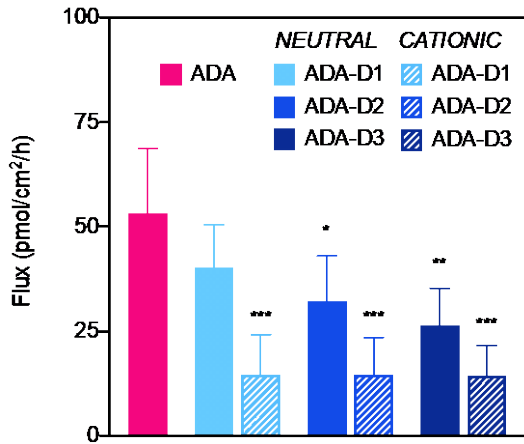


Fig. 6-4: Flux in ng/cm²/h of ADA and the cationic and neutral charged ADA-nanocomplexes of different molar equivalents, showing the effect of size and cationic charge on permeation of the nanocomplexes. Mean \pm SD; n=6; ANOVA + Dunnett's multiple comparison test; significant differences: '*' ($p < 0.05$), '**' ($p < 0.01$), '***' ($p < 0.001$) compared to ADA solution.

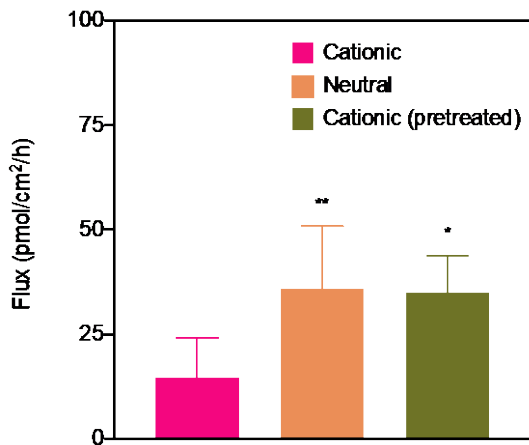


Fig. 6-5: Flux in ng/cm²/h of the ADA-D1 nanocomplex formed by either cationic or neutrally charged dextran and of tissue pretreated with high concentration unlabeled DEAE-dextran solution, showing the effect of size and cationic charge on permeation of the nanocomplexes. Mean \pm SD; n=6; ANOVA + Dunnett's multiple comparison test; significant differences: '*' ($p < 0.05$), '**' ($p < 0.01$) compared to the cationic ADA nanocomplex.

6 Polyelectrolyte nanocomplexes to increase intraarticular residence of adalimumab injections

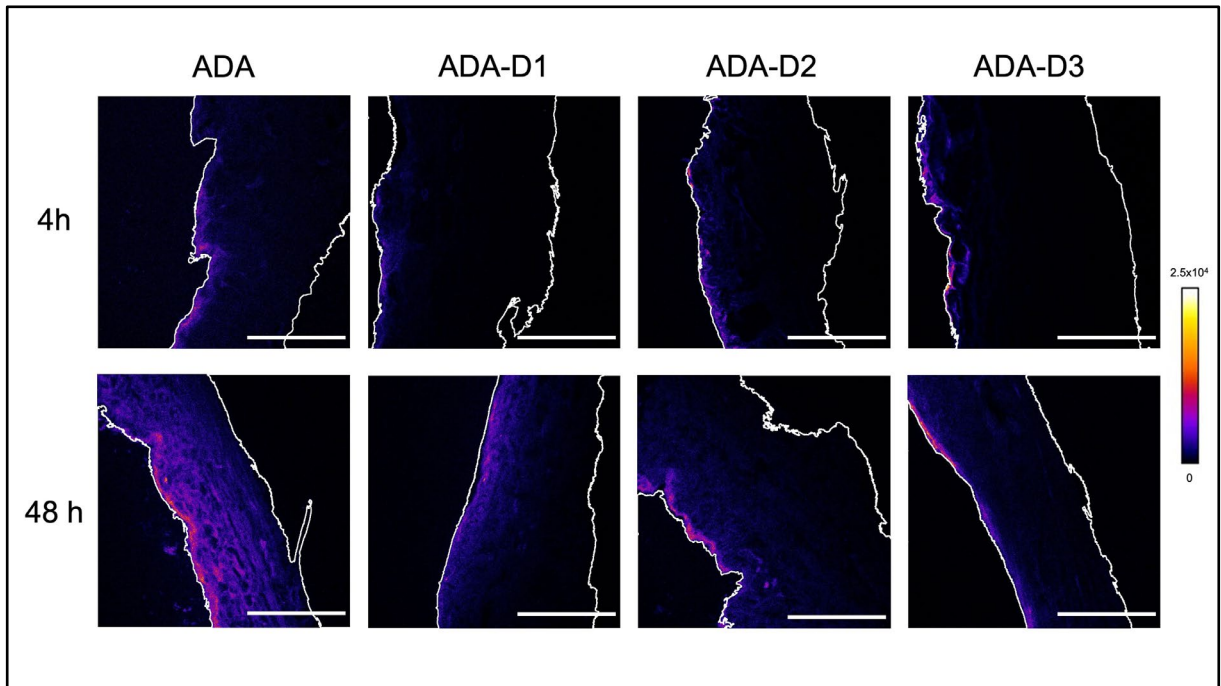


Fig. 6-6: CLSM images of *ex-vivo* synovium cross-sections after 4 h as well as 48 h showing the retention of rhodamine-labeled ADA in cationic nanocomplexes with different molar equivalents of cationic DEAE-dextran compared to solution. Direction of diffusion from left (luminal) to right (basolateral); Scale bar: 500 μ m.

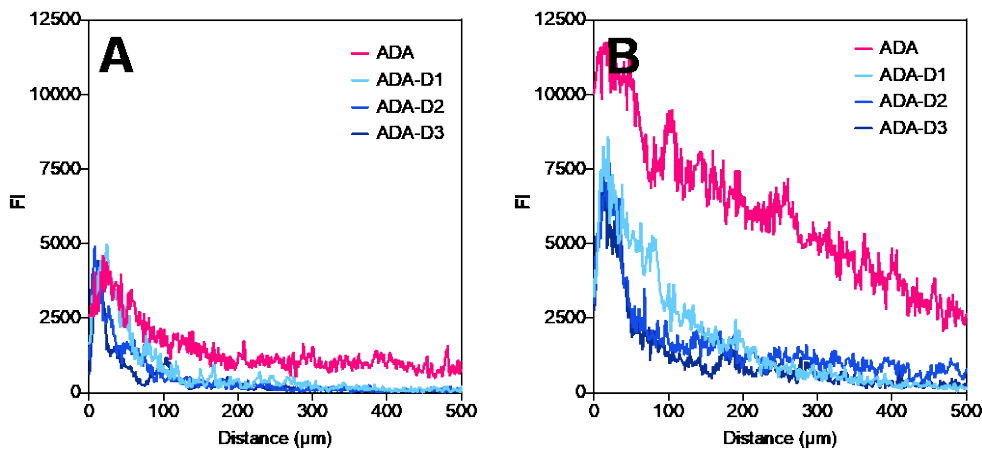


Fig. 6-7: Plot profiles generated from CLSM images of the measured fluorescence intensities (FI) of rhodamine-labeled ADA from ADA solution and ADA-D1, ADA-D2, and ADA-D3 nanocomplexes (n=3) after 4 h (A) and 48 h (B). Error bars were omitted for clarity reasons.

6.6.3 ADA-nanocomplex antigen recognition

The relative binding affinity of complex-bound ADA to TNF- α was assessed by a fluorescence-linked immunoassay in comparison to free ADA, whose activity was set 100%. As shown in **Fig. 6-8**, the antigen recognition of ADA was found to be decreased slightly after oxidation and biotinylation of the antibody ($91.5 \pm 6.2\%$)

in the biotinylation steps, as well as after binding to avidin ($96.2 \pm 4.4\%$), although the differences were not statistically significant ($p > 0.05$). Linkage with the biotinylated DEAE-dextran resulted in a decrease in activity of the conjugated ADA ($p < 0.05$). Thereby, ADA-D1 showed a percentage antigen recognition of $83.0 \pm 8.1\%$, ADA-D2 was measured $84.4 \pm 3.6\%$ and ADA-D3 was $82.3 \pm 3.4\%$ which were all assessed as significantly different compared to free ADA (< 0.05). However, no significant differences in activity were observed between ADA-D1, ADA-D2 and ADA-D3 ($p > 0.05$). There was also no significant effect on antigen recognition post permeation across the synovial membrane ($p > 0.05$). For ADA, a slight decrease in activity was observed, but the complexes remained at the same activity level as measured pre-permeation.

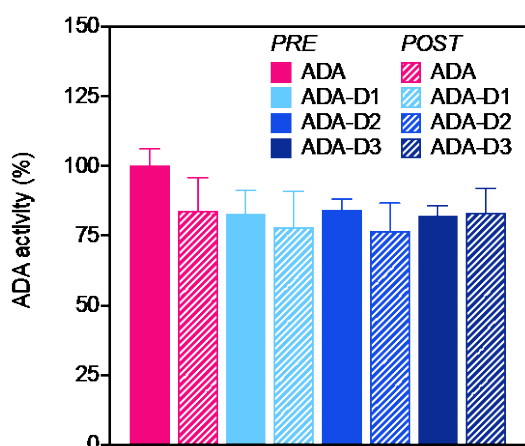


Fig. 6-8: *Pre:* Activity of ADA to bind TNF- α in Solution and as nanocomplexes with DEAE-dextran in different molar ratios (ADA-D1-3) after 48 h of incubation at 37° C in PBS. *Post:* Activity of ADA to bind TNF- α in Solution and as nanocomplexes with DEAE-dextran in different molar ratios (ADA-D1-3) following the permeation study as sampled from the acceptor chamber; Mean \pm SD; n=3; ANOVA+ Dunnett's multiple comparison test; significant differences: '*' ($p < 0.05$), '**' ($p < 0.01$) compared to ADA Solution (ADA).

6.6.4 Synovial cell viability in presence of nanocomplexes

Synovial metabolic activity decreased non-significantly to approximately $92.5 \pm 7.6\%$ on addition of ADA over the duration of the experiment (48 h) at 37 °C compared to the viability of the untreated tissue control right after dissection, which was normalized to 100 % (**Sup. Fig. 6-5**). Nanocomplex formation led to a slight yet general trend of decreasing viability with increasing amounts of polyelectrolyte. More precisely, ADA-D1 showed a synovial viability of $86.7 \pm 10.4\%$, ADA-D2 of 83.3 ± 12.5 and ADA-D3 of 79.6 ± 4.46 after 48 h of incubation. However, the differences were not significant except for ADA-D3 as compared freshly dissected tissue ($p < 0.05$) and none of the nanocomplex formulation

samples showed significant deviation from tissue treated with ADA solution alone ($p > 0.05$).

6.7 Discussion

In this work, we present a nanocarrier model that significantly decelerates the permeation of a therapeutic antibody across the synovial barrier due to ionic interactions with the surrounding tissue. Accurate conjugation of the stoichiometrically defined avidin-mediated complex was obtained by linking one biotinylated ADA via the spacer to one to three equivalents of biotinylated DEAE-dextran as was proven via the HABA assay. Thereby, it could be demonstrated, that with the addition of each molar equivalent of biotin-coupled macromolecule, the absorbance decreased by approximately 25%, which is explained by the four biotin binding sites of avidin. Further, absence of the absorption peak on addition of three or more molar equivalents of polyelectrolyte showed that all biotin binding sites of ADA-Avidin were occupied by one equivalent of DEAE-dextran, proving a correct stoichiometry of the complexes. In consistency with previous studies on the hydrodynamic radius, [26,27] the determined Z-average value of ADA was estimated approx. 12 nm, whereby a small increase in size was observed upon the conjugation of biotin, that was attributed to the spacing EZ linker. With progressive introduction of DEAE-dextran, a gradual increase in the size of the complexes formed was observed. Thereby increased polydispersity was observed, which can be explained by the fact that the complexes are generated on the basis of calculated equivalents and steric shielding, so that statistical distributions are to be expected. Consequently, there is a decrease in PDI with increasing DEAE-dextran content, since in ADA-D3 all avidin binding sites were occupied and thus the homogeneity of the formulation increased. The synovial membrane represents the main barrier for fluid exchange in and out of the joint space. Due to the structure of the synovial extracellular matrix, whose pores are defined by intercalated polyelectrolytes and a polarization layer of the hyaluronic acid on the tissue-fluid interface [28], the synovial membrane forms a ultra-filtrating barrier with a high negative fixed charge density. Synovial permeability and hence elimination of macromolecules depends on both the molecular size and the net charge of the applied drug or dosage form [15,29]. Ranging from 19.3 to 34.5 nm in size all complexes fall below the effective pore size of 33-59 nm defined by the extracellular matrix of the synovial membrane [30], which control diffusion across the tissue, so theoretically, based on size alone, complete but

significantly decelerated elimination of the complexes can be expected without prior degradation. However, charge has been found to exert major influence on the diffusion of analytes in galactosamine glycan-rich structures. Whereas anionic charge appears to have a minor influence on tissue permeation as compared to uncharged molecules, cationic charge can significantly accelerate or decelerate diffusion by interaction with the surrounding tissue. Hence, for the penetration of positively charged peptides into cartilage [13] and for diffusion in vitreous humor [31] as well as in mucin [32], it was shown that the diffusion could initially be enhanced by increasing cationic net charge due to weak reversible binding. However, exceeding a certain threshold of cationic charge will cause complete immobilization of the analyte at the tissue surface or within its superficial layers due to strong ionic interactions. This finding was attributed to the cationic total net charge of the sample and immobilization was identified from a detected of about +20 [13,31]. For the DEAE-dextran used, a net charge of approx. +180 was determined by potentiometric titration at physiological pH which results from the permanently charged quaternary amines and the pH-dependently charged tertiary amines. Accordingly, this molecule was found to exhibit almost complete immobilization during permeation tests in the intimal layer of the of synovium. However, we were able to transmit these diffusion characteristics to the otherwise significantly faster permeating ADA by the formation of a biohybrid nanocomplex so that the ADA diffusion is decelerated to the level of the cationic DEAE-dextran. Although there are no comparative studies on the permeation of highly positive charge bearing nanocarriers in synovial tissue, previous work on diffusivity of cationic nanoparticles in alternate galactosamine glycans enriched collagen tissues such as skin also reports immobilizing effects in superficial tissue zones [33,34]. This suggests fusion of therapeutic agents with cationic polymers to be a potentially generally applicable formulation strategy to extend the residence time at the surface or superficial zones of polyanionic tissue layers. The quantity of DEAE-dextran equivalents showed no significant impact on the resulting flux as determined in the diffusion cell, with all formulations prepared having an equally decelerating effect on ADA permeation. Accordingly, charge of the complex displayed the most decisive retarding parameter since fusion of ADA with a single DEAE-dextran had a significantly greater impact on permeation than increasing size of the nanocarrier up to three uncharged dextrans, with the latter passing the tissue more slowly as their size increased, whereas a maximum prolongation of the charged DEAE-dextran flux was already achieved for ADA-D1. Albeit this could be attributable to the fact that cationic preparations can

increase the retention time in the joint space by forming micrometer-sized aggregates with endogenous hyaluronic acid secreted by synoviocytes [35], the high effect of electrochemical interactions with surrounding tissue on the permeation was conversely proven since pretreatment of the tissue with an excess of unlabeled cationic dextran resulted in a suppression of binding of the nanocomplexes to the synovial extracellular matrix. As a result, size became the defining parameter, and the cationic complex permeated non-significantly differently from the uncharged complex. Therefore, both size-dependent and charge-dependent effects are believed to prolong the diffusion of the prepared nanocomplexes. This finding coincides with a previously published study, where charged dextran-based drug carriers for intradiscal injection had both size and charge potentiated effects on the residence time of the conjugate in the nucleus pulposus [36]. However, upon examination of the CLSM plot profiles, a trend in terms of decreasing fluorescence intensity at increasing distance with an ascending number of conjugated equivalents of DEAE-dextran became apparent. An increased immobilization of ADA in the superficial tissue layers of the synovial tissue mediated synergistically through size and charge would provide an elevated therapeutic value, since in chronic arthritis strong expression of proinflammatory cytokines is particularly found within the intimal lining layer [37]. In the osteoarthritic situation, synovitis alters the permeability of the synovial membrane, resulting in reduced size selectivity, i.e., faster elimination of large molecules due to catabolic processes in the ECM [38–40]. However, as was shown in previous studies, these effects were not observed for high cationic charged macromolecules such as DEAE-dextran [15]. Therefore, it can be assumed that the permeability of the nanocomplexes is the same even in the pathologically affected joints, whereas uncharged complexes were expected to leak out of the joint space more rapidly. It is also worth noting that it has been shown that puncturing of the synovium, as occurs in vivo when the drug is injected, leads to some dose dumping, visible in an increased flux over the first 6 h, out of the joint space. Due to the adhesion of the cationic formulation to the tissue, this effect was observed for the nanocomplexes, which can be seen as another advantage over other injected drug delivery systems. The stability of the ADA-DEAE-dextran complexes over the duration of the permeation studies in its physiological environment could be evaluated by the simultaneous labeling of both ADA and DEAE-dextran with two different fluorophores. The images show almost congruent fluorescence-distance profiles, suggesting identical localization of both molecules in the tissue, and thus sufficient stability of the conjugation can

be assumed for all formulations prepared. Moreover, it could be shown by FLISA that neither oxidation nor conjugation with either the linker or avidin, nor the presence of DEAE-dextran had a negative influence on the antigen recognition of ADA towards TNF- α and therefore an equivalent or greater potency of the formulations may be expected relative to the injection of unmodified antibody. Apart from ADA-D3, the MTT assay indicated no significant reduction in metabolic cell activity, suggesting high tolerance of the complexes. However, since a slight trend in the decrease of metabolic activity with increasing amounts of dextran could be noticed and one conjugated DEAE-dextran molecule alone was found prevent rapid diffusion out of the injection site, the complexation of one antibody with one cationic dextran polymer may be considered as the most advantageous for reasons of maximum compatibility at a maximum protein diffusion-delaying effect. However, the biocompatibility of the pharmacokinetically versatile nanocomplexes has yet to be tested *in-vivo*, as cationic polymers in general may have the potential to affect ECM homeostasis or lead to destabilization of cell membranes. In addition, they may interact with serum proteins, leading to toxicity, especially if the agents enter the systemic circulation. Compared to other IA drug delivery systems, the cationic nanoconstructs offer several advantages in terms of preserving bioactivity within the formulation and the tissue and providing a simple but effective increase in joint residence time. Unlike conventional methods for the formation of particulate carriers, neither organic solvents nor elevated temperatures, sonification or shear stresses are required, which is generally considered critical to maintain the full activity of a protein drug. [41–43]. In addition, given their low viscosity, they are easy to inject and, unlike implants or larger particulate systems, have no potential to provoke irritation in the inflamed joint space as a result of mechanical friction. Thus, the rational exploration of the joint environment by means of a cationic charged nanocomplex using biodegradable polyelectrolytes can provide a facile but nonetheless potent solution to the more widely investigated IA depot dosage forms such as hydrogels or synthetic particles to retain protein drugs within the joint cavity, thereby maintaining bioactivity of the protein drug.

6.8 Conclusion

The investigated nanocomplex offers high translational possibilities to improve the pharmacokinetics of IA injected therapeutic antibodies and illustrates how protein diffusion can be rationally modulated using bioelectricity, thereby

effectively exploiting physiological environments through drug delivery strategies. ADA-DEAE-dextran nanocomplexes exhibited a significant prolongation of the permeation through synovial membrane without adverse effect on antigen recognition or biocompatibility in *ex-vivo* experiments, thus providing a promising novel formulation principle for intra-articular injections.

6.9 Acknowledgements

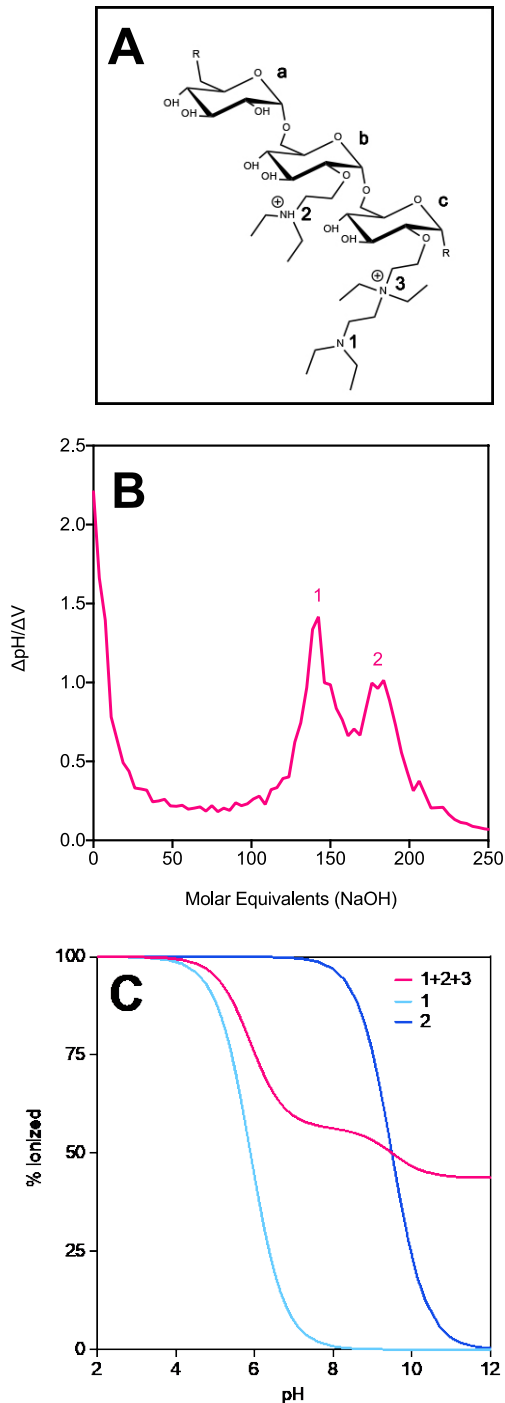
Ferring Pharmaceuticals Inc. sponsored the research that is the subject of the manuscript. Employees of the sponsor were involved in the conceptualization and design of the study.

6.10 Author contributions

Conceptualization, T.S., A.L.; methodology, T.S.; software, T.S.; validation, T.S.; formal analysis, T.S.; investigation, T.S.; resources, A.L., S.B., D.P., C.B., C.C.L.; data curation, T.S.; writing-original draft preparation, T.S.; writing-review and editing, T.S., A.L., S.B.; visualization, T.S.; supervision, A.L.; project administration A.L., S.B., D.P., C.B., C.C.L.; funding acquisition, A.L., S.B., D.P., C.B., C.C.L.

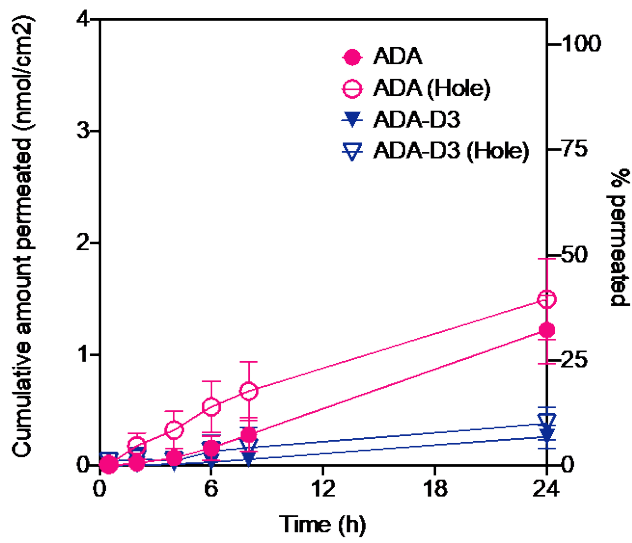
All authors have read and agreed to the published version of the manuscript.

6.11 Supplementary data

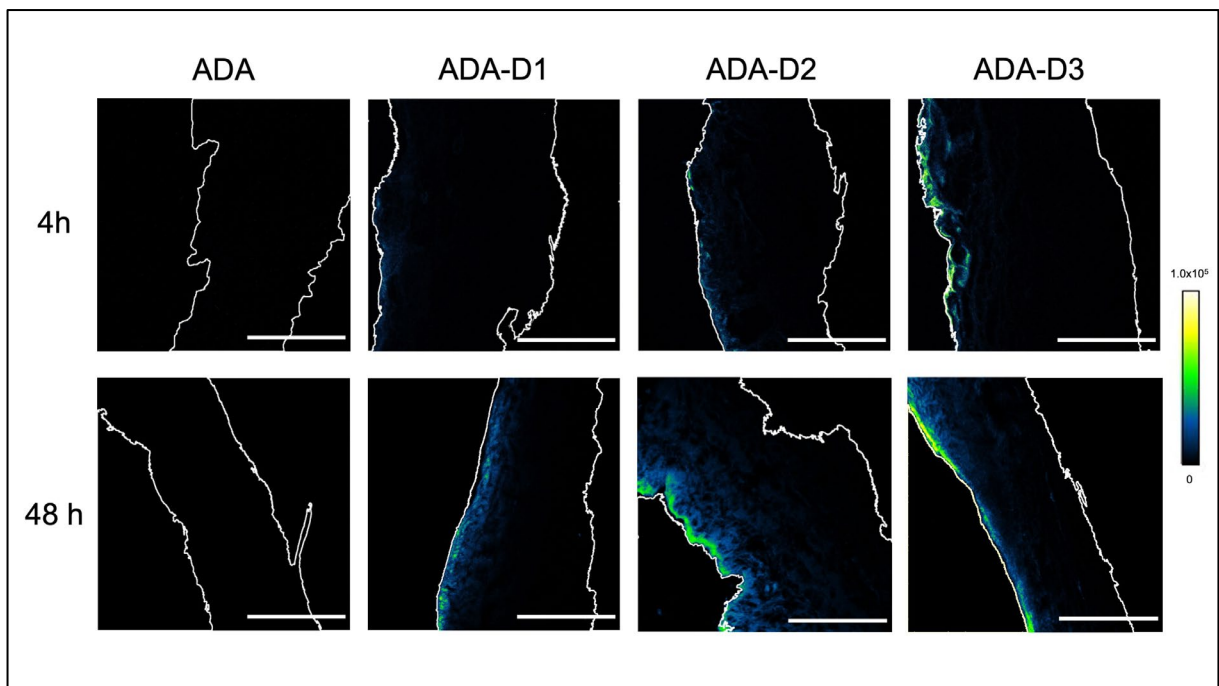


Sup. Fig. 6-1 (A) Chemical structure of DEAE-dextran which consists of three different monomers (a, b, c) where the substituents include two tertiary amines (1, 2) and a quaternary amine. (3). **(B)** As determined by potentiometric titration, the plot of $\Delta pH/\Delta V$ vs. molar equivalents of NaOH, shows the point of complete deionization of each of the two tertiary amines (1,2). **(C)** Proportion of ionized tertiary amines (1,2) at different pH values, as well as of the total molecule including the permanent charged quaternary amine group (1+2+3). At physiological pH, 58% of the amines are positively charged, corresponding to a total net charge of approximately +187 for the 150 kDa DEAE-dextran.

6 Polyelectrolyte nanocomplexes to increase intraarticular residence of adalimumab injections

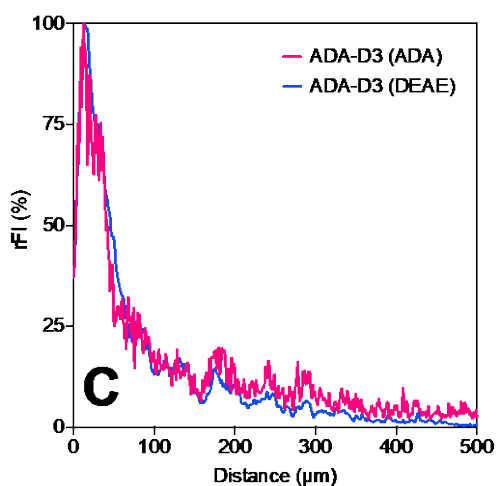
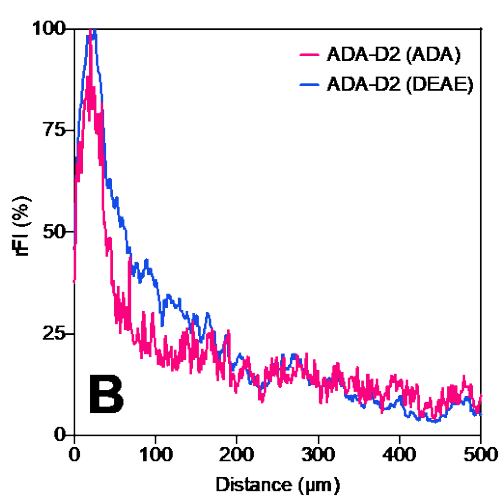
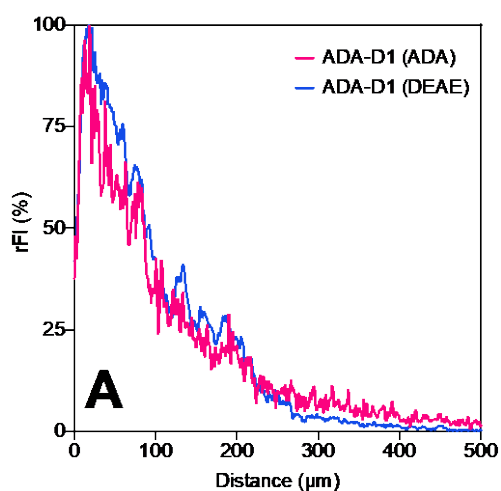


Sup. Fig. 6-2: Comparison of permeation of ADA as a solution and in complex across an untreated and a cannula punctured synovial membrane. Mean \pm SD; n=6.



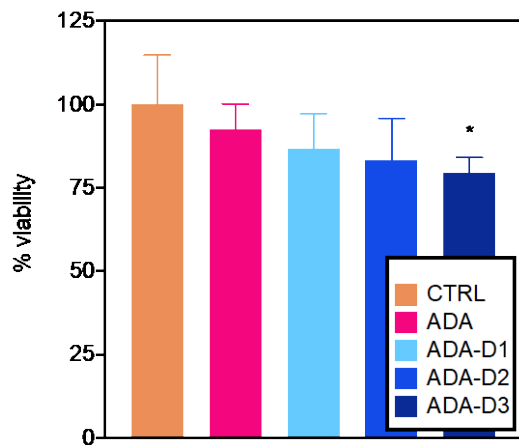
Sup. Fig. 6-3: CLSM images of *ex-vivo* synovium after 4 h as well as 48 h showing the retention of FITC-labeled DEAE-dextran in cationic ADA-nanocomplexes with different molar equivalents of cationic DEAE-dextran. Direction of diffusion from left (luminal) to right (basolateral); Scale bar: 500 μ m.

6 Polyelectrolyte nanocomplexes to increase intraarticular residence of adalimumab injections



Sup. Fig. 6-4: Plot profiles generated from CLSM images of the measured fluorescence intensities of rhodamine-labeled ADA and FITC-labeled DEAE-dextran from ADA-D1 (**A**), ADA-D2 (**B**), and ADA-D3 (**C**) nanocomplexes ($n=3$) after and 48 h proofing simultaneous diffusion and thus stability of the complexes in the tissue. Error bars were omitted for clarity reasons.

6 Polyelectrolyte nanocomplexes to increase intraarticular residence of adalimumab injections



Sup. Fig. 6-5: % viability of synovial tissue in presence of nanocomplex formulations in different molar ratios (ADA-D1-3) after 48 h of incubation at 37° C as determined by MTT-assay. Mean ± SD; n=5; ANOVA+ Dunnett's multiple comparison test; significant differences: none of the formulations was significantly different compared to ADA alone (ADA); '*' (p < 0.05) compared to freshly dissected tissue.

6.12 References

- [1] M.B. Goldring, S.R. Goldring, Osteoarthritis, *J. Cell. Physiol.* 213 (2007) 626–634. <https://doi.org/10.1002/jcp.21258>.
- [2] D. Pereira, E. Ramos, J. Branco, Osteoarthritis, *Acta Médica Port.* Vol 28 No 1 2015 January-Febr. (2014). <https://doi.org/10.20344/amp.5477>.
- [3] S. Orita, T. Koshi, T. Mitsuka, M. Miyagi, G. Inoue, G. Arai, T. Ishikawa, E. Hanaoka, K. Yamashita, M. Yamashita, Y. Eguchi, T. Toyone, K. Takahashi, S. Ohtori, Associations between proinflammatory cytokines in the synovial fluid and radiographic grading and pain-related scores in 47 consecutive patients with osteoarthritis of the knee, *BMC Musculoskelet. Disord.* 12 (2011) 144. <https://doi.org/10.1186/1471-2474-12-144>.
- [4] M.B. Goldring, M. Otero, Inflammation in osteoarthritis, *Curr. Opin. Rheumatol.* 23 (2011) 471–478. <https://doi.org/10.1097/BOR.0b013e328349c2b1>.
- [5] X. Chevalier, F. Eymard, P. Richette, Biologic agents in osteoarthritis: hopes and disappointments, *Nat. Rev. Rheumatol.* 9 (2013) 400–410. <https://doi.org/10.1038/nrrheum.2013.44>.
- [6] W.P. Maksymowych, A.S. Russell, P. Chiu, A. Yan, N. Jones, T. Clare, R.G. Lambert, Targeting tumour necrosis factor alleviates signs and symptoms of inflammatory osteoarthritis of the knee, *Arthritis Res. Ther.* 14 (2012) R206. <https://doi.org/10.1186/ar4044>.
- [7] G. Verbruggen, R. Wittoek, B.V. Cruyssen, D. Elewaut, Tumour necrosis factor blockade for the treatment of erosive osteoarthritis of the interphalangeal finger joints: a double blind, randomised trial on structure modification, *Ann. Rheum. Dis.* 71 (2012) 891. <https://doi.org/10.1136/ard.2011.149849>.
- [8] C.H. Evans, V.B. Kraus, L.A. Setton, Progress in intra-articular therapy, *Nat. Rev. Rheumatol.* 10 (2014) 11–22. <https://doi.org/10.1038/nrrheum.2013.159>.
- [9] S.H.R. Edwards, Intra-articular drug delivery: The challenge to extend drug residence time within the joint, *Vet. J.* 190 (2011) 15–21. <https://doi.org/10.1016/j.tvjl.2010.09.019>.
- [10] M.D. Smith, The Normal Synovium, *Open Rheumatol. J.* 5 (2011) 100–106. <https://doi.org/10.2174/1874312901105010100>.

- [11] S. Sabaratnam, P.J. Coleman, R.M. Mason, J.R. Levick, Interstitial matrix proteins determine hyaluronan reflection and fluid retention in rabbit joints: effect of protease: Hyaluronan reflection mediated by interstitial matrix proteins, *J. Physiol.* 578 (2007) 291–299. <https://doi.org/10.1113/jphysiol.2006.119446>.
- [12] A. Vedadghavami, C. Zhang, A.G. Bajpayee, Overcoming negatively charged tissue barriers: Drug delivery using cationic peptides and proteins, *Nano Today*. 34 (2020) 100898. <https://doi.org/10.1016/j.nantod.2020.100898>.
- [13] A. Vedadghavami, E.K. Wagner, S. Mehta, T. He, C. Zhang, A.G. Bajpayee, Cartilage penetrating cationic peptide carriers for applications in drug delivery to avascular negatively charged tissues, *Acta Biomater.* 93 (2019) 258–269. <https://doi.org/10.1016/j.actbio.2018.12.004>.
- [14] I. Tabujew, K. Peneva, CHAPTER 1. Functionalization of Cationic Polymers for Drug Delivery Applications, in: S. Samal, P. Dubruel (Eds.), *Polym. Chem. Ser.*, Royal Society of Chemistry, Cambridge, 2014: pp. 1–29. <https://doi.org/10.1039/9781782620105-00001>.
- [15] T. Siefen, J. Lokhnauth, A. Liang, C.C. Larsen, A. Lamprecht, An ex-vivo model for transsynovial drug permeation of intraarticular injectables in naive and arthritic synovium, *J. Controlled Release.* (2021). <https://doi.org/10.1016/j.jconrel.2021.03.008>.
- [16] F. Ennen, S. Boye, A. Lederer, M. Cernescu, H. Komber, B. Brutschy, B. Voit, D. Appelhans, Biohybrid structures consisting of biotinylated glycodendrimers and proteins: influence of the biotin ligand's number and chemical nature on the biotin–avidin conjugation, *Polym Chem.* 5 (2014) 1323–1339. <https://doi.org/10.1039/C3PY01152F>.
- [17] A. Jain, K. Cheng, The principles and applications of avidin-based nanoparticles in drug delivery and diagnosis, *J. Controlled Release.* 245 (2017) 27–40. <https://doi.org/10.1016/j.jconrel.2016.11.016>.
- [18] B. Sterner, M. Harms, S. Wöll, M. Weigandt, M. Windbergs, C.M. Lehr, The effect of polymer size and charge of molecules on permeation through synovial membrane and accumulation in hyaline articular cartilage, *Eur. J. Pharm. Biopharm.* 101 (2016) 126–136. <https://doi.org/10.1016/j.ejpb.2016.02.004>.

- [19] Y. Guang, A.L. Davis, T.M. McGrath, C.T.N. Pham, J.A.J. Fitzpatrick, L.A. Setton, Size-Dependent Effective Diffusivity in Healthy Human and Porcine Joint Synovium, *Ann. Biomed. Eng.* (2021). <https://doi.org/10.1007/s10439-020-02717-4>.
- [20] C. Siewert, H. Haas, T. Nawroth, A. Ziller, S.S. Nogueira, M.A. Schroer, C.E. Blanchet, D.I. Svergun, A. Radulescu, F. Bates, Y. Huesemann, M.P. Radsak, U. Sahin, P. Langguth, Investigation of charge ratio variation in mRNA – DEAE-dextran polyplex delivery systems, *Biomaterials*. 192 (2019) 612–620. <https://doi.org/10.1016/j.biomaterials.2018.10.020>.
- [21] T. Masuko, A. Minami, N. Iwasaki, T. Majima, S.-I. Nishimura, Y.C. Lee, Carbohydrate analysis by a phenol–sulfuric acid method in microplate format, *Anal. Biochem.* 339 (2005) 69–72. <https://doi.org/10.1016/j.ab.2004.12.001>.
- [22] S.L. Kuan, S. Fischer, S. Hafner, T. Wang, T. Syrovets, W. Liu, Y. Tokura, D.Y.W. Ng, A. Riegger, C. Förtsch, D. Jäger, T.F.E. Barth, T. Simmet, H. Barth, T. Weil, Boosting Antitumor Drug Efficacy with Chemically Engineered Multidomain Proteins, *Adv. Sci.* 5 (2018) 1701036. <https://doi.org/10.1002/advs.201701036>.
- [23] P.C. Weber, J.J. Wendoloski, M.W. Pantoliano, F.R. Salemme, Crystallographic and thermodynamic comparison of natural and synthetic ligands bound to streptavidin, *J. Am. Chem. Soc.* 114 (1992) 3197–3200. <https://doi.org/10.1021/ja00035a004>.
- [24] J. Weyermann, D. Lochmann, A. Zimmer, A practical note on the use of cytotoxicity assays, *Int. J. Pharm.* 288 (2005) 369–376. <https://doi.org/10.1016/j.ijpharm.2004.09.018>.
- [25] C. Desvignes, S.R. Edupuganti, F. Darrouzain, A.-C. Duvéau, A. Loercher, G. Paintaud, D. Mulleman, Development and validation of an enzyme-linked immunosorbent assay to measure adalimumab concentration, *Bioanalysis*. 7 (2015) 1253–1260. <https://doi.org/10.4155/bio.15.30>.
- [26] M. Ries, B. Moulari, M.A. Shetab Boushehri, M.E. Ali, D. Molnar, A. Béduneau, Y. Pellequer, A. Lamprecht, Adalimumab Decorated Nanoparticles Enhance Antibody Stability and Therapeutic Outcome in Epithelial Colitis Targeting, *Pharmaceutics*. 14 (2022) 352. <https://doi.org/10.3390/pharmaceutics14020352>.

- [27] N.D. Vlieland, M.R. Nejadnik, H. Gardarsdottir, S. Romeijn, A.S. Sediq, M.L. Bouvy, A.C.G. Egberts, B.J.F. van den Bemt, W. Jiskoot, The Impact of Inadequate Temperature Storage Conditions on Aggregate and Particle Formation in Drugs Containing Tumor Necrosis Factor-Alpha Inhibitors, *Pharm. Res.* 35 (2018) 42. <https://doi.org/10.1007/s11095-017-2341-x>.
- [28] D. Scott, P.J. Coleman, R.M. Mason, J.R. Levick, Action of polysaccharides of similar average mass but differing molecular volume and charge on fluid drainage through synovial interstitium in rabbit knees, *J. Physiol.* 528 (2000) 609–618. <https://doi.org/10.1111/j.1469-7793.2000.00609.x>.
- [29] T.K. Mwangi, I.M. Berke, E.H. Nieves, R.D. Bell, S.B. Adams, L.A. Setton, Intra-articular clearance of labeled dextrans from naive and arthritic rat knee joints, *J. Controlled Release.* 283 (2018) 76–83. <https://doi.org/10.1016/j.jconrel.2018.05.029>.
- [30] S. Sabaratnam, V. Arunan, P.J. Coleman, R.M. Mason, J.R. Levick, Size selectivity of hyaluronan molecular sieving by extracellular matrix in rabbit synovial joints: Hyaluronan chain length and interstitial matrix sieving, *J. Physiol.* 567 (2005) 569–581. <https://doi.org/10.1113/jphysiol.2005.088906>.
- [31] B.T. Käsdorf, F. Arends, O. Lieleg, Diffusion Regulation in the Vitreous Humor, *Biophys. J.* 109 (2015) 2171–2181. <https://doi.org/10.1016/j.bpj.2015.10.002>.
- [32] L.D. Li, T. Crouzier, A. Sarkar, L. Dunphy, J. Han, K. Ribbeck, Spatial Configuration and Composition of Charge Modulates Transport into a Mucin Hydrogel Barrier, *Biophys. J.* 105 (2013) 1357–1365. <https://doi.org/10.1016/j.bpj.2013.07.050>.
- [33] R. Gupta, B. Rai, Effect of Size and Surface Charge of Gold Nanoparticles on their Skin Permeability: A Molecular Dynamics Study, *Sci. Rep.* 7 (2017) 45292. <https://doi.org/10.1038/srep45292>.
- [34] J.H. van den Berg, K. Oosterhuis, W.E. Hennink, G. Storm, L.J. van der Aa, J.F.J. Engbersen, J.B.A.G. Haanen, J.H. Beijnen, T.N. Schumacher, B. Nuijen, Shielding the cationic charge of nanoparticle-formulated dermal DNA vaccines is essential for antigen expression and immunogenicity, *J. Controlled Release.* 141 (2010) 234–240. <https://doi.org/10.1016/j.jconrel.2009.09.005>.

- [35] S.R. Kim, M.J. Ho, E. Lee, J.W. Lee, Y.W. Choi, M.J. Kang, Cationic PLGA/Eudragit RL nanoparticles for increasing retention time in synovial cavity after intra-articular injection in knee joint, *Int. J. Nanomedicine*. 10 (2015) 5263–5271. <https://doi.org/10.2147/IJN.S88363>.
- [36] E.K. Wagner, A. Vedadghavami, T.D. Jacobsen, S.A. Goel, N.O. Chahine, A.G. Bajpayee, Avidin grafted dextran nanostructure enables a month-long intradiscal retention, *Sci. Rep.* 10 (2020) 12017. <https://doi.org/10.1038/s41598-020-68351-1>.
- [37] C.A. Ambarus, T. Noordenbos, M.J. de Hair, P.P. Tak, D.L. Baeten, Intimal lining layer macrophages but not synovial sublining macrophages display an IL-10 polarized-like phenotype in chronic synovitis, *Arthritis Res. Ther.* 14 (2012) R74. <https://doi.org/10.1186/ar3796>.
- [38] S.L. Myers, K.D. Brandt, O. Eilam, Even low-grade synovitis significantly accelerates the clearance of protein from the canine knee: implications for measurement of synovial fluid “markers” of osteoarthritis, *Arthritis Rheum.* 38 (1995) 1085–1091. <https://doi.org/10.1002/art.1780380810>.
- [39] A. Mathiessen, P.G. Conaghan, Synovitis in osteoarthritis: current understanding with therapeutic implications, *Arthritis Res. Ther.* 19 (2017) 18. <https://doi.org/10.1186/s13075-017-1229-9>.
- [40] D. Scott, P.J. Coleman, A. Abiona, D.E. Ashhurst, R.M. Mason, J.R. Levick, Effect of depletion of glycosaminoglycans and non-collagenous proteins on interstitial hydraulic permeability in rabbit synovium, *J. Physiol.* 511 (1998) 629–643. <https://doi.org/10.1111/j.1469-7793.1998.629bh.x>.
- [41] N. Gerwin, C. Hops, A. Lucke, Intraarticular drug delivery in osteoarthritis, *Adv. Drug Deliv. Rev.* 58 (2006) 226–242. <https://doi.org/10.1016/j.addr.2006.01.018>.
- [42] D.J.A. Crommelin, R.D. Sindelar, B. Meibohm, eds., *Pharmaceutical Biotechnology: Fundamentals and Applications*, Springer International Publishing, Cham, 2019. <https://doi.org/10.1007/978-3-030-00710-2>.
- [43] M. van de Weert, W.E. Hennink, W. Jiskoot, Protein Instability in Poly(Lactic-co-Glycolic Acid) Microparticles, *Pharm. Res.* 17 (2000) 1159–1167. <https://doi.org/10.1023/A:1026498209874>.

7. Summary and outlook

IA injections of biologic agents, whether protein, gene, or cell therapies most certainly represent the future in pharmacologic therapy for osteoarthritis to achieve more long-term and causal success than existing regimens are capable to provide [1,2]. Biologics offer a wide range of targeted applications and can intercept catabolic events or induce anabolic activity and promote regeneration of deteriorated tissues in the joint [3]. However, intensive research efforts will yet be required before such therapies can become established in clinical practice, not only in the discovery of potential target structures and the development of active pharmaceutical ingredients, but in particular in their delivery to the joint space with the aim of overcoming biopharmaceutical challenges so as to achieve sufficient duration of action in the joint cavity and a reasonable injection frequency.

With the initiation of this research to develop a formulation for IA delivery of biologics, the initial key question was to determine how the joint residence time of the drug dosage form could be tested in a biorelevant but yet simple screening. While there are methods described in the literature to address this concern, they usually involve either basic dissolution experiments or complex and expensive animal models. For the investigation of parenteral depot drug forms in general, scientists often rely on artificial membrane-based models such as the USP apparatus III (reciprocal cylinder) and IV (flow cell), the rotating dialysis cell or assimilated membrane-separated diffusion chambers such as the Ussing chamber [4–7]. However, these models are primarily applicable to simple drug formulations and only infer release but not elimination or distribution kinetics in the joint, as they do not reflect the physiological environment and no material-tissue interplay is involved. Animal models, on the other hand, present much more thorough insights as they include physiological and metabolic factors as well as long-term changes in tissue structure and joint composition. However, whilst they generate valuable data, they are highly complex to interpret, involve ethical concerns, and are both challenging and costly to execute. Accordingly, animal studies are rather inappropriate for preliminary screenings of joint residence time in the stage of early development, especially since individual processes or compartments are difficult to evaluate in isolation as they are influenced by multiple variables. To fill this gap in between dissolution and *in-vivo* studies and allow relevant decisions to be made at the very earliest stages, an *ex-vivo* permeation model was developed, which adopts the membrane-based methodology of conventional release models, but combines it with a viable

synovial membrane, thus providing simultaneous assessment of drug dosage release and tissue permeability and thus local elimination processes. The conceived model was characterized in-depth using fluorescence-labeled dextrans, which are widely employed as standards for assessing permeability in tissues [8–10]. Thereby, different molecular sizes and charge were examined, and the conceived model was proven to exhibit an excellent translatability to existing *in-vivo* studies on IA administered dextran into rats via an IVIVC [11]. Since further studies have also reported good correlation of diffusion amidst *ex-vivo* porcine and human synovial membranes [12], a high relevance of the acquired data is to be expected. The *ex-vivo* model thus fulfilled the expectations by offering a convenient technique for predicting elimination kinetics in the earliest stages of development involving only modest resources and costs. Furthermore, due to the viable nature of the membrane a simulation of arthritic tissue structures could be achieved via LPS stimulation, thus allowing conclusions on synovially altered permeabilities. This represents a novelty for the assessment of synovial permeability and provides yet deeper mechanistic insights, since an injection is commonly administered into inflamed joints. Contrary to former practiced procedures of developing a formulation and subsequently testing it, modern drug delivery research usually first identifies the biopharmaceutical barriers and designs criteria before formulations are developed, thus placing a greater emphasis on the physiological environment. [13]. While this approach is not yet widely employed in pharmaceutical osteoarthritis research, the present work adopted this workflow and first identified key factors affecting synovial permeability through characterization of permeation with the *ex-vivo* model and then deduced formulation strategies. This concept allowed physiological conditions to be leveraged for engaging rational guidelines for the development of IA therapeutics, with the data elaborated providing a sound basis for a rational selection and development of potential drug candidates to be considered for sustained release intra-articular drug delivery. In this context, it was observed that increasing molecular weight as well as positive charge led to a prolongation of transsynovial diffusion.

Based on these findings, the drug ADA was selected as a suitable agent for IA injections because it not only has promising therapeutic potential, but is expected to be eliminated more slowly compared to other protein drugs due to its large molecular size and basic patches [14]. However, these properties should be further optimized by drug delivery design in order to exploit the full potential of the agent. In a first formulation approach, a binary hydrogel system of HA and

PVP was investigated with respect to the extension of the joint residence time of ADA as well as of HA, which is likewise possessing pharmacological activity within the joint. For this purpose, a DOE was used to find an optimal ratio of the polymers, which necessitated a rather large number of samples. Here, the strength of the test system was highlighted in its ability to perform extensive screening and yet offering straightforward insights into drug release as well as delivering information on the tissue permeability. Viscosupplementation by injection of HA is an integral element of current OA therapy regimens to alleviate patients' symptoms [15]. In addition to decelerating drug diffusion, the designed delivery system was found to provide viscosupplementative qualities owing to the viscosity of the selected polymers HA and PVP. Hence, it was possible to achieve not only a retarded permeation of ADA across the synovial membrane but simultaneously achieve optimization of the lubricating capacities and thus resulting in a multimodal therapy approach. Based on rheological and tribological analyses it may thereby be assumed that the effect is at least equal to that of approved HA viscosupplements, although it should be mentioned that these assumptions are based only on the physical properties of the formulations and not on preclinical or clinical trials.

The concept of leveraging biopharmaceutical conditions for formulation design is even more evident in the development of the second drug delivery system. The discovery that DEAE-derivatized dextrans penetrate the synovial membrane much more slowly than uncharged dextrans of the same size gave rise to the idea of linking the cationic polysaccharides to the API via an avidin-mediated complex, which perfectly exemplifies the described development workflow. Electrostatic interaction has already been exploited for controlling intra-joint distribution of small molecules by increasing their uptake into the articular cartilage [16,17]. In the present work, however, the net positive charge of the excipient was yet increased, so that instead of deep penetration into articular compartments, which have a high negative fixed charge density, immobilization was observed within superficial layers of the synovium. Given that synoviocytes and synovial macrophages, which secrete inflammatory mediators into the joint space in OA and thus contribute to cartilage degeneration and inflammation, are located in intimal layers, these tissue layers were considered an ideal target for ADA delivery.

The novel approach of anchoring biologics in superficial tissue zones using charged nanocomplexes to decelerate intrusion into joint biobarriers represents a promising delivery strategy, particularly since no detrimental effects on the

activity of the antibody or the viability of synovial cells could be measured. Since this second approach is based on material-tissue interaction, which can usually only be estimated in a relevant way by animal models or complex 3D cell cultures [18], the advantages of the permeation model in the development of IA drug delivery systems over conventional artificial membranes, which would not have been able to represent the observed effects, were once more demonstrated.

To conclude, the *ex-vivo* permeation model has successfully introduced a tool that allows for biorelevant screening of release as well as pharmacokinetics at an early stage of development, thus narrowing the gap between dissolution and *in-vivo* testing. In addition, this platform offers the opportunity to incorporate novel formulation development practices into the research of IA drug delivery systems through enhanced understanding of material-tissue interactions, thus enabling researchers to observe, evaluate, and adapt the design of more efficient and intelligent drug carriers in their biopharmaceutical environment. Two very different delivery concepts have been developed. On the one hand a co-formulated hydrogel-based system, which combines the sustained release of a biologic with an optimized viscosupplementation and thus presents a novel multimodal therapeutic approach and on the other hand an innovative system, which decelerates the diffusion a biologic via cationic nanocomplexes and leads to immobilization of the anti-inflammatory drug in superficial layers of the synovium. For these very diverse approaches, advantages in terms of quantitative capacity and qualitative performance of the *ex-vivo* model compared to conventional test methods have been demonstrated. The developed model provides an in-depth understanding of potential retention mechanisms in order to gain sustained release upon intra-articular administration of drugs. We therefore trust to have contributed to more sophisticated assessment and development workflow of pioneering IA formulation and to have expanded the testing capabilities by an additional biopharmaceutical tool that provides early and profound insights and understanding into elimination and distribution kinetics of drugs from the joint space.

For future applications and optimization of the predictions of the applied model, it would be of great value to conduct equivalent animal studies in order to assess the pharmacokinetics of drugs alone, but also of formulations, by means of *in-vivo*-imaging methods. *In vivo* imaging would enable tracking of fluorescent drugs from the joint and thus provide conclusions to be drawn about the distribution processes in the living model with all vital parameters. This would allow for even more precise predictability of the data generated by the *ex-vivo* model. In this

context, pharmacokinetic modelling software should support the identification of potential agents or drug delivery systems for application as IA injections based on a small number of *ex-vivo* screenings, with the aim of predicting relevant *in-vivo* processes while further reducing the number of necessary experiments. In the way, the effectiveness of the system would again be enhanced. However, at present, no IA modelling software is on the market, as existing software is generally restricted to the more traditional routes of administration, in particular p.o. medicines. Further improvement of the model could be achieved in future research by accelerating the test process. Especially for slow permeating agents or sustained formulations, the model encounters limitations due to the restricted stability and viability of biological tissue, as the specified test periods of 48 h should not be exceeded. Through quantification of tissue cross-sections in the CLSM, as was already applied in chapter III, this problem could be mitigated, so that short and thus efficient test periods would suffice for all samples. Using a computational finite dose simulation for scaling would allow a simplified translation of the results, whilst equalizing the bias of intra-individual thickness variations of the synovial membranes. So, while there are yet more exciting projects ahead to increase the efficiency and adaptability of IA *in-vitro* or rather *ex-vivo* testing, this work had its share in pioneered biopharmaceutical pharmacokinetic screening in the field of IA drug delivery systems and will likely bring inspiration and support for the evolution of new ideas for researchers in the field of sustained IA injection for the treatment of OA.

7.1 References

- [1] M.M. Richards, J.S. Maxwell, L. Weng, M.G. Angelos, J. Golzarian, Intra-articular treatment of knee osteoarthritis: from anti-inflammatories to products of regenerative medicine, *Phys. Sportsmed.* 44 (2016) 101–108. <https://doi.org/10.1080/00913847.2016.1168272>.
- [2] I.A. Jones, R. Togashi, M.L. Wilson, N. Heckmann, C.T. Vangsnes, Intra-articular treatment options for knee osteoarthritis, *Nat. Rev. Rheumatol.* 15 (2019) 77–90. <https://doi.org/10.1038/s41584-018-0123-4>.
- [3] X. Chevalier, F. Eymard, P. Richette, Biologic agents in osteoarthritis: hopes and disappointments, *Nat. Rev. Rheumatol.* 9 (2013) 400–410. <https://doi.org/10.1038/nrrheum.2013.44>.
- [4] D.J. Burgess, D.J.A. Crommelin, A.S. Hussain, M.-L. Chen, Assuring quality and performance of sustained and controlled release parenterals: EUFEPS workshop report, *AAPS PharmSci.* 6 (2004) 100–111. <https://doi.org/10.1208/ps060111>.
- [5] B.T. Pedersen, J. Østergaard, S.W. Larsen, C. Larsen, Characterization of the rotating dialysis cell as an in vitro model potentially useful for simulation of the pharmacokinetic fate of intra-articularly administered drugs, *Eur. J. Pharm. Sci.* 25 (2005) 73–79. <https://doi.org/10.1016/j.ejps.2005.01.019>.
- [6] N. Joshi, J. Yan, S. Levy, S. Bhagchandani, K.V. Slaughter, N.E. Sherman, J. Amirault, Y. Wang, L. Riegel, X. He, T.S. Rui, M. Valic, P.K. Vemula, O.R. Miranda, O. Levy, E.M. Gravallesse, A.O. Aliprantis, J. Ermann, J.M. Karp, Towards an arthritis flare-responsive drug delivery system, *Nat. Commun.* 9 (2018). <https://doi.org/10.1038/s41467-018-03691-1>.
- [7] T. Noda, T. Okuda, R. Mizuno, T. Ozeki, H. Okamoto, Two-Step Sustained-Release PLGA/Hyaluronic Acid Gel Formulation for Intra-articular Administration, *Biol. Pharm. Bull.* 41 (2018) 937–943. <https://doi.org/10.1248/bpb.b18-00091>.
- [8] Y. Ito, A. Ise, N. Sugioka, K. Takada, Molecular weight dependence on bioavailability of FITC-dextran after administration of self-dissolving micropile to rat skin, *Drug Dev. Ind. Pharm.* 36 (2010) 845–851. <https://doi.org/10.3109/03639040903541179>.

- [9] Y. Olsson, E. Svensjö, K.-E. Arfors, D. Hultström, Fluorescein labelled dextrans as tracers for vascular permeability studies in the nervous system, *Acta Neuropathol. (Berl.)*. 33 (1975) 45–50. <https://doi.org/10.1007/BF00685963>.
- [10] J.R. Sanders, N.A. Pou, R.J. Roselli, Neutral and DEAE dextrans as tracers for assessing lung microvascular barrier permeability and integrity, *J. Appl. Physiol.* 93 (2002) 251–262. <https://doi.org/10.1152/japplphysiol.00635.2000>.
- [11] T.K. Mwangi, I.M. Berke, E.H. Nieves, R.D. Bell, S.B. Adams, L.A. Setton, Intra-articular clearance of labeled dextrans from naive and arthritic rat knee joints, *J. Controlled Release*. 283 (2018) 76–83. <https://doi.org/10.1016/j.jconrel.2018.05.029>.
- [12] Y. Guang, A.L. Davis, T.M. McGrath, C.T.N. Pham, J.A.J. Fitzpatrick, L.A. Setton, Size-Dependent Effective Diffusivity in Healthy Human and Porcine Joint Synovium, *Ann. Biomed. Eng.* (2021). <https://doi.org/10.1007/s10439-020-02717-4>.
- [13] W. Sun, Q. Hu, W. Ji, G. Wright, Z. Gu, Leveraging Physiology for Precision Drug Delivery, *Physiol Rev.* 97 (2017) 37. <https://doi.org/10.1152/physrev.00015.2016>.
- [14] A. Goyon, M. Excoffier, M.-C. Janin-Bussat, B. Bobaly, S. Fekete, D. Guillaume, A. Beck, Determination of isoelectric points and relative charge variants of 23 therapeutic monoclonal antibodies, *J. Chromatogr. B*. 1065–1066 (2017) 119–128. <https://doi.org/10.1016/j.jchromb.2017.09.033>.
- [15] E. Balazs, J. Denlinger, Viscosupplementation: a new concept in the treatment of osteoarthritis, *J. Rheumatol. Suppl.* 39 (1993) 3–9.
- [16] A. Vedadghavami, C. Zhang, A.G. Bajpayee, Overcoming negatively charged tissue barriers: Drug delivery using cationic peptides and proteins, *Nano Today*. 34 (2020) 100898. <https://doi.org/10.1016/j.nantod.2020.100898>.
- [17] T. He, C. Zhang, A. Vedadghavami, S. Mehta, H.A. Clark, R.M. Porter, A.G. Bajpayee, Multi-arm Avidin nano-construct for intra-cartilage delivery of small molecule drugs, *J. Controlled Release*. 318 (2020) 109–123. <https://doi.org/10.1016/j.jconrel.2019.12.020>.

[18] R.M. Stefani, S.S. Halder, E.G. Estell, A.J. Lee, A.M. Silverstein, E. Sobczak, N.O. Chahine, G.A. Ateshian, R.P. Shah, C.T. Hung, A Functional Tissue-Engineered Synovium Model to Study Osteoarthritis Progression and Treatment, *Tissue Eng. Part A.* (2018). <https://doi.org/10.1089/ten.tea.2018.0142>.

8. Appendix

8.1 List of abbreviations

ADA	adalimumab
ADAMTS	a disintegrin and metalloproteinase with thrombospondin motifs
ANOVA	analysis of variance test
API	active pharmaceutical ingredient
BMP-7	bone morphogenetic protein 7
CLSM	confocal laser scanning microscopy
CM	carboxymethyl
DEAE	diethylaminoethyl
DLS	dynamic light scattering
DMEM	Dulbecco minimum essential media
DMSO	dimethyl sulfoxide
DOE	design of experiments
ECM	extracellular matrix
ELISA	enzyme-linked immunosorbent assay
FBS	fetal bovine serum
FITC	fluoresceine-isothiocyanate
FGF-18	fibroblast growth factor 18
FLISA	fluorophore-linked immunosorbent assay
GAG	galactosamine glycan
HABA	2-(4'-hydroxyazobenzene)-benzoic acid
IA	intraarticular
IL-1 β	interleukin 1 β
IGF-1	insulin-like-growth factor 1
ITC	isothermal titration calorimetry
IVIVC	<i>in-vivo-in-vitro</i> -correlation
HA	hyaluronic acid
H&E	hematoxylin-eosin
LPS	lipopolysaccharide

8 Appendix

mAb	monoclonal antibody
MMP	matrix-metalloprotease
MTT	methylthiazolyldiphenyl-tetrazolium bromide
NGF	nerve growth factor
OA	osteoarthritis
PBS	phosphate-buffered saline
PDI	polydispersity index
PEG	polyethylene glycol
PLGA	poly(lactic-co-glycolic acid)
PVP	polyvinylpyrrolidone
RA	receptor antagonist
STR	shear thinning ratio
TEER	transepithelial electrical resistance
TNF- α	tumor necrosis factor α
USP	United States Pharmacopeia
ZSV	zero shear viscosity

8.2 List of publications

Parts of this work are published as:

Articles:

- Siefen T, Bjerregaard S, Borglin C, Lamprecht A. Assessment of joint pharmacokinetics and consequences for the intraarticular delivery of biologics. *J Control Release*. 2022 Jun 14:S0168-3659(22)00343-1. doi: 10.1016/j.jconrel.2022.06.015.
- T. Siefen, J. Lokhnauth, A. Liang, C. C. Larsen, and A. Lamprecht, An ex-vivo model for transsynovial drug permeation of intraarticular injectables in naive and arthritic synovium, *Journal of Controlled Release*, Mar. 2021, doi: 10.1016/j.jconrel.2021.03.008.
- Siefen T, Bjerregaard S, Plaksin D, Lokhnauth J, Liang A, Casper Larsen C, Lamprecht A. Co-formulations of adalimumab with hyaluronic acid / polyvinylpyrrolidone to combine intraarticular drug delivery and viscosupplementation. *Eur J Pharm Biopharm*. 2022 Jun 9:S0939-6411(22)00119-9. doi: 10.1016/j.ejpb.2022.06.002.